

CHEMICAL AND PHYSICAL CONTROLS OF TOXIC
METALS REMOVAL

FROM PETROLEUM PRODUCED WATER

BY DOLOMITE FILTRATION

by

KHALID HAJI OMAR

Bachelor of Science in Geology
Salahaddin University
Erbil, Kurdistan, Iraq
2008

Master of Art in Earth Sciences
Western Michigan University
Kalamazoo, Michigan
2017

Submitted to the Faculty of the
Graduate College of the
Oklahoma State University
in partial fulfillment of
the requirements for
the Degree of
DOCTOR OF PHILOSOPHY
May, 2023

CHEMICAL AND PHYSICAL CONTROLS OF TOXIC
METALS REMOVAL
FROM PETROLEUM PRODUCED WATER
BY DOLOMITE FILTRATION

Dissertation Approved:

Dr. Javier Vilcáez

Dissertation Adviser

Dr. Jim Puckette

Dr. Todd Halihan

Dr. Prem Bikkina

ACKNOWLEDGEMENTS

I would like to dedicate this work to my amazing family, my mother and father especially, who with their continuous support and encouragement, led me to where I am today. To my brothers and sisters, for their sacrifices and for filling in on my behalf when needed. I have been able to reach my goals in life and everything that I have gained until now, is because of their love and support.

I want to thank my lovely wife, for being with me during this journey. For her sacrifices and unwavering strength as she held our family together these past four years while I focused on my studies. Without her, this work wouldn't be accomplished. And to my father and mother-in-law, for helping us when we needed it most.

To Dr. Javier Vilcáez, my advisor, my sincere gratitude for all the support during my Ph.D. studies. For his patience, motivation, and encouragement in guiding me through the research and writing of this dissertation. I consider Dr. Vilcáez a lifetime mentor. He shifted my academic career and transformed me into a protean and multi-disciplinary scientist.

I also want to thank my Ph.D. project committee for their time and insights. To Dr. Jim Puckette, words cannot express how much I appreciate him. Whenever I needed him, he was always there for me. Thank you. To Dr. Todd Halihan, I would like to thank him for providing me with the knowledge and for teaching me about hydrogeology. To Dr. Prem Bikkina, I would like to express my gratitude for his time, and insightful comments and support.

I would like to extend special thanks to our head of school, Dr. Camelia Knapp. I will never forget her great aid, support, and care from the first day of the school until now. I would like to extend my sincere appreciation to the Boone Pickens School of Geology faculty, staff, and colleagues. To Dr. Michael Grammar and Dr. Jay Gregg, thank you for your continuous support and teaching, and for keeping your doors open to me during my studies. I would like to extend my gratitude to Tim Sickbert, Sandy Earls, and others for their technical and administrative support during my time at Oklahoma State University (OSU).

I would like to extend my gratitude to the faculty and staff in the School of Engineering at OSU for making their laboratory facilities available to me during my studies. I also would like to thank Brent Johnson and Lisa Whitworth at the Microscopy Lab Facility at OSU for their continuous assistance and support. Special thanks to the Soil, Water, and

Forage Analytical Laboratory staff for their help and facilitation. Many thanks to my funding agencies for helping me to translate my ideas into real work.

Last but not the least, I would like to express my deepest appreciation to all who have greatly influenced me and helped me on my academic journey and provided me with the possibility to complete this dissertation.

Name: KHALID HAJI OMAR

Date of Degree: MAY, 2023

Title of Study: CHEMICAL AND PHYSICAL CONTROLS OF TOXIC METALS
REMOVAL FROM PETROLEUM PRODUCED WATER BY
DOLOMITE FILTRATION

Major Field: GEOLOGY

Abstract: Produced water (PW) from oil and gas reservoirs contains orders of magnitude higher concentrations of toxic metals (heavy metals, metalloids, and alkaline earth metals) than seawater, shallow groundwater, and conventional wastewater. The high concentration of total dissolved salts (TDS) and complex composition of PW hinder the utilization of conventional water treatment technologies to remove toxic metals from PW at an economic cost. To reduce and/or replace the use of expensive conventional technologies to remove high concentrations of toxic metals from huge volumes of PW, the goal of this research was: 1) to assess the potentiality of using dolomite filters made of compressed dolomite grains to remove toxic metals from PW, 2) to determine the chemical (alkalinity, pH, and salinity) and physical (injection rate, dolomite surface area) controls of toxic metals removal by dolomite filtration, 3) to elucidate the changes in the morphology, and mineral and elemental composition of the dolomite surface due to precipitation/co-precipitation and/or sorption reactions of toxic metals, and 4) to mathematically model and simulate the removal of toxic metals from PW by dolomite filtration. The focus was on the most common and abundant toxic metals found in PW (e.g., Sr, Ba, As, Cd, and Pb). The attained removal levels of toxic metals are comparable to those obtained with synthetic materials. It was found that 1) the in-situ generation of alkalinity from the dissolution of dolomite controls the precipitation/coprecipitation of toxic metals as carbonate minerals, 2) the increases of pH that results from the dissolution of dolomite promotes sorption reactions of toxic metals on dolomite, 3) Ba and Sr are removed from PW preferentially via sorption reactions, Pb and As are removed mostly via precipitation/co-precipitation reactions of carbonate minerals, and the removal mechanism of Cd is highly dependent on the PW composition (alkalinity and pH). Carbonate precipitates from PW have complex compositions that reflect the composition of PW, and the lack of thermodynamic data for those complex carbonate minerals hinders the application of reactive transport models to reproduce experimental results. The findings of this research have large implications toward the establishment of a new dolomite filtration technology to treat PW for toxic metals at an economic cost, as well as to predict the fate of toxic metals present in PW commonly disposed into deep dolomite saline aquifers, and/or to recover critical metals from PW by dolomite filtration.

TABLE OF CONTENTS

Chapter	Page
I. INTRODUCTION	1
1.1. Motivation	1
1.2. Significance	3
1.3. Intellectual merit	7
1.4. Organization of the Dissertation	11
1.5. List of Publications.....	12
1.5.1. Published at or Submitted to Peer Reviewed Journals	12
1.5.2. Conference Proceedings and Abstracts	12
1.6. References	15
II. REMOVAL OF TOXIC METALS FROM PETROLEUM PRODUCED WATER BY DOLOMITE FILTRATION	19
2.1. Abstract	19
2.2. Introduction	20
2.3. Materials and methods	23
2.3.1. Dolomite samples	23
2.3.2. Dolomite filters.....	24
2.3.3. Synthetic produced water	25
2.3.4. Core-flooding experiments	27
2.4. Results and discussion.....	28
2.4.1. Effect of salinity and competition of cations.....	28
2.4.2. Effect of flow velocity and grain size.....	32
2.4.3. Effect of guar gum.....	35
2.4.4. Modeling and simulation.....	38
2.5. Conclusions	47
2.6. Acknowledgements	48
2.7. References	48

Chapter	Page
III. ROLE OF ALKALINITY AND DOLOMITE REACTIVITY ON TOXIC METALS REMOVAL FROM PETROLEUM PRODUCED WATER BY DOLOMITE	64
3.1. Abstract	64
3.2. Introduction	65
3.2. Materials.....	68
3.2.1. Dolomite	68
3.2.2. Dolomite grains	70
3.2.3. Synthetic produced water	70
3.3. Methods.....	72
3.3.1. Batch experiments	72
3.3.2. Surface morphology and composition analyses	74
3.4. Results and discussion.....	76
3.4.1. Batch reaction experiments	76
3.4.2. Geochemical modeling.....	103
3.5. Conclusions	107
3.7. Acknowledgments.....	109
3.8. References	109
IV. EFFECT OF CARBONATE MINERALS PRECIPITATION AND SORPTION REACTIONS ON THE TRANSPORT OF TOXIC METALS IN DOLOMITE.....	115
4.1. Abstract	115
4.2. Introduction	116
4.3. Materials.....	121
4.3.1. Dolomite	121
4.3.2. Synthetic dolomite core	123
4.3.3. Synthetic produced water	123
4.4. Methods.....	126
4.4.1. Core-flooding experiments	126
4.4.2. XRD and SEM-EDS analyses	129
4.5. Results and discussion.....	130
4.5.1. Removal levels	130
4.5.2. SEM analysis of changes in the morphology of dolomite surface	140
4.5.3. SEM-EDS analysis of the elemental composition of dolomite surface.....	146
4.5.4. XRD analysis of the mineral composition of precipitates	151

Chapter	Page
4.6. Conclusions	161
4.7. Funding.....	162
4.8. Acknowledgments.....	162
4.9. References	162
V. CONCLUSIONS AND RECOMMENDATIONS	168
5.1. Conclusions	169
5.1.1. Removal of toxic metals from petroleum produced water by dolomite filtration	169
5.1.2. Role of alkalinity and dolomite reactivity on toxic metals removal from petroleum produced water by dolomite	170
5.1.3. Effect of carbonate minerals precipitation and sorption reactions on the transport of toxic metals in dolomite	171
5.2. Recommendations for Future Studies	172
REFERENCES	175

LIST OF TABLES

Table	Page
2.1. Surface complexation reactions (Pokrovsky et al., 2000b).....	40
2.2. Aqueous phase acid-base and complexation reactions.	41
2.3. Dissolution/precipitation reactions of minerals.	42
2.4. Parameters for reactive transport simulations of Sr, Ba, and Cd in dolomite.....	42
3.1. Added salts to prepare synthetic produced water (PW) of different compositions. ...	71
3.2. Composition of the types of freshwater (FW) used for experiments.	72
3.3. Initial composition of the synthetic produced waters (PW) used for experiments.	73
3.4. Initial composition of the synthetic freshwaters (FW) used for experiments.	74
3.5 Toxic metals removal from PW of different compositions, initial pH, and alkalinity (see Table 3.3).....	77
3.6 Toxic metals removal from FW of different compositions, initial pH, and alkalinity (see Table 3.4).....	77
3.7. Aqueous phase equilibrium complexation reactions.	103
3.8. Mineral phase reactions.	104
4.1. Added salts to prepare synthetic produced water (PW).	125
4.2. Added salts to prepare freshwater (FW).	125
4.3. Initial composition of synthetic produced waters (PW).	128
4.4. Initial composition of the synthetic freshwaters (FW).	128
4.5. Toxic metals removal from PW.	131
4.6. Toxic metals removal from FW.	131

LIST OF FIGURES

Figure	Page
2.1. Representative X-ray (left-hand side) and thin-section (right-hand side) analysis of Arbuckle dolomite samples of 98% purity collected from a road-cuts in south-west Missouri.	24
2.2. Procedure to prepare dolomite filters: A) Arbuckle Group outcrop in the south-west Missouri, B) Jaw rock crusher, C) Crushed dolomite samples, D) Sieving shaker machine, E) Sieved dolomite powder, F) Ultrasonic bath, G) Cylindrical stainless-steel mold, I) Carver Laboratory Presser, and J) Dolomite filer warped with aluminum foil.	25
2.3. Schematic of the experimental setup: A) Computer to record pressure, B) Deionized water container, C) Dual syringe high-pressure injection pump, D) Floating piston accumulator containing 1L of synthetic PW, E) Hydraulic hand pump, F) Pressure gauge (confining pressure), G) Hassler-type core-holder, and I) Effluent collector.	28
2.4. Removal of Sr, Ba, and Cd from 1L of synthetic PW at A) 0 g-NaCl/L, B) 11.5 g-NaCl/L, and C) 115.4 g-NaCl/L salinities using filters (1.5-inch diameter and 6-inch length) made of 600-850 μm grain size. Injection rate is 0.5 mL/min.	29
2.5. Removal of Pb, Sr, Ba, As, and Cd from 1 L of synthetic PW using a dolomite filter made of 350-600 μm grain size (1.5-inch diameter and 6-inch length). PW injection rate is 0.1 mL/min, and salinity of PW is 45 g-NaCl/L.	30
2.6. Representative pH of discrete volumes of filtered PW containing Pb, Sr, Ba, As, and Cd. PW injection rate is 0.1 mL/min and salinity of PW is 45 g-NaCl/L.	32
2.7. Removal of Sr, Ba, and Cd from 1L of synthetic PW at A) 0.5 mL/min, B) 0.25 mL/min, and C) 0.1 mL/min injection rates using: I) 600-850 μm grain size and 115.5 g-NaCl/L salinity. II) 600-850 μm grain size and 42 g-NaCl/L salinity. III) 350-600 μm grain size and 42 g-NaCl/L salinity.	33
2.8. Removal of Sr, Ba, and Cd from 1L of synthetic PW containing 0.5 g-Guar gum/L at A) 0.5 mL/min, B) 0.25 mL/min, and C) 0.1 mL/min injection rates using filters made of 350-600 μm grain size. Salinity of the synthetic PW is 42 g-NaCl/L.	35
2.9. Removal of Sr, Ba, and Cd from 1L of synthetic PW: A) 0.0 g-Guar gum/200 g-Dolomite, B) 0.5 g-Guar gum/200 g-Dolomite, C) 1.0 g-Guar gum/200 g-Dolomite. Filters are made of 850-600 μm grain size. Salinity of the synthetic PW is 42 g-NaCl/L. Injection rate is 0.1 mL/min.	37

2.10. Simulated removal of Sr, Ba, and Cd from 1L of synthetic PW at A) 1.0 mL/min, B) 0.25 mL/min, and C) 0.5 mL/min injection rates using filters made of 600-350 μm grain size. Intrinsic stability constant for Sr, Ba, and Cd is the same (Table 1). Salinity of the synthetic PW is 40 g-NaCl/L.	43
2.11. Simulated concentrations of aqueous species (Sr, Ba, Cd, Ca, Mg, and Cl) in mol/L and pH in a dolomite filter made of 350-600 μm grain size after 0.1 days of PW injection at 0.1 mL/min. Two inlet points are at the bottom and out outlet point at the top.	45
2.12. Simulated concentrations of surface species (Sr, Ba, Cd, Ca, and Mg) in mol/L and pH in a dolomite filter made of 350-600 μm grain size after 0.1 days of PW injection at 0.1 mL/min. Two inlet points are located at the bottom and out outlet point at the top.	46
3.1. A) Thin section (scale bare = 200 μm) showing shape and size of dolomite crystals, B) XRD analysis showing that the employed dolomite is mainly composed of dolomite (represented by D only on the 104-dolomite peak) with minor quantities of quartz and calcite cement (represented by Q only on the 101-quartz peak, and C only on 104-calcite peak which is very weak). Dolomite cations (e.g., Mg & Ca) ordering reflections are indicated by asterisks on 101, 015 and 021 dolomite peaks. C) SEM micrograph showing the shape and size of dolomite crystals as well as porosity.	69
3.2. Batch experimental results of single metals removal by dolomite from PW: A) Ba (PW type I); B) Sr (PW type II); C) Cd (PW type III); D) Pb (PW type IV); and E) As (PW type V). All were supplied with CaCO_3 to increase the initial alkalinity (Table 3.3).	79
3.3. Batch experimental results of individual toxic metals removal by dolomite: A) Ba (FW type I); B) Sr (FW type II); C) Cd (FW type III); D) Pb (FW type IV); and E) As (FW type V). All were supplied with CaCO_3 to increase the initial alkalinity.	80
3.4. Batch experimental results of mixed toxic metals removal by dolomite (PW type VI): A) pH profile; B) Toxic metals removal profile. PW type VI was supplied with CaCO_3 to increase the initial alkalinity (Table 3.3).	82
3.5. Batch experimental results of mixed toxic metals removal by dolomite (PW type VII): A) pH profile; B) Toxic metals removal profile. PW type VII was not supplied with CaCO_3 to increase the initial alkalinity (Table 3.3).	83
3.6. Batch experimental results of mixed toxic metals removal by dolomite (FW type VI): A) pH profile; B) Toxic metals removal profile. FW type VI was supplied with CaCO_3 to increase the initial alkalinity (Table 2).	84
3.7. Batch experimental results of mixed toxic metals removal by dolomite (FW type VII): A) pH profile; B) Toxic metals removal profile. FW type VII was not supplied with CaCO_3 to increase the initial alkalinity (Table 3.4).	85

Figure	Page
3.8. SEM analysis of dolomite grain surface after 72 h of batch reaction: A) Ba (PW type I); B) Sr (PW type II); C) Cd (PW type III); D) Pb (PW type IV); and E) As (PW type V). All were supplied with CaCO ₃ to increase the initial alkalinity.	86
3.9. SEM-EDS analysis of dolomite grain surface after 72 h of batch reaction using PW type I (Ba): A) SEM shows Ba precipitates in the middle of the picture as light-colored grains, B) Zoom-in of A, showing Ba precipitate, C) SEM-EDS mapping of B showing Ba precipitate in green color. D) SEM shows Ba precipitates and NaCl grains (light gray), E) Zoom-in of A, showing Ba precipitates associated with NaCl precipitation, and F) EDS mapping of Ba precipitates in blue color.	87
3.10. SEM-EDS mapping of dolomite grain surface after 72 h of batch reaction using PW type I (Ba): A) a SEM micrograph showing toxic metals carbonate phase at the edges of the dolomite grain, B) X-ray spectrum showing elemental composition of the bulk samples, C) EDS mapping, and D) EDS mapping layers for single metals.	88
3.11. SEM-EDS analysis of dolomite grain surface after 72 h of batch reaction using PW type II (Sr): A) SEM shows Sr and NaCl precipitates (light gray), B) Zoom-in of A showing a precipitate, C) EDS mapping of B showing that the precipitate contains Sr, D) SEM of high silica dolomite grain showing NaCl on the upper left side of the image, E) Zoom-in of D showing amorphous silica, and F) SEM-EDS mapping of E showing Sr a sorbed phase on the high silica dolomite grain in orange color.	88
3.12. SEM-EDS mapping of dolomite grain surface after 72 h of batch reaction using PW type II (Sr): A) a SEM micrograph showing toxic metals carbonate phase at the edges of the dolomite grain, B) X-ray spectrum showing elemental composition of the bulk samples, C) EDS mapping, and D) EDS mapping layers for single metals.	89
3.13. SEM-EDS analysis of dolomite grain surface after 72 h of batch reaction using PW type III (Cd): A) SEM shows a high Fe dolomite grain, B) Zoom-in of A showing a cluster-shaped phase of Fe (light color), C) EDS mapping of B showing Cd sorption on dolomite.	90
3.14. SEM-EDS mapping of dolomite grain surface after 72 h of batch reaction using PW type III (Cd): A) a SEM micrograph showing toxic metals carbonate phase at the edges of the dolomite grain, B) X-ray spectrum showing elemental composition of the bulk samples, C) EDS mapping, and D) EDS mapping layers for single metals.	90
3.15. SEM-EDS analysis of dolomite grain surface after 72 h of batch reaction using PW type IV (Pb): A SEM image showing NaCl grains (light gray) precipitated on the dolomite surface, B) Zoom-in of A showing nanoscale Pb precipitates of white color on dolomite grain/crystal edges, C) EDS mapping of B showing Pb precipitates on dolomite.	91

Figure	Page
3.16. SEM-EDS mapping of dolomite grain surface after 72 h of batch reaction using PW type IV (Pb): A) a SEM micrograph showing toxic metals carbonate phase at the edges of the dolomite grain, B) X-ray spectrum showing elemental composition of the bulk samples, C) EDS mapping, and D) EDS mapping layers for single metals.	91
3.17. SEM-EDS analysis of dolomite grain surface after 72 h of batch reaction using PW type V (As): A) SEM image showing a lot of debris, B) Zoom-in of A showing As precipitate of different in bright color on the dolomite crystal face, C) EDS mapping of B showing As as precipitates.....	92
3.18. SEM-EDS mapping of dolomite grain surface after 72 h of batch reaction using PW type V (As): A) a SEM micrograph showing toxic metals carbonate phase at the edges of the dolomite grain, B) X-ray spectrum showing elemental composition of the bulk samples, C) EDS mapping, and D) EDS mapping layers for single metals.	92
3.19. SEM-EDS mapping of dolomite grain surface after 72 h of batch reaction using PW type VI (Ba, Sr, Cd, Pb, and As): A) SEM micrograph showing toxic metals carbonate phase with oval shape in the center, B) X-ray spectrum showing the elemental composition of the bulk samples, C) EDS mapping, and D) EDS mapping layers for single metals. ...	93
3.20. SEM-EDS mapping of dolomite grain surface after 72 h of batch reaction using PW type VII (Ba, Sr, Cd, Pb, and As): A) SEM micrograph showing toxic metals carbonate phase at the edges of the dolomite grain, B) X-ray spectrum showing the elemental composition of the bulk samples, C) EDS mapping, and D) EDS mapping layers for single metals.	94
3.21. Semiquantitative analyses from high-resolution XRD (Fig. S9) conducted on the powdered dolomite samples collected from batch reaction experiments: A) Control sample, B) PW type I (Ba), C) PW type II (Sr), D) PW type III (Cd), E) PW type IV (Pb), F) PW type V (As), G) PW type VI (Ba, Sr, Cd, Pd, and As), and H) PW VII (Ba, Sr, Cd, Pd, and As).....	95
3.22. High-resolution XRD and semiquantitative analyses of the powdered dolomite samples collected from batch reaction experiments: A) Control sample, B) PW type I (Ba), C) PW type II (Sr), D) PW type III (Cd), E) PW type IV (Pb), F) PW type V (As), G) PW type VI (Ba, Sr, Cd, Pd, and As), and H) PW VII (Ba, Sr, Cd, Pd, and As).	101
3.23. Simulated pH variations and concentration profiles of selected toxic metals: (A-B) Accounting only for precipitation reactions, (C-D) Accounting for both sorption and precipitation reactions. PW composition corresponds to PW type VI (Table 3.3).....	106

Figure	Page
4.1. A) Thin section (scale bare = 200 μm) showing shape and size of dolomite crystals, B) XRD analysis showing that the employed dolomite (represented by D only on the 104-dolomite peak) is mainly composed of dolomite with minor quantities of quartz and calcite cement (represented by Q only on the 101-quartz peak, and C only on the 104-calcite peak which is very weak). Dolomite cations (e.g., Mg & Ca) ordering reflections are indicated by asterisks on 101, 015 and 021 dolomite peaks. C) SEM image showing the shape and size of dolomite crystals as well as porosity.....	122
4.2. Representative synthetic dolomite core and sampling of dolomite grains (inlet, center, and outlet)	127
4.3. Toxic metals removal from PW type I (added with CaCO_3) using a 16.9 cm dolomite core: A) pH and alkalinity profiles at the outlet of the dolomite core, and B) Toxic metals removal profiles at the outlet of the dolomite core.....	132
4.4. Toxic metals removal from PW type II (added with CaCO_3) using a 8.2 cm dolomite core: A) pH and alkalinity profiles at the outlet of the dolomite core, and B) Toxic metals removal profiles at the outlet of the dolomite core.....	135
4.5. Toxic metals removal from PW type III (not added with CaCO_3) using a 15.8 cm dolomite core: A) pH and alkalinity profiles at the outlet of the dolomite core, and B) Toxic metals removal profiles at the outlet of the dolomite core.....	136
4.6. Toxic metals removal from PW type IV (added with CaCO_3) using a 8.1 cm dolomite core: A) pH and alkalinity profiles at the outlet of the dolomite core, and B) Toxic metals removal profiles at the outlet of the dolomite core.....	137
4.7. Toxic metals removal from FW type I (not added with CaCO_3) using a 16.3 cm dolomite core: A) pH and alkalinity profiles at the outlet of the dolomite core, and B) Toxic metals removal profiles at the outlet of the dolomite core.....	138
4.8. Toxic metals removal from FW type I (not added with CaCO_3) using a 15.8 cm dolomite core: A) pH and alkalinity profiles at the outlet of the dolomite core, and B) Toxic metals removal profiles at the outlet of the dolomite core.....	139
4.9. SEM images of toxic metals precipitates (bright white) on dolomite surface: A) Control sample, B) Flooded with FW type II (inlet side of the core), and C) Flooded with PW type II (inlet side of the core).....	140
4.10. SEM images of toxic metals precipitates (bright white) on dolomite surface with PW type I (added with CaCO_3): A) Inlet of the dolomite core, B) Zoom-in of A, C) Center of the dolomite core, D) zoom-in of C, E) Outlet of the dolomite core showing huge bright patches of precipitates, and F) zoom-in of E showing precipitates of different size and shapes.....	142

Figure	Page
4.11. Shows SEM micrographs of dolomite surface form column used for filtering PW type II (added with CaCO ₃). Fig. 10 is also showing toxic metals precipitates: A) bottom of the filter, B) Zoom-in of A showing precipitates with cavities, C) center of the filter, D) zoom-in of C, E) top of the filter, and F) zoom-in of E showing precipitates with different shapes.	143
4.12. SEM images of toxic metals precipitates (bright white) on dolomite surface with FW type I, which was added with CaCO ₃ : A) Inlet of the dolomite core, B) Zoom-in of A showing precipitates of different shapes and sizes, C) Center of the dolomite core showing hexagonal-shaped precipitates, D) zoom-in of C, E) Outlet of the dolomite core showing huge bright patches of precipitates, and F) zoom-in of E showing precipitates with irregular shapes.	144
4.13. SEM images of toxic metals precipitates (bright white) on dolomite surface with FW type II (not added with CaCO ₃ to increase alkalinity): A) Inlet of the dolomite core showing precipitates on highly dissolved dolomite surface, B) Zoom-in of A showing precipitates of different shapes and sizes, C) Center of the dolomite core showing precipitates around pore throat, D) zoom-in of C, E) Outlet of the dolomite core, and F) zoom-in of E showing precipitates.	145
4.14. SEM-EDS mapping of toxic metals on dolomite surface with PW type I at the inlet of the dolomite core: A) SEM micrograph showing carbonate precipitates of oval shapes, B) EDS spectrum showing the elemental composition of the bulk dolomite sample, C) EDS mapping of metals, and D) EDS mapping layers of individual metals.	147
4.15. SEM-EDS mapping of toxic metals on dolomite surface with PW type II (added with CaCO ₃ to increase alkalinity) at the inlet of the dolomite core: A) SEM micrograph showing carbonate precipitates of circular shapes on cavities of oval shapes, B) EDS spectrum showing the elemental composition of the bulk dolomite sample, C) EDS mapping of metals, and D) EDS mapping layers of individual metals.	147
4.16. SEM-EDS mapping of toxic metals on dolomite surface with PW type IV (not added with CaCO ₃) at the inlet of the dolomite core: A) SEM micrograph showing carbonate precipitates, B) EDS spectrum showing the elemental composition of the bulk dolomite sample, C) EDS mapping of metals, and D) EDS mapping layers of individual metals.	148
4.17. SEM-EDS mapping of toxic metals on dolomite surface with FW type I (added with CaCO ₃) at the outlet of the dolomite core: A) SEM image showing carbonate precipitates of circular shape and cavities, B) EDS spectrum showing the elemental composition of the bulk dolomite sample, C) EDS mapping of metals, and D) EDS mapping layers of individual metals.	149

Figure	Page
4.18. SEM-EDS mapping of toxic metals on dolomite surface with FW type II (not added with CaCO ₃) at the inlet of the dolomite core: A) SEM image showing carbonate precipitates of different shape and size, B) EDS spectrum showing the elemental composition of the bulk dolomite sample, C) EDS mapping of metals, and D) EDS mapping layers of individual metals.	149
4.19. SEM-EDS mapping of the dolomite surface from the top of the filter after core flooding using FW type II (not added with CaCO ₃): A) SEM micrograph showing toxic metals carbonate phase with different shapes, B) EDS spectrum showing the elemental composition of the bulk samples, C) EDS mapping, and D) EDS mapping layers for individual elements.	150
4.20. Semiquantitative analyses from high-resolution XRD (Fig. 4.21) conducted on the powdered dolomite samples collected from dolomite core flooded with PW type I: A) Control sample, B) Inlet, C) Center, and D) Outlet.	152
4.21. Semiquantitative analyses from high-resolution XRD conducted on the powdered dolomite samples collected from filter that filtered PW type I: A) Control sample, B) Inlet sample, C) Center sample, and D) Outlet sample.....	155
4.22. Semiquantitative analyses from high-resolution XRD (Fig. 4.24) conducted on the powdered dolomite samples collected from dolomite core injected with FW type II: A) Control sample, B) Inlet sample, C) Center sample, and D) Outlet sample.	156
4.24 Semiquantitative analyses from high-resolution XRD conducted on the powdered dolomite samples collected from filter that filtered FW type II: A) Control sample, B) Inlet sample, C) Center sample, and D) Outlet sample.....	159

CHAPTER I

INTRODUCTION

1.1. Motivation

Produced water (PW) is the wastewater generated from conventional and unconventional oil and gas production. Since most of the world's oil and gas are being depleted, water to oil or gas ratio has been significantly increasing resulting in huge quantities of PW that needs to be managed to prevent environmental pollution. PW is characterized by high concentrations of total dissolved solids (TDS). According to Bureau of Reclamation the TDS in PW ranges from 100 mg/L to over 400,000 mg/L. TDS includes mostly NaCl followed by a broad suite of metals and metalloids (e.g., Ca, Mg, Ba, Sr, As, Se, Pb, and Cd), and naturally occurring radioactive materials (NORM) (Guerra et al., 2011c).

To reinforce the freshwater resources, PW was proposed to be integrated into industrial and agricultural uses. However, to accomplish this process successfully, PW needs to be treated not only for salinity (NaCl) but also for high concentrations of toxic metals and metalloids. The main barrier hindering the utilization of conventional wastewater treatment technologies to treat PW for high concentrations of toxic metals and metalloids is cost.

Most conventional wastewater treatment technologies are not economically feasible technologies to remove high concentrations of coexisting toxic metals and metalloids from PW. Therefore, and based on previous experimental and computational results showing high removal levels of heavy metals using powdered dolomite as sorption and filtration material, the goal of this research is to understand the removal mechanism and controlling variables of selected individual and coexisting toxic heavy metals, metalloids, and alkaline earth metals by dolomite over a range of salinity, pH, and PW composition conditions to enable the development of dolomite filtration for treating PW.

All dolomite samples used in this research project were collected from the Arbuckle Group in Oklahoma and southwest Missouri. Unlike other carbonate mineral, dolomite has a very complex structure and chemistry with chemical composition of $\text{CaMg}(\text{CO}_3)_2$ (Tucker and Wright, 2009). The origin and formation of dolomite in geological strata is still unclear, commonly referred to as ‘dolomite problem’ by the scientific community.

The focus of this dissertation is on toxic alkaline earth metals (Ba and Sr), heavy metals (Pb and Cd), and metalloids (As). These contaminants are commonly found in PW and their concentrations can be in the order of hundreds of mg/L. For the purpose of this dissertation, they will be referred to as toxic metals. The underlying hypotheses of this research are outlined below:

Hypothesis 1 – The use of filters made of powdered dolomite can result in the near complete removal of high concentrations of coexisting toxic metals from PW.

Hypothesis 2 – The uptake of toxic metals by dolomite at ionic strengths of PW is controlled by the competition of cations for hydration sites of dolomite, the surface morphology of dolomite, and the precipitation/co-precipitation of toxic metals.

Hypothesis 3 – The uptake of toxic metals by dolomite at ionic strengths of PW can be represented by surface complexation, equilibrium, and kinetic model equations.

These hypotheses were tested in three stages with the following specific aims:

Specific Aim 1: To assess the potentiality of mixture toxic metals removal by dolomite filtration.

Specific Aim 2: To experimentally determine the physical and chemical factors controlling the removal of mixture toxic metals from PW by dolomite filtration.

Specific Aim 3: To determine the effect of changes in the mineral phase (surface morphology and composition) on the uptake of mixture metals by dolomite.

The above research hypotheses were tested by using experimental and computational work. Experimental work included batch reaction and core-flooding experiments, whereas the changes in the aqueous and mineral phases were analyzed by ICP-OES, XRD, SEM, and SEM-EDS analytical methods. The computational work involved the development of a sorption complexation model for the mixture toxic metals and the formulation of a 3D reactive transport model implemented using CrunchFlow and TOUGHREACT geochemical reactive transport programs.

1.2. Significance

Heavy metals are elements possessing large atomic weights and density with a specific gravity greater than 5.0 (Fu and Wang, 2011; Srivastava and Majumder, 2008). They are not biodegradable and tend to accumulate in living organisms. Accumulation of

heavy metals in humans is known to cause toxic effects and cancer (Fu and Wang, 2011). For instance, lead (Pb) is characterized by toxic effects on the hematopoietic, renal, reproductive, and central nervous system due to its ability to interfere with cellular processes and enzyme systems (Flora et al., 2012). Arsenic (As) is a human carcinogen that can cause skin and bladder cancers, as well as keratosis, hypertension, and cardiovascular diseases even at low levels (Jensen, 2020; Koutros et al., 2018; Ng et al., 2003; Smith et al., 2002). Long term exposure of cadmium (Cd) results in kidney dysfunction and high levels of exposure will result in death. Some alkaline earth metals such as strontium (Sr) and barium (Ba) are also toxic when ingested in high amount (Gutiérrez-Ravelo et al., 2020b). According to the World Health Organization (WHO), high Sr intakes can cause phosphorus deficiency and an increase in bone density (Watts and Howe, 2010). Moreover, Scientific Committee on Health and Environmental Risk (SCHER) showed that chronic exposure to high Ba can cause tachycardia (i.e., heart diseases), hypertension, hypotension, muscle weakness and paralysis (SCHER, 2012).

Oklahoma ranks third in natural gas production and fourth in crude oil production in the U.S. and production continues to rise in Oklahoma. With new technologies making oil and natural gas production more efficient, and considering that U.S. shale gas production continues to increase, with the estimation to be 19.8 tcf in 2040 (Engle et al., 2014), the need to establish cost effective methods to remove not only salinity (NaCl) but also toxic metals from PW, for its reutilization in oil and natural gas operations and/or for its integration into industrial uses, will continue to rise.

Concentration and type of metals in PW varies substantially depending on the geographical location, the geochemistry of the producing formation, the type of

hydrocarbon produced, the characteristics of the producing well, and the extracting technique (Guerra et al., 2011c; Jiménez et al., 2018). Igunnu and Chen (Igunnu and Chen, 2014) classified PW based on its origin into oilfield PW, natural gas PW and coal bed methane (CBM) PW. Most common toxic metals in PW from Oklahoma oil wells are Ca, Mg, Ba, Sr, As, and Cd (Collins, 1969). For instance, concentrations of some these metals in 72 brine samples from Mississippian and Pennsylvanian age sediments are 0-600 mg-Ba/L and 0-3,400 mg-Sr/L. The type of metals found in PW are different from typical metals (e.g., Pb, Cu, Zn, Cd, Hg, and Ni) found in seawater, shallow aquifers, and conventional wastewater. Moreover, while the concentration of metals in PW is in the order of mg/L, typical concentration of metals in seawater, shallow aquifers, and conventional wastewater is in the order of $\mu\text{g/L}$. Concentrations of toxic metal and metalloids in PW greatly exceed the maximum contaminant levels established by U.S. Environmental Protection Agency (EPA) for drinking water (Yost et al., 2016). As such, technologies developed to remove trace concentrations ($\mu\text{g/L}$) of metals from low salinity waters are seriously challenged by the different composition and high salinity of PW.

Conventional technologies that could be used to remove toxic metals from PW include membrane filtration, chemical precipitation, sorption, ion exchange, electrochemical deposition, electrodialysis, and biosorption (Fu and Wang, 2011). However, high concentrations of TDS (mostly NaCl, Ca, and Mg) in PW, limits the application of conventional technologies to remove toxic metals from PW. For instance, NaCl, Ca, and Mg cause severe fouling of membrane materials as well as inhibition of sorption, ion exchange, and precipitation reactions (Hakami et al., 2013a). Membrane filters which are widely employed to remove TDS including metals from seawater, shallow

aquifers, and conventional wastewater, undergo fast fouling due to scale formation and internal blockage of pores by biomass (oil hydrocarbons and microbes) existing in PW.

This new dolomite filtration technology to remove high concentrations of toxic metals (i.e., heavy metals, alkaline earth metals, metalloids, and possible NORM) from PW will replace and/or reduce the cost of using membrane filtration technologies. Dolomite filtration consists of filters made of compressed powdered dolomite. Here, dolomite works as an adsorption medium for metals and polymer molecules trapped in small pore throats function as a secondary filtration medium for metals. The remaining trace concentrations of metals (if any) can be removed, for instance, by conventional membrane and activated carbon filtration technologies. Likewise, salinity (NaCl) can be reduced using conventional seawater desalination technology such as mechanical vapor compression, membrane distillation, and forward osmosis (Shaffer et al., 2013) in subsequent treatment stages.

The positive outlook on this treatment method of PW is on the following scientific and practical considerations: 1) dolomites represent a superior sorption capacity for heavy metals than other natural sorption materials such as sandstone; 2) metals removal via sorption in dolomite filters presents flexibility in operation since the sorption capacity of the dolomite filter can be restored by back washing; 3) and dolomites are abundant in the Arbuckle Group of Oklahoma, Missouri, and Kansas where oil and natural gas activities are intensive. The focus is on Ba, Sr, As, and Cd because they constitute the most common metals present in PW from Oklahoma, USA (Kharaka et al., 2007b; Morton, 1986b; Zielinski and Budahn, 2007). However, Pb will be included in my experiment for comparison purposes. Guar gum is selected as a polymer due to its relatively low cost and common use as viscosifier additive of hydraulic fracturing fluids (Hanes et al., 2003a;

Rozell and Reaven, 2012a). In the proposed dolomite filtration method, it is hypothesized that guar gum occupying small pore throats of the dolomite filter can work as a secondary filtration media to increase the removal of metals from PW.

The new filtration method presented in this dissertation has many outcomes and applications. For instance, it will contribute to solving the environmental issues related to oil and gas industry through reducing the treatment cost of PW and making this water more beneficial to be reused and integrated for industrial and agricultural purposes. This will reduce the disposal of PW by injection into the deep saline aquifers and eventually prevent the induced seismicity events from happening. Likewise, the findings of this dissertation will serve to predict the mobility and transport of toxic metals in dolomite saline aquifers where PW is commonly disposed in Oklahoma. This will help evaluating and preventing the vulnerable underground drinking water from potential contamination by possible PW upward migration. In addition to facility scale, this dolomite filtration method can be applied at regional scale by using subsurface dolomite units among geological strata (e.g., Arbuckle dolomite) as mega filters. Finally, dolomite filtration can be applied for PW mining (e.g., Li and Co) as well as CO₂ sequestration.

1.3. Intellectual merit

In general, interactions between filtration materials and solutes can be categorized into physical and chemical interactions. Physical removal of solutes involves the physical trapping of the solute by the filter material due to a difference in size between the pore throat and solute, whereas chemical removal of solutes from solvents generally involves

sorption, ion exchange, and/or precipitation reactions. Given the small size of dissolved metals, removal of metals by dolomite filtration relies on the chemical interactions between metals and the surface of dolomite. These interactions are functions of the surface chemistry (e.g., type and concentration of hydration sites) and the crystal surface morphology (e.g., faces and edges) of dolomite, the chemical properties of dissolved metals (e.g., charge, radii, and coordination numbers), and changes in the composition of PW.

The reactivity of dolomite in aqueous solutions has been extensively studied in the past (Pokrovsky et al., 2000a; Pokrovsky and Schott, 2002; Pokrovsky et al., 1999b; Van Cappellen et al., 1993). Those studies included surface speciation studies not only for dolomite but also for calcite and magnesite carbonate minerals, metal sorption on dolomite, modeling of surface complexation reactions on dolomite, and dissolution/precipitation of dolomite. From those studies, it is generally accepted that dolomite has three primary hydration sites ($>CaOH^0$, $>MgOH^0$, and $>CO_3H^0$) that can form complex species with Ca^{2+} , Mg^{2+} , and H^+ , and other dissolved metals. The existence of these primary hydration sites is supported by spectroscopy data as well as by surface complexation models formulated to represent sorption of Ca, Mg, and the number of metals. However, this information was generated using low salinity (< 10 g-TDS/L) waters and ambient temperature conditions, and the analyzed metals were trace metals (< 1 mg/L) found in seawater, shallow aquifers, and conventional wastewaters (e.g., Co, Ni, Cu, Zn, As, and Pb) (Brown and Parks, 2001b).

The formation of surface complex species on dolomite at salinity levels of PW (100 - 300 g-TDS/L) for toxic metals (e.g., Ba, Sr, As, and Cd), found in PW at high concentrations (> 10 mg/L), is yet to be fully assessed. Of particular relevance is the

competition of not only divalent cations but also monovalent cations (Na), whose concentration is the highest in PW, and precipitation and co-precipitation of divalent cations at salinity levels of PW.

Therefore, in order to understand the mechanisms and controlling variables of the removal of metals by dolomite, batch reactions and core flooding experiments were used. In addition, to elucidate the precipitation and co-precipitation of cations on the dolomite surface, XRD and SEM-EDS were analysis. Geochemical sorption and 3D reactive transport models were developed for representing the removal of toxic metals by dolomite filtration.

Several other experimental/spectroscopy and modeling studies have been conducted on the sorption of trace elements on mineral surfaces in the marine environment (Brown and Parks, 2001b). Although those studies account for the effect of sea salinity levels, most studies aimed to understand the partition of metals between aqueous solutions and metal-(oxyhydro)oxides (metal oxides, metal oxyhydroxides, and metal hydroxides) commonly found in feldspar and clay minerals (Brown and Parks, 2001b). From those studies it is known that, for instance, the affinity of transition metals for metal-(oxyhydro)oxides is $\text{Cu} \approx \text{Pb} > \text{Zn} > \text{Co} > \text{Ni} > \text{Cd}$, and the affinity of alkaline earth metals for metal-(oxyhydro)oxides is $\text{Mg} > \text{Ca} > \text{Sr} > \text{Ba}$, which correlates with their first hydrolysis constants and ionic radius values. However, this is not always the case, depending on their reactivity, crystal structure, and/or morphology of the sorption material which determines the density of surface hydration/binding sites that came into play.

This research will bridge the knowledge gap regarding the affinity of metals found in PW for dolomite at background electrolyte concentrations of PW. Interestingly, despite

the common occurrence of carbonate minerals, literature is more overwhelmed by metal-(oxyhydro)oxides more than by carbonate minerals when it comes to metal sorption. Consequently, most surface complexation models (SCM) have been formulated to represent the sorption of metals on metal-(oxyhydro)oxides minerals (Brown and Parks, 2001b). These models (SCM) account for the electrochemical properties of the mineral and electrolyte phases and thus account for the electrostatic interactions occurring within single, double, and triple layers of water molecules covering the mineral surface. Although SCMs have been successfully formulated to represent the sorption of metals on dolomite, the applicability of these models is limited to low salinity waters and/or metals commonly found in seawater, shallow aquifers and conventional wastewater, which are different from those found in PW.

Given that dolomite filters can be made of specific surface area and porosity/permeability properties, to enable the development of dolomite filtration technology for treating PW, the goal of this research is twofold; first is to understand the mechanisms and controlling factors of the removal of metals by dolomite over a range of salinity, pH, and PW composition conditions; and second is to elucidate the impact of the operational variables of dolomite filters (grain size/surface area, injection flow rate) on the removal of metals.

This dissertation presents the first effort to understand the mechanisms and controlling variables of mixture toxic metals removal by dolomite at salinity and alkalinity levels of PW, the behavior and fate of toxic metals in the porous medias, and to determine the potentiality of using dolomite filtration to remove coexisting toxic metals from high salinity waters.

1.4. Organization of the Dissertation

This research consists of five chapters and the main results and discussion of this dissertation are presented in chapters 2, 3, and 4 which have already been published at or submitted to peer-reviewed journals. In the following, I briefly explained the subject of each chapter and highlight the main problems that are addressed:

Chapter 1 addresses the dissertation general introduction including motivation, significance, and intellectual merit of the dissertation.

Chapter 2 exhibits the results of core flooding experiments that were conducted to elucidate the physical and chemical controlling factors of removal of toxic metal and metalloid by dolomite from PW. These physical factors are illustrated by using different injection flow rates of synthetic PW into dolomite filters made from powdered dolomite from different homogenized grain size ranges. However, the chemical controlling factors were tested by applying synthetic PW with different salinity, pH, and guar gum content conditions. The experimental results were captured and represented via developed 3D transport reactive modeling and simulations.

Chapter 3 illustrates the experimental results from batch sorption reactions which were conducted to elucidate the effects of dolomite reactivity and alkalinity on removal of individual as well as coexisting toxic metal by dolomite. These experimental results were validated by matching them with results obtained from XRD and SEM-EDS analysis. The findings are also illustrated via geochemical models that accounted for precipitation-coprecipitation then for both sorption and precipitation-coprecipitation reactions of toxic metals on the dolomite surface.

Chapter 4 presents the experimental results obtained from conducting core flooding experiments to predict and evaluate the fate and co-transport of toxic metals through carbonate porous media. This was tested by preparing synthetic PW and freshwater (FW) then injected into the dolomite column made of compacted dolomite powder. The obtained experimental results were confirmed by conducting XRD and SEM-EDS analyses.

Chapter 5 condenses the dissertation main conclusions, presents the future work, and provides recommendations.

1.5. List of Publications

1.5.1. Published at or Submitted to Peer Reviewed Journals

1. **Omar, K.** and Vilcáez, J., 2023. Effect of carbonate minerals precipitation and sorption reactions on the transport of toxic metals in dolomite (submitted to Science of the Total Environment in April 2023).

2. **Omar, K.** and Vilcáez, J., 2023. Role of alkalinity and dolomite reactivity on toxic metals removal from petroleum produced water by dolomite. Science of the Total Environment (Peer reviewing).

3. **Omar, K.** and Vilcáez, J., 2022. Removal of toxic metals from petroleum produced water by dolomite filtration. Journal of Water Process Engineering, 47, p.102682.

<https://doi.org/10.1016/j.jwpe.2022.102682>

1.5.2. Conference Proceedings and Abstracts

1. **Omar, K.** and Vilcáez, J., 2023. Dolomite filtration: A new method for removing toxic metals from petroleum produced water. The Geological Society of America, South-Central Section Meeting, Stillwater, OK.
2. **Omar, K.** and Vilcáez, J., 2022. Removal of toxic metals from petroleum produced water by dolomite filtration. The American Geophysical Union Fall Meeting, Chicago, IL
3. **Omar, K.** and Vilcáez, J., 2022. Removal of toxic metals from petroleum produced water by dolomite filtration. Oklahoma Geological Survey Fall Meeting, Oklahoma City, OK
4. **Omar, K.** and Vilcáez, J., 2022. Removal of toxic metals from petroleum produced water by dolomite filtration. Association of Environmental & Engineering Geologists 65th Annual Meeting, Las Vegas, NV
5. **Omar, K.** and Vilcáez, J., 2022. Removal of toxic metals from petroleum produced water by dolomite filtration. The Geological Society of America South-Central Meeting, Petroleum-Produced Water Section. McAllen, TX.
6. **Omar, K.** and Vilcáez, J., 2022. Removal of mixture heavy metals and metalloids from petroleum produced water by dolomite filtration. TechFest Annual Meeting, Oklahoma State University, Stillwater, OK.
7. **Omar, K.** and Vilcáez, J., 2021. Removal of mixture heavy metals and metalloids from petroleum produced water by dolomite filtration. The American Association of Petroleum Geologists, Mid-Continent Section Convention, Tulsa, OK
8. **Omar, K.** and Vilcáez, J., 2021. A new dolomite filtration method for removal of heavy metals and metalloids from petroleum produced water. The American Geophysical Union Fall Meeting, San Francisco, CA.

9. **Omar, K.** and Vilcáez, J., 2021. A new dolomite filtration method for removal of heavy metals and metalloids from petroleum produced water. The Society of Explorational Geophysicists Annual Meeting, Houston, TX.

1.6. References

- Brown, J. G. E., and Parks, G. A., 2001, Sorption of trace elements on mineral surfaces: Modern perspectives from spectroscopic studies, and comments on sorption in the marine environment.: *International Geology Review*, , v. 43(11), pp.963-1073.
- Collins, A. G., 1969, Chemistry of some Anadarko basin brines containing high concentrations of iodide: *Chemical Geology*, v. 4, no. 1-2, p. 169-187.
- Engle, M. A., Cozzarelli, I. M., and Smith, B. D., 2014, USGS investigations of water produced during hydrocarbon reservoir development, US Department of the Interior, US Geological Survey.
- Fu, F., and Wang, Q., 2011, Removal of heavy metal ions from wastewaters: a review: *Journal of environmental management*, v. 92, no. 3, p. 407-418.
- Guerra, K., Dahm, K., and Dunderf, S., 2011, Oil And Gas Produced Water Management And Beneficial Use in the Western United States,: US Department of the Interior,, p. p. 157.
- Gutiérrez-Ravelo, A., Gutiérrez, Á. J., Paz, S., Carrascosa-Iruzubieta, C., González-Weller, D., Caballero, J. M., Revert, C., Rubio, C., and Hardisson, A., 2020, Toxic metals (Al, cd, pb) and trace element (b, ba, co, cu, cr, fe, li, mn, mo, ni, sr, v, zn) levels in sarpa salpa from the north-eastern atlantic ocean region: *International Journal of Environmental Research and Public Health*, v. 17, no. 19, p. 7212.

- Hakami, M., Tizaoui, C., Kochkodan, V., and Hilal, N., 2013, Effect of hydrodynamic operations, salinity, and heavy metals on ha removal by microfiltration ceramic tubular membrane: *Separation Science and Technology*, v. 48, no. 4, p. 564-570.
- Hanes, R., Parker, M., Slabaugh, B., Weaver, J., and Walters, H., Analytical methods for maintaining quality assurance of recycled fracturing fluids, *in Proceedings International Symposium on Oilfield Chemistry*2003, OnePetro.
- Igunnu, E. T., and Chen, G. Z., 2014, Produced water treatment technologies: *International journal of low-carbon technologies*, v. 9, no. 3, p. 157-177.
- Jensen, J., 2020, The Role of Carbonate Minerals in Arsenic Mobility in a Shallow Aquifer Influenced by a Seasonally Fluctuating Groundwater Table (Masters thesis, Utah State University).
- Jiménez, S., Micó, M., Arnaldos, M., Medina, F., and Contreras, S., 2018, State of the art of produced water treatment: *Chemosphere*, v. 192, p. 186-208.
- Kharaka, Y. K., Kakouros, E., Thordsen, J. J., Ambats, G., and Abbott, M. M., 2007, Fate and groundwater impacts of produced water releases at OSPER “B” site, Osage County, Oklahoma: *Applied geochemistry*, v. 22, no. 10, p. 2164-2176.
- Morton, R. B., 1986, Effects of brine on the chemical quality of water in parts of Creek, Lincoln, Okfuskee, Payne, Pottawatomie, and Seminole Counties, Oklahoma, University of Oklahoma.
- Pokrovsky, O., Mielczarski, J., Barres, O., and Schott, J., 2000, Surface speciation models of calcite and dolomite/aqueous solution interfaces and their spectroscopic evaluation: *Langmuir*, v. 16, no. 6, p. 2677-2688.

- Pokrovsky, O., and Schott, J., 2002, Surface chemistry and dissolution kinetics of divalent metal carbonates: *Environmental science & technology*, v. 36, no. 3, p. 426-432.
- Pokrovsky, O. S., Schott, J., and Thomas, F., 1999, Dolomite surface speciation and reactivity in aquatic systems: *Geochimica et Cosmochimica Acta*, v. 63, no. 19-20, p. 3133-3143.
- Rozell, D. J., and Reaven, S. J., 2012, Water pollution risk associated with natural gas extraction from the Marcellus Shale: *Risk Analysis: An International Journal*, v. 32, no. 8, p. 1382-1393.
- Shaffer, D. L., Arias Chavez, L. H., Ben-Sasson, M., Romero-Vargas Castrillón, S., Yip, N. Y., and Elimelech, M., 2013, Desalination and Reuse of High-Salinity Shale Gas Produced Water: Drivers, Technologies, and Future Directions: *Environmental Science & Technology*, v. 47, no. 17, p. 9569-9583.
- Srivastava, N. K., and Majumder, C. B., 2008, Novel biofiltration methods for the treatment of heavy metals from industrial wastewater: *Journal of Hazardous Materials*, v. 151, no. 1, p. 1-8.
- Tucker, M. E., and Wright, V. P., 2009, *Carbonate Sedimentology*, Wiley.
- Van Cappellen, P., Charlet, L., Stumm, W., and Wersin, P., 1993, A surface complexation model of the carbonate mineral-aqueous solution interface: *Geochimica et Cosmochimica Acta*, v. 57, no. 15, p. 3505-3518.
- Watts, P., and Howe, P., 2010, Strontium and strontium compounds, *World Health Organization*, v. 77.
- Yost, E. E., Stanek, J., DeWoskin, R. S., and Burgoon, L. D., 2016, Overview of Chronic Oral Toxicity Values for Chemicals Present in Hydraulic Fracturing Fluids,

Flowback, and Produced Waters: Environmental Science & Technology, v. 50, no. 9, p. 4788-4797.

Zielinski, R. A., and Budahn, J. R., 2007, Mode of occurrence and environmental mobility of oil-field radioactive material at US Geological Survey research site B, Osage-Skiatook Project, northeastern Oklahoma: Applied Geochemistry, v. 22, no. 10, p. 2125-2137.

Scientific Committee on Health and Environmental Risk, 2012. Assessment of the tolerable daily intake of barium.

Groundwater Protection Council, 2015. Produced Water Reuse in Oklahoma: Regulatory Considerations and References.

CHAPTER II

REMOVAL OF TOXIC METALS FROM PETROLEUM PRODUCED WATER BY DOLOMITE FILTRATION

2.1. Abstract

We conducted experiments and reactive transport simulations to assess the removal of high concentrations of toxic metals (100 mg/L) commonly found in produced water from high saline waters (45,000 – 115,000 mg/L) using dolomite filters made of compressed powdered dolomite. The focus was on Ba, Sr, Cd, Pb, and As, as well as on guar gum as a metal complexing additive. We found that salinity has a significant impact on the removal of Sr and Ba but a mild impact on the removal of Cd. An increase of pH due the dissolution of dolomite increases the removal of Cd more significantly than the removal of Ba and Sr. The formation of guar-gum complexes of metals in the aqueous phase attenuates the removal of Sr, Ba, and Cd by dolomite filtration. This attenuation process is more significant for Cd than for Sr and Ba. The affinity sequence for the sorption of toxic metals at salinity levels of PW is $Pb > Cd > As > Ba > Sr$. Higher removal levels predicted for Sr than for Ba and over predictions of Cd removal using previously proposed surface complexation models for dolomite highlights the necessity of further experimental research to incorporate molecular scale surface crystal structure parameters into surface complexation models

2.2. Introduction

Produced water (PW) from conventional and unconventional oil and gas reservoirs contains high concentrations of dissolved salts, mostly NaCl, CaCO₃, MgCO₃, and organic and inorganic contaminants. Heavy metals, alkaline earth metals, metalloids, and naturally occurring radioactive materials (NORM) constitute the most abundant inorganic contaminants in PW (Guerra et al., 2011b). Their concentrations greatly exceed the maximum contaminant levels established by the USA environmental protection agency (EPA) for drinking water (Yost et al., 2016).

To prevent contamination of surface and underground sources of drinking water (USDW), PW is frequently disposed by injection into deep saline aquifers (Lutz et al., 2013). The depth of disposal wells ranges between few hundreds to thousands of meters depending on the geology of the play. For instance, since the discovery of oil and gas in Oklahoma, USA, huge volumes of PW have been injected into dolomite saline aquifers of the Arbuckle Group. According to Clark and Veil (2009), in 2007 the total volume of PW in Oklahoma was ~2.2 Bbbl and the total volume of PW in U.S. was ~20 Bbbl/year, which ranked Oklahoma fifth in the U.S. in PW. However, according to a more recent study conducted in 2020 (Scanlon et al., 2020), Oklahoma might rank first in PW in the U.S. The medium depth of PW injection into the Arbuckle Group is 2,088 m, and the volumes of PW injection has substantially increased between 2009 and 2014 from 434 MMbbl to more than 1,046 MMbbl (Murray, 2014). PW injection into deep geological formations synchronized with increasing seismic events in Oklahoma. Consequently, public concerns have grown regarding the possibility of USDW contamination by contaminants present in PW. Mechanical failures of the injection well and naturally or induced basement fractures

can facilitate the upward migration of contaminants present in PW to USDW. Previous studies on the transport of toxic metals present in PW aimed to elucidate the chemical and physical factors controlling the transport of Ba in dolomite saline aquifers (Ebrahimi and Vilcáez, 2018a, b, 2019a). In light of those studies showing that dolomite has a superior sorption capacity for Ba than other natural rock materials (e.g., sandstone), and given the observed retarding effect of guar gum on the transport of Ba through dolomite cores, the goal of this study is twofold: first is to fill the knowledge gap regarding the chemical and physical factors controlling the removal of mixture toxic metals by dolomite, and second is to assess the feasibility of removing high concentrations of mixture toxic metals from PW by using dolomite filters made of compressed powdered dolomite and guar gum as metal complexing agent.

Previous studies on the removal of metals by dolomite focused on the removal of trace concentrations of single metals from low salinity waters (Ghaemi et al., 2011; Gruszecka-Kosowska et al., 2017; Mohammadi et al., 2015). The focus of this study is on alkaline earth metals (Ba and Sr), and a heavy metal (Cd) whose concentrations in PW can be in the order of hundreds of mg/L. Ba, Sr, and Cd are commonly found in PW from Oklahoma, USA (Kharaka et al., 2007a; Morton, 1986a; Zielinski and Budahn, 2007) and pose a risk to human health and the environment. Long time exposure of Cd results in kidney dysfunction, and high levels of exposure will result in death. Sr and Ba are also toxic when ingested in high amount (Gutiérrez-Ravelo et al., 2020a). According to the world health organization (WHO), high Sr intakes can cause phosphorus deficiency and an increase in bone density (Watts et al., 2010), and the scientific committee on health and

environmental risk (SCHER) showed that chronic exposure to high Ba can cause tachycardia, hypertension, muscle weakness and paralysis.

In the proposed dolomite filtration method, guar gum trapped in small pore throats of the dolomite filter is expected to work as a secondary filtration media to increase the removal of mixture toxic metals from PW. Other methods to improve the removal of toxic metals by dolomite include thermal activation of dolomite (Ivanets et al., 2014) and the use of phosphatized dolomite (Ivanets et al., 2016). Compared to those methods, guar gum is an inexpensive polymer commonly used as a viscosifying additive of hydraulic fracturing fluids (Hanes et al., 2003b; Rozell and Reaven, 2012b). The positive outlook on this treatment method of PW is on the following scientific and practical considerations: 1) dolomite represent a superior sorption capacity for toxic metals than other natural rock materials such as sandstone, 2) removal of toxic metals via sorption in dolomite filters presents flexibility in operation since the sorption capacity of the dolomite filter can be restored by back washing the filter, and 3) dolomite are abundant in the Arbuckle Group of Oklahoma and Kansas where oil and natural gas activities are intensive. Conventional technologies that could be used to remove toxic metals from PW include chemical precipitation, sorption, ion exchange, electrochemical deposition, electrodialysis, and biosorption (Fu and Wang, 2011). However, cost limits the application of these technologies to remove toxic metals from PW since the high salinity of PW cause severe fouling problems, as well as inhibition of sorption, ion exchange, and precipitation reactions (Hakami et al., 2013b). The implementation of this new economic technology could reduce the cost of using conventional technologies, enabling the integration of PW into industrial and agricultural uses. In a previous study we showed a removal level of 1.25

mg-Ba/g-dolomite (Vilcáez, 2020). This removal level of Ba is comparable to removal levels attained with pecan shell based activated carbon (PBAC) (1.85 mg-Ba/g-PBAC) (Kaveeshwar et al., 2018), and MXene (nanosheet material) (9.3 mg-Ba/g-MXene) (Fard et al., 2017), which are expensive to prepare and/or synthesize.

Sorption of metals occurs along with dissolution/precipitation reactions that are a function of many chemical (e.g., pH, ionic strength, surface chemistry and composition) and physical (e.g., injection flow rate, grain size/surface area) factors. Therefore, our approach to elucidate the chemical and physical factors controlling the removal of mixture toxic metals from water at salinity levels of PW, consists of core-flooding experiments to assess the effect of individual chemical and physical factors, and reactive transport modeling and simulations to assess the effect of combined chemical and physical factors.

2.3. Materials and methods

2.3.1. Dolomite samples

Dolomite samples were collected from a road-cuts in south-west Missouri, the site is an extension of the Arbuckle Group where oil and gas production is prominent (Gadhamshetty et al., 2015). X-ray and petrographic analyses showed that dolomite collected from this site is composed of 98% dolomite and 2% blocky calcite cement and amorphous silica (Fig. 2.1). The peaks in the XRD spectra represent the whole mineral composition of the rock sample. The XRD spectra display strong dolomite ordering reflections (101 ($22^{\circ}2\theta$), 015 ($35^{\circ}2\theta$), and 021 ($44^{\circ}2\theta$)) which distinguish dolomite-structure (JCPDS: 79-1342) from calcite-structure (JCPDS: 86-2334) minerals. Minor amounts of calcite is reflected by weak calcite ordering reflections (012 ($24^{\circ}2\theta$), and 104

($31^\circ 2\theta$) (Kaczmarek et al., 2017; Silva et al., 2020). Dolomite crystals vary between planar euhedral to subhedral, and non-planar layers with different crystal sizes ranging between 0.1 mm to 0.6 mm (Fig. 2.1). Scanning electron microscopy analysis shows that pore diameter is greater than 0.25 mm (image not shown), and the pores are poorly connected one another due to calcite cementation.

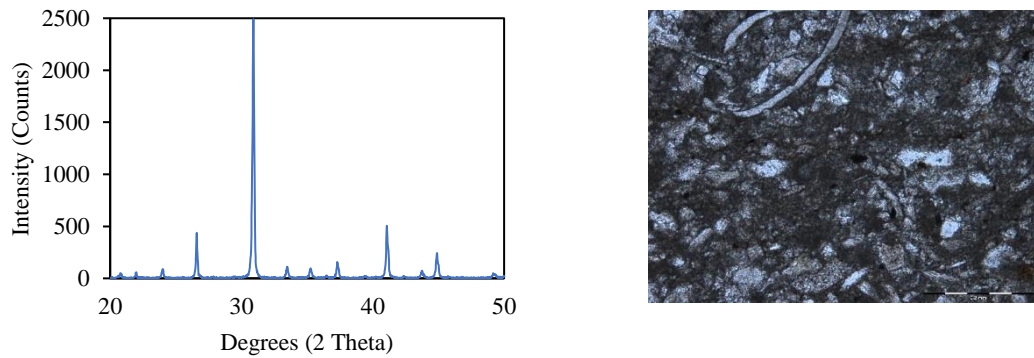


Fig. 2.1. Representative X-ray (left-hand side) and thin-section (right-hand side) analysis of Arbuckle dolomite samples of 98% purity collected from a road-cuts in south-west Missouri.

2.3.2. Dolomite filters

Collected dolomite samples from the Arbuckle Group were used to prepare dolomite filters (1.5-inch diameter and 6-inch length) of same grain size. Powdered dolomite of same grain size was obtained crushing, pulverizing, and sieving (Fig. 2.2). Prior to its utilization to prepare dolomite filters, to remove dust, the obtained powdered dolomite of same grain sizes (600-850 μm and 350-600 μm) was washed several times with deionized water in an ultrasonic bath and then dried by air at room temperature. The procedure to prepare the dolomite filters consisted of mixing 200 g of powdered dolomite of uniform grain size with 10 g of deionized water. The resulting aggregate was poured

into a stainless-steel cylindrical mold. Then, the aggregate was compressed at 4,320 psi for one hour using a uniaxial compaction apparatus (Carver Laboratory Presser (Model 4387)). To assess the effect of guar gum on the removal of mixture toxic metals, additional dolomite filters were prepared mixing 200 g of powdered dolomite with 0.5 g and 1.0 g of guar gum. Fig. 2 includes a picture of the prepared dolomite filter following the described procedure.

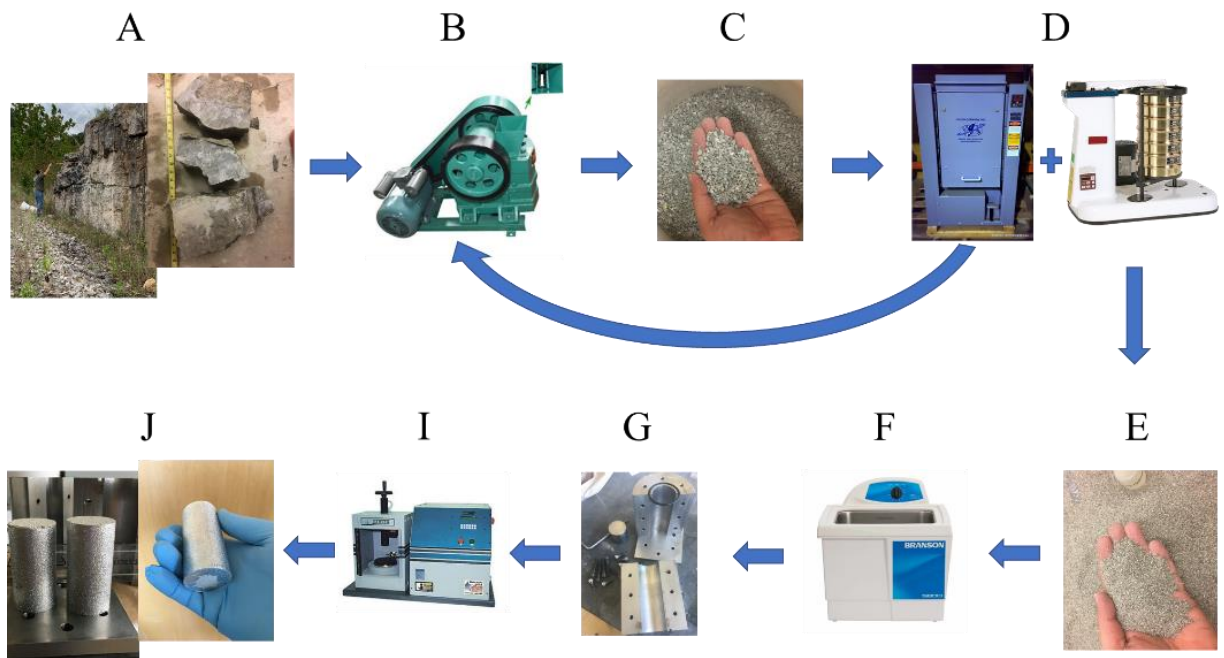


Fig. 2.2. Procedure to prepare dolomite filters: A) Arbuckle Group outcrop in the southwest Missouri, B) Jaw rock crusher, C) Crushed dolomite samples, D) Sieving shaker machine, E) Sieved dolomite powder, F) Ultrasonic bath, G) Cylindrical stainless-steel mold, I) Carver Laboratory Presser, and J) Dolomite filter wrapped with aluminum foil.

2.3.3. Synthetic produced water

Synthetic PW was employed to facilitate the analysis and interpretation of results regarding the chemical factors controlling the removal of mixture toxic metals from PW

by dolomite filtration. Synthetic PW was prepared by adding NaCl, CaCl₂·2H₂O, MgC₂·6H₂O, and two groups of metal salts to deionized water. Group 1 included SrC₂·6H₂O, BaC₂·2H₂O, and CdH₈N₂O₁₀. Group 2 included SrC₂·6H₂O, BaC₂·2H₂O, CdH₈N₂O₁₀, PbCl₂, and AsCl₃ (Fisher Scientific Co. with purity of >99.9%). This work focuses on PW where the concentration of bicarbonate and sulfate anions is practically negligible compared to the concentration of chlorine anions. This is a common type of PW in Oklahoma and surrounding states (US Mid Continent) (Guerra et al., 2011a). The rationale for using an arsenic salt (AsCl₃) instead of arsenate salt is that PW originates from an anaerobic environment and that the oxidation of arsenic to arsenate in the presence of air is very slow. Employed concentrations of Ca (6,000 mg/L) and Mg (1,000 mg/L) correspond to typical concentrations found in PW from Western United States (Guerra et al., 2011b) and they were kept constant in all experiments. To assess the competition of mixture toxic metals for hydration sites of dolomite and complexation reactions with chlorine ions in the aqueous phase, the concentration of Sr, Ba, Cd, Pb, and As was kept the same (100 mg/L) in all experiments. NaCl constitutes the main salt compound in PW, as such variable concentrations of NaCl were employed to obtain synthetic PW of different salinity. In this sense, the term salinity in the present study refers to the concentration of NaCl.

Experiments were conducted with guar gum added to the synthetic PW and with guar gum added to the dolomite filter during its preparation. For the experiments conducted with guar gum added to the synthetic PW, 0.5 g/L of guar gum was added to the synthetic PW 24 hours prior to its use to ensure hydration. The employed guar gum was provided by

PFP Technology that supplies additives to hydraulic fracturing and oil field completion companies in the USA.

2.3.4. Core-flooding experiments

Core-flooding (filtration) experiments were conducted using a Hassler Type core-holder (RCH-series of Core Laboratory). The experimental procedure consisted of placing two prepared dolomite filters into the core-holder under a confining pressure of 2,300 psi. Injection of synthetic PW containing toxic metals was done through the bottom of the core-holder at a constant flow rate. Injection was done using a 260 dual syringe pump (Teledyne ISCO) through a floating piston accumulator containing 1 L of synthetic PW. Temperature was ambient temperature (~20 °C), and the injection pressure of synthetic PW into the dolomite filter was monitored through the pressure transducer of the syringe pump. Samples collected at the inlet and outlet of the core-holder were analyzed for Ca, Mg, Sr, Ba, Cd, Pb, and As by ICP-OES analysis. Meaning that measured concentrations correspond to the total concentrations of metals in solution. Fig. 2.3 shows a schematic representation of the experimental setup used to conduct the experiments. Most experiments were repeated at least two times to verify the reproducibility of results.

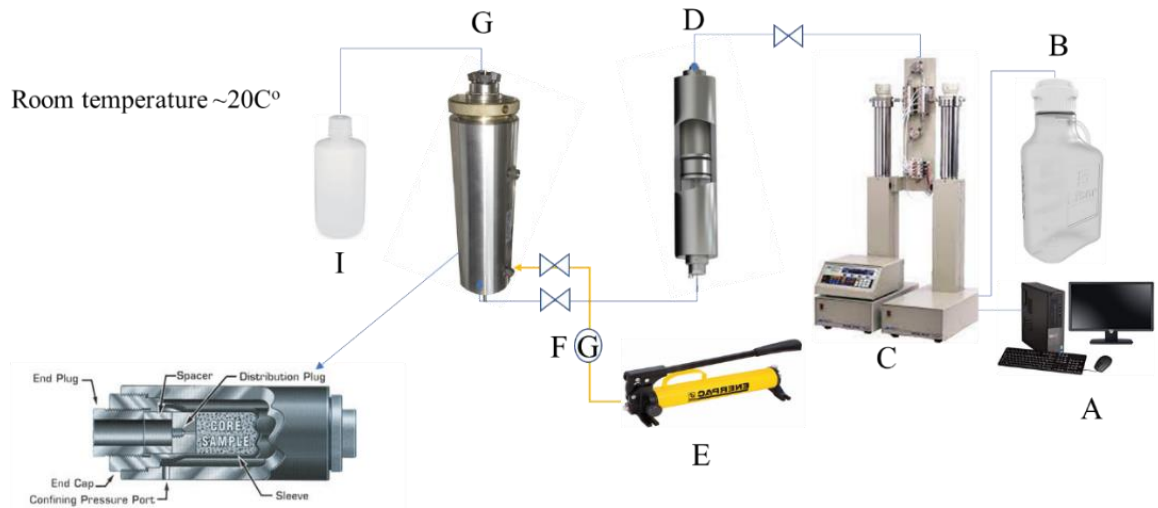


Fig. 2.3. Schematic of the experimental setup: A) Computer to record pressure, B) Deionized water container, C) Dual syringe high-pressure injection pump, D) Floating piston accumulator containing 1L of synthetic PW, E) Hydraulic hand pump, F) Pressure gauge (confining pressure), G) Hassler-type core-holder, and I) Effluent collector.

2.4. Results and discussion

2.4.1. Effect of salinity and competition of cations

Sorption of toxic metals on dolomite is a function of salinity of water and competition of cations for hydration sites of dolomite (Ebrahimi and Vilcez, 2018a; Gruszecka-Kosowska et al., 2017). To bridge the knowledge gap regarding the competition of Ba, Sr, and Cd for hydration sites of dolomite at salinity levels of PW, we conducted core-flooding experiments at an injection rate of 0.5 mL/min using synthetic PW of three different salinities and dolomite filters made of 600-850 μm grain size.

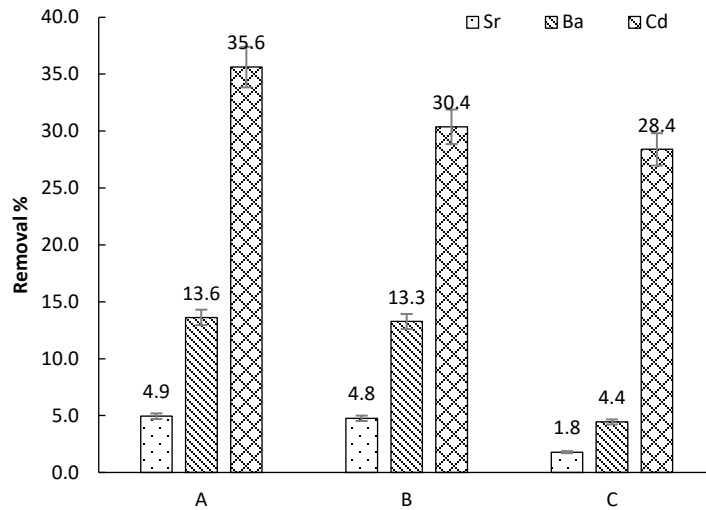


Fig. 2.4. Removal of Sr, Ba, and Cd from 1L of synthetic PW at A) 0 g-NaCl/L, B) 11.5 g-NaCl/L, and C) 115.4 g-NaCl/L salinities using filters (1.5-inch diameter and 6-inch length) made of 600-850 μm grain size. The injection rate is 0.5 mL/min.

Fig. 2.4 shows attained removal levels of 100 mg/L of Sr, Ba, and Cd from 1 L of synthetic PW of 0 g-NaCl/L, 11.55 g-NaCl/L, and 115.4 g-NaCl/L salinities. At a relatively low salinity level of 11.5 g-NaCl/L, attained removal levels of Sr, Ba, and Cd were 4.9%, 13.6%, and 35.6%, respectively, whereas at a salinity level of PW (115.4 g-NaCl/L), attained removal levels of Sr, Ba, and Cd decreased to 1.8%, 4.4%, and 28.4%, respectively. The results show that alkaline earth metals as well as heavy metals sorption on dolomite decreases with increasing salinity. However, the results reveal that salinity has a different impact on the sorption of alkaline earth metals and heavy metals on dolomite. While an increase of salinity from 0 g-NaCl/L to 115.4 g-NaCl/L has a significant impact on the removal of Sr and Ba, the same increase of salinity has a mild impact on the removal of Cd. Removal of Sr and Ba decreases around 65% by increasing salinity from 0 g-NaCl/L to 115.4 g-NaCl/L, whereas removal of Cd only decreases around 20% by the same

increase of salinity. To verify that dolomite has a larger affinity for heavy metals than for alkaline earth metals, we conducted experiments using synthetic PW containing 100 mg/L of Sr, Ba, Cd, Pb, and As. Fig. 2.5 shows attained removal levels from 100 mL, 250 mL, 500 mL, and 1 L of synthetic PW. Highest removal levels attained for Pb and Cd confirm that dolomite has a larger affinity for heavy metals than for alkaline earth metals. A higher removal level attained for As than for Sr and Ba, indicates that dolomite has a larger affinity for metalloids than alkaline earth metals. Furthermore, practically constant removal levels of Sr, Ba, Cd, Pb, and As after 250 mL, suggest surface availability is not a controlling factor. Otherwise, removal levels should decrease with increasing filtered volumes.

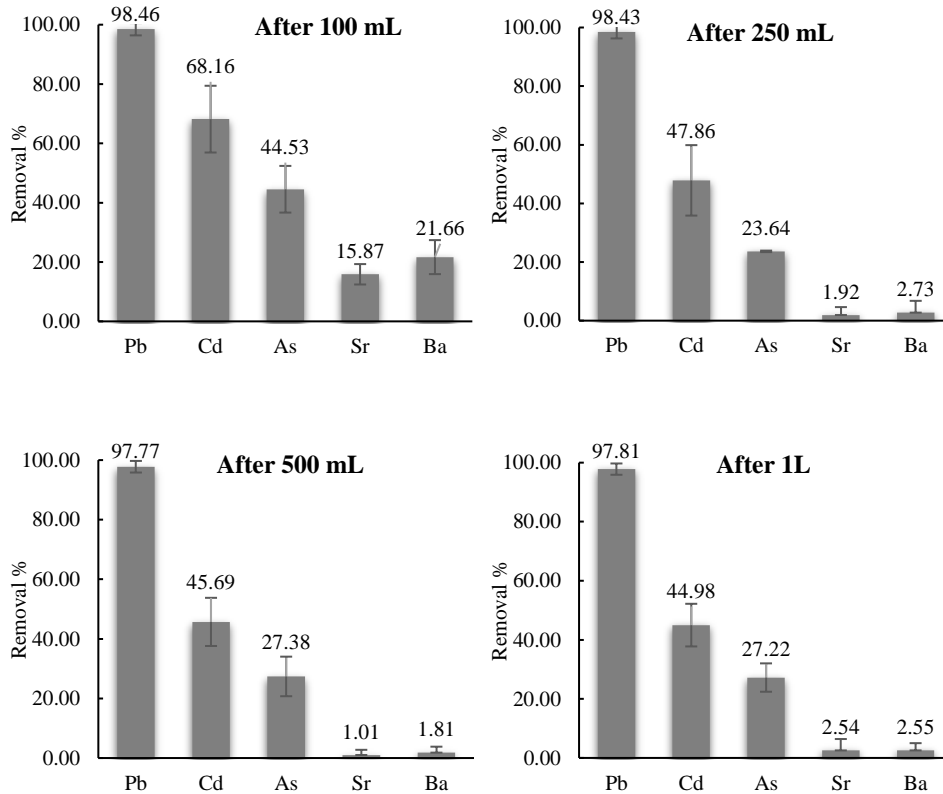


Fig. 2.5. Removal of Pb, Sr, Ba, As, and Cd from 1 L of synthetic PW using a dolomite filter made of 350-600 μm grain size (1.5-inch diameter and 6-inch length). PW injection rate is 0.1 mL/min, and salinity of PW is 45 g-NaCl/L.

The inhibitory effect of salinity on the sorption of metals on dolomite can be attributed to complexation reactions with chlorine ions in the aqueous phase. Chlorine complexes are less prone to be electrostatically attracted by negatively charged hydration sites of dolomite than free divalent cations (Ebrahimi and Vilcáez, 2018a). The larger affinity of dolomite for heavy metals than for alkaline earth metals might be due to the extent of complexation by chlorine in solution, which might be larger for alkaline earth metals than for heavy metals, and/or due to the extent of surface complexation reactions which might be larger for heavy metals than for alkaline earth metals.

Despite of the common occurrence of carbonate minerals like dolomite, previous studies have overwhelmingly focused on metal-(oxyhydro)oxides (Brown and Parks, 2001a). Those studies have shown that alkaline earth metals (Sr and Ba) form weaker surface complexes than heavy metals (Pb and Cd), and they have pointed out the affinity sequence for metal-(oxyhydro)oxides is $Pb > Cd$ and $Sr > Ba$ (Hayes and Katz, 1996; Stumm, 1992). According to our experiments, this affinity sequence holds for heavy metals but not for alkaline earth metals sorption on dolomite. The affinity sequence for the sorption of alkaline earth metals on dolomite at salinity levels of PW is $Ba > Sr$ (Fig. 2.4).

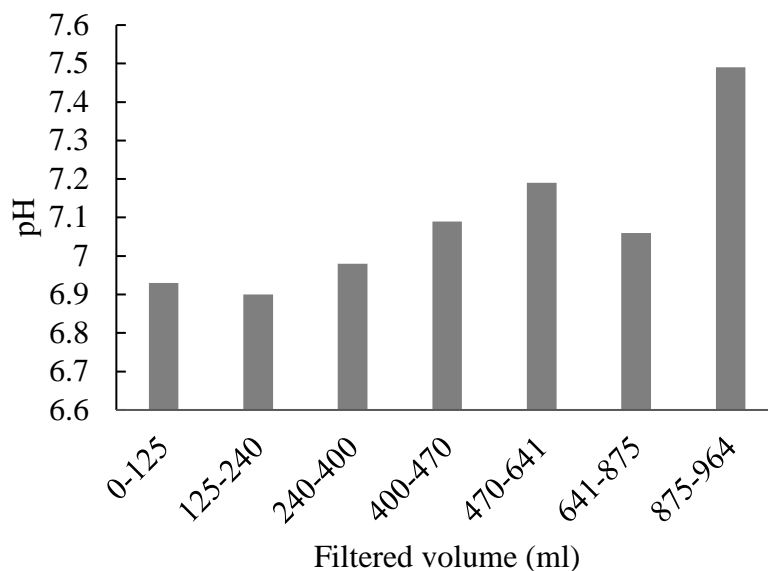


Fig. 2.6. Representative pH of discrete volumes of filtered PW containing Pb, Sr, Ba, As, and Cd. PW injection rate is 0.1 mL/min and salinity of PW is 45 g-NaCl/L.

Fig. 2.6 shows changes of pH in discrete volumes of filtered PW containing Pb, Sr, Ba, As, and Cd. In accordance to previous studies using a single metal (Ba) and the same dolomite sample, pH increases due to the dissolution of dolomite (Ebrahimi and Vilcáez, 2018a, b). An increase of pH is known to increase the removal of metal cations as the concentration of protons competing for hydration sites of dolomite decreases due an increased concentration of bicarbonate ions derived from the dissolution of dolomite (Brady et al., 1999; Pokrovsky et al., 1999a; Yamkate et al., 2017). This implies that dolomite would be more effective removing toxic metals from PW of alkaline pH.

2.4.2. Effect of flow velocity and grain size

To determine whether or not sorption of Sr, Ba, and Cd on dolomite are equilibrium reactions and to assess the degree to which flow velocity and/or grain size affect the removal of mixture toxic metals from PW by dolomite filtration, we conducted core-

flooding experiments at three different injection rates (0.1, 0.25, and 0.5 mL/min) using dolomite filters made of two different grain sizes (600-850 μm and 350-600 μm) and synthetic PW of two different salinities (42g-NaCl/L and 115.4 g-NaCl/L).

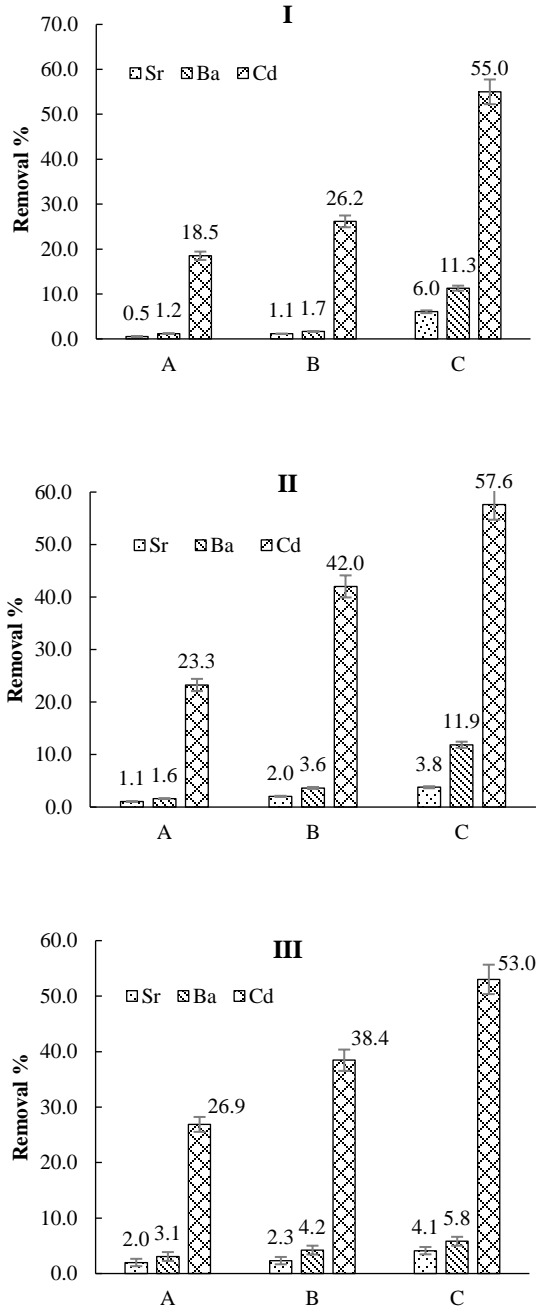


Fig. 2.7. Removal of Sr, Ba, and Cd from 1L of synthetic PW at A) 0.5 mL/min, B) 0.25 mL/min, and C) 0.1 mL/min injection rates using: D) 600-850 μm grain size and 115.5 g-

NaCl/L salinity. II) 600-850 μm grain size and 42 g-NaCl/L salinity. III) 350-600 μm grain size and 42 g-NaCl/L salinity.

Fig. 2.7 shows the obtained results. Removal levels of Sr, Ba, and Cd increase with decreasing the injection rate of PW into the dolomite filter at both salinity and grain size conditions. For instance, at 0.5 mL/min injection rate, removal levels of Sr, Ba, and Cd from synthetic PW of 115.4 g-NaCl/L salinity is only 0.5%, 1.2%, and 21.3%, respectively. Whereas, at 0.1 mL/min injection rate, removal of Sr, Ba, and Cd from synthetic PW of the same salinity increases to 6%, 11.3% and 55%, respectively (Fig. 7.I). This result suggests that sorption of toxic metals on dolomite are kinetic reactions. While removal levels of Sr and Ba are higher with synthetic PW of 42 g-NaCl/L salinity (Fig. 6.II) than with synthetic PW of 115.4 g-NaCl/L salinity (Fig. 7.I), removal levels of Cd remain practically the same. This result confirms that salinity has higher inhibitory effect on alkaline earth metals sorption than on heavy metals sorption, and thus dolomite filters are more efficient removing Cd than Sr and Ba from high salinity waters.

Although dolomite filters made of 350-600 μm grain size have a larger pore surface area than dolomite filters made of 600-850 μm grain size, similar removal levels of Sr, Ba, and Cd are attained with filters made of 600-850 μm (Figure. 7.II) and 350-600 μm (Figure 7.III) grain sizes. This result confirms that sorption reactions of Sr, Ba, and Cd on dolomite are kinetically controlled reactions affected by the dissolution of dolomite. The dissolution of dolomite was reflected by an increase of pH. However, concentration of Ca and Mg in the filtered PW remained practically the same. pH profiles over time and at different salinities can be seen in a previous study where the same dolomite was employed (Ebrahimi and Vilcáez, 2018a, b).

2.4.3. Effect of guar gum

A previous study on the effect of guar gum on the transport of Ba in dolomite suggested that guar gum trapped in small pore throats works as a secondary filtration media retarding the transport of Ba (Ebrahimi and Vilcáez, 2018a). Based on that finding, we conducted core-flooding experiments to assess the feasibility of using guar gum as an aiding agent to enhance the removal of a mixture of toxic metals from PW by dolomite filtration. We tested two guar gum utilization methods, one where guar gum is added to PW prior to its injection into the dolomite filter, and other where guar gum is mixed with powdered dolomite to prepare dolomite filters.

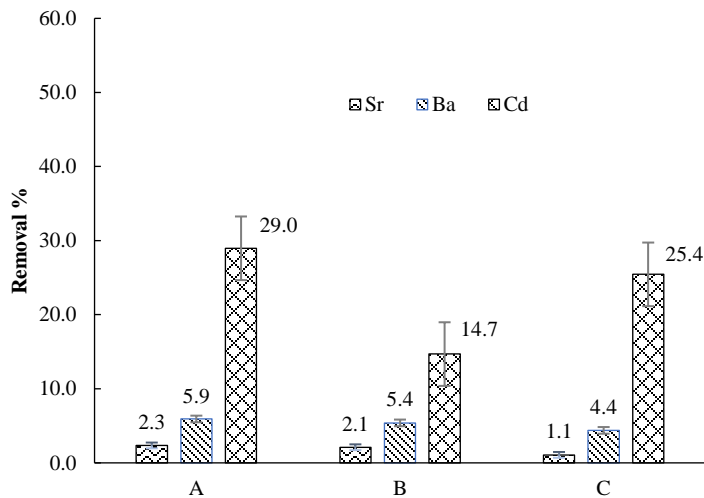


Fig. 2.8. Removal of Sr, Ba, and Cd from 1L of synthetic PW containing 0.5 g-Guar gum/L at A) 0.5 mL/min, B) 0.25 mL/min, and C) 0.1 mL/min injection rates using filters made of 350-600 μ m grain size. Salinity of the synthetic PW is 42 g-NaCl/L.

Fig. 2.8 shows obtained removal levels of Sr, Ba, and Cd at three injection rates (0.1, 0.25, and 0.5 mL/min) using synthetic PW of 42 g-NaCl/L salinity containing 0.5 g-Guar gum/L. Addition of guar gum to PW did not enhance the removal of Sr, Ba, or Cd.

Interestingly, while removal levels of Sr and Ba are practically the same with and without the addition of guar gum, the removal level of Cd decreases with the addition of guar gum. For instance, removal of Cd decreased from 53% (Fig. 7.III) to 25.4% (Fig. 8) due to the addition of guar gum. Guar gum is known to form complexes with metal ions and metal surfaces through its -COOH functional group (Peter et al., 2016). In fact, this property of guar gum has been used to develop a treatment method to remove Pd from conventional wastewater (Mukherjee et al., 2018). Our results indicate a higher degree of complexation of guar gum with heavy metals (Cd) than with alkaline earth metals (Sr and Ba) in the aqueous phase.

Apparently, if pore throats of the dolomite filter are too large to physically trap the formed guar gum-complex of metal ions, guar gum addition to PW can result in low removal levels of Sr, Ba, and Cd, because guar gum-complexes of metal ions form weaker bonds with hydration sites of dolomite than dissolved ions. Contrary to previous results obtained using low porosity dolomite cores where the trapping of guar gum complexes of metal ions was reflected by pressure buildup at the inlet of the core-holder (Ebrahimi and Vilcáez, 2018a), the free flow of gum complexes of metal ions in dolomite filters made of 350-600 and 600-850 μm grain size did not result in a pressure buildup at the inlet of the core-holder.

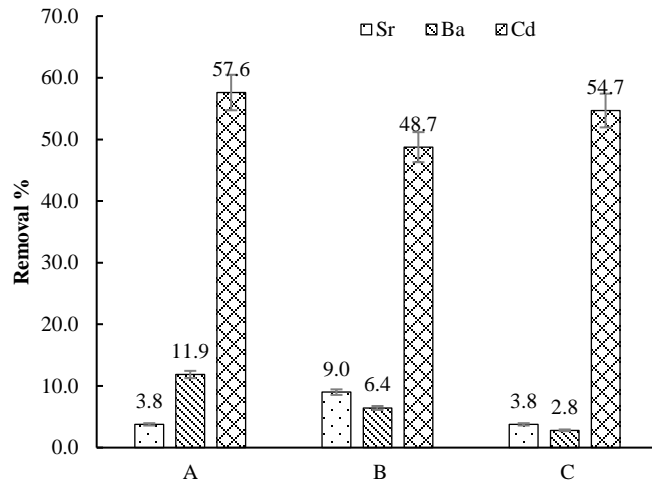


Fig. 2.9. Removal of Sr, Ba, and Cd from 1L of synthetic PW: A) 0.0 g-Guar gum/200 g-Dolomite, B) 0.5 g-Guar gum/200 g-Dolomite, C) 1.0 g-Guar gum/200 g-Dolomite. Filters are made of 850-600 μm grain size. Salinity of the synthetic PW is 42 g-NaCl/L. Injection rate is 0.1 mL/min.

Fig. 2.9 compares removal levels of Sr, Ba, and Cd obtained with dolomite filters prepared mixing powdered dolomite and guar gum. Similar removal levels attained with and without the presence of guar gum in the dolomite filter, suggest that guar gum has less complexation capacity towards heavy metals and alkaline earth metals than towards dolomite. To verify the capacity of dolomite filters to effectively remove Sr, Ba, and Cd from PW, we conducted additional experiments where 1 L of synthetic PW of 42 g-NaCl/L salinity was injected into five dolomite filters (1.5-inch diameter and 6-inch length) of the same grain size (350-600 μm) sequentially. Obtained removal levels of Sr, Ba, and Cd were 9.4%, 31.6%, and 91.8%, respectively. Suggesting that a complete removal of Sr, Ba, and Cd can be obtained by optimizing the relationship between the injection rate and volume of the dolomite filter. To prevent the inhibition of sorption reactions by dissolved oil hydrocarbons which are generally present in PW can be

remove by microbiological methods that consists of the stimulation of indigenous oil degrading methanogenic microbial communities by combining the supply of protein-rich matter and CO₂ (Vilcáez et al., 2018). The remaining trace concentrations of oil hydrocarbons and toxic metals can be removed in subsequent stages using conventional technologies (e.g., membrane filtration).

2.4.4. Modeling and simulation

Different removal levels of heavy metals and alkaline earth metals can be attributed to the different surface complexation of heavy metals and alkaline earth metals on dolomite and/or to the different complexation of heavy metals and alkaline earth metals by chlorine ions in the aqueous phase. To elucidate the relevance of both type of complexation reactions on the removal of mixture toxic metals from PW by dolomite filtration, we conducted 3D reactive transport simulations using a model calibrated to simulate the reactive transport of Ba in dolomite (Vilcáez, 2020). Briefly, the 3D reactive transport model accounts for the kinetic dissolution of dolomite as well as for all possible complexation reactions of ions in the aqueous phase. This is an important feature of the model as it determines the availability of cations (H⁺, Ca²⁺, Mg²⁺, Sr²⁺, Ba²⁺, and Cd²⁺) to form surface complexes with the three types of hydration sites (>CaOH⁰, >MgOH⁰, and >CO₃H⁰) of dolomite. The sorption preference of dolomite for the cations is captured by using an intrinsic stability constant (K_{int}^S) function of the concentration of cations in the aqueous phase and the concentration of available and occupied hydration sites of dolomite:

$$K_{\text{int}}^{\text{S}} = \frac{\{>\text{CO}_3\text{Ms}^+\}\{\text{H}^+\}}{\{>\text{CO}_3\text{H}^0\}\{\text{Ms}^{2+}\}} \quad (1)$$

where Ω denotes the activity of M_s (Ca^{2+} , Mg^{2+} , Sr^{2+} , Ba^{2+} , and Cd^{2+}) at the mineral-solution interface (Pokrovsky et al., 2000b). Intrinsic stability constants have been experimentally measured for Ca and Mg, and fitted to batch sorption experimental results for Ba (Vilcez, 2020). To bridge the knowledge gap regarding the intrinsic stability constants for Sr and Cd, simulations are conducted assuming that Sr, Ba, and Cd have the same intrinsic stability constants. Pb and As are not included in the simulations because their intrinsic stability constants are not available in literature. The kinetic dissolution/precipitation reaction of dolomite is represented by a kinetic model formulated based on the transition state theory (TST) (Lasaga, 2018):

$$-R_{dol}^{min} = A[H^+]^{0.5}k\{1 - \Omega\} \quad (2)$$

where A is the surface area of the mineral, k is the kinetic coefficient of the reaction, and Ω is the saturation index of the reaction. Table 2.1 shows all surface complexation reactions included in the model along with the employed intrinsic stability constant values. The model is implemented in TOUGHREACT reactive transport simulator which includes a thermodynamic data base of gas, aqueous, and mineral phase reactions. TOUGHREACT has been extensively employed to study various types of reactive transport processes in subsurface porous media (Shabani et al., 2020; Shabani and Vilcez, 2017, 2018, 2019).

Tables 2.2 and 2.3 show all aqueous phase complexation reactions and mineral phase dissolution/precipitation reactions along with their corresponding constants. The preparation procedure of dolomite filters involves the mixing of deionized water and

powdered dolomite and compression. Table 2.4 shows reported and measured parameters we employed to simulate the reactive transport of Sr, Ba, and Cd in dolomite. The preparation procedure of dolomite filters involves the mixing of deionized water and powdered dolomite and compression. Therefore, the pore space of the dolomite filter is initially occupied with water and the initial composition of water corresponds to an equilibrium condition with dolomite. Generally, porosity increases with decreasing grain sizes, therefore a porosity of 20% for well sorted 350-600 μm grain size (Ogolo et al., 2015) was used for simulations. Table 2.2 show all other parameters needed to run the simulations.

Table 2.1. Surface complexation reactions (Pokrovsky et al., 2000b).

Sorption reaction	$\log K_{\text{int}}^{\text{s}}$				
	Ca	Mg	Ba	Sr	Cd
1 $> \text{CO}_3\text{H}^{\circ} \leftrightarrow \text{CO}_3^- + \text{H}^+$	-4.8	-4.8	–	–	–
2 $> \text{CO}_3\text{H}^{\circ} + \text{Ms}^{2+} \leftrightarrow \text{CO}_3\text{Ms}^+ + \text{H}^+$	-1.8	-2.0	-3.2*	-3.2†	-3.2†
3 $> \text{MeOH}^{\circ} \leftrightarrow \text{MeO}^- + \text{H}^+$	-12	-12	–	–	–
4 $> \text{MeOH}^{\circ} + \text{H}^+ \leftrightarrow > \text{MeOH}_2^+$	11.5	10.6	–	–	–
5 $> \text{MeOH}^{\circ} + \text{HCO}_3^{2-} + \text{H}^+ \leftrightarrow$ $> \text{MeHCO}_3^{\circ} + \text{H}_2\text{O}$	13.7	13.2	–	–	–
6 $> \text{MeOH}^{\circ} + \text{HCO}_3^{2-} \leftrightarrow > \text{MeCO}_3^- + \text{H}_2\text{O}$	6.3	5.1	–	–	–

*Estimated from batch sorption experimental results (Me: Ca and Mg; Ms: Ca, Mg, and Ba)

†Assumed

Table 2.2. Aqueous phase acid-base and complexation reactions.

Reaction	Log K (25 °C)
$\text{CO}_2(\text{aq}) + \text{H}_2\text{O} \leftrightarrow \text{H}^+ + \text{HCO}_3^-$	-6.342
$\text{CO}_3^{2-} + \text{H}^+ \leftrightarrow \text{HCO}_3^-$	10.325
$\text{OH}^- + \text{H}^+ \leftrightarrow \text{H}_2\text{O}$	13.991
$\text{Ca}(\text{Cl})^+ \leftrightarrow \text{Ca}^{2+} + 2\text{Cl}^-$	0.701
$\text{CaCl}_2(\text{aq}) \leftrightarrow \text{Ca}^{2+} + 2\text{Cl}^-$	0.654
$\text{CaCO}_3(\text{aq}) + \text{H}^+ \leftrightarrow \text{Ca}^{2+} + \text{HCO}_3^-$	7.009
$\text{CaHCO}_3^+ \leftrightarrow \text{Ca}^{2+} + \text{HCO}_3^-$	-1.043
$\text{CaOH}^+ + \text{H}^+ \leftrightarrow \text{Ca}^{2+} + \text{H}_2\text{O}$	12.852
$\text{MgCl}^+ \leftrightarrow \text{Mg}^{2+} + \text{Cl}^-$	0.139
$\text{MgCO}_3(\text{aq}) + \text{H}^+ \leftrightarrow \text{HCO}_3^- + \text{Mg}^{2+}$	7.356
$\text{MgHCO}_3^+ \leftrightarrow \text{HCO}_3^- + \text{Mg}^{2+}$	-1.033
$\text{MgOH}^+ + \text{H}^+ \leftrightarrow \text{H}_2\text{O} + \text{Mg}^{2+}$	11.785
$\text{NaCl}(\text{aq}) \leftrightarrow \text{Na}^+ + \text{Cl}^-$	0.782
$\text{NaCO}_3^- + \text{H}^+ \leftrightarrow \text{HCO}_3^- + \text{Na}^+$	9.816
$\text{NaHCO}_3(\text{aq}) \leftrightarrow \text{HCO}_3^- + \text{Na}^+$	-0.170
$\text{NaOH}(\text{aq}) + \text{H}^+ \leftrightarrow \text{Na}^+ + \text{H}_2\text{O}$	14.154
$\text{BaCO}_3(\text{aq}) + \text{H}^+ \leftrightarrow \text{Ba}^{2+} + \text{HCO}_3^-$	7.691
$\text{Ba}(\text{Cl})^+ \leftrightarrow \text{Ba}^{2+} + 2\text{Cl}^-$	0.503
$\text{BaHCO}_3^+ \leftrightarrow \text{Ba}^{2+} + \text{HCO}_3^-$	-1.012
$\text{Sr}(\text{Cl})^+ \leftrightarrow \text{Sr}^{2+} + \text{Cl}^-$	0.253
$\text{SrCO}_3(\text{aq}) + \text{H}^+ \leftrightarrow \text{Sr}^{2+} + \text{HCO}_3^-$	7.470

$\text{SrHCO}_3^+ \leftrightarrow \text{Sr}^{2+} + \text{HCO}_3^-$	-1.225
$\text{SrOH}^+ + \text{H}^+ \leftrightarrow \text{Sr}^{2+} + \text{H}_2\text{O}$	13.292
$\text{Cd}(\text{OH})^+ + \text{H}^+ \leftrightarrow \text{Cd}^{2+} + \text{H}_2\text{O}$	10.080
$\text{CdCO}_3(\text{aq}) + \text{H}^+ \leftrightarrow \text{Cd}^{2+} + \text{HCO}_3^-$	7.329
$\text{CdHCO}_3^+ \leftrightarrow \text{Cd}^{2+} + \text{HCO}_3^-$	-2.070
$\text{Cd}(\text{Cl})^+ \leftrightarrow \text{Cd}^{2+} + \text{Cl}^-$	-1.966

Table 2.3. Dissolution/precipitation reactions of minerals.

Reaction	Log K (25 °C)
$\text{Dolomite} + 2\text{H}^+ \leftrightarrow \text{Ca}^{2+} + \text{Mg}^{2+} + 2\text{HCO}_3^-$	2.524
$\text{Calcite} + \text{H}^+ \leftrightarrow \text{Ca}^{2+} + \text{HCO}_3^-$	1.854

Table 2.4. Parameters for reactive transport simulations of Sr, Ba, and Cd in dolomite.

Parameter	Value	Source
Grain size diameter (μm)	350-600	Measured
Total reactive surface area (cm^2/g)	2.95×10^5	Ávila et al. (2012)
Sorption surface area (cm^2/g)		
> CO_3H^0	2.95×10^5	Total reactive surface area
> CaOH^0	2.95×10^5	Total reactive surface area
> MgOH^0	2.95×10^5	Total reactive surface area
Sorption site density (mol/m^2)		

> CO ₃ H ^o	8.0×10 ⁻⁶	Pokrovsky et al. (2000b); Pokrovsky et al. (1999a)
> CaOH ^o	7.0×10 ⁻⁶	Pokrovsky et al. (2000b); Pokrovsky et al. (1999a)
> MgOH ^o	14×10 ⁻⁶	Pokrovsky et al. (2000b); Pokrovsky et al. (1999a)
Kinetic coefficient (k, mol/m ² /s)	3.0×10 ⁻⁸	Xu, Sonnenthal, Spycher and Pruess (Xu et al., 2006)

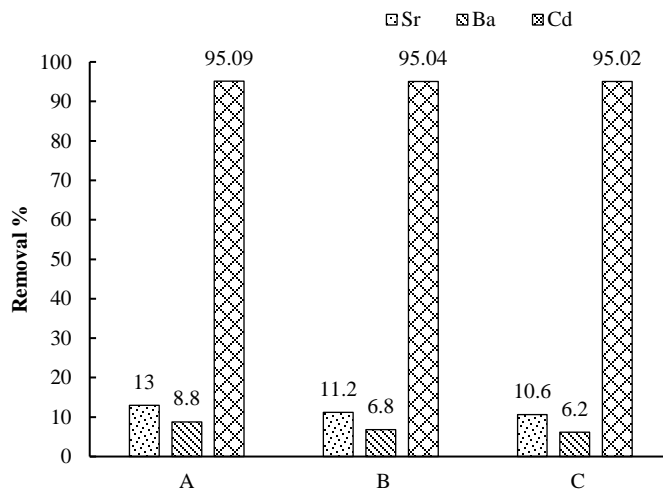


Fig. 2.10. Simulated removal of Sr, Ba, and Cd from 1L of synthetic PW at A) 1.0 mL/min, B) 0.25 mL/min, and C) 0.5 mL/min injection rates using filters made of 600-350 μ m grain size. Intrinsic stability constant for Sr, Ba, and Cd is the same (Table 1). The salinity of the synthetic PW is 40 g-NaCl/L.

Fig. 2.10 shows simulated removal levels of Sr, Ba, and Cd from 1L of synthetic PW of 40 g-NaCl/L salinity at three different injection rates. The model captures the higher removal levels measured for Cd than for Ba and Sr, as well as the increase of Cd, Ba and

Sr removal with decreasing the injection rate. Simulated removal levels of Sr, Ba, and Cd at 0.5 mL/min injection rate are 13.0%, 6.2% and 95.02%, respectively. Decreasing the injection rate to 0.1 mL/min increases the removal of Sr and Ba to 15.6% and 8.8%, respectively, while Cd removal remains practically the same (95.09%). Considering that the model captured the preferential removal of Cd over Ba and Sr using the same intrinsic stability constant value for Cd, Ba and Sr (Table 2.1), our simulation results reveal that removal of Sr, Ba, and Cd from PW by dolomite filtration is largely controlled by the complexation of Sr, Ba, and Cd by chlorine in the aqueous phase. The smaller the equilibrium constant of the metal ion chloro-complex (Table 2.2), the higher removal of Sr, Ba, and Cd by dolomite filtration. Furthermore, considering that surface complexation reactions in the model are equilibrium reactions, our simulation results reveal that higher removal levels at low injection rates are due to the kinetic dissolution of dolomite. Dolomite dissolution is reflected by an increase of pH and thus by a reduction of the concentration of protons in solution, which results in an increase the concentration of surface species (e.g., $>CO_3Sr^+$, $>CO_3Ba^+$ and $>CO_3Cd^+$) according to Eq. (1). However, the model overpredicts the removal levels of Cd, Ba and Sr, and the predicted affinity sequences of alkaline earth metals is opposite (Sr>Ba) to the observed one (Ba>Sr). This is attributed to the surface crystal morphology of dolomite whose effect is yet to be assessed, and due to the intrinsic stability constants of Sr and Cd whose values are yet to be measured at salinity levels of PW. Higher removal levels simulated for Sr than for Ba, suggest a smaller intrinsic stability constant for Ba than for Sr. In a follow-up study, intrinsic stability constant will be estimated from surface titration and electrokinetic measurements (Pokrovsky et al., 2000b; Pokrovsky et al., 1999a) and in-situ molecular

characterization of metals uptake will be done by X-ray adsorption fine structure spectroscopy (EXAFS) (Brown and Parks, 2001a).

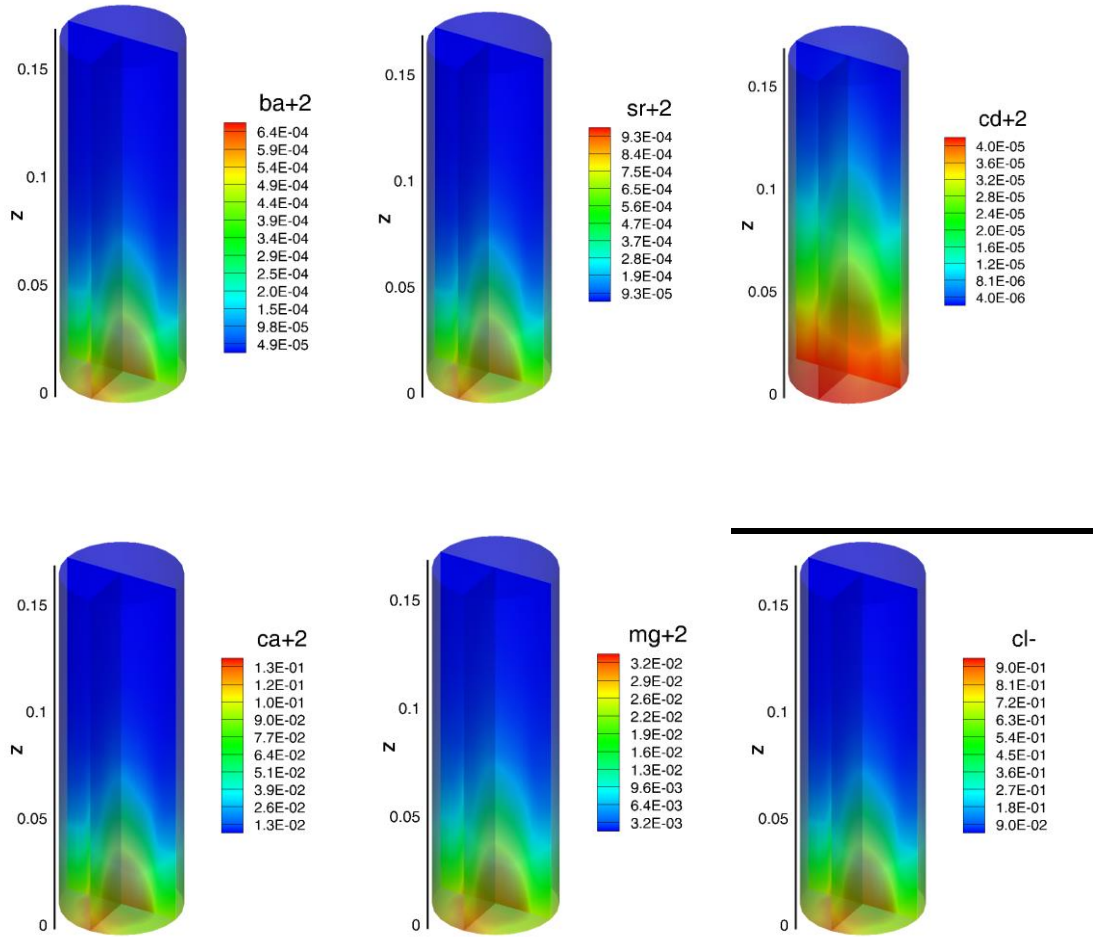


Fig. 2.11. Simulated concentrations of aqueous species (Sr, Ba, Cd, Ca, Mg, and Cl) in mol/L and pH in a dolomite filter made of 350-600 μm grain size after 0.1 days of PW injection at 0.1 mL/min. Two inlet points are at the bottom and out outlet point at the top.

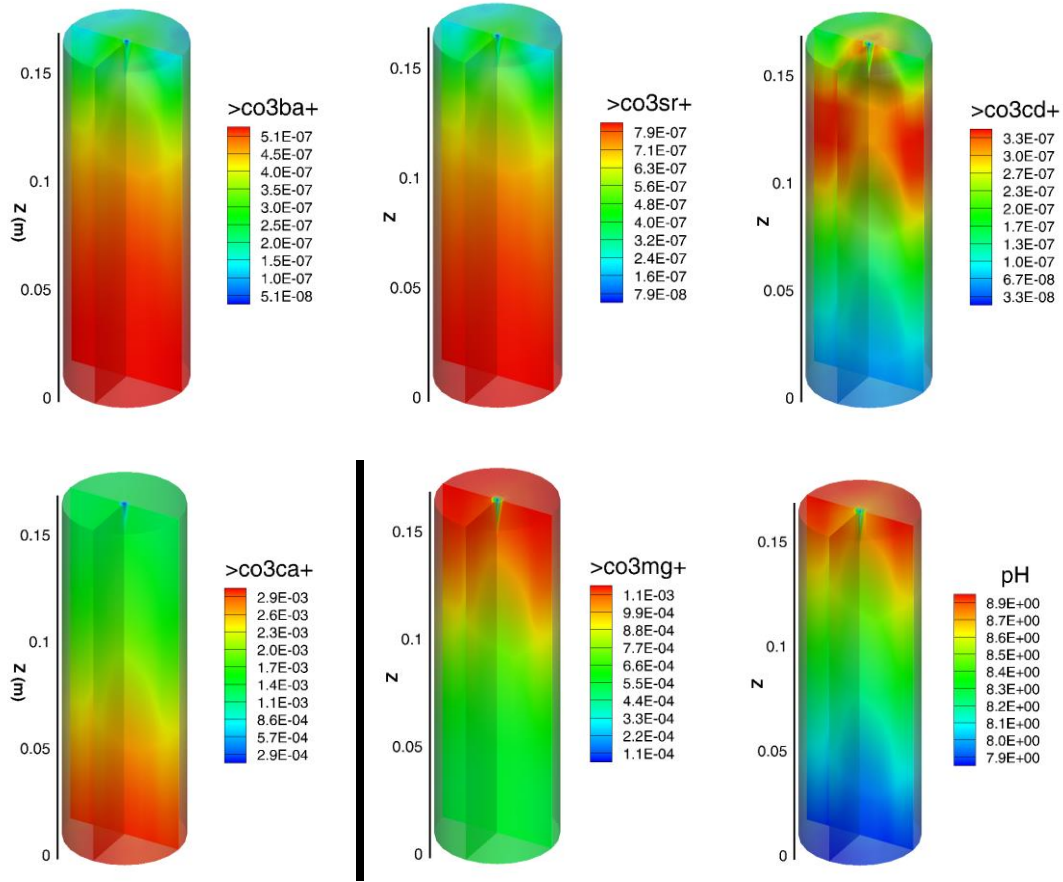


Fig. 2.12. Simulated concentrations of surface species (Sr, Ba, Cd, Ca, and Mg) in mol/L and pH in a dolomite filter made of 350-600 μm grain size after 0.1 days of PW injection at 0.1 mL/min. Two inlet points are located at the bottom and out outlet point at the top.

Figs. 2.11 and 2.12 show representative 3D concentration distributions of aqueous species (Sr^{2+} , Ba^{2+} , Cd^{2+} , Ca^{2+} , Mg^{2+} and Cl^-), surface species ($>\text{CO}_3\text{Sr}^+$, $>\text{CO}_3\text{Ba}^+$ and $>\text{CO}_3\text{Cd}^+$), and pH in a dolomite filter after 0.1 days of injecting synthetic produced PW at 0.1 mL/min into a dolomite filter made of 350-600 μm grain size. As expected, concentrations of aqueous species in the dolomite filter gradually increases from the two inlet points at the bottom to the outlet point at the top (Fig. 2.11). Highest concentrations of Sr, Ba, and Ca surface species occur near the bottom of the dolomite filter while highest concentrations of Cd and Mg surface species occur near the top of the filter (Fig. 2.12).

This behavior is related to the pH which gradually increases from the bottom to the top of the filter due to the dissolution of dolomite. The simulated increase of pH at the outlet of dolomite filter is in accordance with the experimental results (Fig. 2.7). Apparently, the smaller the ability of cations to form chloro-complexes, the lower the enhancing effect of alkaline pH levels on the removal of divalent cations by dolomite.

2.5. Conclusions

Salinity has a significant impact on the removal of Sr and Ba, but a mild impact on the removal of Cd by dolomite filtration. Dolomite filters are more effective removing heavy metals (e.g., Pb and Cd) than alkaline earth metals (e.g., Ba and Sr). At salinity levels of PW, the affinity sequence for the sorption of mixture metals on dolomite is $Pb > Cd > As > Ba > Sr$. Opposite to metal-(oxyhydro)oxides the affinity sequence for dolomite at salinity levels of PW is $Ba > Sr$. Removal of Sr, Ba, and Cd from PW by dolomite filtration are kinetically controlled reactions where an increase of pH due to the dissolution of dolomite increases the removal of Sr, Ba, and Cd. This increase is higher for Cd than for Sr and Ba. Sr, Ba, and Cd complexation by guar gum in the aqueous phase hinders their removal by dolomite filters made of large grain size (e.g., 350-600 μm) where trapping of guar gum in small pore throats is not possible. A complete removal of Sr, Ba, and Cd can be obtained by optimizing the relationship between the injection rate and size of the dolomite filter. Overestimated removal levels of Cd and higher removal levels of Sr than Ba, by the formulated reactive transport model highlights the necessity of further experimental research to be able to incorporate molecular scale surface crystal structure and surface morphology parameters into the model.

2.6. Acknowledgements

We thank the United State Geological Survey (USGS) 104 (b) Program for their partial financial support. This is Oklahoma State University Boone Pickens School of Geology contribution number 2022-127.

2.7. References

- Alexandratos, V. G., Elzinga, E. J., and Reeder, R. J., 2007, Arsenate uptake by calcite: macroscopic and spectroscopic characterization of adsorption and incorporation mechanisms: *Geochimica et Cosmochimica Acta*, v. 71, no. 17, p. 4172-4187.
- Alley, B., Beebe, A., Rodgers Jr, J., and Castle, J. W., 2011, Chemical and physical characterization of produced waters from conventional and unconventional fossil fuel resources.: *Chemosphere*, v. 85(1), pp.74-82.
- Antao, S. M., and Hassan, I., 2009, The orthorhombic structure of CaCO₃, SrCO₃, PbCO₃ and BaCO₃: linear structural trends.: *The Canadian Mineralogist*, v. 47(5), pp.1245-1255.
- Anthony, J. W., Bideaux, R. A., Bladh, K. W., and Nichols, E., Monte C., , 1995, *Handbook of Mineralogy*: Mineralogical Society of America. Chantilly, VA 20151-1110, USA. <http://www.handbookofmineralogy.org/>.
- Anthony, J. W., Bideaux, R. A., Bladh, K. W., and Nichols, M. C., 2007, Borates, Carbonates, Sulfates. In *Handbook of Mineralogy*: Mineralogical Society of America, v. V.

- Ávila, I., Crnkovic, P. M., Milioli, F. E., and Luo, K. H., 2012, Investigation of the pore blockage of a Brazilian dolomite during the sulfation reaction: *Applied Surface Science*, v. 258, no. 8, p. 3532-3539.
- Balci, N., Demirel, C., Ön, S. A., Gültekin, A. H., and Kurt, M. A., 2018, Evaluating abiotic and microbial factors on carbonate precipitation in Lake Acigöl, a hypersaline lake in Southwestern Turkey: *Quaternary International*, v. 486, pp.116-128.
- Ballinger, D. G., 1979, 1979. Methods for chemical analysis of water and wastes. In United States Environmental Protection Agency.: EPA 600/4-79-020. Environmental Monitoring and Support Laboratory Cincinnati, Ohio., p. 353.352-351 to 353.352-355 (nitrate analysis) and 325.352-351 to 325.352-352 (chloride analysis).
- Bettermann, P., and Liebau, F., 1975, The transformation of amorphous silica to crystalline silica under hydrothermal conditions.: *Contributions to Mineralogy and Petrology*, v. 53(1), pp.25-36.
- Brady, P. V., Papenguth, H. W., and Kelly, J. W., 1999, Metal sorption to dolomite surfaces! This work supported by the United States Department of Energy under contract DE-AC04-94AL85000.1: *Applied Geochemistry*, v. 14, no. 5, p. 569-579.
- Brown, G. E., and Parks, G. A., 2001a, Sorption of Trace Elements on Mineral Surfaces: Modern Perspectives from Spectroscopic Studies, and Comments on Sorption in the Marine Environment: *International Geology Review*, v. 43, no. 11, p. 963-1073.
- Brown, J. G. E., and Parks, G. A., 2001b, Sorption of trace elements on mineral surfaces: Modern perspectives from spectroscopic studies, and comments on sorption in the marine environment.: *International Geology Review*, , v. 43(11), pp.963-1073.

- Chen, X., Zhang, D., Larson, S. L., Ballard, J. H., Knotek-Smith, H. M., Nie, J., Hu, N., Ding, D., and Han, F. X., 2021, Microbially Induced Carbonate Precipitation Techniques for the Remediation of Heavy Metal and Trace Element–Polluted Soils and Water.: *Water, Air, & Soil Pollution*, v. 232(7), pp.1-15.
- Clark, C. E., and Veil, J. A., 2009, Produced water volumes and management practices in the United States: Argonne National Laboratory.
- Collins, A. G., 1969, Chemistry of some Anadarko basin brines containing high concentrations of iodide: *Chemical Geology*, v. 4, no. 1-2, p. 169-187.
- Da'ana, D. A., Zouari, N., Ashfaq, M. Y., Abu-Dieyeh, M., Khraisheh, M., Hijji, Y. M., and Al-Ghouti, M. A., 2021, Removal of toxic elements and microbial contaminants from groundwater using low-cost treatment options: *Current Pollution Reports*, v. 7, no. 3, p. 300-324.
- Dixit, S., and Hering, J. G., 2003, Comparison of arsenic (V) and arsenic (III) sorption onto iron oxide minerals: implications for arsenic mobility.: *Environmental science & technology*, v. 37(18), pp.4182-4189.
- Drever, J. I., 1997, The geochemistry of natural waters: surface and groundwater environments., v. 436. p87-105.
- Ebrahimi, P., and Borrok, D. M., 2020, Mobility of Ba, Sr, Se and As under simulated conditions of produced water injection in dolomite: *Applied Geochemistry*, v. 118, p. 104640.
- Ebrahimi, P., and Vilcáez, J., 2018a, Effect of brine salinity and guar gum on the transport of barium through dolomite rocks: Implications for unconventional oil and gas wastewater disposal: *Journal of Environmental Management*, v. 214, p. 370-378.

- , 2018b, Petroleum produced water disposal: Mobility and transport of barium in sandstone and dolomite rocks: *Science of The Total Environment*, v. 634, p. 1054-1063.
- , 2019, Transport of barium in fractured dolomite and sandstone saline aquifers: *Science of The Total Environment*, v. 647, p. 323-333.
- Emmons, R. V., Shyam Sunder, G. S., Liden, T., Schug, K. A., Asfaha, T. Y., Lawrence, J. G., Kirchhoff, J. R., and Gionfriddo, E., 2022, Unraveling the Complex Composition of Produced Water by Specialized Extraction Methodologies.: *Environmental Science & Technology*, v. 56(4), pp.2334-2344.
- Engle, M. A., Cozzarelli, I. M., and Smith, B. D., 2014, USGS investigations of water produced during hydrocarbon reservoir development, US Department of the Interior, US Geological Survey.
- Fard, A. K., McKay, G., Chamoun, R., Rhadfi, T., Preud'Homme, H., and Atieh, M. A., 2017, Barium removal from synthetic natural and produced water using MXene as two dimensional (2-D) nanosheet adsorbent: *Chemical Engineering Journal*, v. 317, p. 331-342.
- Federation, W. E., and Aph Association, 2005, Standard methods for the examination of water and wastewater. : American Public Health Association (APHA): Washington, DC, USA. 21th Edition. , p. pp 4-75 to 74-76 (chloride method 4500-Cl G) and 4504-4127 to 4504-4129 (nitrate method 4500-NO4503 I).
- Flora, G., Gupta, D., and Tiwari, A., 2012, Toxicity of lead: a review with recent updates: *Interdisciplinary Toxicology*, v. 5, no. 2, p. 47-58.

- Fu, F., and Wang, Q., 2011, Removal of heavy metal ions from wastewaters: a review: Journal of environmental management, v. 92, no. 3, p. 407-418.
- Fukushi, K., Munemoto, T., Sakai, M., and Yagi, S., 2011, Monohydrocalcite: a promising remediation material for hazardous anions: Sci Technol Adv Mater, v. 12, no. 6, p. 064702.
- Gadhamshetty, V., Shrestha, N., Chilkoor, G., and Bathi, J. R., 2015, Emerging Environmental Impacts of Unconventional Oil Development in the Bakken Formation in the Williston Basin of Western North Dakota, Hydraulic Fracturing: Environmental Issues, Volume 1216, American Chemical Society, p. 151-180.
- Ghaemi, A., Torab-Mostaedi, M., and Ghannadi-Maragheh, M., 2011, Characterizations of strontium(II) and barium(II) adsorption from aqueous solutions using dolomite powder: Journal of Hazardous Materials, v. 190, no. 1, p. 916-921.
- Gruszecka-Kosowska, A., Baran, P., Wdowin, M., and Franus, W., 2017, Waste dolomite powder as an adsorbent of Cd, Pb(II), and Zn from aqueous solutions: Environmental Earth Sciences, v. 76, no. 15, p. 521.
- Guerra, K., Dahm, K., and Dundorf, S., 2011a, Oil and gas produced water management and beneficial use in the Western United States: US Department of the Interior.
- Guerra, K., Dahm, K., and Dundorf, S., 2011b, Oil and gas produced water management and beneficial use in the Western United States: U.S. Department of the Interior Bureau of Reclamation.
- Guerra, K., Dahm, K., and Dundorf, S., 2011c, Oil And Gas Produced Water Management And Beneficial Use in the Western United States, : US Department of the Interior,, p. p. 157.

- Gutiérrez-Ravelo, A., Gutiérrez Á, J., Paz, S., Carrascosa-Iruzubieta, C., González-Weller, D., Caballero, J. M., Revert, C., Rubio, C., and Hardisson, A., 2020a, Toxic Metals (Al, Cd, Pb) and Trace Element (B, Ba, Co, Cu, Cr, Fe, Li, Mn, Mo, Ni, Sr, V, Zn) Levels in *Sarpa Salpa* from the North-Eastern Atlantic Ocean Region: *Int J Environ Res Public Health*, v. 17, no. 19.
- Gutiérrez-Ravelo, A., Gutiérrez, Á. J., Paz, S., Carrascosa-Iruzubieta, C., González-Weller, D., Caballero, J. M., Revert, C., Rubio, C., and Hardisson, A., 2020b, Toxic metals (Al, cd, pb) and trace element (b, ba, co, cu, cr, fe, li, mn, mo, ni, sr, v, zn) levels in *sarpa salpa* from the north-eastern atlantic ocean region: *International Journal of Environmental Research and Public Health*, v. 17, no. 19, p. 7212.
- Hakami, M., Tizaoui, C., Kochkodan, V., and Hilal, N., 2013a, Effect of hydrodynamic operations, salinity, and heavy metals on ha removal by microfiltration ceramic tubular membrane: *Separation Science and Technology*, v. 48, no. 4, p. 564-570.
- Hakami, M. W., Tizaoui, C., Kochkodan, V., and Hilal, N., 2013b, Effect of Hydrodynamic Operations, Salinity, and Heavy Metals on HA Removal by Microfiltration Ceramic Tubular Membrane: *Separation Science and Technology*, v. 48, no. 4, p. 564-570.
- Hanes, R., Parker, M., Slabaugh, B., Weaver, J., and Walters, H., Analytical methods for maintaining quality assurance of recycled fracturing fluids, *in Proceedings International Symposium on Oilfield Chemistry*2003a, OnePetro.
- Hanes, R., Parker, M., Slabaugh, B., Weaver, J., and Walters, H. G., Analytical Methods for Maintaining Quality Assurance of Recycled Fracturing Fluids, *in Proceedings*

- International Symposium on Oilfield Chemistry 2003b, Volume All Days: SPE-80221-MS.
- Hayes, K. F., and Katz, L. E., 1996, Application of X-Ray Absorption Spectroscopy for Surface Complexation Modeling of Metal Ion Sorption *in* Brady, P. V., ed., Physics and Chemistry of Mineral Surfaces, CRC Press, p. 77.
- Holail, H., and Al-Hajari, S., 1997, Evidence of an authigenic origin for the palygorskite in a Middle Eocene carbonate sequence from North Qatar.: Qatar Univ. Sci. J., , v. 17, 405– 418.
- Igunnu, E. T., and Chen, G. Z., 2014, Produced water treatment technologies: International journal of low-carbon technologies, v. 9, no. 3, p. 157-177.
- Ingles, M., and Anadon, P., 1991, Relationship of clay minerals to depositional environment in the non-marine Eocene Pontils Group, SE Ebro Basin (Spain). J. Sed. Petrol.,, v. 61, 926–939.
- Ivanets, A. I., Kitikova, N. V., Shashkova, I. L., Oleksienko, O. V., Levchuk, I., and Sillanpää, M., 2016, Using of phosphatized dolomite for treatment of real mine water from metal ions: Journal of Water Process Engineering, v. 9, p. 246-253.
- Ivanets, A. I., Shashkova, I. L., Kitikova, N. V., and Drozdova, N. V., 2014, Extraction of Co(II) ions from aqueous solutions with thermally activated dolomite: Russian Journal of Applied Chemistry, v. 87, no. 3, p. 270-275.
- Jensen, J., 2020, The Role of Carbonate Minerals in Arsenic Mobility in a Shallow Aquifer Influenced by a Seasonally Fluctuating Groundwater Table (Masters thesis, Utah State University).

- Jiménez, S., Micó, M., Arnaldos, M., Medina, F., and Contreras, S., 2018, State of the art of produced water treatment: *Chemosphere*, v. 192, p. 186-208.
- Kaasa, B., and Østvold, T., 1996, Alkalinity in oil field waters-what alkalinity is and how it is measured.
- Kaczmarek, S. E., Gregg, J. M., Bish, D. L., Machel, H. G., Fouke, B. W., Macneil, A. J., Lonnee, J., and Wood, R., 2017, Dolomite, very high-magnesium calcite, and microbes—Implications for the microbial model of dolomitization, *Characterization and Modeling of Carbonates—Mountjoy Symposium 1, Volume 109, SEPM (Society for Sedimentary Geology)*, p. 0.
- Kaveeshwar, A. R., Kumar, P. S., Revellame, E. D., Gang, D. D., Zappi, M. E., and Subramaniam, R., 2018, Adsorption properties and mechanism of barium (II) and strontium (II) removal from fracking wastewater using pecan shell based activated carbon: *Journal of Cleaner Production*, v. 193, p. 1-13.
- Kharaka, Y. K., Kakouros, E., Thordsen, J. J., Ambats, G., and Abbott, M. M., 2007a, Fate and groundwater impacts of produced water releases at OSPER "B" site, Osage County, Oklahoma: *Applied Geochemistry*, v. 22, no. 10, p. 2164-2176.
- Kharaka, Y. K., Kakouros, E., Thordsen, J. J., Ambats, G., and Abbott, M. M., 2007b, Fate and groundwater impacts of produced water releases at OSPER "B" site, Osage County, Oklahoma: *Applied geochemistry*, v. 22, no. 10, p. 2164-2176.
- Kim, Y., Kwon, S., and Roh, Y., 2021, Effect of divalent cations (Cu, Zn, Pb, Cd, and Sr) on microbially induced calcium carbonate precipitation and mineralogical properties.: *Frontiers in Microbiology*, v. 12, p.646748.

- Koutros, S., Lenz, P., Hewitt, S. M., Kida, M., Jones, M., Schned, A. R., Baris, D., Pfeiffer, R., Schwenn, M., and Johnson, A., 2018, RE: Elevated bladder cancer in northern new England: The role of drinking water and arsenic: JNCI: Journal of the National Cancer Institute, v. 110, no. 11, p. 1273-1274.
- Kumari, D., Qian, X. Y., Pan, X., Achal, V., Li, Q., and Gadd, G. M., 2016, Microbially-induced carbonate precipitation for immobilization of toxic metals.: Advances in applied microbiology,, v. 94, pp.79-108.
- Lasaga, A. C., 1984, Chemical kinetics of water-rock interactions: Journal of Geophysical Research: Solid Earth, v. 89, no. B6, p. 4009-4025.
- , 2018, Kinetics of Geochemical Processes, *in* Anthonio, C. L., and James, K., eds., CHAPTER 4. TRANSITION STATE THEORY, De Gruyter, p. 135-170.
- Lin, C. Y., Musta, B., and Abdullah, M. H., 2013, Geochemical processes, evidence and thermodynamic behavior of dissolved and precipitated carbonate minerals in a modern seawater/freshwater mixing zone of a small tropical island: Applied geochemistry, v. 29, p. 13-31.
- Lutz, B. D., Lewis, A. N., and Doyle, M. W., 2013, Generation, transport, and disposal of wastewater associated with Marcellus Shale gas development: Water Resources Research, v. 49, no. 2, p. 647-656.
- Mohammadi, M., Ghaemi, A., Torab-Mostaedi, M., Asadollahzadeh, M., and Hemmati, A., 2015, Adsorption of cadmium (II) and nickel (II) on dolomite powder: Desalination and Water Treatment, v. 53, no. 1, p. 149-157.
- Morton, R. B., 1986a, Effects of brine on the chemical quality of water in parts of Creek, Lincoln, Okfuskee, Payne, Pottawatomie, and Seminole Counties, Oklahoma, 89.

- Morton, R. B., 1986b, Effects of brine on the chemical quality of water in parts of Creek, Lincoln, Okfuskee, Payne, Pottawatomie, and Seminole Counties, Oklahoma, University of Oklahoma.
- Mukherjee, S., Mukhopadhyay, S., Zafri, M. Z. B., Zhan, X., Hashim, M. A., and Sen Gupta, B., 2018, Application of guar gum for the removal of dissolved lead from wastewater: *Industrial Crops and Products*, v. 111, p. 261-269.
- Murray, K. E., 2014, Class II underground injection control well data for 2010–2013 by geologic zones of completion, Oklahoma: Oklahoma Geological Survey Open File Report OF1.
- Neuberger, C. S., and Helz, G. R., 2005, Arsenic (III) carbonate complexing: Applied geochemistry, v. 20(6), pp.1218-1225.
- Ng, J. C., Wang, J., and Shraim, A., 2003, A global health problem caused by arsenic from natural sources: *Chemosphere*, v. 52, no. 9, p. 1353-1359.
- Ogolo, N. A., Akinboro, O. G., Inam, J. E., Akpokere, F. E., and Onyekonwu, M. O., Effect of Grain Size on Porosity Revisited, *in Proceedings SPE Nigeria Annual International Conference and Exhibition 2015, Volume All Days: SPE-178296-MS*.
- Omar, K., and Vilcaez, J., 2021, Removal of mixture heavy metals and metalloids from petroleum produced water by dolomite filtration: *Journal of Contaminant Hydrology*, v. Under review.
- Omar, K., and Vilcáez, J., 2022, Removal of toxic metals from petroleum produced water by dolomite filtration.: *Journal of Water Process Engineering*, v. 47, p.102682.

- Peter, A., Sharma, S. K., and Obot, I. B., 2016, Anticorrosive efficacy and adsorptive study of guar gum with mild steel in acidic medium: *Journal of Analytical Science and Technology*, v. 7, no. 1, p. 26.
- Pokrovsky, O., Mielczarski, J., Barres, O., and Schott, J., 2000a, Surface speciation models of calcite and dolomite/aqueous solution interfaces and their spectroscopic evaluation: *Langmuir*, v. 16, no. 6, p. 2677-2688.
- Pokrovsky, O., and Schott, J., 2002, Surface chemistry and dissolution kinetics of divalent metal carbonates: *Environmental science & technology*, v. 36, no. 3, p. 426-432.
- Pokrovsky, O. S., Mielczarski, J. A., Barres, O., and Schott, J., 2000b, Surface Speciation Models of Calcite and Dolomite/Aqueous Solution Interfaces and Their Spectroscopic Evaluation: *Langmuir*, v. 16, no. 6, p. 2677-2688.
- Pokrovsky, O. S., Schott, J., and Thomas, F., 1999a, Dolomite surface speciation and reactivity in aquatic systems: *Geochimica et Cosmochimica Acta*, v. 63, no. 19, p. 3133-3143.
- Pokrovsky, O. S., Schott, J., and Thomas, F., 1999b, Dolomite surface speciation and reactivity in aquatic systems: *Geochimica et Cosmochimica Acta*, v. 63, no. 19-20, p. 3133-3143.
- Ribeiro, L. P. S., Puchala, R., Lalman, D. L., and Goetsch, A. L., 2021, Composition of various sources of water in Oklahoma available for consumption by ruminant livestock.: *Applied Animal Science*, v. 37(5), pp.595-601.
- Rozell, D. J., and Reaven, S. J., 2012a, Water pollution risk associated with natural gas extraction from the Marcellus Shale: *Risk Analysis: An International Journal*, v. 32, no. 8, p. 1382-1393.

- Rozell, D. J., and Reaven, S. J., 2012b, Water pollution risk associated with natural gas extraction from the Marcellus Shale: *Risk Anal*, v. 32, no. 8, p. 1382-1393.
- Ryan, B. H., Kaczmarek, S. E., and Rivers, J. M., 2019, Dolomite dissolution: An alternative diagenetic pathway for the formation of palygorskite clay.: *Sedimentology*, v. 66(5), pp.1803-1824.
- Scanlon, B. R., Reedy, R. C., Xu, P., Engle, M., Nicot, J. P., Yoxtheimer, D., Yang, Q., and Ikonnikova, S., 2020, Can we beneficially reuse produced water from oil and gas extraction in the U.S.?: *Science of The Total Environment*, v. 717, p. 137085.
- Shabani, B., Pashin, J., and Vilcáez, J., 2020, TOUGHREACT-CO2Bio – A new module to simulate geological carbon storage under biotic conditions (Part 2): The biogeochemical reactive transport of CO2-CH4-H2-H2S gas mixtures: *Journal of Natural Gas Science and Engineering*, v. 76, p. 103190.
- Shabani, B., and Vilcáez, J., 2017, Prediction of CO2-CH4-H2S-N2 gas mixtures solubility in brine using a non-iterative fugacity-activity model relevant to CO2-MEOR: *Journal of Petroleum Science and Engineering*, v. 150, p. 162-179.
- , 2018, A fast and robust TOUGH2 module to simulate geological CO2 storage in saline aquifers: *Computers & Geosciences*, v. 111, p. 58-66.
- , 2019, TOUGHREACT-CO2Bio – A new module to simulate geological carbon storage under biotic conditions (Part 1): The multiphase flow of CO2-CH4-H2-H2S gas mixtures: *Journal of Natural Gas Science and Engineering*, v. 63, p. 85-94.
- Shaffer, D. L., Arias Chavez, L. H., Ben-Sasson, M., Romero-Vargas Castrillón, S., Yip, N. Y., and Elimelech, M., 2013, Desalination and Reuse of High-Salinity Shale Gas

- Produced Water: Drivers, Technologies, and Future Directions: Environmental Science & Technology, v. 47, no. 17, p. 9569-9583.
- Silva, C., Smith, B. J., Ray, J. T., Derby, J. R., and Gregg, J. M., 2020, Diagenesis of Hunton Group Carbonates (Silurian) West Carney Field, Logan and Lincoln Counties, Oklahoma, U.S.A: Midcontinent Geoscience, v. 1, p. 30-51.
- Smith, A. H., Lopipero, P. A., Bates, M. N., and Steinmaus, C. M., 2002, Arsenic epidemiology and drinking water standards, Volume 296, American Association for the Advancement of Science, p. 2145-2146.
- Srivastava, N. K., and Majumder, C. B., 2008, Novel biofiltration methods for the treatment of heavy metals from industrial wastewater: Journal of Hazardous Materials, v. 151, no. 1, p. 1-8.
- Steeffel, C. I., and Lasaga, A. C., 1994, A coupled model for transport of multiple chemical species and kinetic precipitation/dissolution reactions with application to reactive flow in single phase hydrothermal systems: American Journal of Science, v. 294, no. 5, p. 529.
- Stumm, W., 1992, Chemistry of the Solid-Water Interface: Processes at the Mineral-Water and Particle-Water Interface in Natural Systems, Wiley.
- Stumm, W., and Morgan, J. J., 1996, Aquatic Chemistry (3rd ed.). New York, Wiley-Interscience. Chaps 3 and 4. Detailed systematics of acid-base reactions, the carbonate system, and alkalinity titrations.
- Tabatabaefar, A., Yuan, Q., Salehpour, A., and Rajabi-Hamane, M., 2020, Batch adsorption of lead (II) from aqueous solution onto novel polyoxyethylene sorbitan monooleate/ethyl cellulose microfiber adsorbent: kinetic, isotherm and

- thermodynamic studies.: *Separation Science and Technology*, , v. 55(6), pp.1051-1061.
- Temple, B. J., Bailey, P. A., and Gregg, J. M., 2020, Carbonate Diagenesis Of The Arbuckle Group North Central Oklahoma To Southeastern Missouri., p. 10-30.
- Tesoriero, A. J., and Pankow, J. F., 1996, Solid solution partitioning of Sr²⁺, Ba²⁺, and Cd²⁺ to calcite: *Geochimica et Cosmochimica Acta*, v. 60, no. 6, p. 1053-1063.
- Thompson, J. B., and Ferris, F. G., 1990, Cyanobacterial precipitation of gypsum, calcite, and magnesite from natural alkaline lake water.: *Geology* v. 18, 995e998.
- Thompson, J. B., Schultze-Lam, S., Beveridge, T. J., and Des Marais, D. J., 1997, Whiting events: Biogenic origin due to the photosynthetic activity of cyanobacterial picoplankton.: *Limnol. Oceanogr.*, v. 42, 133e141.
- Tucker, M. E., and Wright, V. P., 2009, *Carbonate Sedimentology*, Wiley.
- Van Cappellen, P., Charlet, L., Stumm, W., and Wersin, P., 1993, A surface complexation model of the carbonate mineral-aqueous solution interface: *Geochimica et Cosmochimica Acta*, v. 57, no. 15, p. 3505-3518.
- Verrecchia, E. P., and Le Coustumer, M. N., 1996, Occurrence and genesis of palygorskite and associated clay minerals in a Pleistocene calcrete complex, Sde Boqer, Negev Desert, Israel.: *Clay Miner.*, , v. 31, 183–202.
- Vilcáez, J., 2020, Reactive transport modeling of produced water disposal into dolomite saline aquifers: Controls of barium transport: *Journal of Contaminant Hydrology*, v. 233, p. 103600.
- Vilcáez, J., York, J., Youssef, N., and Elshahed, M., 2018, Stimulation of methanogenic crude oil biodegradation in depleted oil reservoirs: *Fuel*, v. 232, p. 581-590.

- Watts, P., England, S., and Howe, P., 2010, Strontium and strontium compounds: World Health Organization, 1020-6167.
- Watts, P., and Howe, P., 2010, Strontium and strontium compounds, World Health Organization, v. 77.
- Wei, H., Shen, Q., Zhao, Y., Wang, D. J., and Xu, D. F., 2003, Influence of polyvinylpyrrolidone on the precipitation of calcium carbonate and on the transformation of vaterite to calcite. : Journal of Crystal Growth, , v. 250(3-4), pp.516-524.
- Wolery, T. J., Jackson, K. J., Bourcier, W. L., Bruton, C. J., Viani, B. E., Knauss, K. G., and Delany, J. M., 1990, Current Status of the EQ3/6 Software Package for Geochemical Modeling, Chemical Modeling of Aqueous Systems II, Volume 416, American Chemical Society, p. 104-116.
- Xu, T., Sonnenthal, E., Spycher, N., and Pruess, K., 2006, TOUGHREACT—A simulation program for non-isothermal multiphase reactive geochemical transport in variably saturated geologic media: Applications to geothermal injectivity and CO₂ geological sequestration: Computers & Geosciences, v. 32, no. 2, p. 145-165.
- Yamkate, N., Chotpantarat, S., and Sutthirat, C., 2017, Removal of Cd²⁺, Pb²⁺, and Zn²⁺ from contaminated water using dolomite powder: Human and Ecological Risk Assessment: An International Journal, v. 23, no. 5, p. 1178-1192.
- Yost, E. E., Stanek, J., DeWoskin, R. S., and Burgoon, L. D., 2016, Overview of Chronic Oral Toxicity Values for Chemicals Present in Hydraulic Fracturing Fluids, Flowback, and Produced Waters: Environmental Science & Technology, v. 50, no. 9, p. 4788-4797.

Zielinski, R. A., and Budahn, J. R., 2007, Mode of occurrence and environmental mobility of oil-field radioactive material at US Geological Survey research site B, Osage-Skiatook Project, northeastern Oklahoma: *Applied Geochemistry*, v. 22, no. 10, p. 2125-2137.

CHAPTER III

ROLE OF ALKALINITY AND DOLOMITE REACTIVITY ON TOXIC METALS REMOVAL FROM PETROLEUM PRODUCED WATER BY DOLOMITE

3.1. Abstract

Most available information on toxic metals removal by dolomite corresponds to trace concentrations (< 1 mg/L) of toxic metals at salinity and alkalinity levels of fresh and seawater. We conducted batch reaction experiments to elucidate the role of alkalinity and reactivity of dolomite on the removal of high concentrations (100 mg/L) of toxic metals (Ba, Sr, Cd, Pb, and As) commonly present in petroleum produced water (PW) at salinity and alkalinity levels of PW. Our results indicate that under alkalinity and salinity levels of PW, the removal of Ba, Sr, and Cd from PW is mostly due to sorption reactions, with sorption reactions and thus removal levels being higher for Cd than for Ba and Sr. In contrast, the removal of Pb and As is largely due to precipitation and coprecipitation reactions on dolomite. Under close to zero alkalinity conditions, the precipitation of toxic metals as carbonate minerals relies on alkalinity generated from the dissolution of dolomite. Ba, Sr, and Cd removal by dolomite is 10, 2, and 4 times, respectively, smaller in PW than in freshwater (FW), while As removal is practically the same regardless of salinity, and Pb is practically insoluble in FW. The composition of precipitated carbonate minerals corresponds to the chemical composition of PW. As such, the complexity of the

precipitated carbonate minerals increase with increasing the number toxic metals in solution. The effect of salinity on sorption reactions as well as the effect of dolomite dissolution on alkalinity can be captured by sorption complexation model and kinetic model equations. However, this study reveals the need of thermodynamic data of complex carbonate minerals to capture the effect of alkalinity on the removal of toxic metals from PW by dolomite.

3.2. Introduction

Conventional and unconventional oil and gas industries produce gigantic amounts of wastewater, commonly called produced water (PW). This wastewater is characterized by high concentrations of total dissolved solid (TDS), dissolved organic matter such as hydrocarbons, and dissolved gases such as carbon dioxide and hydrogen sulfide. TDS mainly consists of chlorine, carbonate, sulfate, and hydroxide salts associated with heavy metal, metalloid, and alkaline earth metal ions, as well as naturally occurring radioactive materials (NORM). Contrary to dissolved organic matter and gases, heavy metals, metalloids, and some alkaline earth metal ions are not biodegradable, and they tend to accumulate in the soil and living tissue causing serious health problems in both animals and humans (Tabatabaefar et al., 2020). Notably, the concentration of toxic metals in PW can be orders of magnitude higher than in shallow groundwater and seawater. Their concentrations greatly exceed the maximum contaminant levels (MCLs) of drinking water standards imposed by the U.S. Environmental Protection Agency (EPA). Therefore, and for economic motives, PW is usually disposed into deep saline aquifers. However, the injection of huge volumes of PW into geologic units induces seismicity episodes even in regions that are not tectonically active, raising the prospect of undersurface drinking water

(USDW) contamination due to the possible upward migration of PW through induced or naturally occurring faults, fractures, and abandoned wells.

To prevent the risk of USDW contamination, in previous studies we investigated the fate and transport of a representative toxic metal (Ba) in dolomite saline aquifers (Ebrahimi and Borrok, 2020; Ebrahimi and Vilcáez, 2018a, b, 2019a; Vilcáez, 2020) as well as the feasibility of using dolomite as filtration media to remove toxic heavy metals, alkaline earth metals, and metalloids from PW (Omar and Vilcáez, 2022). Different from previous studies which focused on relatively low concentrations (<1 mg/L) of toxic metals (e.g., Zn, Cu, and As (V)) commonly present in shallow groundwater systems (TDS < 1,000 mg/L), our studies focus on the reactive transport of high concentrations (~100 mg/L) of toxic heavy metals, alkaline earth metals, and metalloids commonly present in PW (TDS = 40,000-120,000 mg/L). The results of our previous studies suggest that the competition of cations for hydration sites of dolomite and complexation reactions of metals and chlorine ions control the removal of toxic metals from PW by dolomite. Moreover, they revealed higher removal levels of Pb and Cd than Ba, Sr, and As, as well as a different affinity sequence of Ba and Sr at high and low salinity levels (Brown and Parks, 2001b; Omar and Vilcáez, 2022). However, the role of alkalinity and dolomite reactivity on toxic metals removal from high salinity waters (e.g., PW) has not been assessed before. Alkalinity is a critical parameter for describing the composition, pH behavior, buffer capacity, and precipitation potential of cations (scaling) in waters from the oil and gas industry (Kaasa and Østvold, 1996). Water alkalinity is the equivalent sum of the bases that are titratable with strong acids (Stumm and Morgan, 1996). In most natural waters, alkalinity is the sum

of $m\text{HCO}_3^-$ and $2m\text{CO}_3^{2-}$ ions because they are the predominated anions compared to other anion species such as OH^- (Drever, 1997).

Alkalinity concentrations are generally greater in PW than in freshwater (FW). For instance, the alkalinity of FW (TDS of 105-931 mg/L) and brackish water (TDS of 1,037-6900 mg/L) in Oklahoma is typically around 20-250 mg/L (Ribeiro et al., 2021), whereas, alkalinity concentrations in PW from conventional natural gas, conventional oil, shale gas, and coal-bed methane deposits in the continental U.S. has been reported to be 0-285 mg/L, 300-380 mg/L, 160-188 mg/L, and 55-9,450 mg/L, respectively (Alley et al., 2011). Considering the relatively high concentrations of alkalinity in PW, and that dolomite dissolution has been reported as an important factor in the formation of new minerals (Holail and Al-Hajari, 1997; Ingles and Anadon, 1991; Ryan et al., 2019; Verrecchia and Le Coustumer, 1996), the possibility of precipitation and/or coprecipitation of toxic heavy metals, alkaline earth metals, and metalloids present in PW as carbonate minerals in dolomite cannot be discarded. Several studies have been conducted to understand the precipitation of metals as carbonate minerals from seawater (Brown and Parks, 2001b) and freshwater (Alexandratos et al., 2007; Da'ana et al., 2021; Jensen, 2020; Lin et al., 2013; Tesoriero and Pankow, 1996) in different rock and soil materials. From those studies, it is known that carbonate mineral precipitates (e.g., calcite, magnesite, and siderite) can incorporate trace metal cations from seawater and that carbonate minerals precipitation can effectively sequester As from groundwater, for instance. Many other studies have focused on microbial-induced carbonate minerals precipitation (Chen et al., 2021; Kumari et al., 2016). It is known from those studies that bio-precipitation of carbonates can result in the elimination of Pb, Sr, and Cd from freshwater (Kim et al., 2021). Considering these

findings, we hypothesize that in addition and/or in parallel to sorption reactions, and depending on the pH and alkalinity, precipitation and/or coprecipitation reactions can contribute to the removal of toxic heavy metals, alkaline earth metals, and metalloids as carbonate minerals from PW in natural or artificial dolomite porous media. This includes deep dolomite aquifers where PW is commonly disposed as well as engineered dolomite filters made of packed dolomite grains.

To elucidate the role of alkalinity and dolomite reactivity on toxic metals removal from PW by dolomite and to determine the contribution of carbonate minerals precipitation on the observed removal levels of Ba, Sr, Cd, Pb, and As by dolomite (Omar and Vilcaez, 2021), here we conduct batch reaction experiments using synthetic PW and FW of different alkalinity and toxic metals content but same Ca, Mg, and NaCl content. The approach consists of analyzing changes in the morphology and elemental and mineral composition of the dolomite surface due to precipitation/dissolution sorption/desorption reactions. For the sake of simplicity, the toxic heavy metals, alkaline earth metals, and metalloids studied in this work (Ba, Sr, Cd, Pb, and As) are called toxic metals from this point on in this article.

3.2. Materials

3.2.1. Dolomite

Dolomite was collected from the Arbuckle Group outcrop in southwest Missouri, U.S. The dolomite sample was analyzed via Powder X-ray Diffractometer (Bruker XRD D8 ADVANCE Plus). The results confirmed that sample was composed of 98% dolomite and 2% of both blocky calcite cement and amorphous silica. The XRD spectrum distinguished dolomite-structure (JCPDS: 79-1342) from calcite-structure (JCPDS: 86-

2334) minerals. The XRD spectrum displayed the highest intensity of 104 (>2500 counts) at $31^\circ 2\Theta$ as well as strong dolomite cation (e.g., Mg and Ca) ordering peaks (101, 015, and 021 at $22^\circ 2\Theta$, $35^\circ 2\Theta$, and $44^\circ 2\Theta$, respectively) confirming that the samples were near perfect dolomite and suggesting that the collected dolomite had near stoichiometric composition (Mg/Ca~1) (Fig. 3.1).

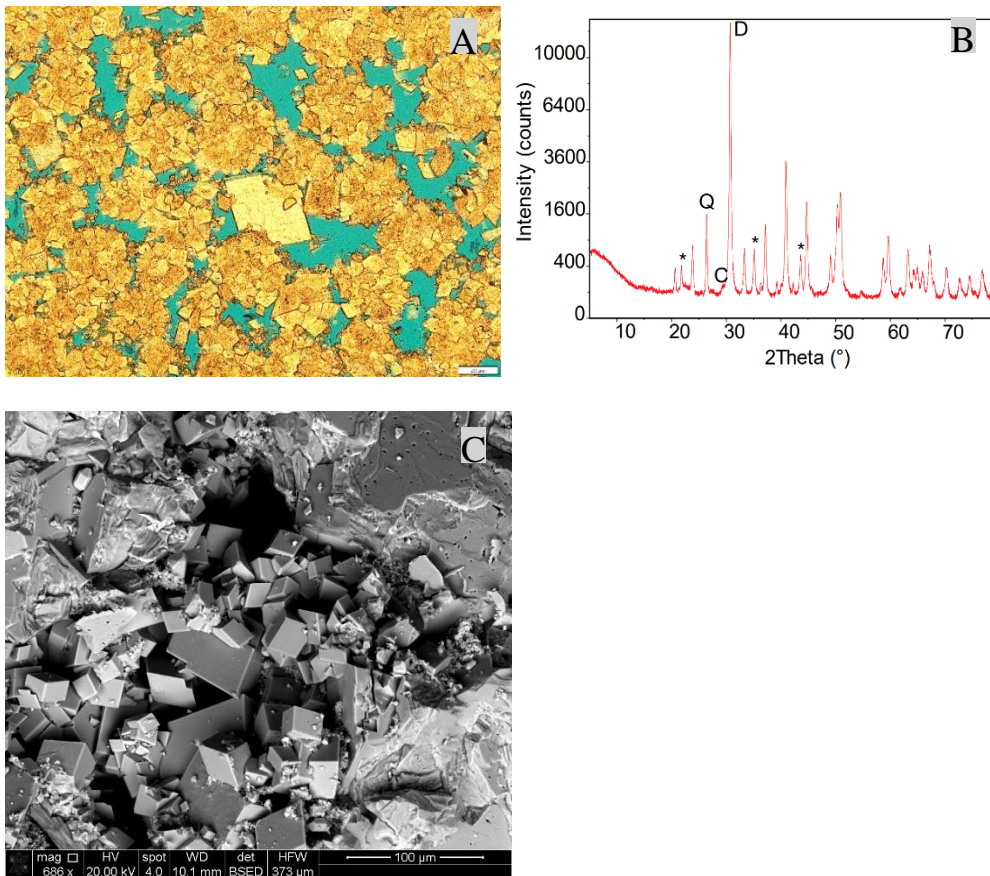


Fig. 3.1. A) Thin section (scale bare = 200 μm) showing shape and size of dolomite crystals, B) XRD analysis showing that the employed dolomite is mainly composed of dolomite (represented by D only on the 104-dolomite peak) with minor quantities of quartz and calcite cement (represented by Q only on the 101-quartz peak, and C only on 104-calcite peak which is very weak). Dolomite cations (e.g., Mg & Ca) ordering reflections are indicated by asterisks on 101, 015 and 021 dolomite peaks. C) SEM micrograph showing the shape and size of dolomite crystals as well as porosity.

3.2.2. Dolomite grains

The collected dolomite was crashed and sieved multiple times to obtain dolomite grains of uniform size (300 - 600 μm). The obtained dolomite grains were washed with ultrapure deionized water in an ultrasonic bath to remove dust particles from the grain surfaces. Then, the dolomite grains were dried at room temperature and characterized by XRD and SEM analyses.

3.2.3. Synthetic produced water

Produced water has very complex chemistry and a detailed compositional analysis is quite challenging due to its high TDS content (Emmons et al., 2022). Since TDS in PW is mostly composed of chloride and carbonate salts, synthetic PW of different alkalinity (HCO_3^- and CO_3^{2-}) and toxic metals content but the same Ca, Mg, and NaCl content was prepared by adding NaCl, $\text{CaCl}_2 \cdot 2\text{H}_2\text{O}$, $\text{MgCa}_2 \cdot 6\text{H}_2\text{O}$, $\text{SrCa}_2 \cdot 6\text{H}_2\text{O}$, $\text{BaCa}_2 \cdot 2\text{H}_2\text{O}$, $\text{CdH}_8\text{N}_2\text{O}_{10}$, PbCl_2 , and AsCl_3 (Fisher Scientific Co. with the purity of >99.9%) to ultrapure deionized water (Table 3.1). TDS of the prepared synthetic PW was 68,000-75,000 mg/L. To determine the effect of salinity, synthetic freshwater (FW) was prepared and used to conduct the same experiments as with synthetic PW. TDS of the prepared synthetic FW was <2,000 mg/L and contained the same salts as the synthetic PW (Table 3.2). The initial alkalinity of the prepared synthetic PW and FW, that results from the dissolution of atmospheric CO_2 , was increased by adding CaCO_3 . To ensure the total dissolution of the added salts, the prepared synthetic PW and FW were stirred for 24 h, and possible undissolved particles in the prepared synthetic PW and FW were removed by filtration using a 0.4 μm cellulose filter.

Seven types of synthetic PW and FW were prepared. PW and FW types I-V contained only one toxic metal, and they were all added with CaCO₃ to increase alkalinity. PW and FW type VI contained all toxic metals, and it was added with CaCO₃ to increase alkalinity, whereas PW and FW type VII contained all toxic metals, but they were not added with CaCO₃ to increase alkalinity (Tables S1 and S2). The resulting concentrations of Ca and Mg in the synthetic PW correspond to PW in Oklahoma (Ribeiro et al., 2021) and U.S. Mid Continent (Guerra et al., 2011c). Concentrations of sulfate in PW are negligible in these regions. Therefore, the prepared synthetic PW and FW did not contain dissolved sulfate. Arsenite (As(III)) salt (AsCl₃) was used instead of arsenate (As(V)) because PW originates under reduced conditions and the oxidation of arsenite to arsenate by dissolved oxygen is very slow (Dixit and Hering, 2003). For the sake of comparisons, the initial concentrations of metals and metalloids (Ca, Mg, Cd, Pb, Sr, Ba, and As) were kept the same in all types of synthetic PW and FW used to conduct the experiments.

Table 3.1. Added salts to prepare synthetic produced water (PW) of different compositions.

Salts (g/L)	Types of produced waters						
	I	II	III	IV	V	VI	VII
NaCl	40	40	40	40	40	40	40
CaCO ₃	5	5	5	5	5	5	0
CaCl ₂ .2H ₂ O	14.7	14.7	14.7	14.7	14.7	14.7	25.7
MgCl ₂ .6H ₂ O	8.4	8.4	8.4	8.4	8.4	8.4	8.4
BaCl ₂ .2H ₂ O	0.18					0.178	0.178
SrCl ₂ .6H ₂ O		0.3				0.304	0.304
CdH ₈ N ₂ O ₁₁			0.27			0.274	0.274
PbCl ₃				0.132		0.132	0.132
AsCl ₃					0.241	0.241	0.241
TDS	68.3	68.4	68.4	68.2	68.3	69.2	75.2

Table 3.2. Composition of the types of freshwater (FW) used for experiments.

Salts (g/L)	Types of freshwaters						
	I	II	III	IV	V	VI	VII
NaCl	0.1038	0.1024	0.1072	0.1047	0.1047	0.1018	0.1054
CaCO ₃						0.35	0
CaCl ₂ .2H ₂ O	0.1805	0.1602	0.1602	0.1607	0.1607	0	0.1577
MgCl ₂ .6H ₂ O	0.196	0.2029	0.2029	0.2009	0.2009	0.1918	0.2041
BaCl ₂ .2H ₂ O	0.178					0.1786	0.1779
SrCl ₂ .6H ₂ O		0.3031				0.3048	0.3045
CdH ₈ N ₂ O ₁₁			0.2734			0.2651	0.2723
PbCl ₃				0.135		0.1351	0.1343
AsCl ₃					0.241	0.241	0.241
TDS	0.6583	0.7686	0.7437	0.6013	0.7073	1.7682	1.5972

3.3. Methods

3.3.1. Batch experiments

Tables 3.3 and 3.4 show the measured alkalinity, initial pH, and composition of all types of synthetic PW and FW used to conduct the batch reaction experiments. All experiments were conducted in duplicate. An amount of 100 mL of each type of synthetic PW or FW was added to 250 mL flasks containing 40 g of dolomite grains. The flasks were placed in an orbital shaking incubator operating at 80 orbits/min. Temperature was fixed at 25 °C. Samples of 1.5 mL were carefully taken hourly for 70 hours, and their composition was analyzed at the Soil, Water, and Forage Analytical Laboratory (SWFAL) of Oklahoma State University (OSU). The analysis included the measurement of all heavy metals, alkaline earth metals, and metalloids (Na, Ca, Mg, Ba, Sr, Cd, Pd, and As), chloride (Cl⁻), as well as pH, and alkalinity (HCO₃⁻ and CO₃²⁻). The concentration of Na, Ca, Mg, Ba, Sr, Cd, Pb, and As were measured by ICP-OES analysis. Alkalinity was measured by

the titration method using a Hach TitraLab AT1000 Series auto-titrator with an autosampler. This method involves the titration of samples with standard 0.02N sulfuric acid (H₂SO₄) titrant to endpoints of pH 8.3 and 4.5. The pH endpoint of 8.3 corresponds to carbonate alkalinity, whereas the pH endpoint of 4.5 corresponds to bicarbonate alkalinity. Chloride was measured by the colorimetric method using ferricyanide in a flow-injection analyzer (Ballinger, 1979; Federation and Aph Association, 2005). Once an equilibrium condition was reached, reflected by a constant pH, dolomite grains were collected and then analyzed by the XRD and SEM-EDS analyses to determine changes in the morphology as well as the elemental and mineral composition of the dolomite surface due to precipitation/dissolution and sorption/desorption reactions.

Table 3.3. Initial composition of the synthetic produced waters (PW) used for experiments.

(mg/L)	Type of produced water (PW)						
	I	II	III	IV	V	VI	VII
Na	15,647.2	17,667.5	18,538.3	18,211.5	17,802.2	17,740.2	18,112.0
Cl	29,996.7	31,305.7	33,926.7	31,656.0	31,070.0	29,385.5	29,938.5
Ca	4,074.9	4,388.2	4,520.9	4,424.2	4,796.7	4,663.8	4,445.6
Mg	9,41.96	1,020.1	1,045.0	1,047.9	1039.8	1,077.0	1,023.7
Ba	92.31					87.88	94.13
Sr		95.0				97.65	98.09
Cd			72.68			68.21	88.47
Pb				85.64		85.64	95.11
As					99.26	91.98	105.25
Alkalinity	11.28	12.16	11.07	16.45	58.42	98.86	0.00*

pH 8.25 8.88 7.98 6.63 6.81 6.64 2.39

*Below detection limit.

Table 3.4. Initial composition of the synthetic freshwaters (FW) used for experiments.

(mg/L)	Type of freshwater (FW)						
	I	II	III	IV	V	VI	VII
Na	26.58	24.92	27.15	26.42	23.98	26.00	26.89
Cl	235.55	272.17	185.42	219.77	344.54	431.17	535.75
Ca	42.87	42.54	39.42	41.35	43.80	107.25	41.96
Mg	10.77	12.12	11.08	10.89	12.50	10.51	11.57
Ba	96.65					97.81	98.73
Sr		97.40				100.79	100.89
Cd			95.29			90.51	97.93
Pb				90.71		0.20	100.67
As					105.18	104.12	103.59
Alkalinity	2.39	4.22	2.20	3.86	0.00*	15.29	0.00*
pH	6.41	5.89	5.63	5.30	2.58	6.36	2.57

*Below detection limit.

3.3.2. Surface morphology and composition analyses

Sorption reactions of cations on minerals is due to physical, electrostatic, and chemical interactions (Drever, 1997). Physical interactions are the attraction between ions and mineral surfaces due to Van Der Waals forces. Whereas electrostatic interactions are the attraction of cations and negatively charged sites on mineral surfaces. Chemical

interactions are chemical bonds between ion molecules and one or more atoms on mineral surfaces. Generally, sorption reactions are the most important interactions affecting the transport of contaminants in groundwater. Therefore, understanding these interactions (physical, electrostatic, and chemical) is important to predict the fate and transport of toxic metals in deep dolomite saline aquifers (where PW is commonly disposed) as well as in filtration materials such as filters made of dolomite grains. However, sorption reactions are not the only possible water-rock reactions that can result in the removal or retardation in the transport of toxic metals in groundwater. Precipitation reactions can also sequester toxic metals into carbonate, silicate, and sulfate mineral and/or salt phases. Precipitation reactions occur due to the changes in the saturation index of dissolved species in the aqueous solutions. In natural carbonate systems, precipitation of metals as a carbonate phase can occur through direct precipitation and/or dissolution/precipitation reactions controlled by thermodynamic (e.g., salts saturation levels, alkalinity, and ionic strength) and kinetic factors (Balci et al., 2018; Thompson and Ferris, 1990; Thompson et al., 1997). Phases of calcium carbonate, for instance, in surface and subsurface environments range from amorphous to crystalline and from anhydrous (e.g., calcite, aragonite, and vaterite) to hydrated (e.g., monohydrocalcite ($\text{CaCO}_3 \cdot \text{H}_2\text{O}$) and ikaite ($\text{CaCO}_3 \cdot 6\text{H}_2\text{O}$)) phases (Anthony et al., 2007; Fukushi et al., 2011).

The methods we used to analyze the changes in the elemental and mineral composition of dolomite surface due to precipitation/dissolution and sorption/desorption reactions of toxic metals consisted of X-ray Powder Diffraction (XRD) and Scanning Electron Microscopy-Dispersive X-ray Spectroscopy (SEM-DES) analyses of dolomite surface. The removal of toxic metals from PW and FW was determined by Inductively

Coupled Plasma-Optical Emission Spectroscopy (ICP-OES) analysis of metals in the aqueous phase. In this study, XRD is used to determine the nature of the toxic metals precipitates on dolomite grains (Wei et al., 2003) whereas SEM-DES is used to map the elemental composition of sorbed and precipitated elements on dolomite (Alexandratos et al., 2007).

High-resolution XRD analyses were conducted on pulverized dolomite grains at the OSU Microscopy Laboratory using a Bruker D8 ADVANCE Plus XRD. The obtained XRD data were semi-quantitatively analyzed via DIFFRAC.EVA software. Dolomite samples were dried but not pulverized for SEM-EDS analysis. This analysis was performed at the OSU Microscopy Laboratory using a SEM FEI Quanta 600 field emission gun ESEM with Bruker EDS and HKL EBSD. Samples for SEM-EDS analysis were coated with carbon (graphite) to prevent artifacts and to optimize the quality of the images. To avoid missing any relevant features and to enhance the generated results, SEM-EDS mapping was performed at different magnification scales (e.g., 1 mm, 100 μm , and 10 μm). XRD and SEM-EDS analyses were done on dolomite grains collected at the beginning and end of the batch experiments, and the results were compared to identify changes.

3.4. Results and discussion

3.4.1. Batch reaction experiments

Batch reaction experiments were designed to elucidate the contribution of precipitation and sorption reactions to the removal of toxic metals from PW and FW by dolomite, as well as to assess the reaction kinetics and removal levels of individual and mixed toxic metals from PW and FW by dolomite. To this aim, we measured the

concentration profiles of toxic metals in solution over time and analyzed the mineral and elemental composition of dolomite grains at the beginning and end of each batch experiment. Experiments were conducted using synthetic PW and FW of different initial compositions (Tables 3.3 and 3.4) until an equilibrium condition reflected by a constant pH was reached.

Table 3.5 Toxic metals removal from PW of different compositions, initial pH, and alkalinity (see Table 3.3)

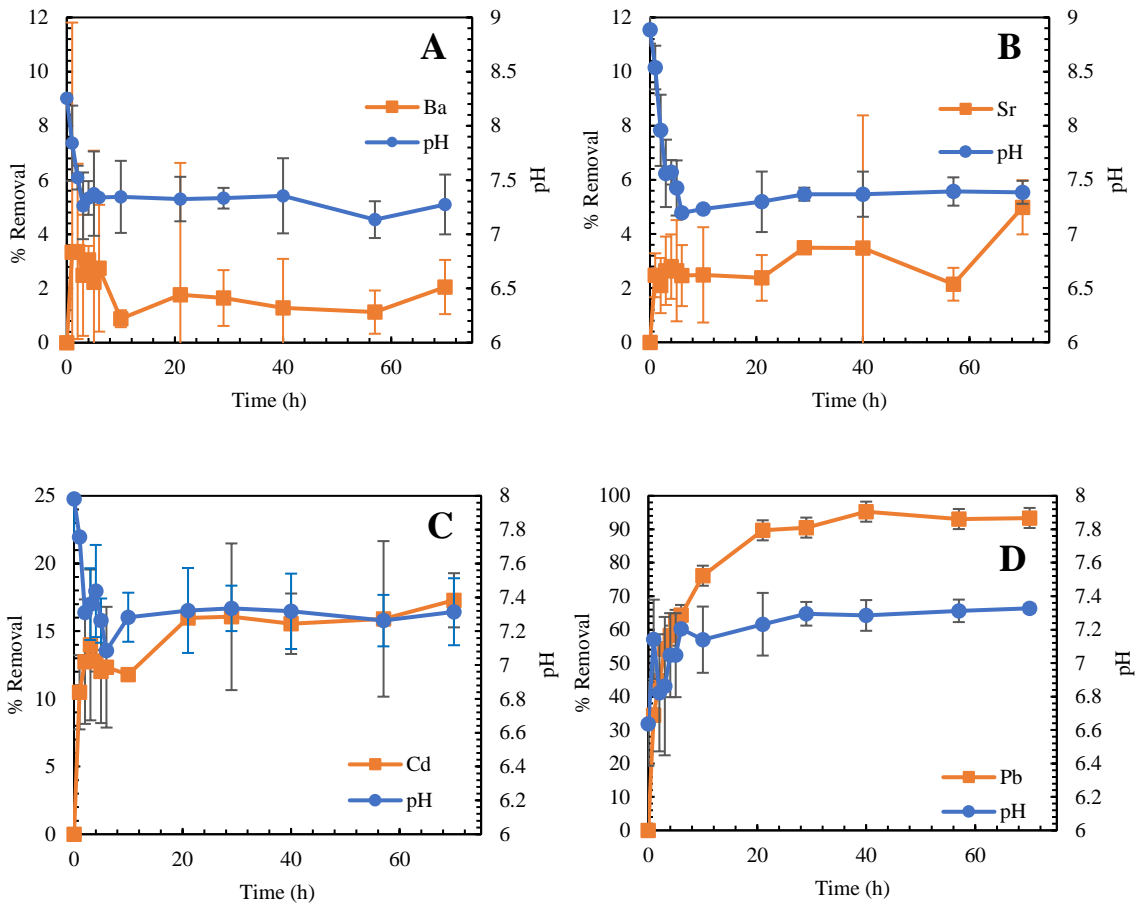
	Type of produced water (PW)						
	I	II	III	IV	V	VI	VII
Final pH	7.08	7.38	7.31	7.32	7.45	7.61	7.26
Alkalinity increment (mg/L)	15.16	13.62	12.77	10.58	-22.34	-43.77	23.24
Ba removal (%)	2.05					3.61	2.1
Sr removal (%)		4.90				3.72	1.28
Cd removal (%)			17.29			15.16	8.19
Pb removal (%)				93.39		98.48	96.16
As removal (%)					4.75	12.57	17.73

Table 3.6 Toxic metals removal from FW of different compositions, initial pH, and alkalinity (see Table 3.4)

	Types of produced water (FW)						
	I	II	III	IV	V	VI	VII
Final pH	7.58	7.96	7.05	7.83	8.06	7.1	6.83
Alkalinity increment (mg/L)	47.80	43.90	3.90	42.20	43.80	-4.00	8.20
Ba removal (%)	22.02					12.19	5.54

Sr removal (%)	8.94	6.08	2.06	
Cd removal (%)	68.20	63.68	38.29	
Pb removal (%)	99.78	N/A*	99.48	
As removal (%)		5.48	4.68	15.07

*Solubility of Pb in FW type V was practically zero.



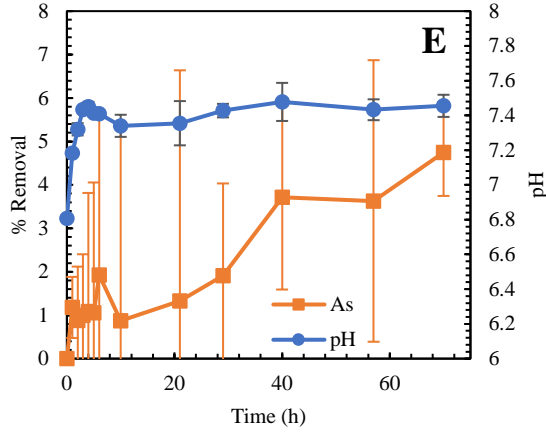
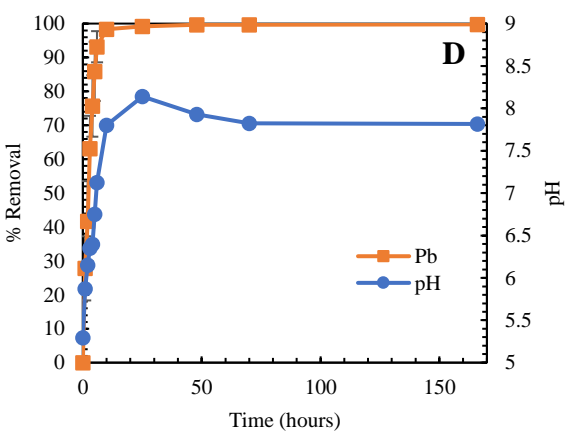
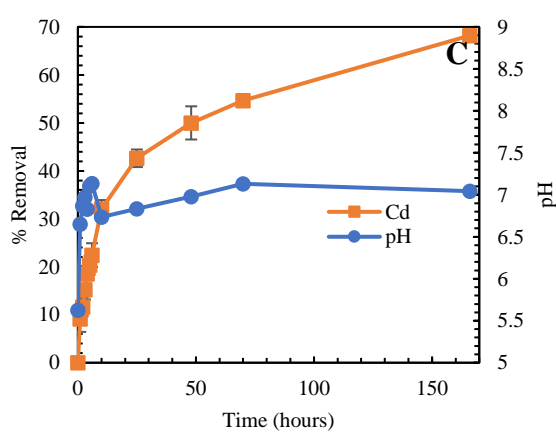
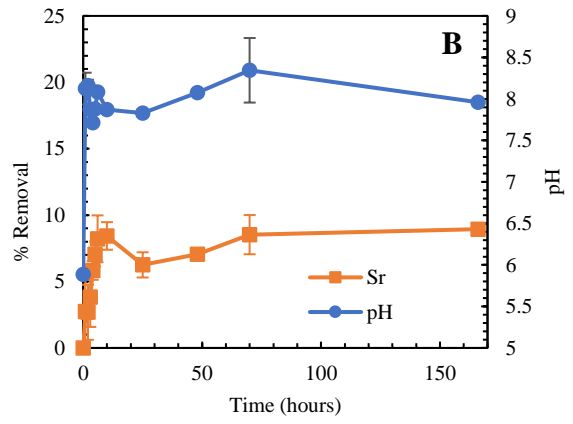
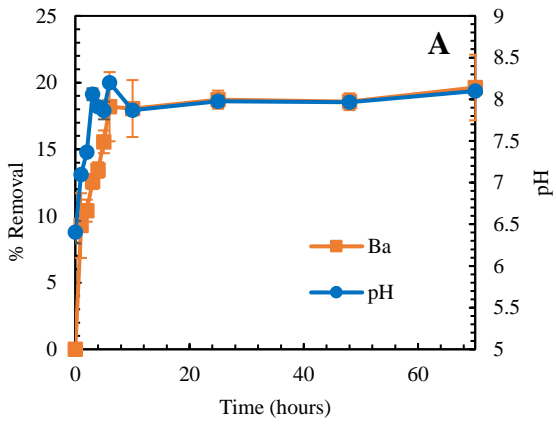


Fig. 3.2. Batch experimental results of single metals removal by dolomite from PW: A) Ba (PW type I); B) Sr (PW type II); C) Cd (PW type III); D) Pb (PW type IV); and E) As (PW type V). All were supplied with CaCO_3 to increase the initial alkalinity (Table 3.3).



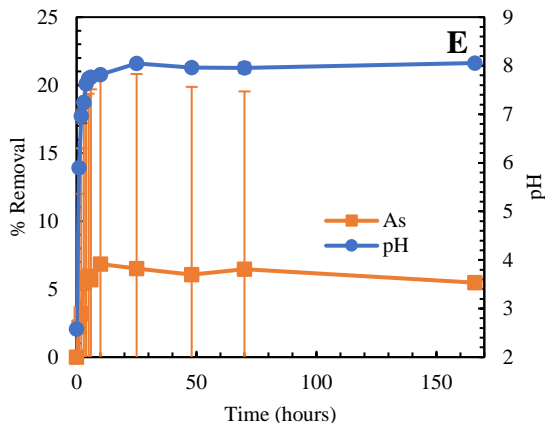


Fig. 3.3. Batch experimental results of individual toxic metals removal by dolomite: A) Ba (FW type I); B) Sr (FW type II); C) Cd (FW type III); D) Pb (FW type IV); and E) As (FW type V). All were supplied with CaCO_3 to increase the initial alkalinity.

Fig. 3.2 shows Ba, Sr, Cd, Pb, and As removal and pH profiles over time obtained using PW types I-V (Table 3.3), which contained single toxic metals. During the first 6 hours, pH decreases from 8.2 to 7 concomitantly with Ba concentration in solution. However, Ba concentration in solution rebounds after the first 6 hours reaching a constant Ba removal level of about 2% after 72 hours. pH remains practically constant after 6 hours (Fig. 3.2A). Apparently, a fast decrease in Ba concentration in solution and pH is due to both sorption and precipitation reactions. Alkaline pH is known to promote sorption reactions of metals, and pH should have increased due to the dissolution of dolomite if carbonate ions (alkalinity) had not precipitated. A subsequent rebound of Ba concentration in solution is most likely due to an increase of Ca and Mg concentrations due to the dissolution of dolomite. Ca and Mg are known to compete for hydration sites of dolomite with metal cations such as Ba.

Similar behavior of Ba (Fig. 3.2A) is observed with Sr (Fig. 3.2B), though the removal levels at equilibrium conditions are higher for Sr (5%) than for Ba (2%). Like with Ba and Sr, pH decreases with Cd removal from an alkaline pH to a close to neutral pH due to sorption and possibly precipitation reactions (Fig. 3.2C). However, different from Ba

and Sr whose removal are relatively small, the removal level of Cd at equilibrium conditions reaches 15% and the rebound of Cd concentration in solution after the initial stages of the reaction (when Cd removal is highest) is less pronounced than with Ba and Sr. Suggesting that sorption reactions are more prominent for Cd than for Ba and Sr. If Cd precipitation reactions were more prominent than sorption reactions, lower alkalinity levels would have been observed with Cd than with Ba and Sr. Conversely, the initial and final alkalinity levels for Ba, Sr, and Cd as well as final pH are practically the same (Table 3.5).

Much higher removal levels were attained for Pb (93.39%) (Fig. 3.2D) than for Ba (2%), Sr (5%), and Cd (15%). Different from the concentration profiles observed with Ba, Sr, and Cd where a fast decrease of their concentrations during the early stages of the reaction is followed up by a rebound of their concentrations in solution, the concentration of Pb in solution gradually decreases over time by 93.39%, and the initial pH, which was slightly acidic, increased gradually to ~7.3 (equilibrium pH). This behavior suggests that Pb sorption on dolomite is controlled by the dissolution of dolomite and that Pb precipitation as a carbonate mineral might play an important role. Note that the net increase of alkalinity for Pb due to the dissolution of dolomite is smaller with Pb than with Ba, Sr, and Cd (Table 3.5).

Fig 3.2E. shows As removal and pH profiles over time obtained using PW type 5 (Table 3.3). The higher initial alkalinity for PW type 5 than for the PW types I-IV was due to the formation of hydrochloric acid according to the following reaction: $\text{AsCl}_3 + 3\text{H}_2\text{O} = \text{As}(\text{OH})_3 + 3\text{HCl}$. The formed acid resulted in a pH of ~2 before adding CaCO_3 . This acidic pH facilitated the dissolution of the supplied CaCO_3 resulting in a pH of 6.8 and an initial alkalinity of 58.2 mg/L. Interestingly, alkalinity decreases instead of increasing despite the

dissolution of dolomite. This behavior suggests that As removal under the tested conditions takes place through the precipitation of As as a carbonate mineral. However, the removal level does not exceed 5%, suggesting that Ca and/or Mg precipitation might be the dominant precipitation reaction sequestering As. Analogous behavior has been observed in groundwater systems as implied by previous studies (Alexandratos et al., 2007; Da'ana et al., 2021; Jensen, 2020; Lin et al., 2013; Tesoriero and Pankow, 1996).

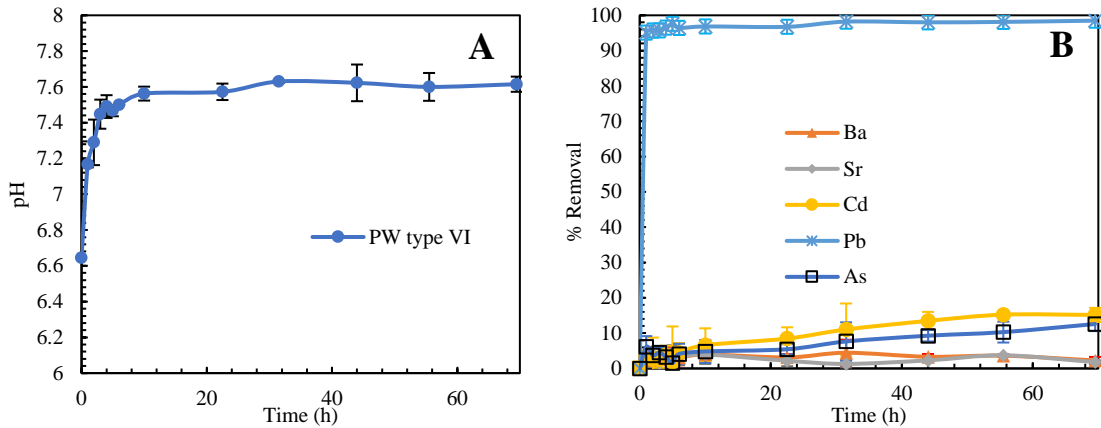


Fig. 3.4. Batch experimental results of mixed toxic metals removal by dolomite (PW type VI): A) pH profile; B) Toxic metals removal profile. PW type VI was supplied with CaCO_3 to increase the initial alkalinity (Table 3.3).

To detect possible reaction interferences, we conducted experiments using synthetic PW type VI, which contained mixed toxic metals (Ba, Sr, Cd, Pb, and As). Fig. 3.4 shows their removal and pH profiles over time. The initial alkalinity of PW type VI was 98.86 mg/L (Table 3.3). With this alkalinity, removal of Pb from solution (85.64%) happened practically instantaneously and the removal of As increased from 4.75% with an initial alkalinity of 58.2 mg/L (PW type V) to 12.57% with an initial alkalinity of 98.86 mg/L (PW type VI). The concentration profiles of the rest of the toxic metals follow the same trend as when their behavior was analyzed individually (Fig. 3.2). This behavior strongly supports the hypothesis that precipitation reactions and thus alkalinity play an

important role in the removal of Pb and As from PW, and that there are minor interferences between Ba, Sr, Cd, Pb, and As removal by dolomite at salinity and alkalinity levels of PW.

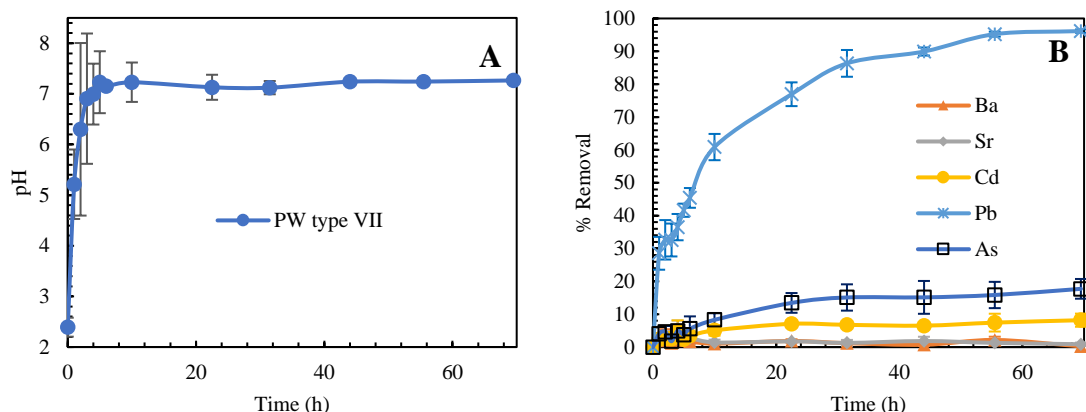


Fig. 3.5. Batch experimental results of mixed toxic metals removal by dolomite (PW type VII): A) pH profile; B) Toxic metals removal profile. PW type VII was not supplied with CaCO_3 to increase the initial alkalinity (Table 3.3).

To determine if the addition of CaCO_3 to increase alkalinity played a role in the observed removals of Ba, Sr, Cd, Pb, and As, we conducted experiments using synthetic PW type VII, which was not supplied with CaCO_3 . Fig. 3.5 shows Ba, Sr, Cd, Pb, and As removal and pH profiles over time obtained using PW type VII (Table 3.3). The initial pH was acidic due to the formation of hydrochloric acid. Different from the profiles obtained with PW type VI (Fig. 3.4) where Pb and As removal increase is relatively fast, the profiles displayed with PW type VII show Pb and As removal increase at slower rates. Slower removal rates of these two toxic metals support the hypothesis that precipitation/coprecipitation reactions of Pb and As as carbonate minerals contribute to the removal of Pb and As from PW more than to the removal of Ba, Sr, and Cd. Apparently, under low alkalinity conditions, the precipitation of toxic metals as carbonates relies on alkalinity generated from the dissolution of dolomite.

To elucidate a possible different response of toxic metals to alkalinity and dolomite reactivity at FW salinity levels, we conducted experiments using synthetic FW containing single (FW types I-V) and mixed (FW types VI and VII) toxic metals (Table 3.5). In accordance with previous studies showing that salinity (NaCl) inhibits sorption reactions, higher removal levels were obtained with FW for Ba (22.02%), Sr (8.94%), Cd (68.2%), Pb (99.78%), and As (5.48%) (Fig. 3.3 and Table 3.5). However, despite the same initial concentration of toxic metals and Ba removal increases ten times while Sr removal only increases two times due to the reduction of salinity. Moreover, interestingly As removal remains practically the same with PW and FW. The results highlight the different behavior of toxic metals in FW and PW. The inhibitory effect of salinity on sorption reactions is different depending on the type of toxic metal and initial alkalinity. Ba, Sr, and Cd removal decreases 10, 2, and 4 times by increasing salinity from ~6,00 mg/L to ~68,000 mg/L, while As removal is practically the same regardless of salinity.

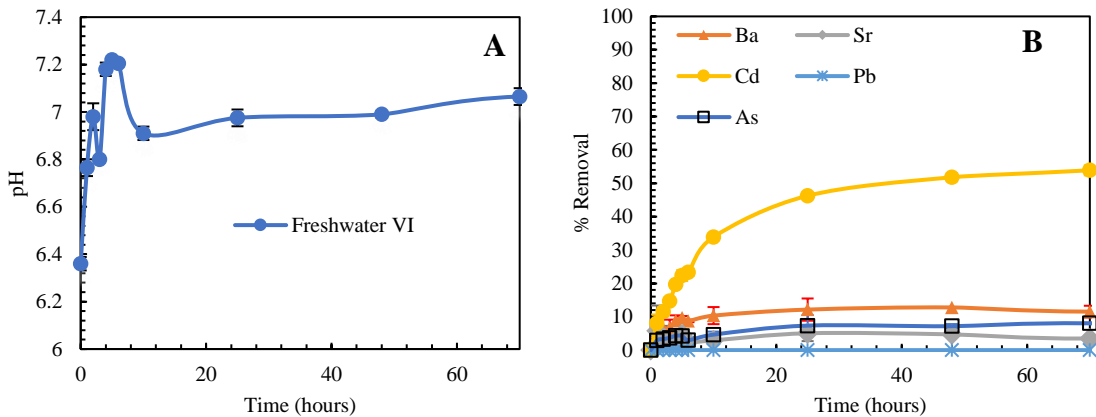


Fig. 3.6. Batch experimental results of mixed toxic metals removal by dolomite (FW type VI): A) pH profile; B) Toxic metals removal profile. FW type VI was supplied with CaCO₃ to increase the initial alkalinity (Table 2).

Fig. 3.6 shows Ba, Sr, Cd, Pb, and As removal and pH profiles over time obtained using FW type VI that had an initial alkalinity of 15.29 mg/L. Different from PW type VI, which was also added with CaCO₃ to increase alkalinity, Pb solubility was practically zero in FW, highlighting the different solubility of toxic metals in PW and FW. Similar removal levels (Table 3.6) obtained for Ba, Sr, Cd, and As as individual (FW type 1-V) and mixed toxic metals (FW type VI) confirms that their removals do not interfere with each other in both FW and PW.

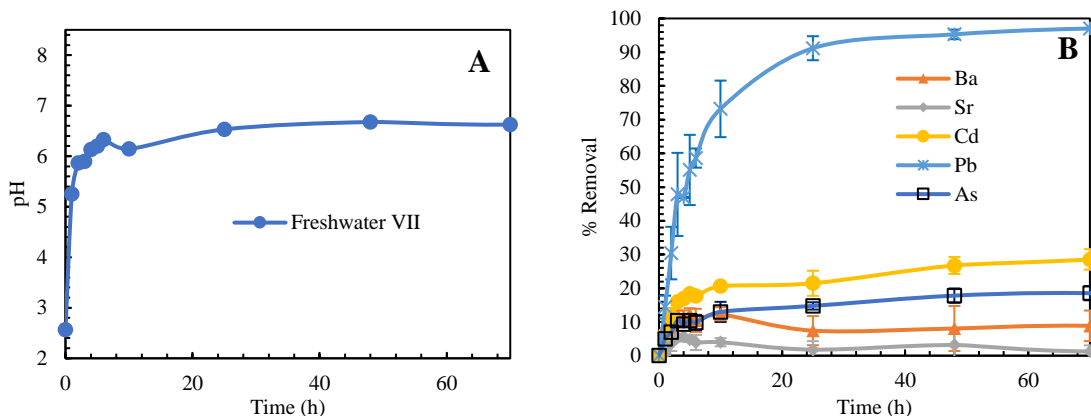


Fig 3.7. Batch experimental results of mixed toxic metals removal by dolomite (FW type VII): A) pH profile; B) Toxic metals removal profile. FW type VII was not supplied with CaCO₃ to increase the initial alkalinity (Table 3.4).

To determine the role of alkalinity in toxic metals precipitation from FW, we conducted batch experiments using FW type VII that was not added with CaCO₃ to increase alkalinity. In accordance with our hypothesis regarding the role of alkalinity, Pb did not precipitate immediately as it did with FW type VI. Its removal rate was slow as dolomite dissolution provided the required alkalinity for Pb precipitation. This is reflected by a concomitant increase of pH and removal of Pb (Fig. 3.7). Most importantly, lower removal levels of Ba, Sr, and Cd were obtained with FW type VII than with FW type VI. This

confirms that the removal of Ba, Sr, and Cd by sorption reactions decreases with decreasing pH, and that alkalinity promotes the removal of Pb and As as carbonate minerals, regardless of salinity.

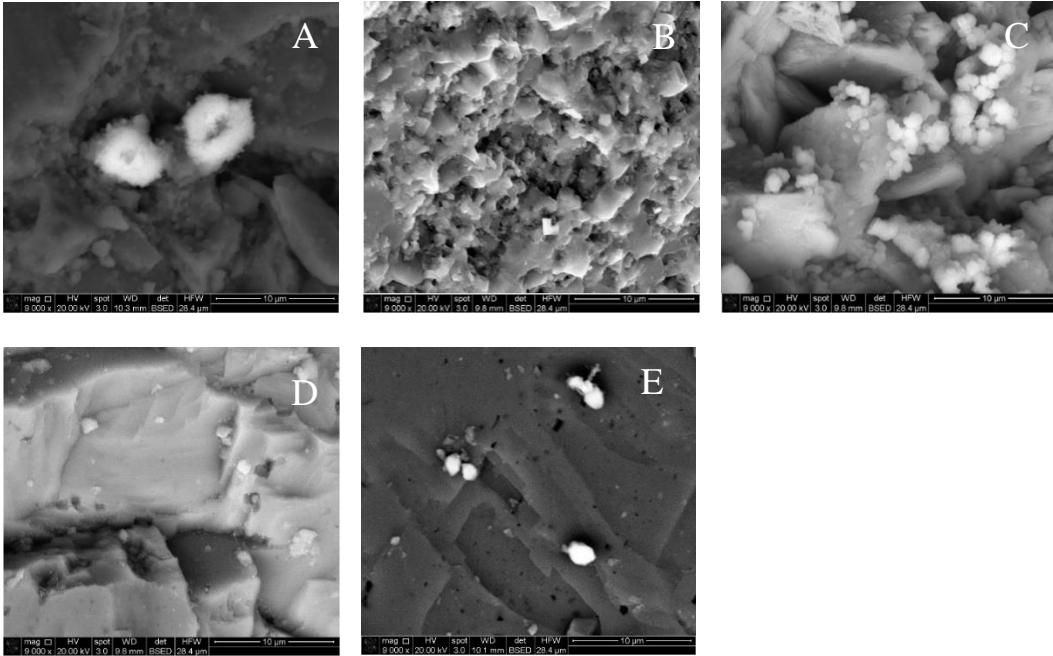


Fig. 3.8. SEM analysis of dolomite grain surface after 72 h of batch reaction: A) Ba (PW type I); B) Sr (PW type II); C) Cd (PW type III); D) Pb (PW type IV); and E) As (PW type V). All were supplied with CaCO₃ to increase the initial alkalinity.

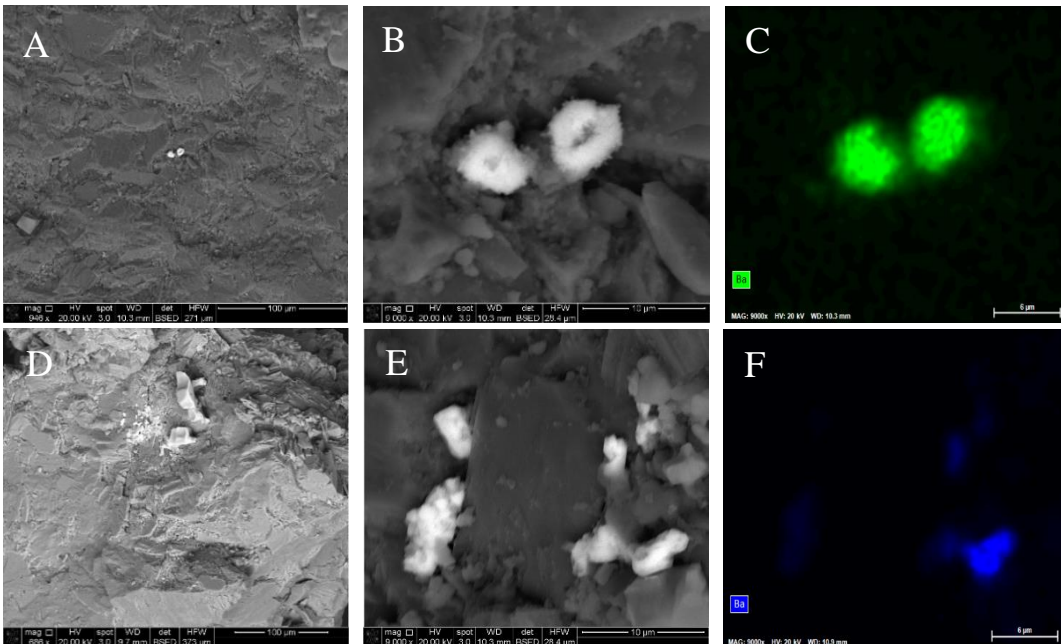
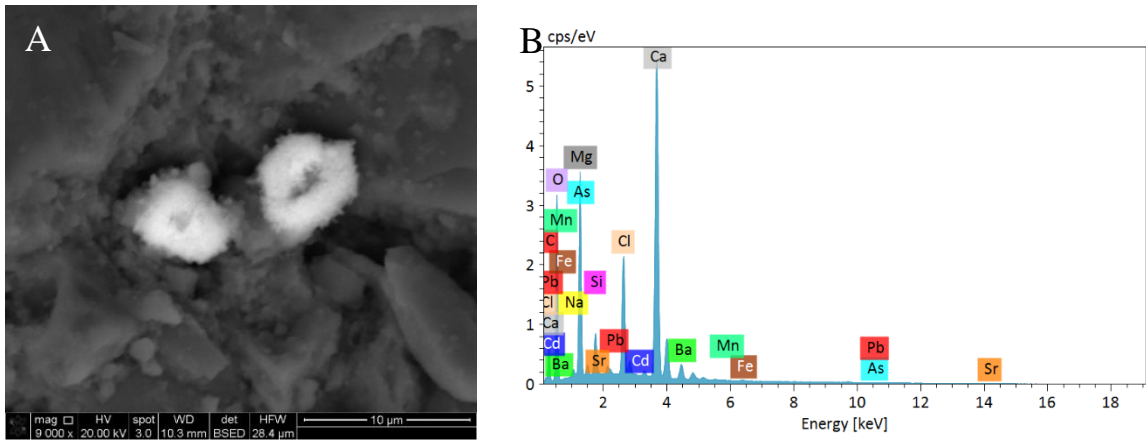


Fig. 3.9. (Previous page) SEM-EDS analysis of dolomite grain surface after 72 h of batch reaction using PW type I (Ba): A) SEM shows Ba precipitates in the middle of the picture as light-colored grains, B) Zoom-in of A, showing Ba precipitate, C) SEM-EDS mapping of B showing Ba precipitate in green color. D) SEM shows Ba precipitates and NaCl grains (light gray), E) Zoom-in of A, showing Ba precipitates associated with NaCl precipitation, and F) EDS mapping of Ba precipitates in blue color.

To confirm the formation of precipitates, we analyzed the surface morphology of dolomite grains collected from the batch reactors after 72 h of reaction. Fig. 3.8 shows SEM images of dolomite grains surface using PW types I-V. Ba precipitates were rarely found (Fig. 3.9). The detected Ba precipitates were characterized by having rough surfaces, irregular shapes, and different sizes (2-10 μm). Notably, Ba precipitates were found only in cavities on the dolomite surface or between dolomite crystals. According to literature (Tesoriero and Pankow, 1996), Ba in nature can precipitate as witherite (BaCO_3) (Antao and Hassan, 2009), coprecipitate with carbonate minerals such as calcite, and/or it can form hydrated amorphous carbonate phases. In our experiments, Ba precipitates were found along with NaCl precipitates (Fig. 3.10).



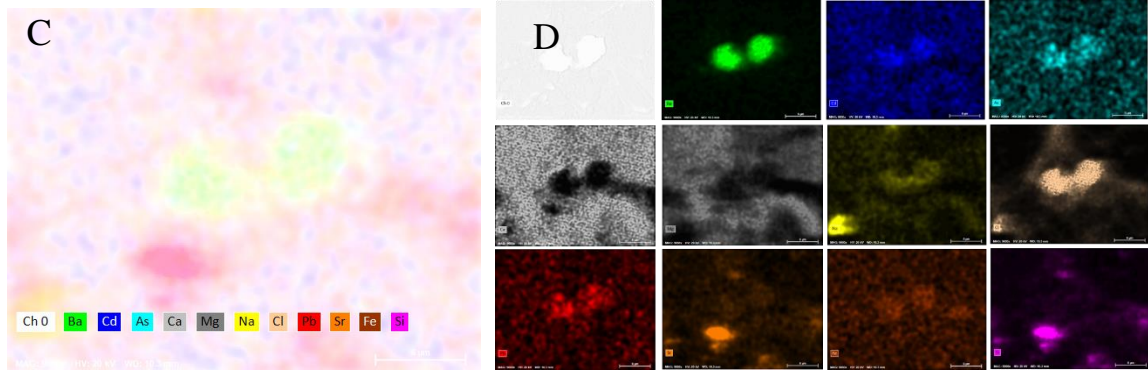


Fig. 3.10. SEM-EDS mapping of dolomite grain surface after 72 h of batch reaction using PW type I (Ba): A) a SEM micrograph showing toxic metals carbonate phase at the edges of the dolomite grain, B) X-ray spectrum showing elemental composition of the bulk samples, C) EDS mapping, and D) EDS mapping layers for single metals.

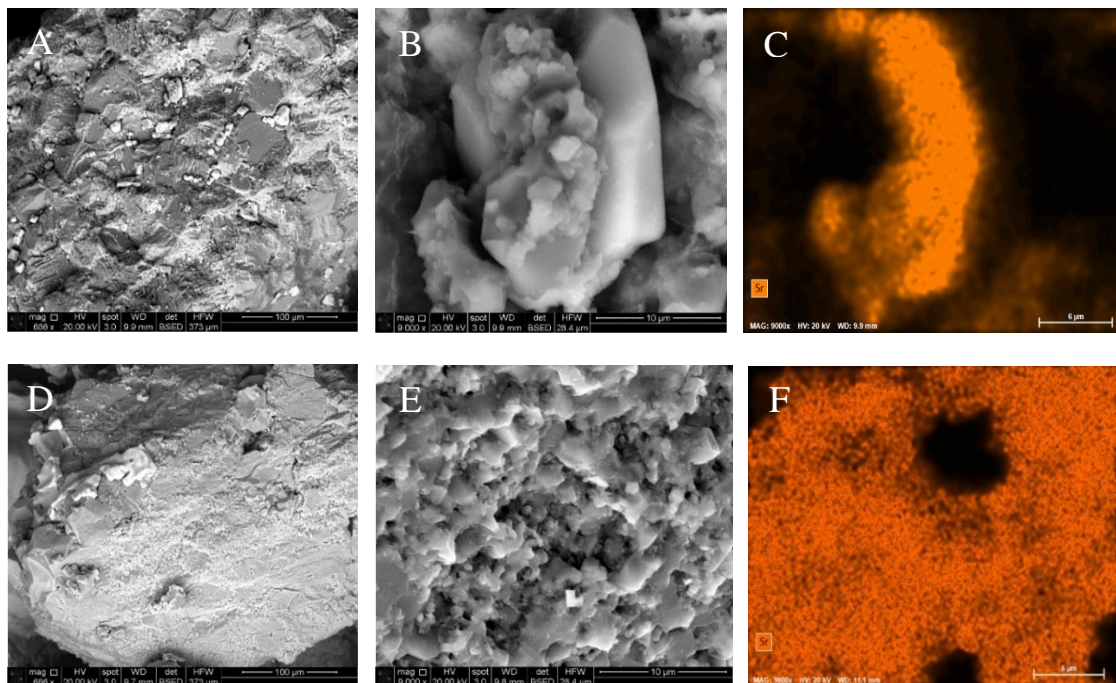


Fig. 3.11. SEM-EDS analysis of dolomite grain surface after 72 h of batch reaction using PW type II (Sr): A) SEM shows Sr and NaCl precipitates (light gray), B) Zoom-in of A showing a precipitate, C) EDS mapping of B showing that the precipitate contains Sr, D) SEM of high silica dolomite grain showing NaCl on the upper left side of the image, E) Zoom-in of D showing amorphous silica, and F) SEM-EDS mapping of E showing Sr a sorbed phase on the high silica dolomite grain in orange color.

Sr was found on the dolomite grains surface as precipitate and sorbed species (Fig. 3.11). However, like Ba, Sr precipitates were scarce and characterized by angular surfaces, larger sizes (~20 μm long), and they were also found along with NaCl precipitates. Interestingly, Sr mainly sorbed on quartz (SiO_2) which is a minor component of Arbuckle dolomite (Fig. 3.12). This observation suggests that Sr has a higher affinity for quartz than for dolomite.

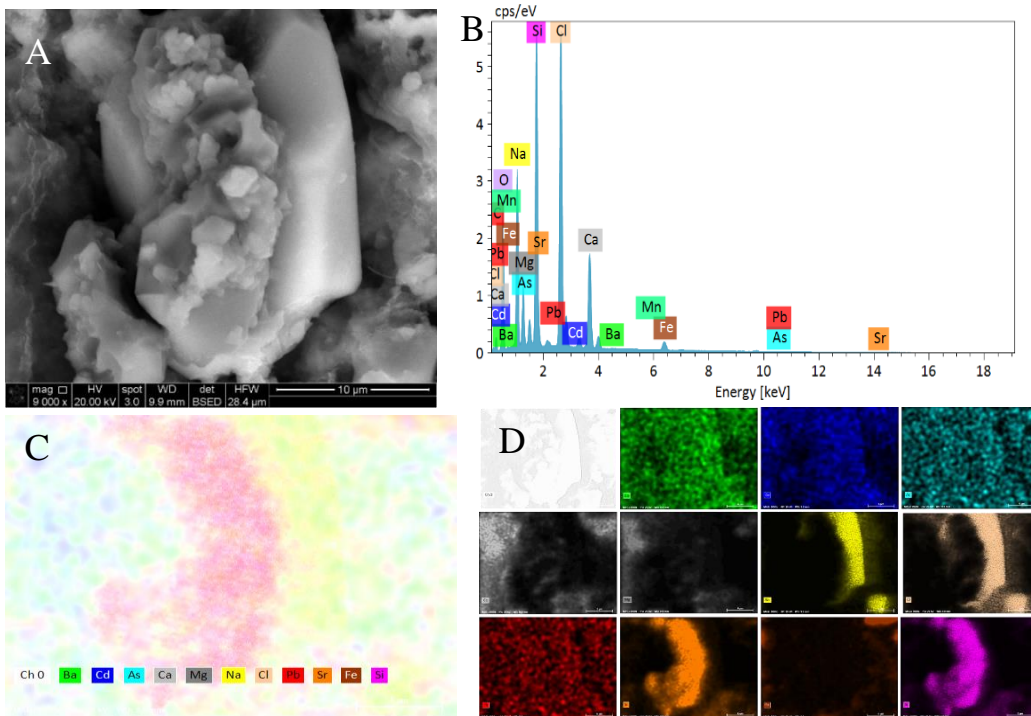


Fig. 3.12. SEM-EDS mapping of dolomite grain surface after 72 h of batch reaction using PW type II (Sr): A) a SEM micrograph showing toxic metals carbonate phase at the edges of the dolomite grain, B) X-ray spectrum showing elemental composition of the bulk samples, C) EDS mapping, and D) EDS mapping layers for single metals.

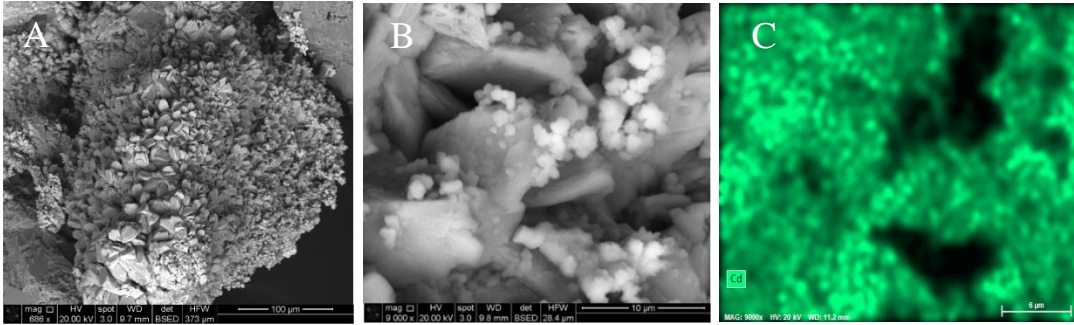


Fig. 3.13. SEM-EDS analysis of dolomite grain surface after 72 h of batch reaction using PW type III (Cd): A) SEM shows a high Fe dolomite grain, B) Zoom-in of A showing a cluster-shaped phase of Fe (light color), C) EDS mapping of B showing Cd sorption on dolomite.

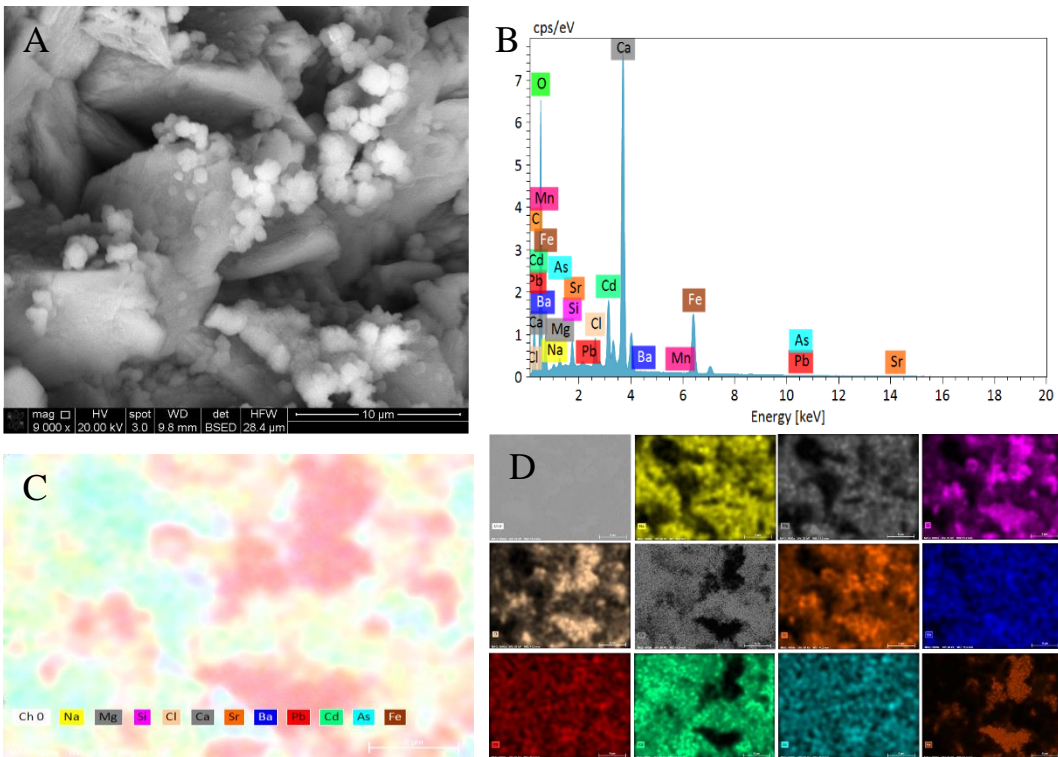


Fig. 3.14. SEM-EDS mapping of dolomite grain surface after 72 h of batch reaction using PW type III (Cd): A) a SEM micrograph showing toxic metals carbonate phase at the edges of the dolomite grain, B) X-ray spectrum showing elemental composition of the bulk samples, C) EDS mapping, and D) EDS mapping layers for single metals.

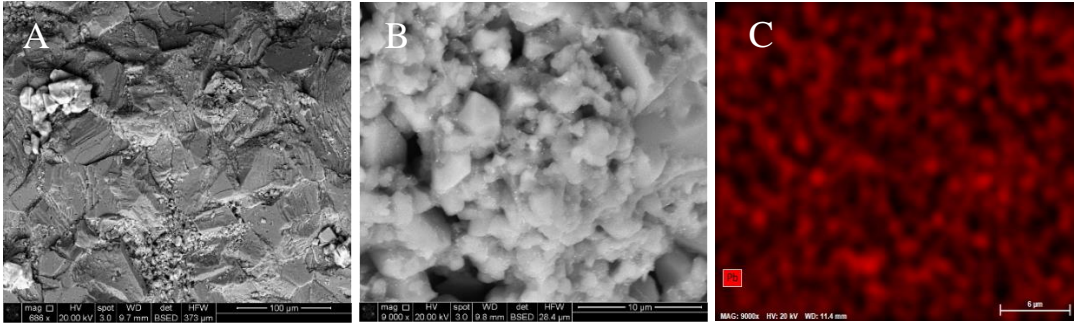


Fig 3.15. SEM-EDS analysis of dolomite grain surface after 72 h of batch reaction using PW type IV (Pb): A SEM image showing NaCl grains (light gray) precipitated on the dolomite surface, B) Zoom-in of A showing nanoscale Pb precipitates of white color on dolomite grain/crystal edges, C) EDS mapping of B showing Pb precipitates on dolomite.

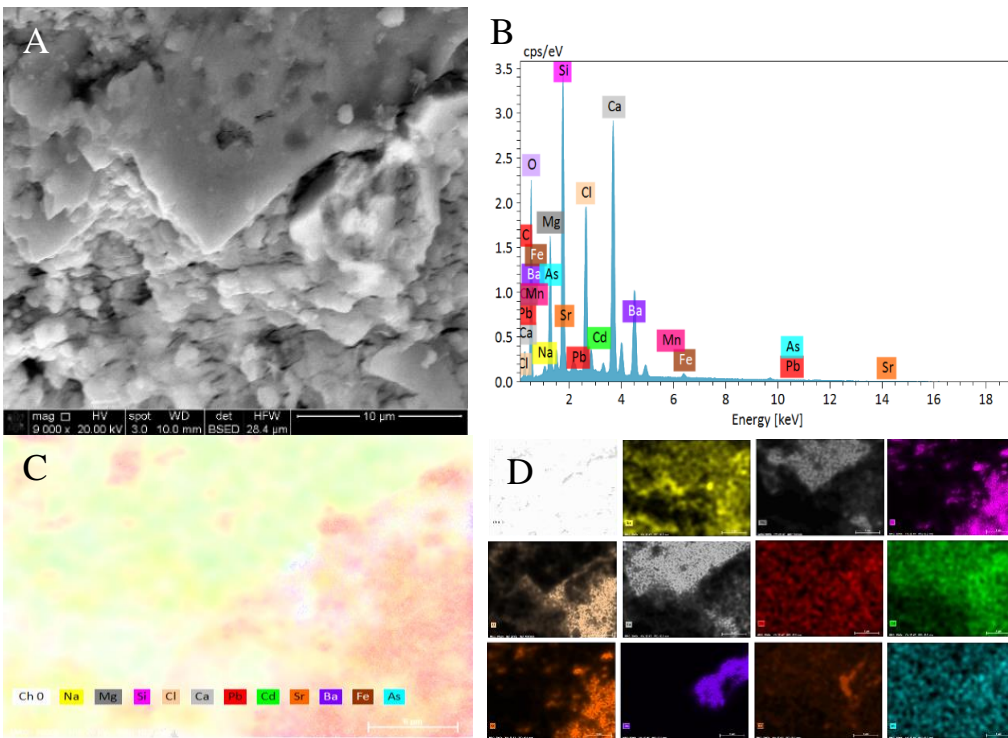


Fig. 3.16. SEM-EDS mapping of dolomite grain surface after 72 h of batch reaction using PW type IV (Pb): A) a SEM micrograph showing toxic metals carbonate phase at the edges of the dolomite grain, B) X-ray spectrum showing elemental composition of the bulk samples, C) EDS mapping, and D) EDS mapping layers for single metals.

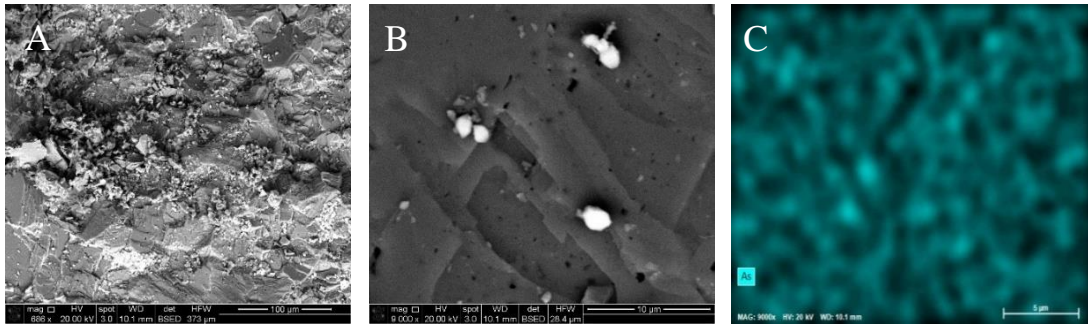


Fig. 3.17. SEM-EDS analysis of dolomite grain surface after 72 h of batch reaction using PW type V (As): A) SEM image showing a lot of debris, B) Zoom-in of A showing As precipitate of different in bright color on the dolomite crystal face, C) EDS mapping of B showing As as precipitates.

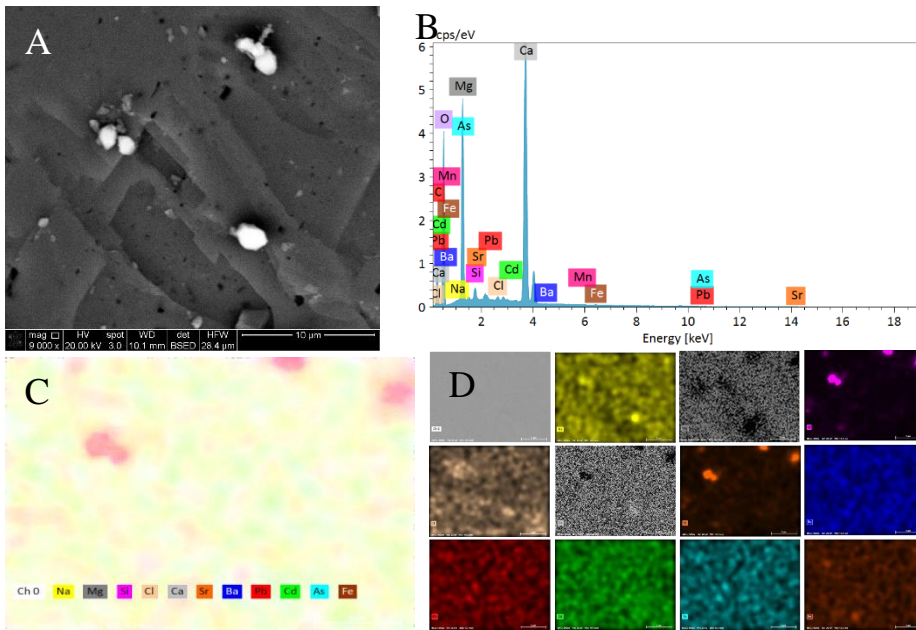


Fig. 3.18. SEM-EDS mapping of dolomite grain surface after 72 h of batch reaction using PW type V (As): A) a SEM micrograph showing toxic metals carbonate phase at the edges of the dolomite grain, B) X-ray spectrum showing elemental composition of the bulk samples, C) EDS mapping, and D) EDS mapping layers for single metals.

Notably, Cd was never found as a precipitate in the experiments that we conducted for individual toxic metals. Cd was only detected as sorbed phase on ferric dolomite grains (Fig. 3.13 and Fig. 3.14), indicating that the high removal of Cd (17.29%) was mostly due

to sorption reactions. Conversely, Pb was commonly found as a precipitate on the dints or inside edges of dolomite grains/crystals (Fig. 3.15 and Fig 3.16). Pb precipitates are characterized by nanoscale oval shape precipitates. As was found as 1-3 μm precipitates with irregular shapes on the dolomite (Fig. 3.17). Different from the other toxic metals, As precipitated directly on the crystal face of dolomite, and it was detected as precipitate and sorbed phases (Fig. 3.17 and Fig. 3.18).

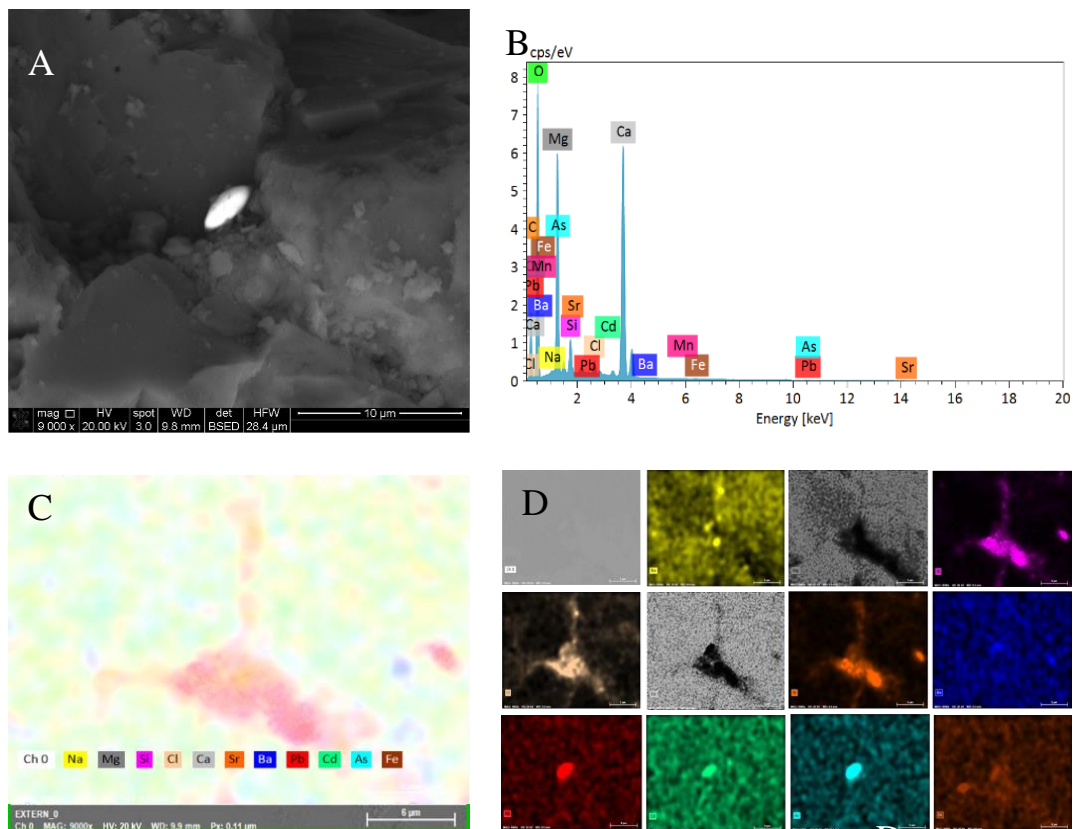


Fig. 3.19. SEM-EDS mapping of dolomite grain surface after 72 h of batch reaction using PW type VI (Ba, Sr, Cd, Pb, and As): A) SEM micrograph showing toxic metals carbonate phase with oval shape in the center, B) X-ray spectrum showing the elemental composition of the bulk samples, C) EDS mapping, and D) EDS mapping layers for single metals.

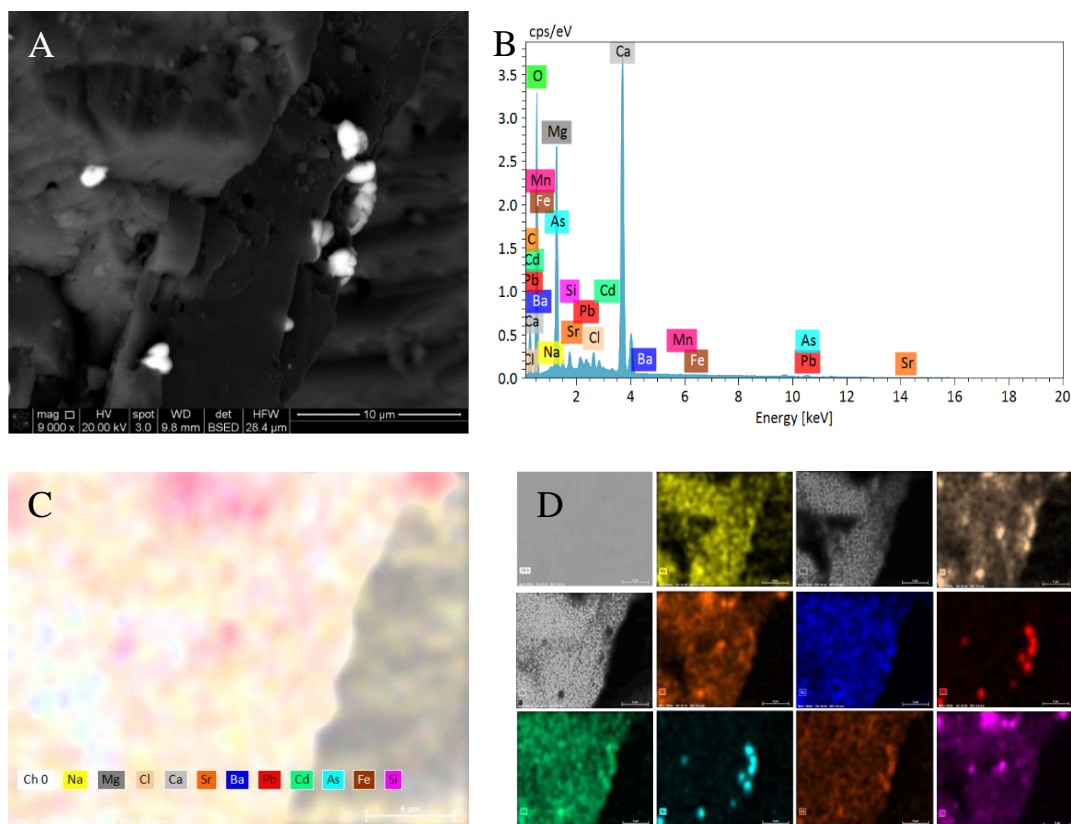


Fig. 3.20. SEM-EDS mapping of dolomite grain surface after 72 h of batch reaction using PW type VII (Ba, Sr, Cd, Pb, and As): A) SEM micrograph showing toxic metals carbonate phase at the edges of the dolomite grain, B) X-ray spectrum showing the elemental composition of the bulk samples, C) EDS mapping, and D) EDS mapping layers for single metals.

To identify which toxic metals form part of the precipitates when they are all present in PW, we mapped the elemental composition of the dolomite grains by SEM-EDS analysis. Figs. 3.19 and 3.20 show SEM-EDS images of the dolomite surface at the end of the experiments conducted with synthetic PW types VI (with added alkalinity) and VII (without added alkalinity). The analysis confirms the sorption of all tested toxic metals on dolomite. However, and more importantly, in accordance with the concentration profiles of Pb and As, SEM-EDS analysis suggests that their precipitation as carbonates plays a prominent role in their removal by dolomite. The SEM-EDS images show that the bright white spots in the SEM images contain Pb and/or As.

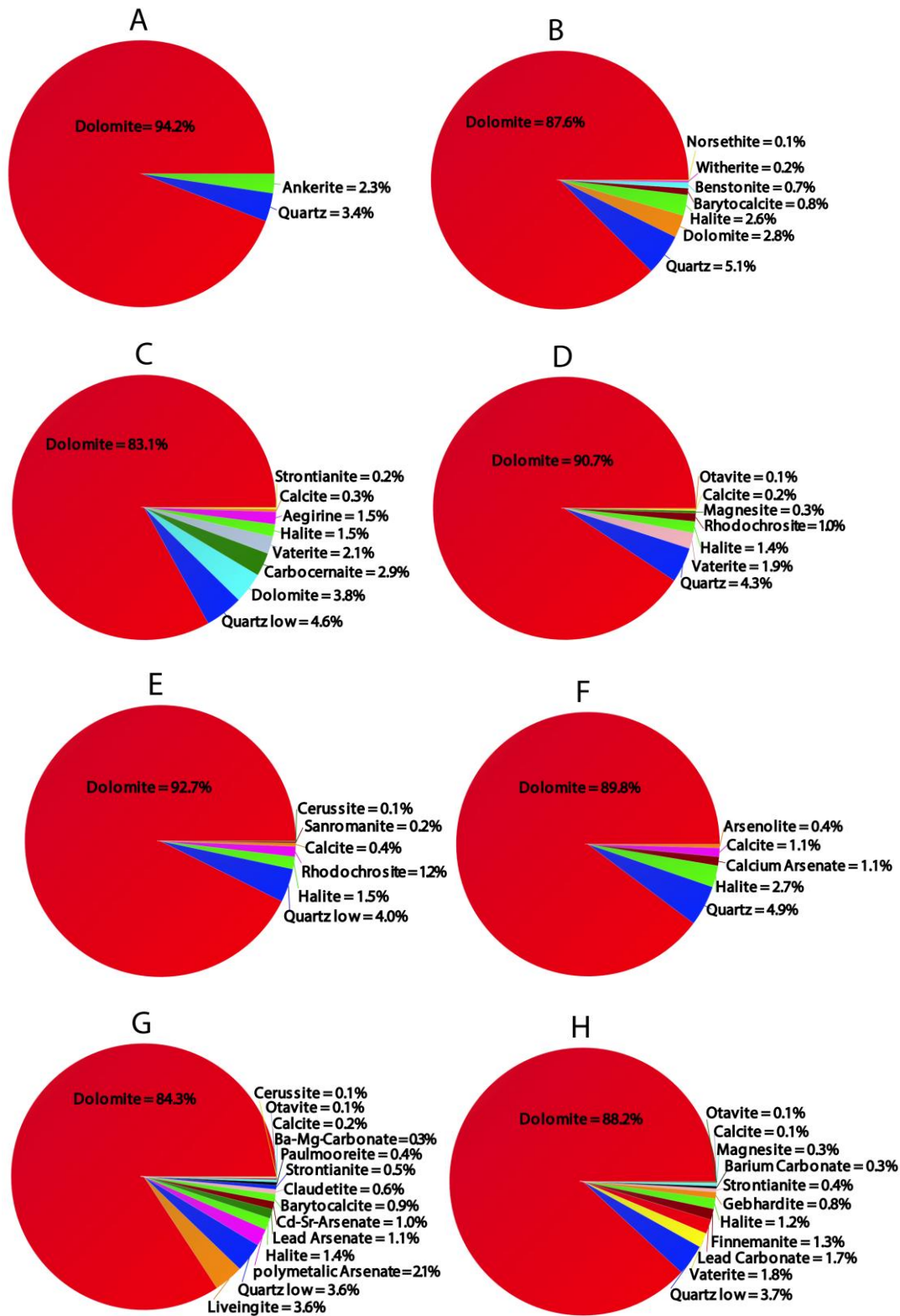
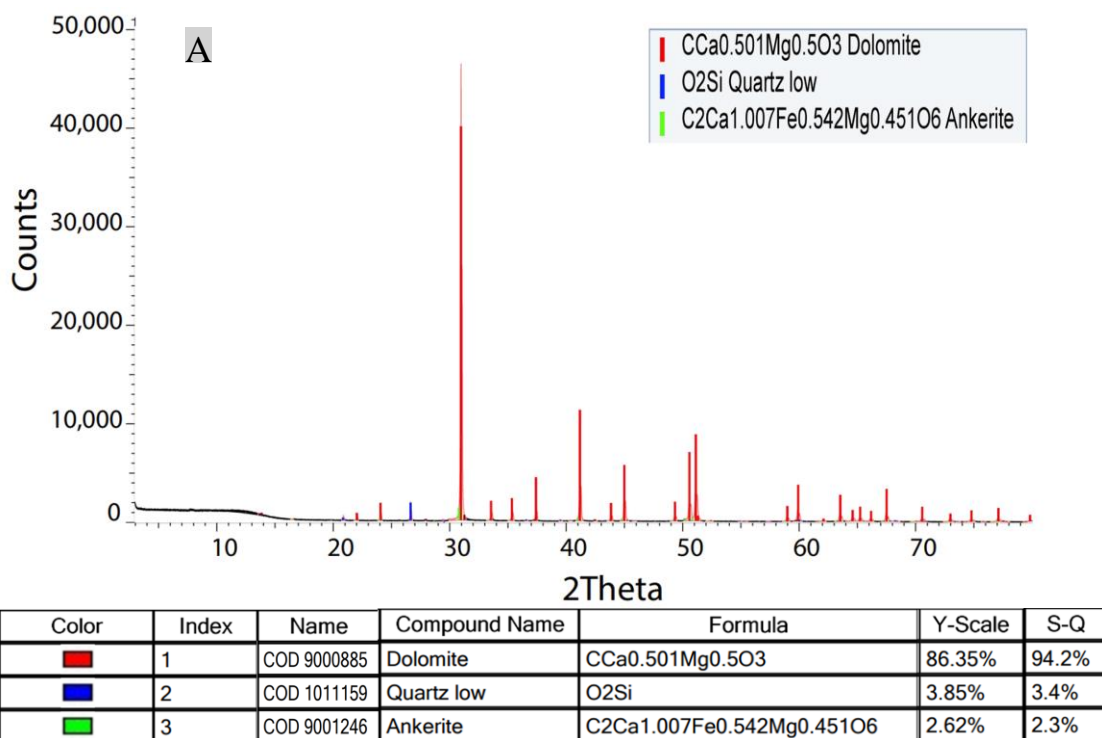
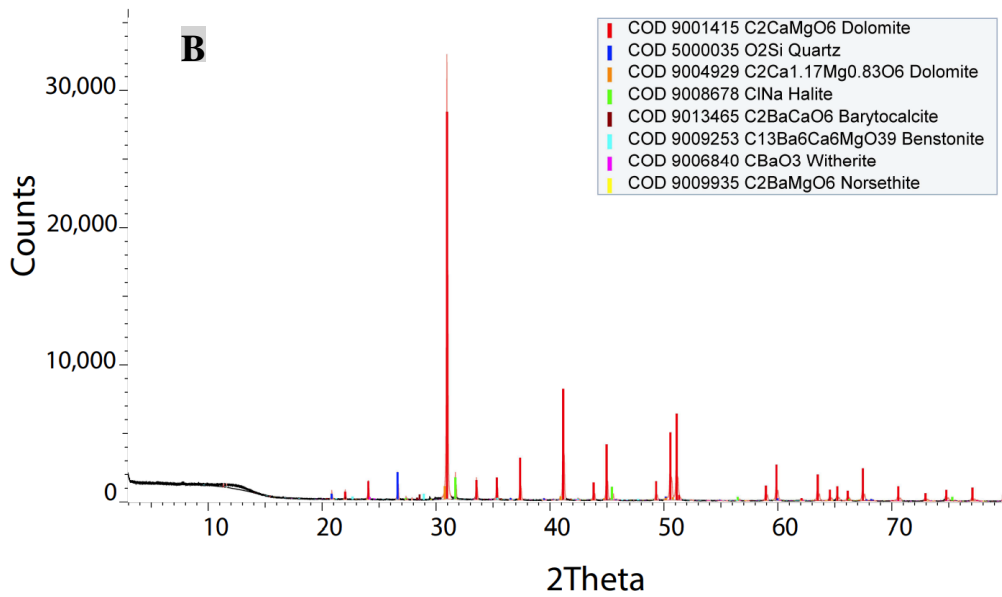


Fig. 3.21. Semiquantitative analyses from high-resolution XRD (Fig. S9) conducted on the powdered dolomite samples collected from batch reaction experiments: A) Control sample,

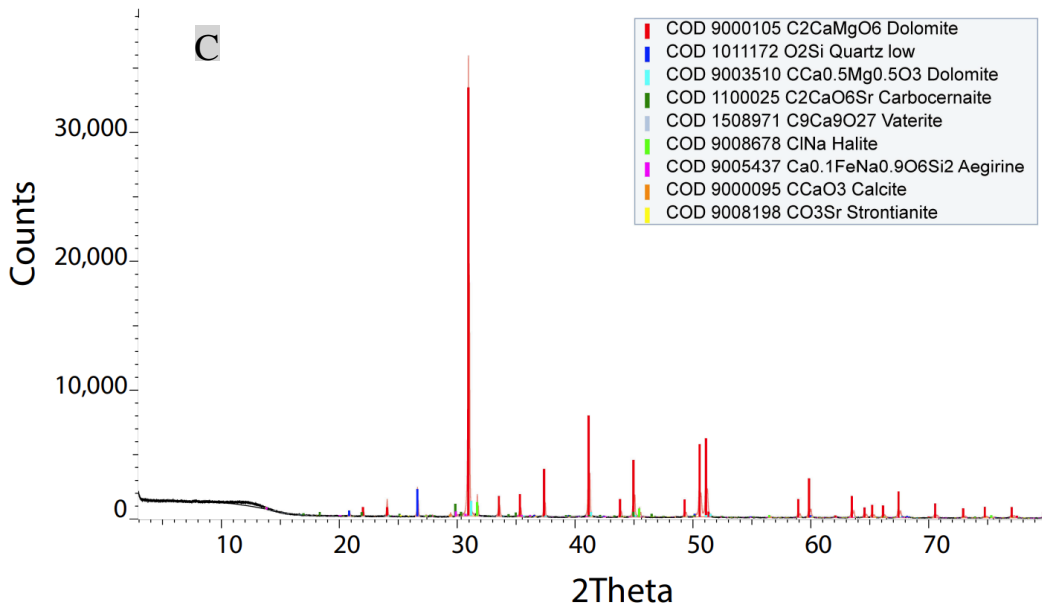
B) PW type I (Ba), C) PW type II (Sr), D) PW type III (Cd), E) PW type IV (Pb), F) PW type V (As), G) PW type VI (Ba, Sr, Cd, Pd, and As), and H) PW VII (Ba, Sr, Cd, Pd, and As).

To elucidate whether the observed precipitates are crystallized carbonates and to determine the mineral composition of the precipitates, we conducted high-resolution XRD analyses. Fig. 3.21 shows all the minerals detected through semiquantitative analysis of high-resolution XRD data. Analysis was done on a control dolomite sample (e.g., Fig. 3.21A) as well as on samples collected before and after each batch experiment (Fig. 3.21B-H).

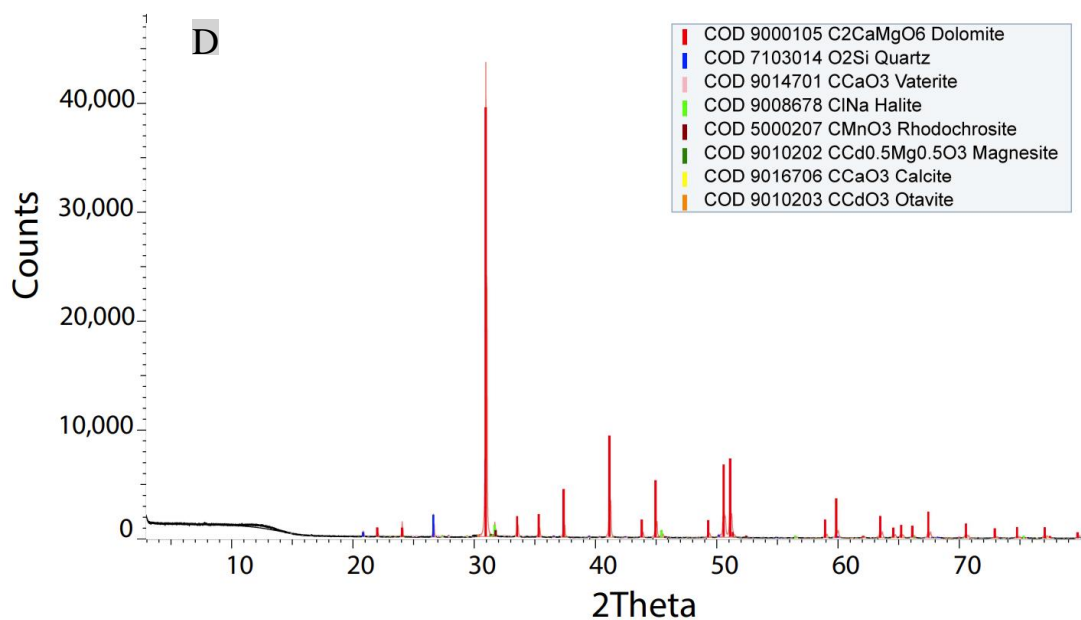




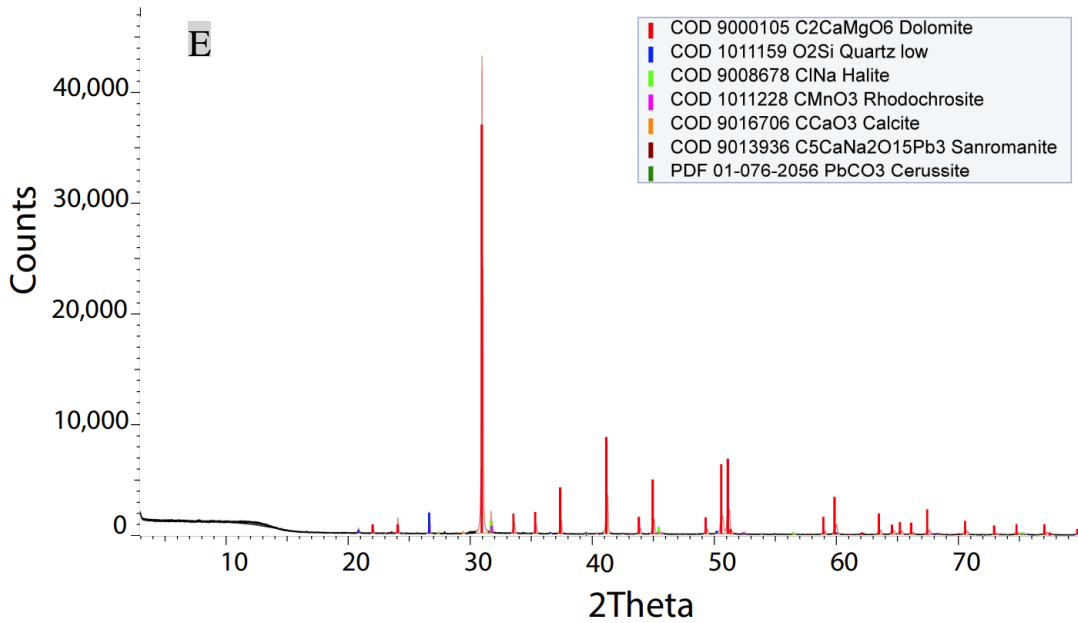
Icon	Color	Index	Name	Compound Name	Formula	S-Q
		1	COD 9001415	Dolomite	C ₂ CaMgO ₆	87.6%
		2	COD 5000035	Quartz	O ₂ Si	5.1%
		3	COD 9004929	Dolomite	C ₂ Ca _{1.17} Mg _{0.83} O ₆	2.8%
		4	COD 9008678	Halite	ClNa	2.6%
		5	COD 9013465	Barytocalcite	C ₂ BaCaO ₆	0.8%
		6	COD 9009253	Benstonite	C ₁₃ Ba ₆ Ca ₆ MgO ₃₉	0.7%
		7	COD 9006840	Witherite	CBaO ₃	0.2%
		8	COD 9009935	Norsethite	C ₂ BaMgO ₆	0.1%



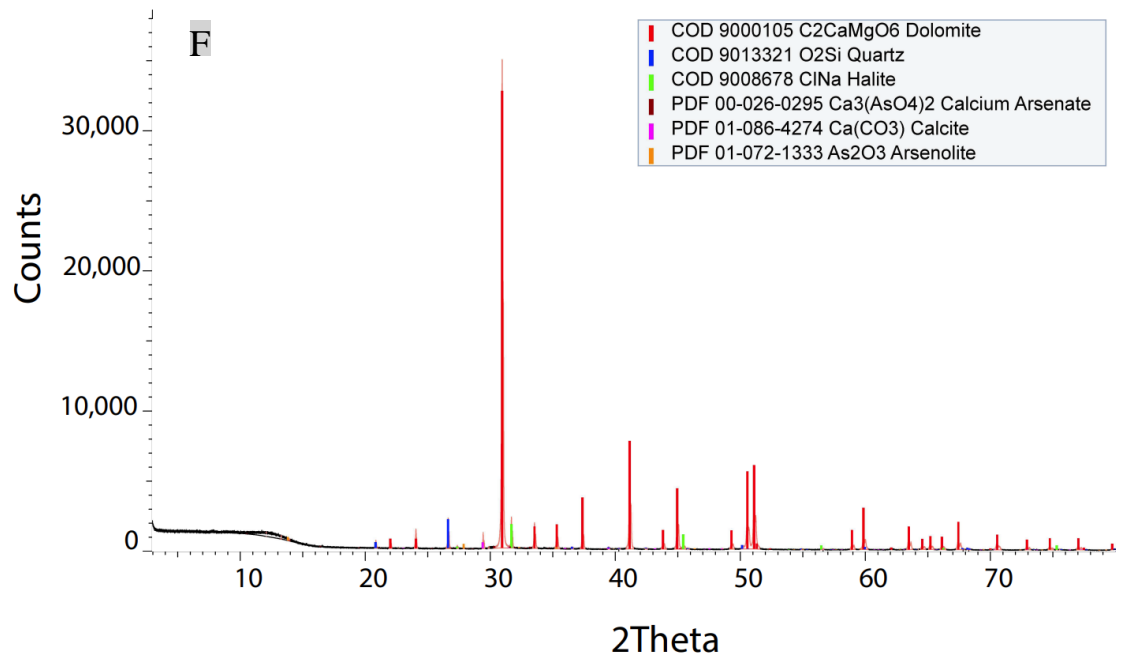
Color	Index	Name	Compound Name	Formula	Y-Scale	S-Q
Red	1	COD 9000105	Dolomite	C2CaMgO6	93.10%	83.1%
Blue	2	COD 1011172	Quartz low	O2Si	5.85%	4.6%
Cyan	3	COD 9003510	Dolomite	CCa0.5Mg0.5O3	3.17%	3.8%
Green	4	COD 1100025	Carbocernaite	C2CaO6Sr	2.64%	2.9%
Light Blue	5	COD 1508971	Vaterite	C9Ca9O27	0.20%	2.1%
Light Green	6	COD 9008678	Halite	ClNa	2.94%	1.5%
Purple	7	COD 9005437	Aegirine	Ca0.1FeNa0.9O6Si2	1.06%	1.5%
Orange	8	COD 9000095	Calcite	CCaO3	0.43%	0.3%
Yellow	9	COD 9008198	Strontianite	CO3Sr	0.34%	0.2%



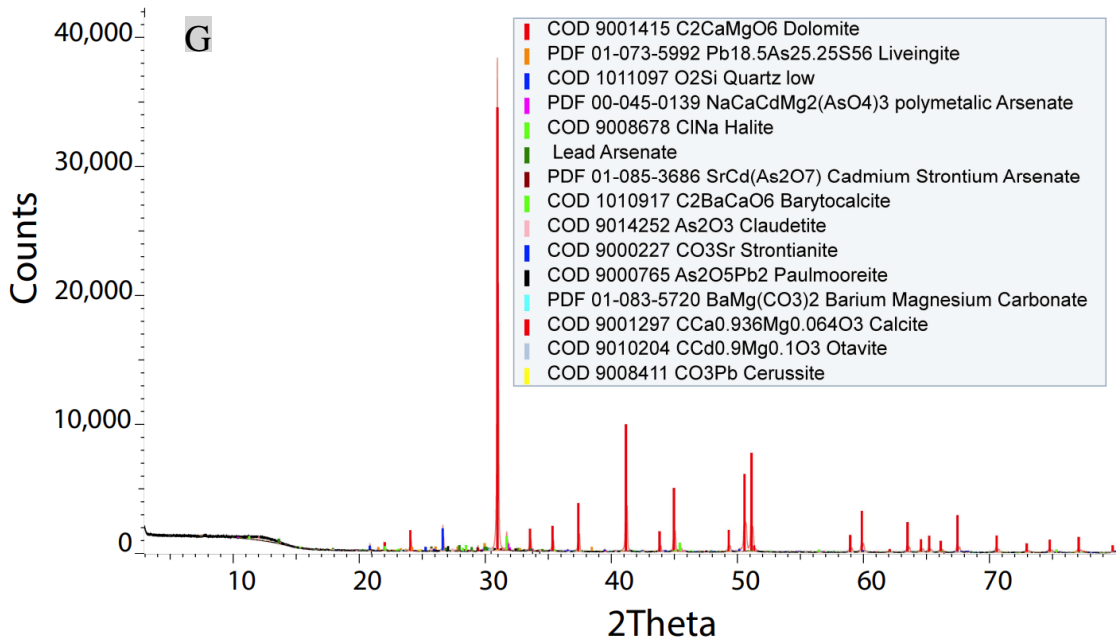
Color	Index	Name	Compound Name	Formula	Y-Scale	S-Q
Red	1	COD 9000105	Dolomite	C2CaMgO6	90.53%	90.4%
Blue	2	COD 7103014		O2Si	4.62%	4.3%
Pink	3	COD 9014701	Vaterite	CCaO3	0.41%	1.9%
Green	4	COD 9008678	Halite	ClNa	2.42%	1.4%
Dark Red	5	COD 5000207	Rhodochrosite	CMnO3	1.28%	1.0%
Dark Green	6	COD 9010202	Magnesite	CCd0.5Mg0.5O3	0.52%	0.3%
Black	7	COD 9010214	Magnesite	CCd0.45Mg0.55O3	0.38%	0.2%
Yellow	8	COD 9016706	Calcite	CCaO3	0.19%	0.2%
Orange	9	COD 9010203	Otavite	CCdO3	0.30%	0.1%
Light Blue	10	COD 9006689	Monteponite	CdO	0.07%	0.0%
Purple	11	COD 1010883		Ca0.75Cd0.25O	0.14%	0.1%



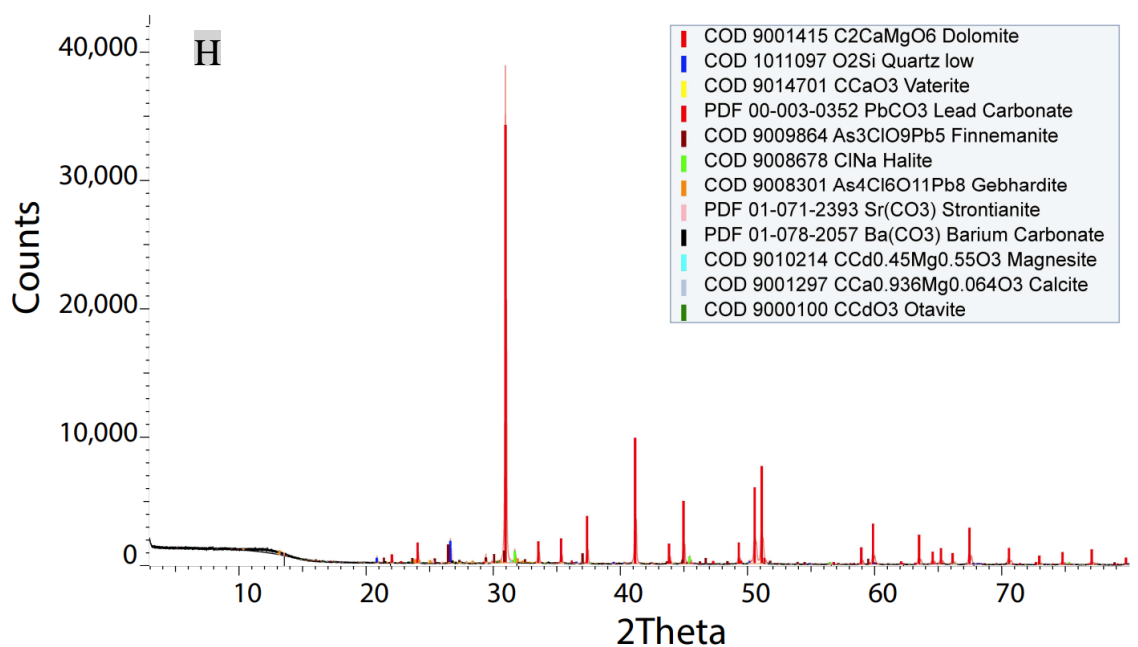
Color	Index	Name	Compound Name	Formula	Y-Scale	S-Q
Red	1	COD 9000105	Dolomite	C ₂ CaMgO ₆	85.64%	92.7%
Blue	2	COD 1011159	Quartz low	O ₂ Si	4.28%	4.0%
Green	3	COD 9008678	Halite	ClNa	2.35%	1.5%
Magenta	4	COD 1011228	Rhodochrosite	CMnO ₃	1.45%	1.2%
Orange	5	COD 9016706	Calcite	CCaO ₃	0.38%	0.4%
Brown	6	COD 9013936	Sanromanite	C ₅ CaNa ₂ O ₁₅ Pb ₃	0.41%	0.2%
Dark Green	7	PDF 01-076-2056	Cerussite	PbCO ₃	0.27%	0.1%



Color	Index	Name	Compound Name	Formula	Y-Scale	S-Q
■	1	COD 9000105	Dolomite	C2CaMgO6	93.59%	89.8%
■	2	COD 9013321	Quartz	O2Si	5.89%	4.9%
■	3	COD 9008678	Halite	ClNa	4.78%	2.7%
■	4	PDF 00-026-0295	Calcium Arsenate	Ca3(AsO4)2	0.39%	1.1%
■	5	PDF 01-086-4274	Calcite	Ca(CO3)	1.26%	1.1%
■	6	PDF 01-072-1333	Arsenolite	As2O3	0.97%	0.4%



Color	Index	Name	Compound Name	Formula	Y-Scale	S-Q
■	1	COD 9001415	Dolomite	C2CaMgO6	89.98%	84.3%
■	2	PDF 01-073-5992	Liveingite	Pb18.5As25.25S56	1.52%	3.6%
■	3	COD 1011097	Quartz low	O2Si	4.54%	3.6%
■	4	PDF 00-045-0139	polymetalic Arsenate	NaCaCdMg2(AsO4)3	1.37%	2.1%
■	5	COD 9008678	Halite	ClNa	2.81%	1.4%
■	6	PDF 01-079-0114	Lead Arsenate	PbAs2O4	1.19%	1.1%
■	7	PDF 01-085-3686	Cadmium Strontium Arsenate	SrCd(As2O7)	0.75%	1.0%
■	8	COD 1010917	Barytocalcite	C2BaCaO6	1.24%	0.9%
■	9	COD 9014252	Claudetite	As2O3	0.54%	0.6%
■	10	COD 9000227	Strontianite	CO3Sr	0.84%	0.5%
■	11	COD 9000765	Paulmooreite	As2O5Pb2	0.96%	0.4%
■	12	PDF 01-083-5720	Barium Magnesium Carbonate	BaMg(CO3)2	0.34%	0.3%
■	13	COD 9001297	Calcite	CCa0.936Mg0.064O3	0.21%	0.2%
■	14	COD 9010204	Otavite	CCd0.9Mg0.1O3	0.40%	0.1%
■	15	COD 9008411	Cerussite	CO3Pb	0.32%	0.1%



Color	Index	Name	Compound Name	Formula	Y-Scale	S-Q
Red	1	COD 9001415	Dolomite	C ₂ CaMgO ₆	88.09%	88.2%
Blue	2	COD 1011097	Quartz low	O ₂ Si	4.43%	3.7%
Yellow	3	COD 9014701	Vaterite	CCaO ₃	0.39%	1.8%
Dark Red	4	PDF 00-003-0352	Lead Carbonate	PbCO ₃	0.63%	1.7%
Brown	5	COD 9009864	Finnemanite	As ₃ ClO ₉ Pb ₅	3.69%	1.3%
Green	6	COD 9008678	Halite	ClNa	2.29%	1.2%
Orange	7	COD 9008301	Gebhardite	As ₄ Cl ₆ O ₁₁ Pb ₈	0.86%	0.8%
Pink	8	PDF 01-071-2393	Strontianite	Sr(CO ₃)	0.58%	0.4%
Black	9	PDF 01-078-2057	Barium Carbonate	Ba(CO ₃)	0.55%	0.3%
Cyan	10	COD 9010214	Magnesite	CCd _{0.45} Mg _{0.55} O ₃	0.43%	0.3%
Grey	11	COD 9001297	Calcite	CCa _{0.936} Mg _{0.064} O ₃	0.17%	0.1%
Dark Green	12	COD 9000100	Otavite	CCdO ₃	0.37%	0.1%

Fig. 3.22. High-resolution XRD and semiquantitative analyses of the powdered dolomite samples collected from batch reaction experiments: A) Control sample, B) PW type I (Ba), C) PW type II (Sr), D) PW type III (Cd), E) PW type IV (Pb), F) PW type V (As), G) PW type VI (Ba, Sr, Cd, Pd, and As), and H) PW VII (Ba, Sr, Cd, Pd, and As).

The obtained XRD spectra (Fig. 3.22) display major (>5%), minor (<5%), and even trace (<1%) mineral concentrations. The major minerals in the control sample were dolomite and quartz. However, XRD spectra showed minor content of silica (quartz) and carbonate (ankerite) minerals in some control samples. The origin of detected silica minerals could be either from terrigenous siliciclastic sand grains entered by different

transportation mechanisms such as wind into the precursor carbonate depositional settings, or from amorphous biogenic silica crystallization by complex hydrothermal diagenetic processes that Arbuckle Group had undergone (Bettermann and Liebau, 1975; Temple et al., 2020). Carbonate minerals such as calcite and vaterite were only found in samples collected at the end of the batch reaction experiments, confirming that these minerals were precipitated during the experiments. Evaporate minerals (e.g., halite) were also detected in all samples collected at the end of the experiments but not in the control samples, confirming that halite was precipitated during the experiments or during the drying of samples for XRD analysis. Remarkably, and based on the XRD semiquantitative analysis (Fig. 3.21), the detected minerals are significantly diverse from sample to sample. At first glance, this might be expected because we used natural dolomite rocks. Traces of minerals might be slightly different from sample to sample even for the same rock. However, with more careful examination, we see that the chemistry of these traces of minerals corresponds to the chemical composition of the employed PW. For example, carbonate minerals detected in samples collected from experiments conducted using PW type I-V are witherite (BaCO_3), strontianite (SrCO_3), otavite (CdCO_3), cerussite (PbCO_3), and calcium arsenate ($\text{Ca}_3(\text{AsO}_4)_2$) (Fig. 3.21 B-F), which are known to be more thermodynamically feasible at standard conditions (Antao and Hassan, 2009; Anthony et al., 1995). In addition to these minerals, several other carbonate and oxide phases were also detected. For instance, As oxides were found in the samples collected from experiments conducted using PW type V (Fig. 3.21F). This is probably due to the tendency of As to form oxide phases in the aqueous environments (Neuberger and Helz, 2005). However, it is known that As can also coprecipitate with carbonate minerals during the transformation of hydrated (e.g.,

monohydrocalciteto) to anhydrous (e.g., calcite and aragonite) carbonate phases in saline water (Fukushi et al., 2011).

XRD analysis on samples collected from experiments conducted using PW types VI and VII, which contained mixed toxic metals, show very complex polymetallic minerals. Contrary to the results obtained using PW types I-V, the detected phases were largely arsenate minerals and coprecipitated arsenate phases such as strontium cadmium arsenate ($\text{SrCd}(\text{As}_2\text{O}_7)$) and lead arsenate (PbAs_2O_4) (Fig. 3.21G-H).

3.4.2. Geochemical modeling

Measuring the fraction of toxic metals removal from PW by sorption and precipitation reactions presents several challenges and it requires additional analytical methods. To confirm the thermodynamic feasibility and to determine the possible extent of precipitation reactions under the tested PW conditions, here we simulate the conducted experiments using CrunchFlow geochemical modeling software (Steeffel and Lasaga, 1994). CrunchFlow incorporates the EQ3/EQ6 thermodynamic database (Wolery et al., 1990). Due to the unavailability of thermodynamic data for Ba and As precipitation reactions, simulations are done for synthetic PW type VI containing only Sr, Cd, and Pb.

Table 3.7. Aqueous phase equilibrium complexation reactions.

Reaction	Log K_{eq} (25°C)
$\text{OH}^- + \text{H}^+ \leftrightarrow \text{H}_2\text{O}$	13.991
$\text{CO}_2(\text{aq}) + \text{H}_2\text{O} \leftrightarrow \text{H}^+ + \text{HCO}_3^-$	-6.342
$\text{CO}_3^{2-} + \text{H}^+ \leftrightarrow \text{HCO}_3^-$	10.325

$\text{CaOH}^+ + \text{H}^+ \leftrightarrow \text{Ca}^{2+} + \text{H}_2\text{O}$	12.852
$\text{SrOH}^+ + \text{H}^+ \leftrightarrow \text{Sr}^{2+} + \text{H}_2\text{O}$	13.290
$\text{CdOH}^+ + \text{H}^+ \leftrightarrow \text{Cd}^{2+} + \text{H}_2\text{O}$	10.075
$\text{PbOH}^+ + \text{H}^+ \leftrightarrow \text{Pb}^{2+} + \text{H}_2\text{O}$	7.695
$\text{CaCO}_3(\text{aq}) + \text{H}^+ \leftrightarrow \text{Ca}^{2+} + \text{HCO}_3^-$	7.009
$\text{MgCO}_3(\text{aq}) + \text{H}^+ \leftrightarrow \text{HCO}_3^- + \text{Mg}^{2+}$	7.356
$\text{SrCO}_3(\text{aq}) + \text{H}^+ \leftrightarrow \text{Sr}^{2+} + \text{HCO}_3^-$	7.470
$\text{CdCO}_3(\text{aq}) + \text{H}^+ \leftrightarrow \text{Cd}^{2+} + \text{HCO}_3^-$	7.328
$\text{PbCO}_3(\text{aq}) + \text{H}^+ \leftrightarrow \text{Pb}^{2+} + \text{HCO}_3^-$	3.748
$\text{CaCl}^+ \leftrightarrow \text{Ca}^{2+} + 2\text{Cl}^-$	0.701
$\text{MgCl}^+ \leftrightarrow \text{Mg}^{2+} + \text{Cl}^-$	0.139
$\text{SrCl}^+ \leftrightarrow \text{Sr}^{2+} + \text{Cl}^-$	0.253
$\text{CdCl}^+ \leftrightarrow \text{Cd}^{2+} + \text{Cl}^-$	-2.706
$\text{PbCl}^+ \leftrightarrow \text{Pb}^{2+} + \text{Cl}^-$	-1.432
$\text{CO}_2(\text{g}) + \text{H}_2\text{O} \leftrightarrow \text{H}^+ + \text{HCO}_3^-$	-7.809

Table 3.8. Mineral phase reactions.

Carbonate	Reaction	Log K_{eq} (25°C)
Dolomite	$\text{CaMg}(\text{CO}_3)_2 + 2\text{H}^+ \leftrightarrow \text{Ca}^{2+} + \text{Mg}^{2+} + 2\text{HCO}_3^-$	-0.7717
Calcite	$\text{CaCO}_3 + \text{H}^+ \leftrightarrow \text{Ca}^{2+} + \text{HCO}_3^-$	-0.8070
Magnesite	$\text{MgCO}_3 + \text{H}^+ \leftrightarrow \text{Mg}^{2+} + \text{HCO}_3^-$	-1.5934
Strontionite	$\text{SrCO}_3 + \text{H}^+ \leftrightarrow \text{Sr}^{2+} + \text{HCO}_3^-$	-0.7702

Otavite	$\text{CdCO}_3 + \text{H}^+ \leftrightarrow \text{Cd}^{2+} + \text{HCO}_3^-$	-1.2378
Cerussite	$\text{PbCO}_3 + \text{H}^+ \leftrightarrow \text{Pb}^{2+} + \text{HCO}_3^-$	1.0681

Tables 3.7 and 3.8 show the aqueous phase complexation and carbonate precipitations reactions along with corresponding equilibrium constants used for simulations. Details on the employed sorption complexation model can be found in Ebrahimi and Vilcaez (2019). Briefly, the model accounts for the three types of hydration sites of dolomite ($>\text{CaOH}^0$, $>\text{MgOH}^0$, and $>\text{CO}_3\text{H}^0$). An intrinsic stability constant (K_{int}) that determines the concentration of divalent cations on the surface of dolomite is given by:

$$K_{\text{int}} = \frac{[>\text{CO}_3\text{Me}^+][\text{H}^+]}{[>\text{CO}_3\text{H}^0][\text{Me}^{2+}]} \quad (1)$$

where Me is Ca^{2+} , Mg^{2+} , Sr, Cd, or Pb. Employed log values of K_{int} for these metals are -1.8, -2.0, -4.66, -0.233, and -2.33, respectively. K_{int} for Ca and Mg correspond the measured values at low salinity conditions, whereas K_{int} for Sr, Cd, and Pb are assumed values based on observed removal levels.

Except for dolomite, precipitation/dissolution reactions of carbonate minerals (Table 7) are assumed to be equilibrium (instantaneous) reactions. The kinetic dissolution/precipitation of dolomite is represented by the transition state theory (TST) model (Lasaga, 1984):

$$-R_{\text{Dolomite}} = Ak_m[\text{H}^+] \left\{ 1 - \frac{[\text{HCO}_3^-]^2[\text{Ca}^{2+}][\text{Mg}^{2+}]}{[\text{H}^+]K_{\text{eq}}} \right\} \quad (2)$$

where k_m is the intrinsic rate constant, K_{eq} is the equilibrium constant of dolomite dissolution/precipitation (Table 8), and A is the surface area of dolomite. k_m and K_{eq} values

included in the widely employed EQ2/EQ6 database are used for simulations. Other parameter values for dolomite including references can be found in (Ebrahimi and Vilcáez, 2018a).

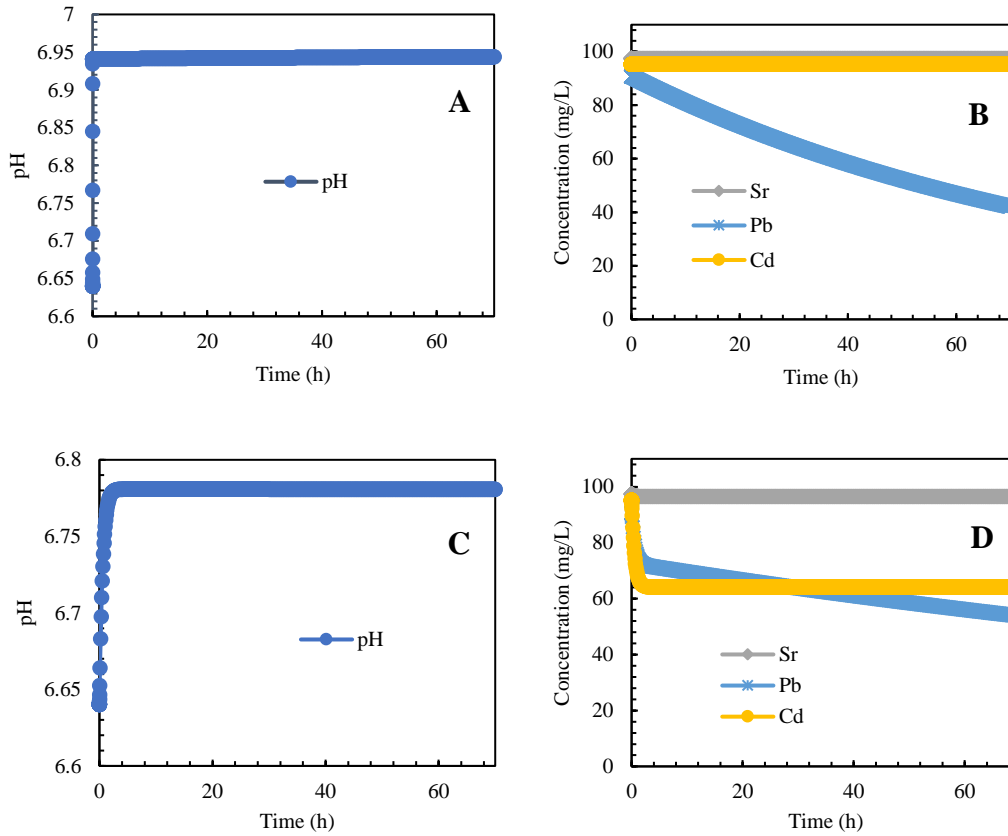


Fig. 3.23. Simulated pH variations and concentration profiles of selected toxic metals: (A-B) Accounting only for precipitation reactions, (C-D) Accounting for both sorption and precipitation reactions. PW composition corresponds to PW type VI (Table 3.3).

Fig. 3.23A-B shows concentration profiles of Sr, Cd, and Pb simulated assuming only precipitation/dissolution reactions are possible. The simulation results indicate that without sorption reactions, concentrations of Sr and Cd in PW type VI should have remained practically constant because precipitation of strontianite and otavite is thermodynamically not favored. Only the concentration of Pb should have decreased since its precipitation as cerussite is thermodynamically favored. This simulation results confirm that sorption is the main reaction controlling the removal of Ba, Sr, and Cd by dolomite

and that indeed the amount of strontianite and otavite that precipitates on dolomite is negligible as shown by the SEM-EDS analyses. Fig. 3.23C-D shows profiles of Sr, Cd, and Pb simulated accounting for the possibility of precipitation/dissolution and sorption reactions. Interestingly, the concentration profiles resemble measured removal levels of Sr, Cd, and Pb. However, the simulated removal level for Pb is not as high as the measured one. This simulation result confirms the precipitation and coprecipitation of Pb as complex carbonate minerals. Their formation would need to be included in the model to reproduce experimental results. pH in both cases increases and is in accordance with measured values suggesting that pH and thus alkalinity is a function of the reactivity of dolomite. Note that the model captures the dependency of cerussite precipitation on dolomite dissolution.

3.5. Conclusions

Batch reaction experiments were conducted to assess the role of alkalinity and dolomite reactivity on the removal of high concentrations (100 mg/L) of toxic metals (Ba, Sr, Cd, Pb, and As) from PW (TDS > 68,000 mg/L) and FW (TDS < 2,000 mg/L) by dolomite.

Ba, Sr, Cd, Pb, and As undergo sorption and precipitation reactions. However, the degree and therefore relevance of both reactions at salinity and alkalinity levels of PW are different depending on the type of metal. Ba, Sr, and Cd mostly undergo sorption reactions, whereas Pb and As undergo both sorption and precipitation reactions. Alkalinity promotes the removal of Ba, Sr, and Cd through sorption reactions by reducing the concentration of H^+ which competes for hydration (sorption) sites of dolomite. Whereas alkalinity (CO_3^{2-} and HCO_3^{2-}) promotes the removal of Pb and As by forming carbonate minerals. Given the role of alkalinity in the removal of Ba, Sr, Cd, Pb and As by sorption and precipitation

reactions, dolomite dissolution plays an important role in the removal of toxic metals from PW. This is particularly the case of Pb whose removal rate is proportional to the dissolution rate of dolomite. This conclusion is supported by SEM-EDS mapping results showing different ratios of sorbed and precipitated phases of Ba, Sr, Cd, Pb, and As on dolomite grains, as well as by XRD analysis showing the precipitation of Ba, Sr, Cd, and Pb as carbonate minerals (e.g., witherite, strontionite, otavite, and cerussite), As as oxide (calcium arsenate), and several other minerals phases with complex composition, such as strontium cadmium arsenate ($\text{SrCd}(\text{As}_2\text{O}_7)$) and lead arsenate (PbAs_2O_4) when they are all present in PW. Ba precipitates in cavities or between dolomite crystals, Sr on quartz in dolomite, Cd on ferric dolomite grains, Pb on the dints or inside edges of dolomite grains, and As precipitates directly on the surface of dolomite.

Simulations accounting for complexation reactions in the aqueous and mineral phases, equilibrium precipitation reactions of carbonate minerals, and kinetic dissolution/precipitation reaction of dolomite, confirms the thermodynamic feasibility of small amounts of Sr, and Cd precipitation and much larger precipitation amounts of Pb as carbonate minerals. Comparison between attained removal levels of Ba, Sr, Cd, Pb, and As from PW and FW of the same alkalinity shows that the effect of salinity is very different depending on the type of toxic metal. Salinity inhibits sorption reactions of Ba, Sr, and Cd and it promotes the solubility of Pb, but it does not seem to have any effect on As removal by dolomite.

The findings of this study have large practical implications to predict the fate and transport of toxic metals in saline aquifers injected with PW and to design optimum operational conditions to remove toxic metals from PW by dolomite filtration.

3.7. Acknowledgments

This work was supported by the National Science Foundation under Grant CBET-220036. This is Oklahoma State University Boone Pickens School of Geology contribution number 2023-xx.

3.8. References

- Alexandratos VG, Elzinga EJ, Reeder RJ. Arsenate uptake by calcite: macroscopic and spectroscopic characterization of adsorption and incorporation mechanisms. *Geochimica et Cosmochimica Acta* 2007; 71: 4172-4187.
- Alley B, Beebe A, Rodgers Jr J, Castle JW. Chemical and physical characterization of produced waters from conventional and unconventional fossil fuel resources. *Chemosphere*, 2011; 85(1), pp.74-82.
- Antao SM, Hassan I. The orthorhombic structure of CaCO₃, SrCO₃, PbCO₃ and BaCO₃: linear structural trends. *The Canadian Mineralogist*, 2009; 47(5), pp.1245-1255.
- Anthony JW, Bideaux RA, Bladh KW, Nichols E, Monte C., . *Handbook of Mineralogy*. Mineralogical Society of America. Chantilly, VA 20151-1110, USA. <http://www.handbookofmineralogy.org/> 1995.
- Anthony JW, Bideaux RA, Bladh KW, Nichols MC. Borates, Carbonates, Sulfates. In *Handbook of Mineralogy*. Mineralogical Society of America 2007; V.
- Balci N, Demirel C, Ön SA, Gültekin AH, Kurt MA. Evaluating abiotic and microbial factors on carbonate precipitation in Lake Acigöl, a hypersaline lake in Southwestern Turkey. *Quaternary International* 2018; 486, pp.116-128.
- Ballinger DG. 1979. Methods for chemical analysis of water and wastes. In United States Environmental Protection Agency. EPA 600/4-79-020. Environmental Monitoring

and Support Laboratory Cincinnati, Ohio. 1979: 353.2-1 to 353.2-5 (nitrate analysis) and 325.2-1 to 325.2-2 (chloride analysis).

Bettermann P, Liebau F. The transformation of amorphous silica to crystalline silica under hydrothermal conditions. *Contributions to Mineralogy and Petrology*, 1975; 53(1), pp.25-36.

Brown JGE, Parks GA. Sorption of trace elements on mineral surfaces: Modern perspectives from spectroscopic studies, and comments on sorption in the marine environment. *International Geology Review*, 2001; 43(11), pp.963-1073.

Chen X, Zhang D, Larson SL, Ballard JH, Knotek-Smith HM, Nie J, et al. Microbially Induced Carbonate Precipitation Techniques for the Remediation of Heavy Metal and Trace Element-Polluted Soils and Water. *Water, Air, & Soil Pollution*, 2021; 232(7), pp.1-15.

Da'ana DA, Zouari N, Ashfaq MY, Abu-Dieyeh M, Khraisheh M, Hijji YM, et al. Removal of toxic elements and microbial contaminants from groundwater using low-cost treatment options. *Current Pollution Reports* 2021; 7: 300-324.

Dixit S, Hering JG. Comparison of arsenic (V) and arsenic (III) sorption onto iron oxide minerals: implications for arsenic mobility. *Environmental science & technology*, 2003; 37(18), pp.4182-4189.

Drever JI. *The geochemistry of natural waters: surface and groundwater environments*. 1997; 436. p87-105.

Ebrahimi P, Borrok DM. Mobility of Ba, Sr, Se and As under simulated conditions of produced water injection in dolomite. *Applied Geochemistry* 2020; 118: 104640.

- Ebrahimi P, Vilcáez J. Effect of brine salinity and guar gum on the transport of barium through dolomite rocks: Implications for unconventional oil and gas wastewater disposal. *Journal of Environmental Management* 2018a; 214: 370-378.
- Ebrahimi P, Vilcáez J. Petroleum produced water disposal: Mobility and transport of barium in sandstone and dolomite rocks. *Science of The Total Environment* 2018b; 634: 1054-1063.
- Ebrahimi P, Vilcáez J. Transport of barium in fractured dolomite and sandstone saline aquifers. *Science of The Total Environment* 2019; 647: 323-333.
- Emmons RV, Shyam Sunder GS, Liden T, Schug KA, Asfaha TY, Lawrence JG, et al. Unraveling the Complex Composition of Produced Water by Specialized Extraction Methodologies. *Environmental Science & Technology*, 2022; 56(4), pp.2334-2344.
- Federation WE, Aph Association. Standard methods for the examination of water and wastewater. . American Public Health Association (APHA): Washington, DC, USA. 21th Edition. 2005: pp 4-75 to 4-76 (chloride method 4500-Cl G) and 4-127 to 4-129 (nitrate method 4500-NO3 I).
- Fukushi K, Munemoto T, Sakai M, Yagi S. Monohydrocalcite: a promising remediation material for hazardous anions. *Sci Technol Adv Mater* 2011; 12: 064702.
- Guerra K, Dahm K, Dundorf S. Oil And Gas Produced Water Management And Beneficial Use in the Western United States,. US Department of the Interior, 2011: p. 157.
- Holail H, Al-Hajari S. Evidence of an authigenic origin for the palygorskite in a Middle Eocene carbonate sequence from North Qatar. *Qatar Univ. Sci. J.*, 1997; 17, 405–418.

- Ingles M, Anadon P. Relationship of clay minerals to depositional environment in the non-marine Eocene Pontils Group, SE Ebro Basin (Spain). *J. Sed. Petrol.*, 1991; 61, 926–939.
- Jensen J. The Role of Carbonate Minerals in Arsenic Mobility in a Shallow Aquifer Influenced by a Seasonally Fluctuating Groundwater Table (Masters thesis, Utah State University). 2020.
- Kaasa B, Østvold T. Alkalinity in oil field waters-what alkalinity is and how it is measured. 1996.
- Kim Y, Kwon S, Roh Y. Effect of divalent cations (Cu, Zn, Pb, Cd, and Sr) on microbially induced calcium carbonate precipitation and mineralogical properties. *Frontiers in Microbiology*, 2021; 12, p.646748.
- Kumari D, Qian XY, Pan X, Achal V, Li Q, Gadd GM. Microbially-induced carbonate precipitation for immobilization of toxic metals. *Advances in applied microbiology*, 2016; 94, pp.79-108.
- Lasaga AC. Chemical kinetics of water-rock interactions. *Journal of Geophysical Research: Solid Earth* 1984; 89: 4009-4025.
- Lin CY, Musta B, Abdullah MH. Geochemical processes, evidence and thermodynamic behavior of dissolved and precipitated carbonate minerals in a modern seawater/freshwater mixing zone of a small tropical island. *Applied geochemistry* 2013; 29: 13-31.
- Neuberger CS, Helz GR. Arsenic (III) carbonate complexing. *Applied geochemistry* 2005; 20(6), pp.1218-1225.

- Omar K, Vilcaez J. Removal of mixture heavy metals and metalloids from petroleum produced water by dolomite filtration. *Journal of Contaminant Hydrology* 2021; Under review.
- Omar K, Vilcáez J. Removal of toxic metals from petroleum produced water by dolomite filtration. *Journal of Water Process Engineering*, 2022; 47, p.102682.
- Ribeiro LPS, Puchala R, Lalman DL, Goetsch AL. Composition of various sources of water in Oklahoma available for consumption by ruminant livestock. *Applied Animal Science*, 2021; 37(5), pp.595-601.
- Ryan BH, Kaczmarek SE, Rivers JM. Dolomite dissolution: An alternative diagenetic pathway for the formation of palygorskite clay. *Sedimentology*, 2019; 66(5), pp.1803-1824.
- Steeffel CI, Lasaga AC. A coupled model for transport of multiple chemical species and kinetic precipitation/dissolution reactions with application to reactive flow in single phase hydrothermal systems. *American Journal of Science* 1994; 294: 529.
- Stumm W, Morgan JJ. *Aquatic Chemistry* (3rd ed.). New York, Wiley-Interscience. Chaps 3 and 4. Detailed systematics of acid-base reactions, the carbonate system, and alkalinity titrations. 1996.
- Tabatabaeefar A, Yuan Q, Salehpour A, Rajabi-Hamane M. Batch adsorption of lead (II) from aqueous solution onto novel polyoxyethylene sorbitan monooleate/ethyl cellulose microfiber adsorbent: kinetic, isotherm and thermodynamic studies. *Separation Science and Technology*, 2020; 55(6), pp.1051-1061.
- Temple BJ, Bailey PA, Gregg JM. Carbonate Diagenesis Of The Arbuckle Group North Central Oklahoma To Southeastern Missouri. 2020: 10-30.

- Tesoriero AJ, Pankow JF. Solid solution partitioning of Sr^{2+} , Ba^{2+} , and Cd^{2+} to calcite. *Geochimica et Cosmochimica Acta* 1996; 60: 1053-1063.
- Thompson JB, Ferris FG. Cyanobacterial precipitation of gypsum, calcite, and magnesite from natural alkaline lake water. *Geology* 1990; 18, 995e998.
- Thompson JB, Schultze-Lam S, Beveridge TJ, Des Marais DJ. Whiting events: Biogenic origin due to the photosynthetic activity of cyanobacterial picoplankton. *Limnol. Oceanogr.* 1997; 42, 133e141.
- Verrecchia EP, Le Coustumer MN. Occurrence and genesis of palygorskite and associated clay minerals in a Pleistocene calcrete complex, Sde Boqer, Negev Desert, Israel. *Clay Miner.*, 1996; 31, 183–202.
- Vilcáez J. Reactive transport modeling of produced water disposal into dolomite saline aquifers: Controls of barium transport. *Journal of Contaminant Hydrology* 2020; 233: 103600.
- Wei H, Shen Q, Zhao Y, Wang DJ, Xu DF. Influence of polyvinylpyrrolidone on the precipitation of calcium carbonate and on the transformation of vaterite to calcite. *Journal of Crystal Growth*, 2003; 250(3-4), pp.516-524.
- Wolery TJ, Jackson KJ, Bourcier WL, Bruton CJ, Viani BE, Knauss KG, et al. Current Status of the EQ3/6 Software Package for Geochemical Modeling. *Chemical Modeling of Aqueous Systems II*. 416. American Chemical Society, 1990, pp. 104-116.

CHAPTER IV

EFFECT OF CARBONATE MINERALS PRECIPITATION AND SORPTION REACTIONS ON THE TRANSPORT OF TOXIC METALS IN DOLOMITE

4.1. Abstract

Predicting the fate and transport of toxic metals present in petroleum produced water (PW) disposed into dolomite saline aquifers is important to protect underground sources of drinking water and public health. In this study we assessed the effect of toxic metals (Ba, Sr, Cd, Pd, and As) precipitation as carbonate minerals, sorption reactions, and dolomite dissolution on the transport of toxic metals in dolomite. The assessment consisted of core-flooding experiments using synthetic PW, BSEs SEM, SEM-EDS, and high-resolution XRD analysis. Our results show higher removal levels of all tested toxic metals under flow than under no-flow (batch reaction) conditions, with the removal of heavy metals (Pb and Cd) being higher than the removal of metalloids (As) and alkaline earth metals (Ba and Sr). The surface morphology as well as the mineral and elemental composition of dolomite grains changed with changing the alkalinity of PW. The results support previous findings regarding the key role of alkalinity and dolomite reactivity in toxic metals removal from PW via precipitation/coprecipitation as carbonate minerals and sorption reactions. Pb and As precipitates were mainly found close to the inlet, Ba and Sr

precipitates were mainly found at the center, while Cd precipitates were generally found close to the outlet side of the dolomite core. The toxic metals concentrations, alkalinity, and pH profiles observed at the outlet of the dolomite core can be explained in terms of a transition from a stage where the removal of toxic metals is controlled by sorption and precipitation reactions driven by the initial pH and alkalinity of PW to a stage where the removal of toxic metals is controlled by sorption and precipitation reactions driven by the dissolution rate of dolomite. These new results provide critical insights into the potential impact of the initial alkalinity and pH of PW and dolomite reactivity on the transport of toxic metals in dolomite.

4.2. Introduction

Wastewater from conventional and unconventional oil and gas industries commonly called produced water (PW) is characterized by high concentrations of total dissolved solids (TDS), dissolved organic matter, and dissolved gases. TDS mainly consists of chlorine, carbonate, and sulfate salts of heavy metals, metalloids, and toxic alkaline earth metals, as well as naturally occurring radioactive materials (NORM). Dissolved organic matter is mainly dissolved hydrocarbons and dissolved gases are CO₂, CH₄, and H₂S. Opposite to dissolved organic matter, heavy metals, metalloids, and alkaline earth metals are not biodegradable, and they tend to accumulate in the soil and living tissue causing serious health problems in both animals and humans (Tabatabaeefar et al., 2020). Among all metals and metalloids in PW, Pb, Cd, As, Ba, and Sr are of special concern due to their severe toxicity (Kharaka et al., 2007b; Yin et al., 2019). Pb is characterized by toxic effects on the hematopoietic, renal, reproductive, and central nervous system due to its

ability to interfere with cellular processes and enzyme systems (Flora et al., 2012). As is a human carcinogen that can cause skin and bladder cancers, it can cause keratosis, hypertension, and cardiovascular diseases even at low levels (Jensen, 2020; Koutros et al., 2018; Ng et al., 2003; Smith et al., 2002). Long-term exposure to Cd results in kidney dysfunction and high level of exposure cause neurotoxicity and carcinogenicity that can significantly increase the risk of brain damage and perturb cell signaling pathways and eventually death (Yin et al., 2019; Zheng et al., 2017). Chronic exposure to high levels of Ba causes tachycardia, hypertension, muscle weakness, and paralysis (Kowalczyk et al., 2022). High Sr intakes can cause phosphorus deficiency and an increase in bone density (WHO) (Watts and Howe, 2010).

The concentration of Pb, Cd, As, Ba, and Sr in PW can be orders of magnitude higher than in shallow groundwater and seawater. Their concentrations exceed the drinking water standards regulated by the U.S. Environmental Protection Agency (EPA). Therefore, and for economic motives, PW is usually disposed into deep dolomite saline aquifers. However, the injection of huge volumes of PW into geologic units induces seismicity episodes even in regions that are not tectonically active, raising the prospect of underground sources of drinking water (USDW) contamination due to the possible upward migration of PW through induced or naturally occurring faults, fractures, and abandoned wells. Thus, understanding the mobility and transport of toxic metals in dolomite is important to assess the risk of USDW contamination, and/or the determine the feasibility of using dolomite as a filtration medium to remove toxic metals from PW on the surface.

In previous studies we investigated the transport of a representative toxic metal (Ba) in dolomite saline aquifers (Ebrahimi and Vilcáez, 2018c, 2019b), and we assessed the

feasibility of using dolomite as filtration medium to remove common toxic heavy metals, alkaline earth metals, and metalloids (Ba, Sr, Cd, Pb, and As) from PW (Omar and Vilcáez, 2022). Different from previous studies which focused on the transport of relatively low concentrations (<1 mg/L) of toxic metals (e.g., Zn, Cu, and As (V)) commonly present in shallow groundwater systems (TDS < 1,000 mg/L), our studies focus on the transport of high concentrations (~100 mg/L) of toxic heavy metals, alkaline earth metals, and metalloids commonly present in PW (TDS>40,000-120,000 mg/L) in dolomite. The results of our previous studies suggest that at salinity levels of PW, the competition of cations for hydration sites of dolomite and complexation reactions of metals and chlorine ions in solution control the transport of toxic metals in dolomite. However, the focus of those studies was on sorption reactions of metals in dolomite, and they were conducted using synthetic produced water (PW) of alkalinity derived only from the dissolution of atmospheric CO₂.

Sorption reactions of cations on minerals like dolomite can be due to physical, electrostatic, and chemical interactions (Drever, 1997). Physical interactions are the attraction between ions and mineral surfaces due to Van Der Waals forces. Whereas electrostatic interactions are the attraction of cations and negatively charged sites on mineral surfaces. Chemical interactions are chemical bonds between ion molecules and one or more atoms on mineral surfaces. Generally, sorption reactions are the most important interactions affecting the transport of contaminants in groundwater. Therefore, understanding these interactions (physical, electrostatic, and chemical) is important to predict the transport of toxic metals in dolomite saline aquifers (the common place of PW disposal) as well as in filters made of dolomite grains.

However, and in addition to sorption reactions, precipitation reactions of carbonate, silicate, and sulfate minerals can also affect the transport of toxic metals in dolomite if the solubility product of the mineral is exceeded. Among which, carbonate minerals precipitation is the most relevant in the carbonate rocks such as dolomite. In general, carbonate minerals precipitation is controlled by water chemistry, water temperature, and biological activity. For a carbonate mineral to precipitate, water must be saturated with a metal cation (e.g., Ca, Mg, Ba, Sr, Cd, Pb, and As) and carbonate anions (CO_3^{2-}).

In a previous study we conducted batch reaction experiments to elucidate the role of alkalinity on the removal of Ba, Sr, Cd, Pb, and As from PW by sorption and precipitation reactions on dolomite. The results indicated that under high alkalinity conditions and salinity levels of PW all tested toxic metals undergo both sorption and precipitation reactions, with Ba, Sr, and Cd undergoing mostly sorption reactions and Pb and As undergoing mostly precipitation reactions (Omar and Vilcaez, 2023). Moreover, we found that the rate of toxic metals removal by mineral precipitation reactions is proportional to the dissolution rate of dolomite which provides alkalinity (CO_3^{2-} and HCO_3^-) and cations (Ca and Mg) that compete for the sorption sites of dolomite. Building on this knowledge, the objective of this study is to elucidate the effect of both precipitation and sorption reactions on the transport of Ba, Sr, Cd, Pb, and As in dolomite, at high alkalinity conditions and salinity levels of PW. It is noteworthy that numerous previous studies have been conducted to understand the fate and transport of toxic metals in reactive porous media (e.g., graphite oxides, quartz sand, iron oxide sediments) (Jensen, 2020; Saha et al., 2020; Yin et al., 2019). However, a study to understand the fate and transport of high

concentrations of toxic metals commonly present in PW at salinity and possible alkalinity levels of PW in dolomite rocks has not been done before.

Our experimental approach consisted of core-flooding using synthetic dolomite cores made of compressed dolomite grains of the same grain size. The use of synthetic dolomite cores of the same surface area and flow and transport properties (e.g., permeability, dispersivity, and tortuosity) enabled us to conduct reproducible experiments such that we could focus on the reactive component of the transport process of the selected toxic metals.

The analytical methods we used to analyze the effect of precipitation and sorption reactions on the transport of Ba, Sr, Cd, Pb, and As in dolomite consisted of X-ray Powder Diffraction (XRD), Scanning Electron Microscopy-Dispersive X-ray Spectroscopy (SEM-EDS), backscattered electrons (BSEs) SEM analyses of dolomite grains surface, and Inductively Coupled Plasma-Optical Emission Spectroscopy (ICP-OES) analysis of the aqueous phase. XRD is commonly used to analyze the mineral composition of dry rock grains. It has been used before to determine the precipitation process and formation of calcite crystals from an amorphous CaCO_3 phase (Wei et al., 2003), for instance. XRD in this study is used to determine the nature and mineral composition of carbonate precipitates. SEM-EDS is a cutting-edge technology that shows the morphology of grains/crystals at the nano-scale level and enables the elemental classification of particles. In this study, SEM-EDS is used to map the elemental composition and morphology of sorbed and precipitated elements on dolomite. Previous studies have shown the potential of SEM-DES to analyze the sorption and mineral precipitation of heavy metals on agricultural byproducts (e.g., walnut shell and tea powder waste) (Çelebi et al., 2020; Feizi

and Jalali, 2015) and minerals (Alexandratos et al., 2007) using BSEs SEM analysis. During BSEs SEM imaging, materials are shot with high energy (eV) onto the sample surface. Elements with higher density can reflect more energy back to the detector. Thus, BSEs-SEM can differentiate sample minerals based on the density of their elements, the denser the elements in the mineral, the brighter the mineral will be displayed in the SEM image. For instance, the higher density (2.87g/cm^3) of dolomite than calcite (2.71g/cm^3) results in higher brightness for calcite than for dolomite in the SEM image due to the higher Ca (Ca is denser than Mg) content in calcite. Thus, BSEs SEM images in this study was helpful to determine changes in the morphology and composition of the dolomite surface due to dissolution-precipitation reactions.

The results of this study are presented in terms of the removal profiles of toxic metals under different alkalinity and salinity conditions, and the results obtained from analyzing the surface of dolomite by BSEs SEM, SEM-EDS, and XRD. For the sake of readability, Ba, Sr, Cd, Pb, and As are called toxic metals in this work.

4.3. Materials

4.3.1. Dolomite

Arbuckle Group dolomite was collected from the outcrop in southwest Missouri. To confirm the purity of dolomite, samples were analyzed via Powder X-ray Diffraction (Bruker XRD D8 ADVANCE Plus) analysis. The analysis confirmed that samples were composed of 98% dolomite and 2% of both blocky calcite and silica cement. The XRD spectrum distinguished dolomite-structure (JCPDS: 79-1342) from calcite structure (JCPDS: 86-2334) minerals by displaying the highest intensity of 104 (>2500 counts) at

31° 2θ as well as the strong dolomite cation (e.g., Mg and Ca) ordering peaks (101, 015, and 021 at 22° 2θ, 35° 2θ, and 44° 2θ, respectively). The samples are near perfect dolomite and thus have near stoichiometric composition (Mg/Ca~1). Our petrographic analysis demonstrated that the dolomite crystals vary between planar euhedral to subhedral, and non-planar which are in agreement with previous studies done on the Arbuckle Group dolomite in Missouri and Oklahoma (Temple et al., 2020). Our analysis also showed different crystal sizes ranging between 5 μm to 0.6 mm (Fig. 4.1).

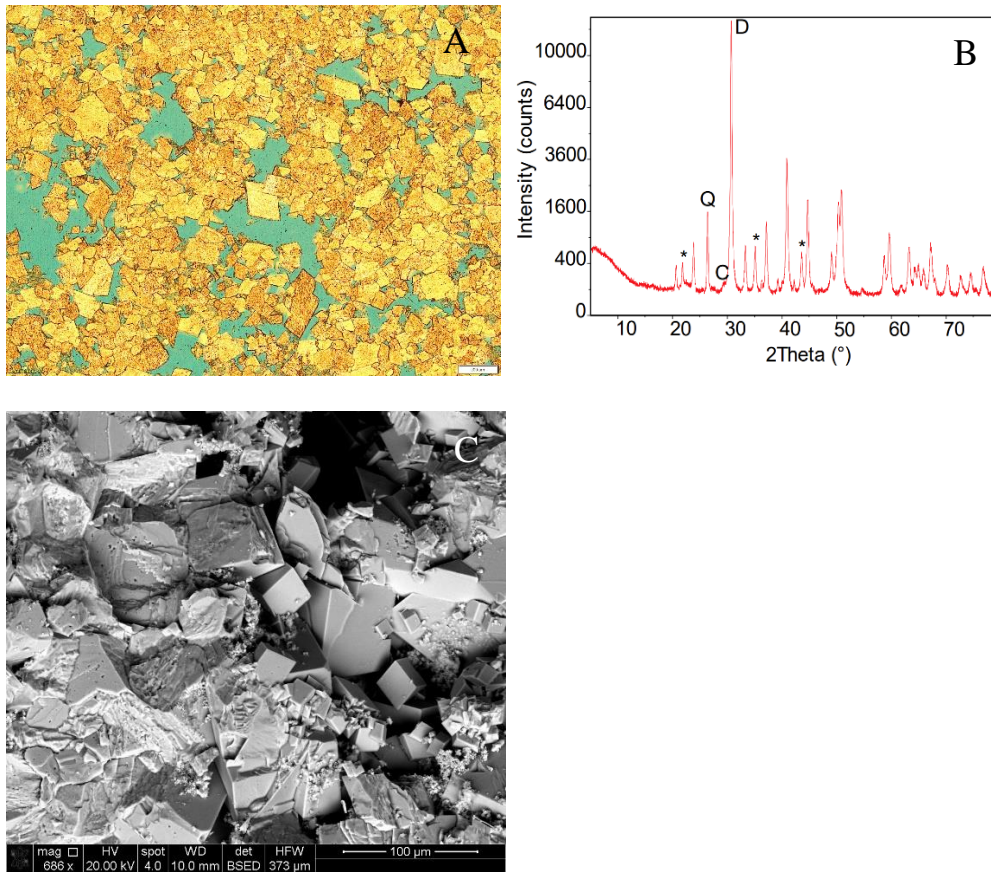


Fig. 4.1. A) Thin section (scale bare = 200 μm) showing shape and size of dolomite crystals, B) XRD analysis showing that the employed dolomite (represented by D only on the 104-dolomite peak) is mainly composed of dolomite with minor quantities of quartz and calcite cement (represented by Q only on the 101-quartz peak, and C only on the 104-calcite peak which is very weak). Dolomite cations (e.g., Mg & Ca) ordering reflections

are indicated by asterisks on 101, 015 and 021 dolomite peaks. C) SEM image showing the shape and size of dolomite crystals as well as porosity.

4.3.2. Synthetic dolomite core

The collected dolomite was crashed and sieved multiple times to obtain dolomite grains of 300-600 μm size. Prior to their utilization, dolomite grains were washed with ultrapure deionized water in an ultrasonic bath to remove dust particles. The prepared dolomite grains were used to make synthetic dolomite cores. Firstly, 200 g of dried powdered dolomite and 10 g of ultrapure deionized water was placed in the beaker then mixed very well. Secondly, the resulting aggregate was put into a stainless-steel cylindrical mold. Next, the mold was placed inside a uniaxial compaction apparatus (Carver Laboratory Presser (Model 4387)) exerting a pressure of 4,320 psi for one hour. The dimensions of the resulting synthetic dolomite core were 3.8 cm diameter and ~8.1 cm length with porosity and permeability of 15% and 1000 mD, receptivity. Finally, one or two of these filters were placed into the core holder of a core-flooding system to conduct the core-flooding experiments using synthetic PW or freshwater.

4.3.3. Synthetic produced water

Since TDS in PW is mostly composed of chloride and carbonate salts, synthetic PW of different coexisting metals, alkalinity, and salinity (NaCl) was prepared by adding NaCl, $\text{CaCl}_2 \cdot 2\text{H}_2\text{O}$, $\text{MgCa}_2 \cdot 6\text{H}_2\text{O}$, $\text{SrCa}_2 \cdot 6\text{H}_2\text{O}$, $\text{BaCa}_2 \cdot 2\text{H}_2\text{O}$, $\text{CdH}_8\text{N}_2\text{O}_{10}$, PbCl_2 , and AsCl_3 (Fisher Scientific Co. with the purity of >99.9%) into ultrapure deionized water (Table 4.1). TDS of the prepared synthetic PW was 69,200-77,300 mg/L. To confirm the

different behavior of the tested toxic heavy metals in PW (high salinity water) and freshwater (low salinity water), synthetic freshwater (FW) was prepared and used to conduct the same experiments as with synthetic PW. TDS of the prepared synthetic FW was $<1,700$ mg/L and contained the same salts as the synthetic PW (Table 4.2). The initial alkalinity of the prepared synthetic PW and FW that resulted from the dissolution of atmospheric CO_2 , was increased by adding CaCO_3 . To ensure the total dissolution of the added salts, the prepared synthetic PW and FW were stirred overnight. Possible undissolved particles in the prepared synthetic PW and FW were removed by filtration using a $0.4 \mu\text{m}$ cellulose filter. Two types of synthetic PW and FW were prepared. PW types I and II and FW type I were added with CaCO_3 to increase alkalinity, whereas PW types III & IV and FW type II were not added with CaCO_3 to increase alkalinity (Table 4.1 and 4.2).

We used concentrations of Ca and Mg in the synthetic PW that correspond to PW in Oklahoma (Ribeiro et al., 2021) and U.S. Mid Continent (Guerra et al., 2011c). Since concentrations of sulfate in PW are negligible in these regions, sulfate is not considered in this work and the prepared synthetic PW and FW did not contain sulfate. Arsenite (As (III)) salt (AsCl_3) was used instead of arsenate (As(IV)) because PW originates under reduced conditions and the oxidation of arsenite to arsenate by dissolved oxygen is very slow (Dixit and Hering, 2003). For the sake of assessing the effect of alkalinity on the removal of toxic metals, salinity (NaCl) and the initial concentrations of metals and metalloids (Ca, Mg, Cd, Pb, Sr, Ba, and As) were kept the same in all types of synthetic PW and FW used to conducted the core-flooding experiments.

Table 4.1. Added salts to prepare synthetic produced water (PW).

Salts (g/L)	Type of PW			
	I	II	III	IV
NaCl	40	40	42	42
CaCO ₃	5	5	0	0
CaCl ₂ .2H ₂ O	14.7	14.7	25.7	25.7
MgCl ₂ .6H ₂ O	8.4	8.4	8.4	8.4
BaCl ₂ .2H ₂ O	0.1782	0.1783	0.178	0.1787
SrCl ₂ .6H ₂ O	0.3023	0.3024	0.304	0.3035
CdH ₈ N ₂ O ₁₁	0.27455	0.2724	0.275	0.2749
PbCl ₃	0.1305	0.1296	0.135	0.1341
AsCl ₃	0.241	0.241	0.241	0.241
TDS	69.22655	69.2237	77.233	77.2322

Table 4.2. Added salts to prepare freshwater (FW).

Salts (g/L)	Types of FW	
	I	II
NaCl	0.1081	0.1006
CaCO ₃	0.2551	0
CaCl ₂ .2H ₂ O	0	0.15905
MgCl ₂ .6H ₂ O	0.1973	0.2
BaCl ₂ .2H ₂ O	0.1774	0.17705

SrCl ₂ .6H ₂ O	0.3077	0.304
CdH ₈ N ₂ O ₁₁	0.2747	0.2748
PbCl ₃	0.1367	0.1349
AsCl ₃	0.241	0.241
TDS	1.698	1.5914

4.4. Methods

4.4.1. Core-flooding experiments

The core-flooding experiments consisted of injecting 1 L of synthetic PW into the prepared dolomite core placed in a Hassler Type core-holder (RCH-series of Core Laboratory). Confining pressure in the core-holder was 2,300 psi. The injection operation was done using a floating piston accumulator connected to a 260 dual syringe pump (Teledyne ISCO). Water was injected at a constant flow rate of 0.1 mL/min through two inlet points at the bottom of the core-holder. The inlet pressure was monitored through the pressure transducer of the syringe pump. Water samples were collected at the inlet and outlet of the core holder. Their compositions were analyzed at the Soil, Water, and Forage Analytical Laboratory (SWFAL) of Oklahoma State University. The analysis included the measurement of all heavy metals, alkaline earth metals, and metalloids (Na, Ca, Mg, Ba, Sr, Cd, Pd, and As), chloride (Cl⁻), as well as pH and total alkalinity (CO₃²⁻ and HCO₃⁻). The concentration of Na, Ca, Mg, Ba, Sr, Cd, Pb, and As were measured by ICP-OES analysis. Alkalinity was measured by the titration method using a Hach TitraLab AT1000 Series auto-titrator with an autosampler. This method involves the titration of samples with standard 0.02N sulfuric acid (H₂SO₄) titrant to endpoints of pH 8.3 and 4.5. The pH

endpoint of 8.3 corresponds to carbonate alkalinity, whereas the pH endpoint of 4.5 corresponds to bicarbonate alkalinity. Chloride was measured by the colorimetric method using ferricyanide in a flow-injection analyzer (Ballinger, 1979; Federation and Aph Association, 2005). At the end of the experiments, dolomite grains (~3g) were sampled from the bottom (inlet), center, and top (outlet) of the filter for BSEs SEM, XRD, and SEM-EDS analyses to determine changes in the morphology as well as the elemental and mineral composition of the dolomite grains surface due to precipitation/dissolution sorption/desorption reactions (Fig. 4.2). For the sake of results validation, experiments were repeated at least two times. Tables 4.2 and 4.3 show the measured alkalinity, initial pH, and composition of all synthetic PW and FW used to conduct the core-flooding experiments.

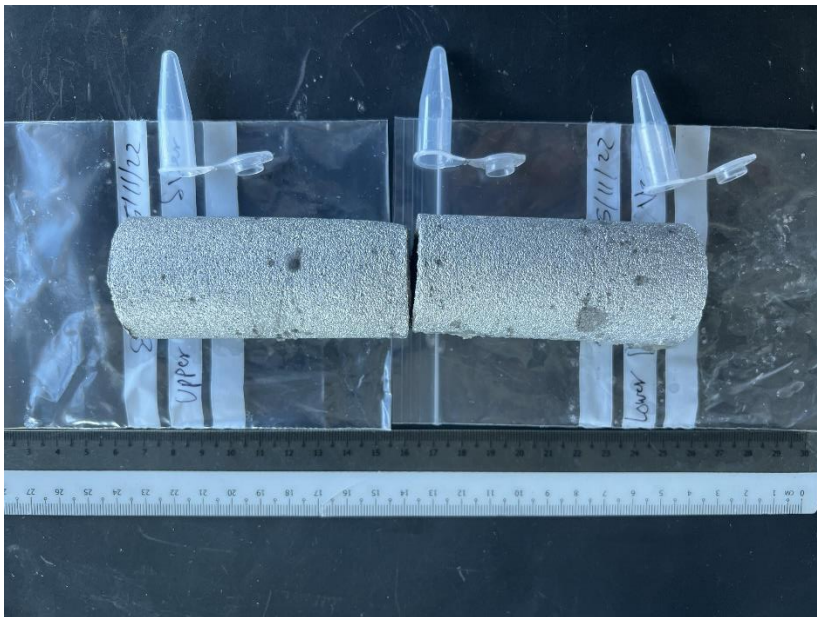


Fig. 4.2. Representative synthetic dolomite core and sampling of dolomite grains (inlet, center, and outlet).

Table 4.3. Initial composition of synthetic produced waters (PW).

(mg/L)	Type of produced water (PW)			
	I	II	III	IV
Na	15943.5	16957.8	17,273.40	17935.3
Cl	31310.5	31353.5	41,965.50	43536
Ca	4014.7	4191.6	7175.5	7484.3
Mg	940.2	974.3	1011.9	815.6
Ba	90.3	87	97.7	79.9
Sr	91.3	88.3	102.1	81.9
Cd	71.3	61.1	97.6	72.8
Pb	3.8	3.9	67.3	81.1
As	93.3	83.8	93.6	84.4
Alkalinity	101.7	79.6	0	0
pH	6.9	6.9	2.61	2.1

Table 4.4. Initial composition of synthetic freshwaters (FW).

(mg/L)	Type of freshwater (FW)	
	I	II
Na	31.2	38.3
Cl	436.6	607.1
Ca	100.4	45.6
Mg	11.2	21.9

Ba	97	98.2
Sr	101	99.1
Cd	95.8	99.4
Pb	33.7	99
As	95.8	106.8
Alkalinity	2.8	0
pH	6	2.7

4.4.2. XRD and SEM-EDS analyses

To determine the impact of sorption and precipitation reactions on the transport of toxic metals in dolomite, we used SEM-EDS and XRD analyses. SEM-EDS analysis was used to identify changes in the surface morphology of the dolomite grains due to the precipitation of amorphous and/or crystal phases of metals, and to map the elemental distribution of metals (sorbed and precipitated) on the surface of dolomite. Dolomite samples were dried but not pulverized for SEM-EDS analysis. This analysis was performed at the OSU Microscopy Laboratory using a SEM FEI Quanta 600 field emission gun ESEM with Bruker EDS and HKL EBSD. Samples for SEM-EDS analysis were coated with carbon (graphite) to prevent artifacts and to optimize the quality of the microphotographs. To avoid missing any relevant features and enhance the generated results, SEM-EDS mapping was performed at different magnification scales (e.g., 1 mm, 100 μm , and 10 μm). The samples used for SEM-EDS analysis were used to conduct BSEs SEM analysis. Since SEM-EDS analysis does not provide information on the mineral and/or amorphous

composition of precipitates, we used powder XRD for this purpose. XRD is commonly used for identifying mineral crystals and their polymorphs in the rocks. A quantitative application of this analytical method presents several challenges and limitations. Thus, we did a semiquantitative analysis of the precipitates. To this aim, high-resolution XRD analyses were conducted on pulverized dolomite grains at the Microscopy Laboratory of Oklahoma State University, using a Bruker D8 ADVANCE Plus XRD. The obtained XRD data were semi-quantitatively analyzed via DIFFRAC.EVA software using the ICDD-PDF-2-2022 and Crystallography Open Database (COD).

4.5. Results and discussion

Core flooding experiments were conducted to analyze the effect of precipitation and sorption reactions on the transport Ba, Sr, Cd, Pb, and As in dolomite. To this aim we measured the removal levels of Ba, Sr, Cd, Pb, and As by the dolomite cores, and we analyzed changes in the morphology of the dolomite grains surface, as well as changes in the mineral and elemental composition of dolomite grains collected from different points in the dolomite core after each core-flooding experiment. The core-flooding experiments consisted of flooding synthetic dolomite cores with 1L of synthetic PW and FW whose compositions are shown in Tables 1 and 2. We used two lengths of dolomite cores (~8.1 and ~16.2 cm length).

4.5.1. Removal levels

Table 4.5. Toxic metals removal from PW.

	Type of produced water (PW)			
	I	II	III	IV
Final pH	7.57	7.51	7.2	7.37
Alkalinity increment (mg/L)	6.59	-8	0*	0*
Ba removal (%)	3.45	2.86	4.43	1.34
Sr removal (%)	2.8	0.36	2.59	1.06
Cd removal (%)	64.77	44.86	44.81	11.89
Pb removal (%)	96.42	94.89	97.57	95.89
As removal (%)	28.26	17.17	29.19	25.42

*Below detection limits

I and III: Used with 8.1 cm dolomite core length.

II and IV: Used with 16.2 cm dolomite core length.

Table 4.6. Toxic metals removal from FW

	Type of freshwater (FW)	
	I	II
Final pH	7.59	7.85
Alkalinity increment (mg/L)	16.04	32.84
Ba removal (%)	11.79	16.46
Sr removal (%)	7.59	11.13

Cd removal (%)	85.61	94.42
Pb removal (%)	99.41	99.98
As removal (%)	11.79	18.51

I and II: Used with 16.2 cm dolomite core length.

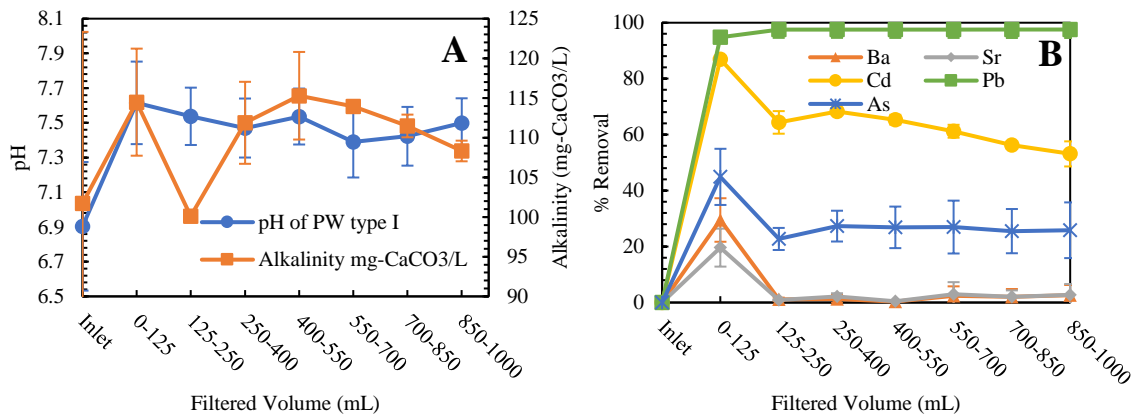


Fig. 4.3. Toxic metals removal from PW type I (added with CaCO₃) using a 16.9 cm dolomite core: A) pH and alkalinity profiles at the outlet of the dolomite core, and B) Toxic metals removal profiles at the outlet of the dolomite core.

Fig. 4.3 shows Ba, Sr, Cd, Pb, As removals, total alkalinity concentrations, and pH profiles at the outlet of the core-holder using PW type I of 102 mg/L total alkalinity (Table 4.3) and a dolomite core of 16.9 cm length. Lower concentrations of all toxic metals at the outlet than at the inlet confirm their removal by dolomite due to precipitation and sorption reactions. In accordance with our previous study showing that at high alkalinity and salinity conditions of PW, precipitation reactions contribute to the removal of Pb and As, the removal of Pb and As is higher than the removal of Ba and Sr whose removal is mostly due to sorption reactions. However, opposite to the removal sequence observed in batch reaction experiments, higher removal levels are observed for Cd than for As under flow conditions. This behavior suggests that the removal of Ca and Mg from the pore space of

dolomite by advection favors the sorption of Cd more than it does the sorption of As. It is well-known that Ca and Mg competes with other cations for hydration sites of dolomite, as such their removal by advection from the dolomite results in different sorption degrees determined by an intrinsic stability constant:

$$K_{\text{int}}^s = \frac{[>\text{CO}_3\text{Ms}^+][\text{H}^+]}{[>\text{CO}_3\text{H}^0][\text{Ms}^{2+}]} \quad (1)$$

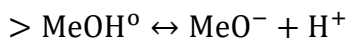
where $[\text{Ms}^{2+}]$ and $[>\text{CO}_3\text{Ms}^+]$ are the activity of Ms (Ca, Mg, Ba, Sr, Cd, and Pb) in solution and on the hydration sites of dolomite ($>\text{CaOH}^0$, $>\text{MgOH}^0$, and $>\text{CO}_3\text{H}^0$).

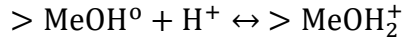
A higher removal level of all toxic metals at the beginning than at the subsequent stages of the flooding process can be attributed to a transition stage where sorption and precipitation reactions control the removal of toxic metals, to a stage where the dissolution of dolomite controls the removal of toxic metals by both precipitation and sorption reactions according to the following main reactions:

Dolomite dissolution:



Sorption reactions (Ebrahimi and Vilcez, 2019a; Pokrovsky et al., 1999c):





where Me is Ca and Mg.

Representative precipitation reaction:



According to this mechanism, during the initial stages (0-125 mL) where sorption reactions (Eq. (4)) control the removal of toxic metals, dolomite dissolution (Eq. (2)) results in an increase of pH from 6.9 to ~7.6 and alkalinity from 102 to 114 mg/L. During the transition stage where sorption and precipitation reactions (Eq. (5)) control the removal of toxic metals by dolomite, the removal of Ba, Sr, Cd, and As reach highest levels. However, precipitation reactions of toxic metals cause a drop of alkalinity reflected by a decrease of the removal of toxic metals, except for Pb whose solubility as PbCO_3 is smaller than the solubility of Ba as BaCO_3 , for instance. Eventually, during the later stages (>125 mL) pH and alkalinity reach a steady condition controlled by the dissolution of dolomite. This is reflected by practically a constant rate of toxic metals removal by sorption and/or precipitation reactions. Apparently, depending on the initial concentrations of Ca and Mg, alkalinity, and pH, dolomite dissolution can favor sorption reactions by increasing the pH, or it can oppose sorption reactions by increasing the concentration of cations (Ca and Mg) that compete for the hydration sites of dolomite. Whereas, depending on the initial alkalinity of PW, alkalinity, which is also generated from the dissolution of dolomite, favors precipitation and/or coprecipitation of toxic metals.

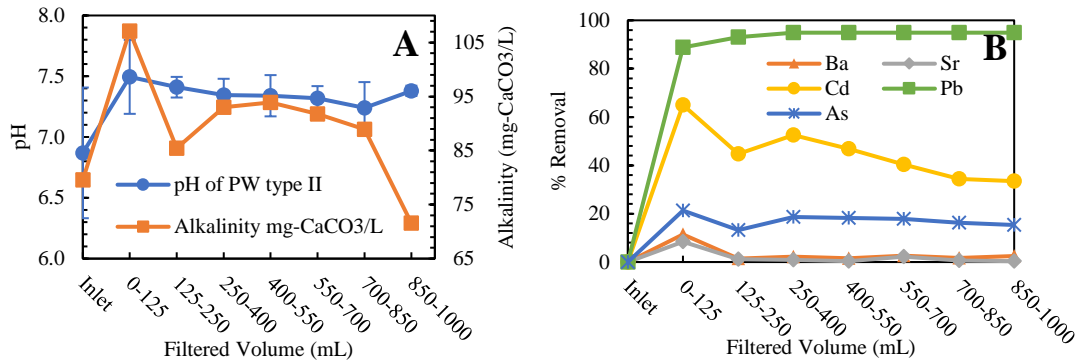


Fig. 4.4. Toxic metals removal from PW type II (added with CaCO₃) using a 8.2 cm dolomite core: A) pH and alkalinity profiles at the outlet of the dolomite core, and B) Toxic metals removal profiles at the outlet of the dolomite core.

To verify the effect of dolomite dissolution on the removal of toxic metals under flow conditions, we repeated the experiments using a shorter synthetic dolomite core (~8 cm length). Fig. 4.4 shows Ba, Sr, Cd, Pb, As removals, total alkalinity concentrations, and pH profiles at the outlet of the core-holder using PW type II of 79.6 mg/L total alkalinity (Table 4.3) and a dolomite core of 8.2 cm length. The same profiles obtained with a larger dolomite core (Fig. 4.3) confirm the transition from a stage controlled by sorption and precipitation reactions to a stage controlled by dolomite dissolution. Interestingly, practically the same removal levels of toxic metals are obtained during the initial stages (0-125 mL) of the flooding process, confirming that this stage is controlled by sorption and precipitation reactions, and it is not limited by the availability of hydration sites or alkalinity. However, the removal levels decrease during the later stages (>125 mL) where dolomite dissolution controls the removal of toxic metals. This decrease is larger than the decrease observed with the larger size dolomite core, confirming that the amount of alkalinity generated from the dissolution of dolomite plays an important role in the removal of toxic metals by dolomite because it ends up controlling both sorption and precipitation

reactions according to the proposed mechanism (Eqs. (2)-(5)). Consequently, the larger the size of the dolomite core, the larger the removal levels of toxic metals that can be achieved. This has practical implications to predict the fate of toxic metals in PW disposed in deep saline aquifers and to design dolomite filters to remove toxic metals from PW on the surface.

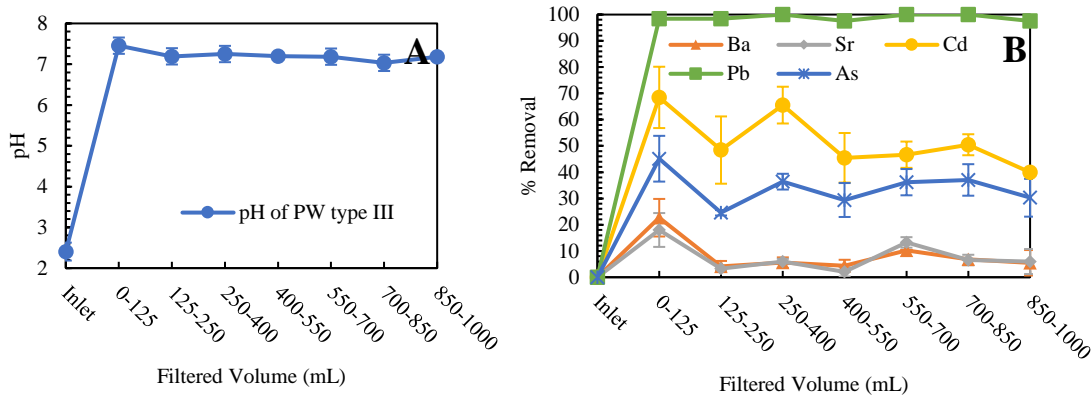


Fig. 4.5. Toxic metals removal from PW type III (not added with CaCO_3) using a 15.8 cm dolomite core: A) pH and alkalinity profiles at the outlet of the dolomite core, and B) Toxic metals removal profiles at the outlet of the dolomite core.

Given the fact that alkalinity in PW is variable and that some PW have close to zero alkalinity, we conducted experiments using PW type III that was not added with CaCO_3 to increase alkalinity. Fig. 4 shows Ba, Sr, Cd, Pb, As, and total alkalinity concentrations, and pH profiles at the outlet of the core-holder using PW type III of total alkalinity below detection limits (Table 4.3) and a dolomite core of 15.8 cm length. The inlet pH was acidic due to the formation of hydrochloric acid according to the following reaction: $\text{AsCl}_3 + 3\text{H}_2\text{O} = \text{As}(\text{OH})_3 + 3\text{HCl}$. The formed acid resulted in a pH of ~ 2.4 . The fast dissolution of dolomite under acidic conditions (Eq. (2)), results in a fast increase of pH to ~ 7.5 and remains practically constant throughout the remainder of the experiment. Like the toxic metal removal profiles obtained with PW type I whose initial alkalinity was increased by

adding CaCO_3 , removal levels of toxic metals with PW type III (Fig. 3) reach highest levels during the initial stages of the flooding process (0-125 mL) where sorption and precipitation reactions control the removal of Ba, Sr, Cd, and As, and Pb, respectively. Apparently, the acidic pH of PW type III, resulted in fast dissolution rate of dolomite providing alkalinity for the continuous removal of Pb. However, given low pH and thus higher concentration of protons (H^+) which also compete for hydration sites of dolomite (Eq. (4)), attained removal levels of Ba, Sr, and Cd whose removal is mostly due to sorption reactions, reached lower levels with PW type III than with PW type I. Fluctuations in the removal of toxic metals following the initial stages (0-125 mL) might be due to fluctuations between the stages controlled by sorption/precipitation reactions and dolomite dissolution reactions derived from the close to zero initial alkalinity of PW type III injected into the dolomite core.

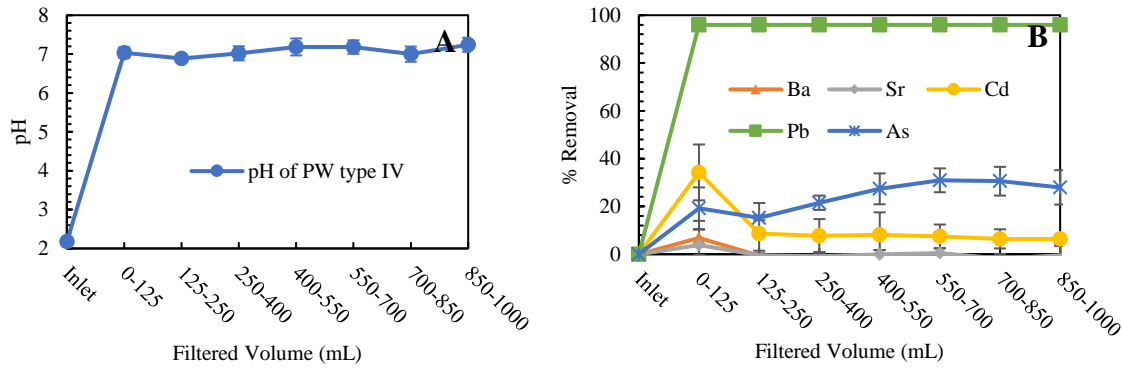


Fig. 4.6. Toxic metals removal from PW type IV (not added with CaCO_3) using an 8.1 cm dolomite core: A) pH and alkalinity profiles at the outlet of the dolomite core, and B) Toxic metals removal profiles at the outlet of the dolomite core.

To further investigate the role of dolomite dissolution and alkalinity on the removal of toxic metals, we repeated the previous experiment using PW type IV which was not supplied with CaCO_3 using a shorter dolomite core (8.1 cm length). Fig. 4.6 shows Ba, Sr,

Cd, Pb, As removals, total alkalinity concentrations, and pH profiles at the outlet of the core-holder using PW type IV of total alkalinity below detection limits (Table 4.3) and a dolomite core of 8.1cm length. The profiles are like those obtained using a shorter dolomite core, and as expected, lower removal levels are attained for Ba, Sr, Cd, and As using a 8.1 cm length than a 16.2 cm length dolomite core because dolomite dissolution favors toxic metals removal by increasing alkalinity and pH. However, higher removal levels are obtained for As than for Cd with a shorter dolomite core. This is opposite to the behavior observed using a longer dolomite core. This behavior is attributed to the lower pH of PW type IV compared to PW type III. The initial pH of PW type III was 2.6, whereas the initial pH of PW was 2.1. Given the logarithmic relationship between pH and the concentration of H^+ , a $10^{0.5}$ difference in the concentration of H^+ resulted in higher dissolution rates of dolomite that promoted the coprecipitation of As, and an inhibition of Cd sorption which are the most relevant reactions controlling the removal of these two toxic metals (Omar and Vilcáez, 2022).

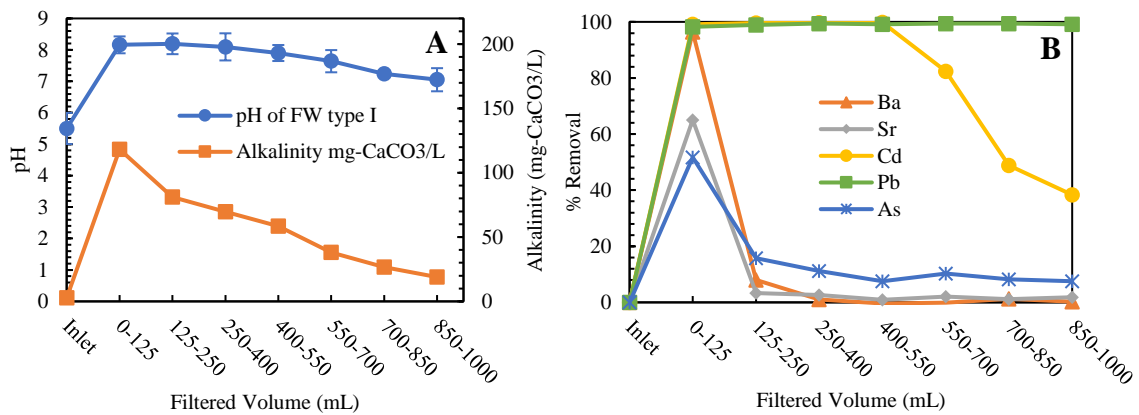


Fig. 4.7. Toxic metals removal from FW type I (added with CaCO₃) using a 15.8 cm dolomite core: A) pH and alkalinity profiles at the outlet of the dolomite core, and B) Toxic metals removal profiles at the outlet of the dolomite core.

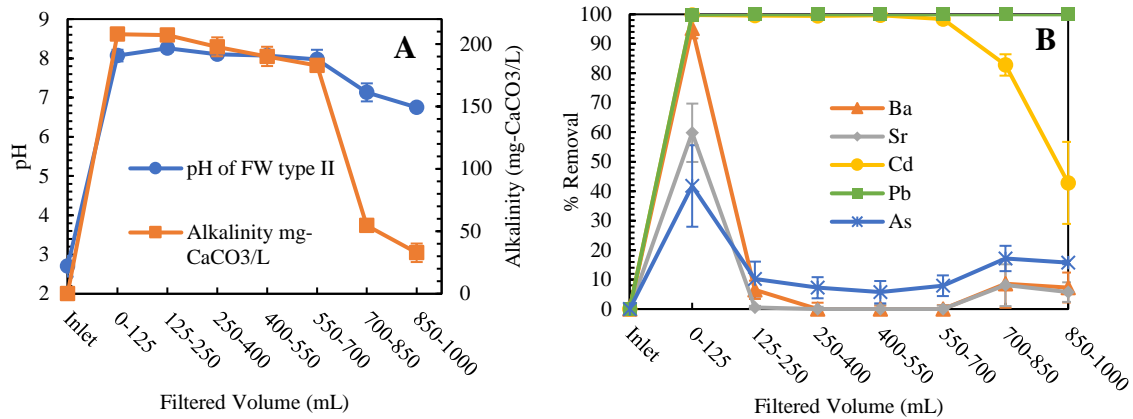


Fig. 4.8. Toxic metals removal from FW type II (not added with CaCO₃) using a 16.3 cm dolomite core: A) pH and alkalinity profiles at the outlet of the dolomite core, and B) Toxic metals removal profiles at the outlet of the dolomite core.

Another important goal of this study was to identify differences between the removal of toxic metals by dolomite from PW and FW. To this aim, we conducted core-flooding experiments using FW (Table 4.4) instead of PW (Table 4.3). Fig. 4.7 shows Ba, Sr, Cd, Pb, As removals, total alkalinity concentrations, and pH profiles at the outlet of the core-holder using FW type I of 2.8 mg/L total alkalinity (Table 4.4) and a dolomite core of 15.8 cm length.

In accordance with the results obtained from batch reaction experiments, higher removal levels of toxic metals are obtained with FW than with PW, and in agreement with the new finding regarding the effect of competing cations (Ca and Mg) removal by advection on the removal toxic metals by dolomite, higher removals were obtained in core-flooding than in the batch reaction experiments. The removal levels during the initial stages (0-125 mL) of the flooding process reach much higher levels with FW type I than with PW type I of 101.7 mg/L total alkalinity (Tables 4.5 and 4.6). This behavior is attributed to the faster dissolution rate of dolomite with FW type I than with PW type I (Eq. (2)) as indicated by the higher alkalinity and pH levels attained during the initial stages with FW type I (~8

and 118 mg/L) than with PW type I (~7.6 and 112 mg/L), as well as to the to the lower complexation degree of free toxic metals with chlorine anions according to: $Ms^{2+} + 2Cl^{-} \leftrightarrow (MsCl_2)^{+}$ with FW than with PW. Higher alkalinity and pH levels with FW type I than with PW type I is due to the low pH of FW type I (5.5) compared to the pH of PW type I (6.9). In accordance with our batch reaction experiment results regarding the removal of Cd by mostly sorption reactions (Omar and Vilcáez, 2022), a decrease in alkalinity and thus pH during the latest stage due to precipitation reactions is accompanied by a decrease in the removal levels of Cd.

4.5.2. SEM analysis of changes in the morphology of dolomite surface

To confirm the formation of precipitates, we analyzed the surface morphology of dolomite grains sampled from dolomite powder before core preparation and from the inlet, center, and outlet sides of the cores after been flooded with PW and FW (Fig. 4.2).

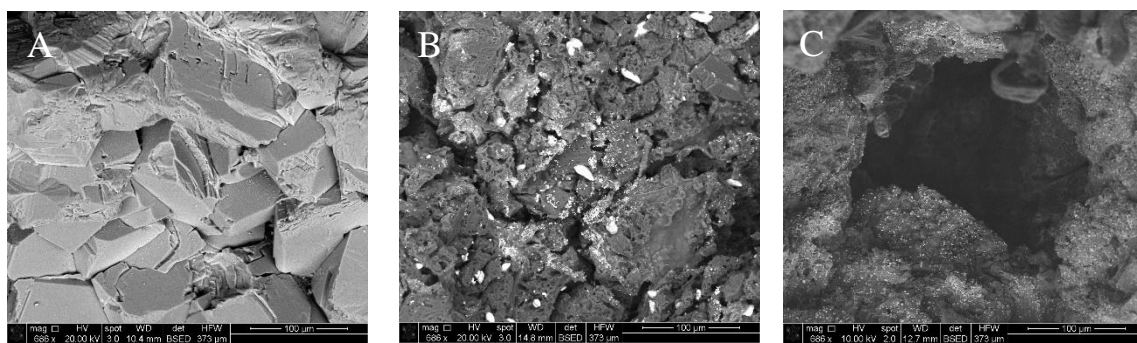


Fig. 4.9. SEM images of toxic metals precipitates (bright white) on dolomite surface: A) Control sample, B) Flooded with FW type II (inlet side of the core), and C) Flooded with PW type II (inlet side of the core)

Fig. 4.9 shows representative SEM images comparing the surface morphology of dolomite grains collected from the inlet, center, and outlet of the dolomite core flooded with PW type II (without added CaCO_3) and FW II (without added CaCO_3). The surface morphology of dolomite changed after the core-flooding experiment owing to dissolution of dolomite and carbonate minerals precipitation. Different from batch reaction experiments where Ba and Sr precipitates were rarely found, all toxic metals were found as precipitates but at different amounts through the dolomite cores. The precipitates had different shapes, roundness, and sizes. The shapes of precipitates range from circular, oval, and polygonal to irregular forms with smooth perfect to etched angular roundness. The precipitates were commonly seen with cavities or as partially eroded particles, especially with PW.

The ways of deposition and arrangement of the precipitates were different from place to place within the same dolomite core with PW and FW (Figs 4.10 - 4.13). Particle precipitates were found as a single particle mainly at the center of the dolomite core whereas the precipitates at the inlet and outlet sides were mainly clustered to clumped particles. Moreover, the precipitated particles were of various sizes ranging from several nanometers to several micrometers and the larger particles were commonly observed at the inlet side of the column. The number of precipitates was significantly larger in locations surrounding the pore troughs on edges and cavities, and on grain surfaces facing the fluid flow direction.

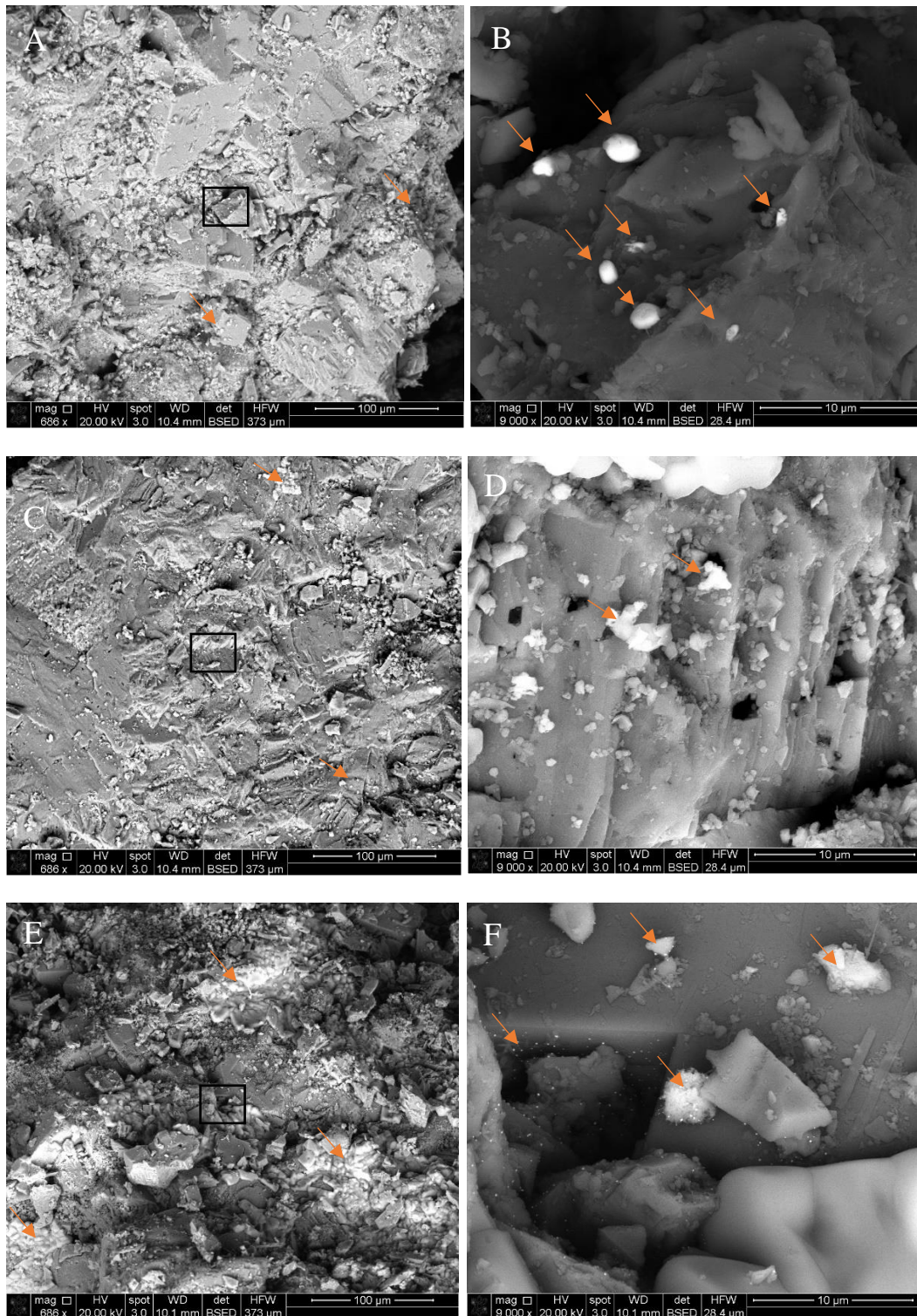


Fig. 4.10. SEM images of toxic metals precipitates (bright white) on dolomite surface with PW type I (added with CaCO_3): A) Inlet of the dolomite core, B) Zoom-in of A, C) Center of the dolomite core, D) zoom-in of C, E) Outlet of the dolomite core showing huge bright patches of precipitates, and F) zoom-in of E showing precipitates of different size and shapes.

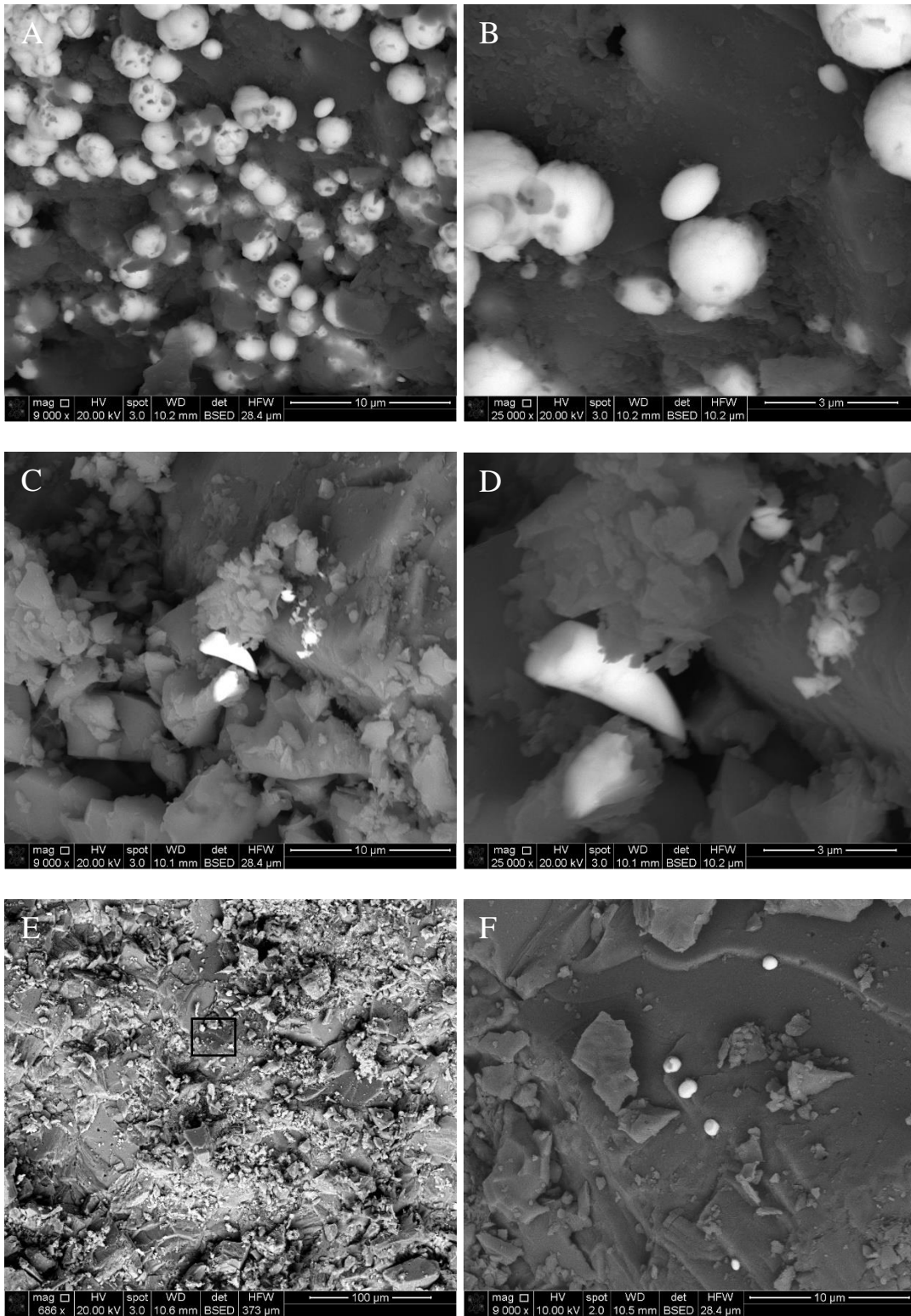


Fig. 4.11. Shows SEM micrographs of dolomite surface form column used for filtering PW type II (added with CaCO_3). Fig. 10 also shows toxic metals precipitates: A) bottom of the filter, B) Zoom-in of A showing precipitates with cavities, C) center of the filter, D) zoom-in of C, E) top of the filter, and F) zoom-in of E showing precipitates with different shapes.

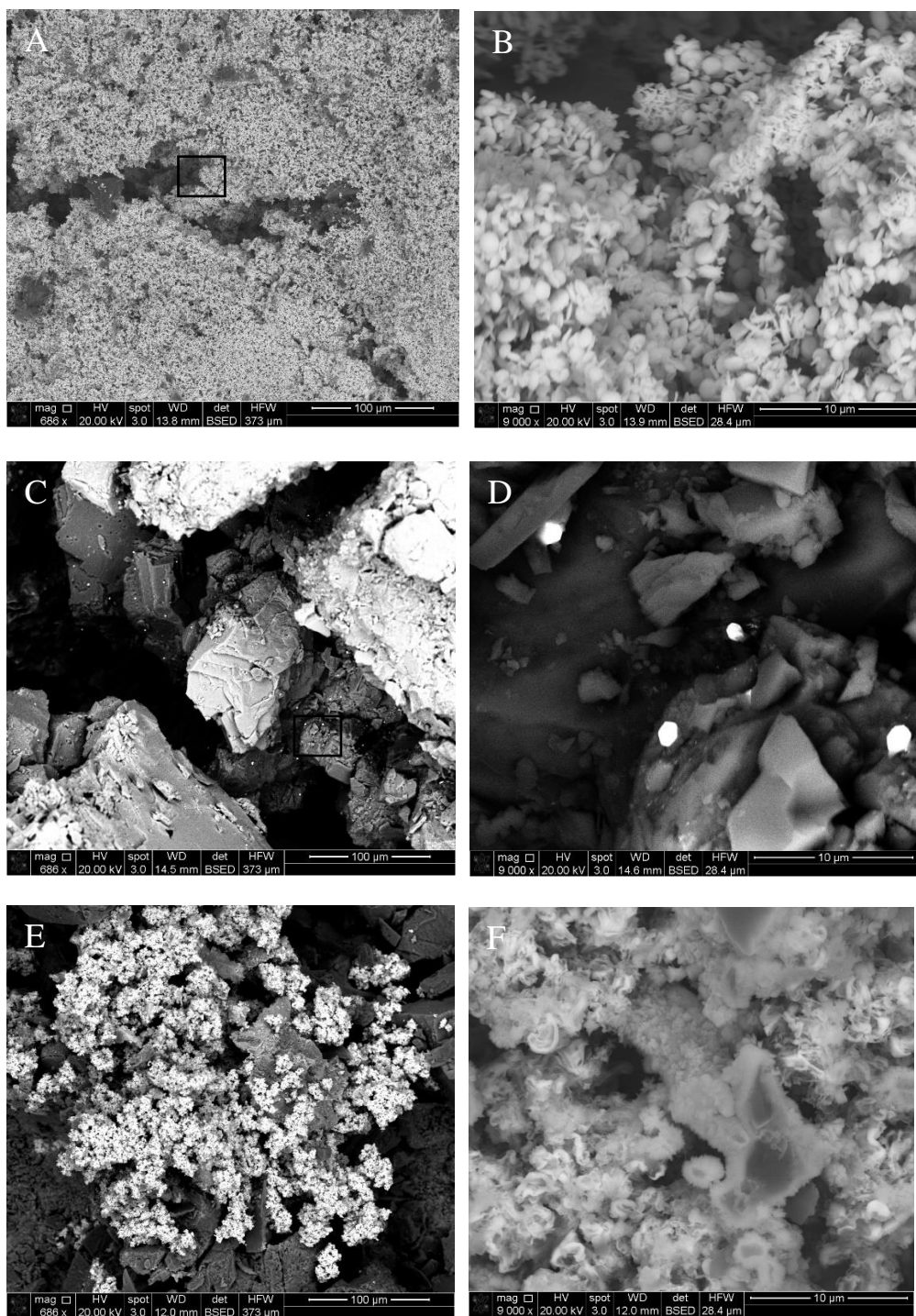


Fig. 4.12. SEM images of toxic metals precipitates (bright white) on dolomite surface with FW type I, which was added with CaCO_3 : A) Inlet of the dolomite core, B) Zoom-in of A showing precipitates of different shapes and sizes, C) Center of the dolomite core showing hexagonal-shaped precipitates, D) zoom-in of C, E) Outlet of the dolomite core showing huge bright patches of precipitates, and F) zoom-in of E showing precipitates with irregular shapes.

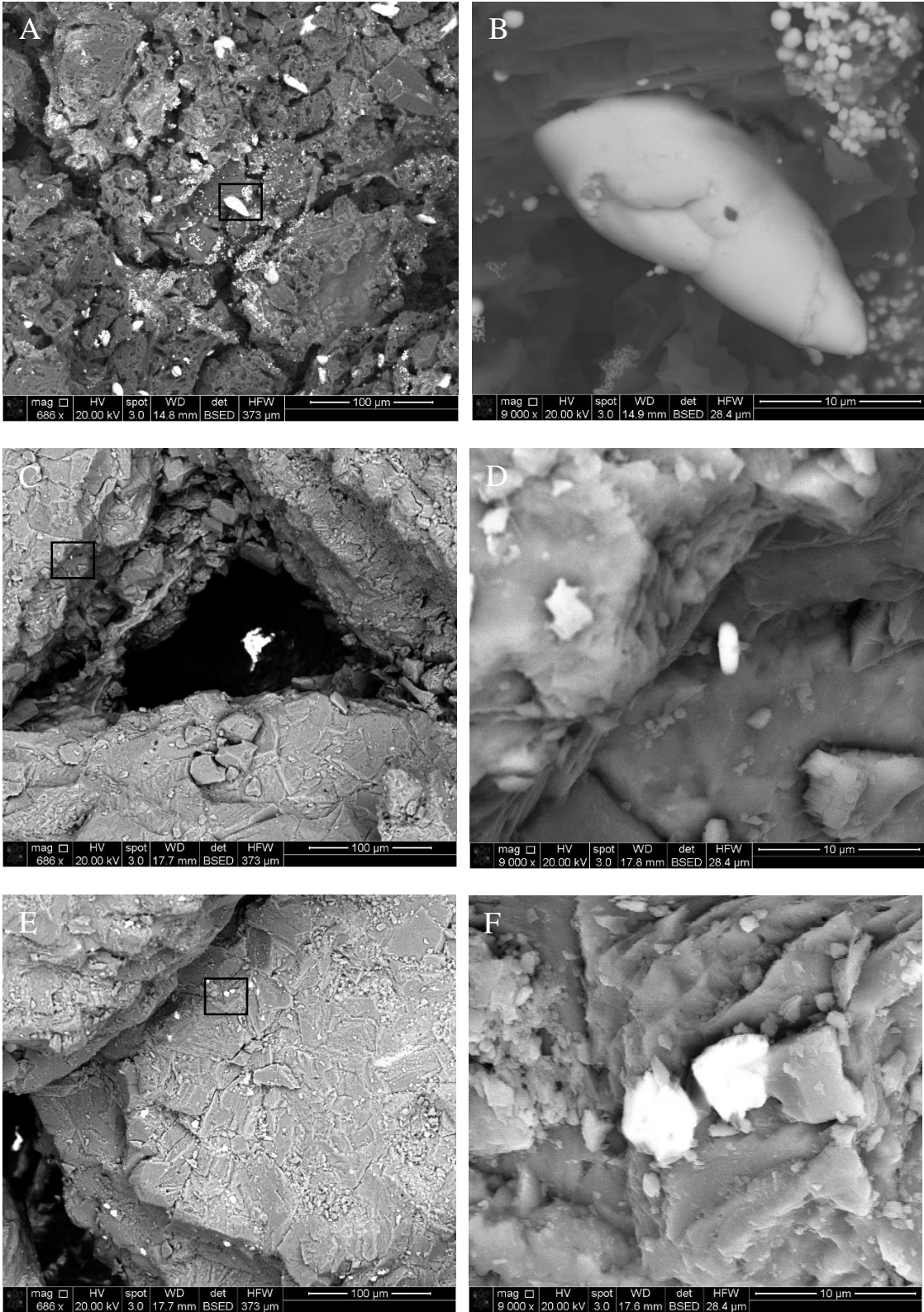
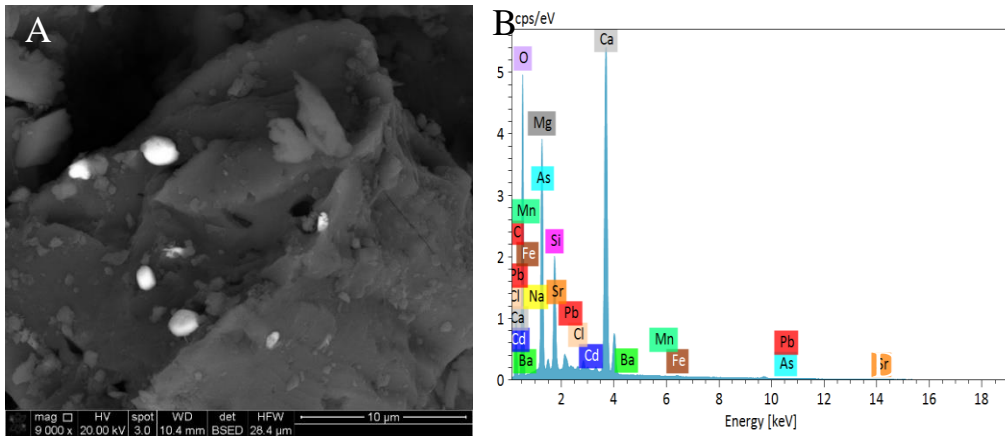


Fig. 4.13. SEM images of toxic metals precipitates (bright white) on dolomite surface with FW type II (not added with CaCO_3 to increase alkalinity): A) Inlet of the dolomite core

showing precipitates on highly dissolved dolomite surface, B) Zoom-in of A showing precipitates of different shapes and sizes, C) Center of the dolomite core showing precipitates around pore throat, D) zoom-in of C, E) Outlet of the dolomite core, and F) zoom-in of E showing precipitates.

4.5.3. SEM-EDS analysis of the elemental composition of dolomite surface

To identify the elemental composition of the precipitated and sorbed phases in the dolomite cores flooded with PW and FW, we mapped the elemental composition of dolomite grains samples by SEM-EDS analysis. Figs. 4.14 to 4.19 show SEM-EDS images of the dolomite grain samples after the dolomite cores were flooded with 1 L of PW type I, II (added with CaCO_3), and IV (not added with CaCO_3), and FW type I (added with CaCO_3), and type II (not added with CaCO_3). The analysis confirms the sorption and precipitation of all toxic metals in the dolomite cores. In accordance with the removal profiles of Pb and As, SEM-EDS analysis confirms that their precipitation as carbonates/oxides plays a prominent role in their removal by dolomite.



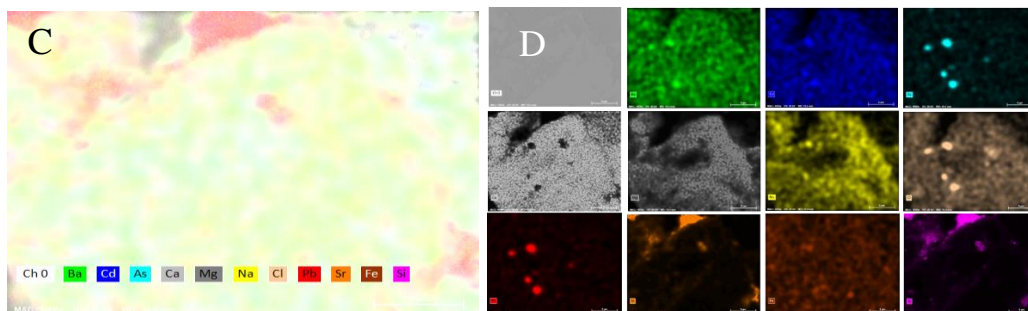


Fig. 4.14. SEM-EDS mapping of toxic metals on dolomite surface with PW type I at the inlet of the dolomite core: A) SEM micrograph showing carbonate precipitates of oval shapes, B) EDS spectrum showing the elemental composition of the bulk dolomite sample, C) EDS mapping of metals, and D) EDS mapping layers of individual metals.

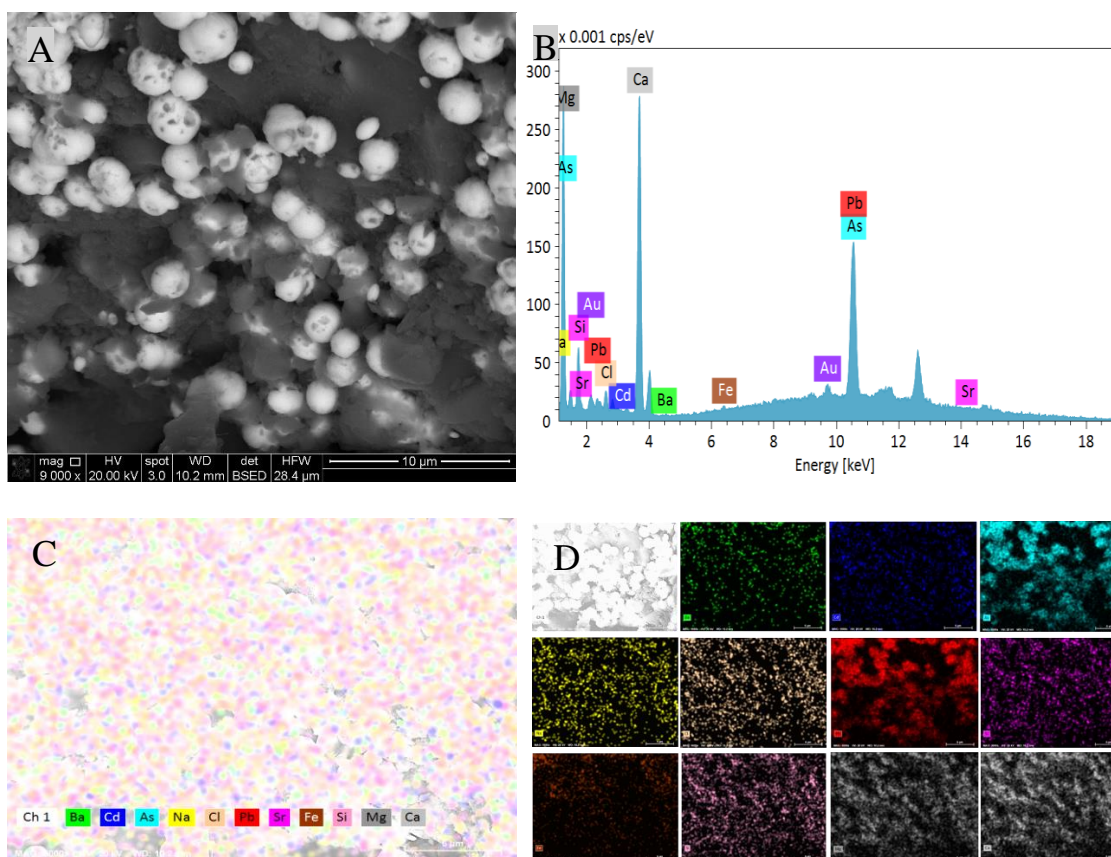


Fig. 4.15. SEM-EDS mapping of toxic metals on dolomite surface with PW type II (added with CaCO_3 to increase alkalinity) at the inlet of the dolomite core: A) SEM micrograph showing carbonate precipitates of circular shapes on cavities of oval shapes, B) EDS spectrum showing the elemental composition of the bulk dolomite sample, C) EDS mapping of metals, and D) EDS mapping layers of individual metals.

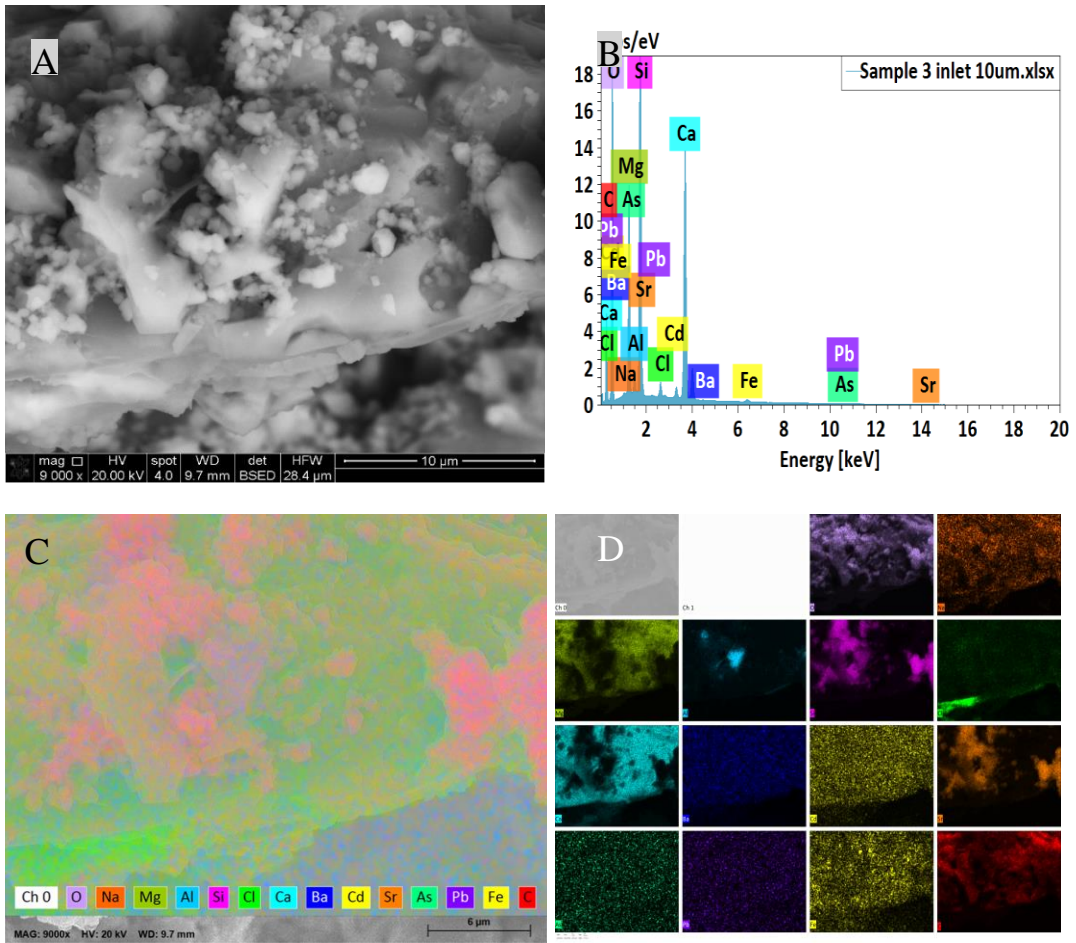
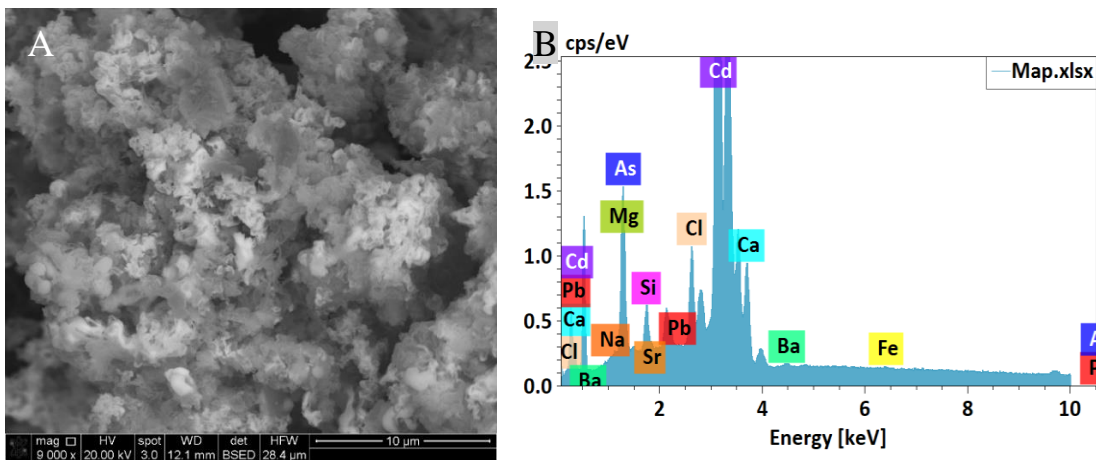


Fig. 4.16. SEM-EDS mapping of toxic metals on dolomite surface with PW type IV (not added with CaCO_3) at the inlet of the dolomite core: A) SEM micrograph showing carbonate precipitates, B) EDS spectrum showing the elemental composition of the bulk dolomite sample, C) EDS mapping of metals, and D) EDS mapping layers of individual metals.



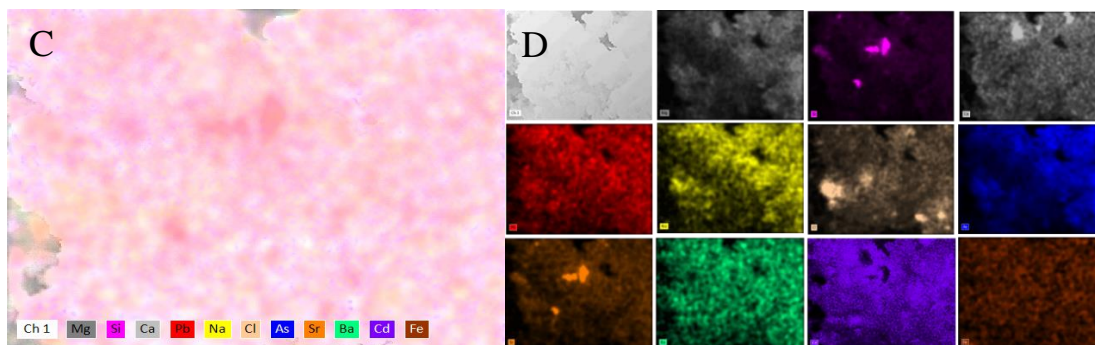


Fig. 4.17. SEM-EDS mapping of toxic metals on dolomite surface with FW type I (added with CaCO_3) at the outlet of the dolomite core: A) SEM image showing carbonate precipitates of circular shape and cavities, B) EDS spectrum showing the elemental composition of the bulk dolomite sample, C) EDS mapping of metals, and D) EDS mapping layers of individual metals.

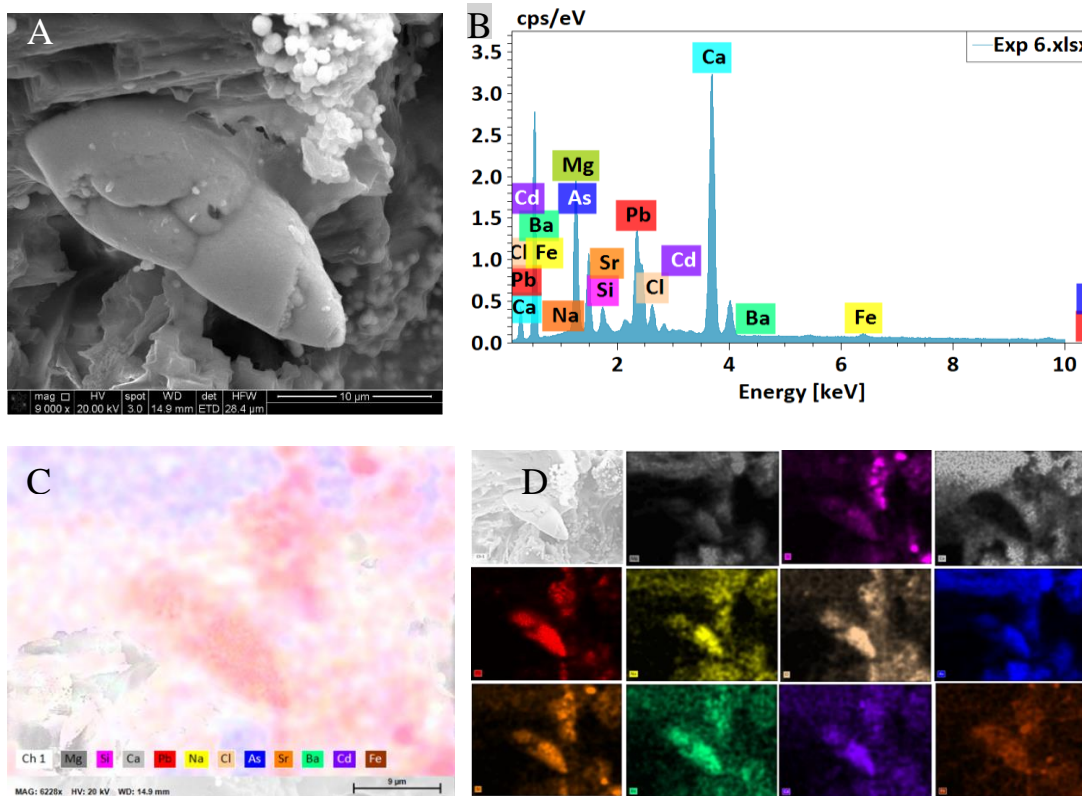


Fig. 4.18. SEM-EDS mapping of toxic metals on dolomite surface with FW type II (not added with CaCO_3) at the inlet of the dolomite core: A) SEM image showing carbonate precipitates of different shape and size, B) EDS spectrum showing the elemental composition of the bulk dolomite sample, C) EDS mapping of metals, and D) EDS mapping layers of individual metals.

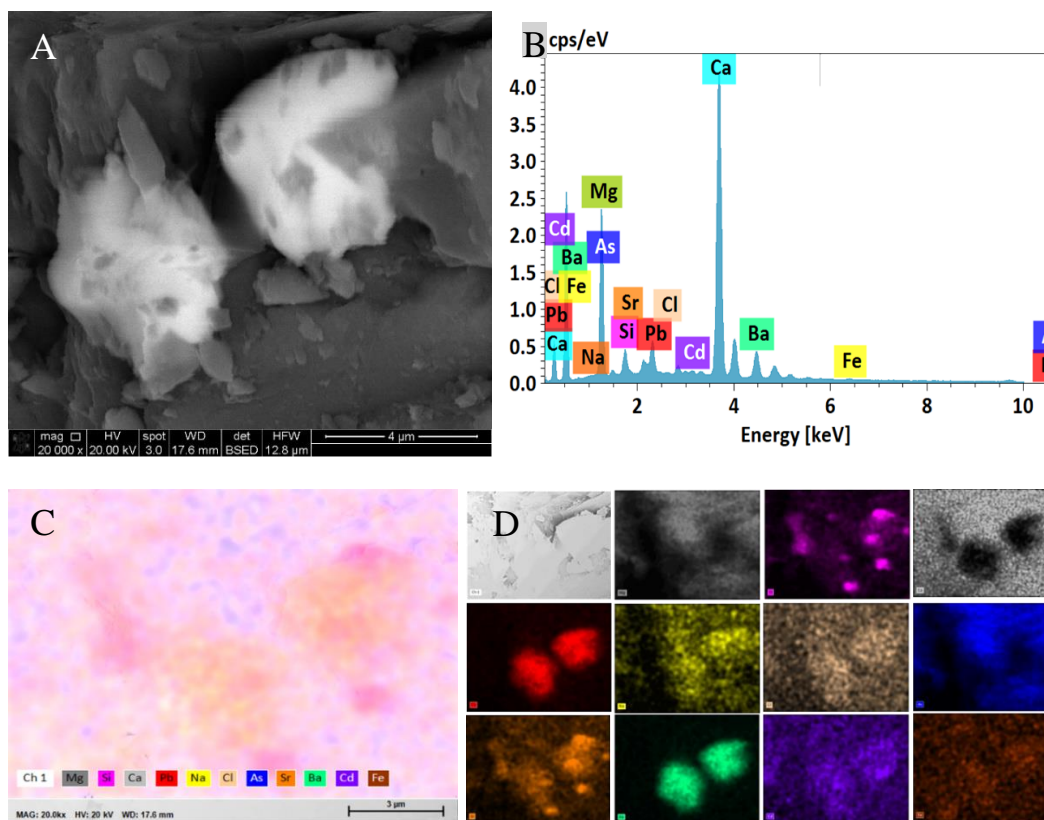


Fig. 4.19. SEM-EDS mapping of the dolomite surface from the top of the filter after core flooding using FW type II (not added with CaCO_3): A) SEM micrograph showing toxic metals carbonate phase with different shapes, B) EDS spectrum showing the elemental composition of the bulk samples, C) EDS mapping, and D) EDS mapping layers for individual elements.

A comparison between the SEM images of precipitates and EDS maps of elements reveals that precipitates of heavy metals and metalloids are more abundant than precipitates of alkaline earth metals. This agrees with the removal levels of Sr and Ba which were relatively smaller than the removal levels of Cd, Pb, and As. Overall, SEM-EDS analysis confirms that the removal of Ba and Sr from PW is controlled by sorption reactions with minor precipitation/coprecipitation reactions. However, the removal of Pb and As is mainly controlled by precipitation/coprecipitation reactions. Contrary to the batch reaction experiments where Cd was never found as a precipitate, in core-flooding experiments, Cd

was commonly found as precipitates on the dolomite grains (Fig. 4.17), indicating that the high removal of Cd was mostly due to precipitation/coprecipitation reactions.

Like in the batch experiment, Sr was found as sorbed and co-precipitated species on dolomite (Fig. 4.18). Sr was predominantly associated with other metals in the precipitates. In accordance with the relatively low levels of Sr removal, Sr precipitates were less frequently found than other toxic metal precipitates. Ba was found as a sorbed ions and co-precipitated particles of polygonal to irregular shapes of 2-4 μm size that precipitated in the cavities of dolomite surface or between dolomite crystals (Figs. 4.13 and 4.18). At ambient conditions, Ba can precipitate as witherite (BaCO_3) in natural waters (Tesoriero and Pankow, 1996), coprecipitate with carbonate minerals such as calcite, and/or it can form hydrated amorphous carbonate phases (Antao and Hassan, 2009; Tesoriero and Pankow, 1996). Like in batch reaction experiments, Pb precipitation was commonly found inside dints or at the edges of dolomite grains/crystals (Fig. 4.17). Pb precipitates occurred as cluster and clumped oval shape precipitates of nano to micro scale size. Moreover, Pb and As were commonly found in precipitates close to the inlet of the dolomite core (Figs. 4.14 and 4.15). This confirms that the precipitation reaction rates of Pb and As are faster than the precipitation rates of Ba, Sr, and Cd that accumulate away from the inlet point.

4.5.4. XRD analysis of the mineral composition of precipitates

To elucidate whether the observed precipitates are crystallized carbonates and to determine their spatial distribution, we conducted high-resolution XRD analyses. Figs. 4.20 and 4.21 show all the minerals detected through semiquantitative analysis of high-

resolution XRD data. Analysis was done on a control dolomite sample collected before preparing the dolomite cores for the core-flooding experiment as well as on samples collected from the inlet, center, and outlet of the dolomite core after being flooded with 1 L of PW or FW.

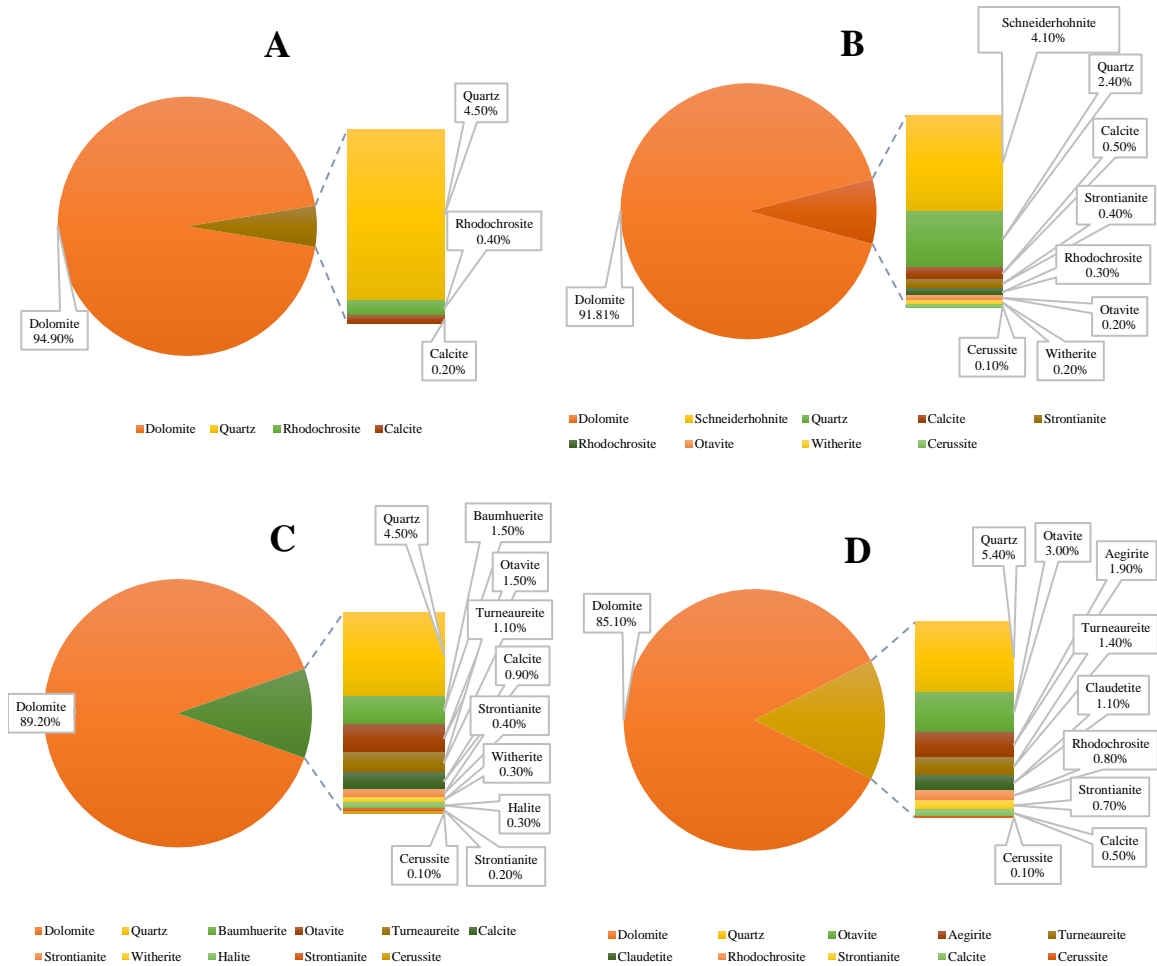
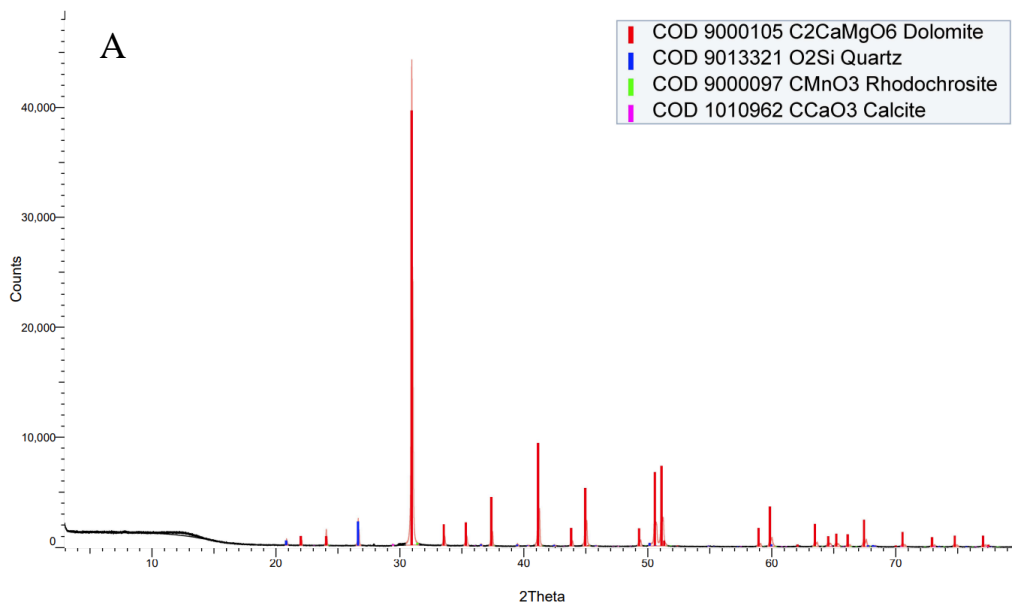
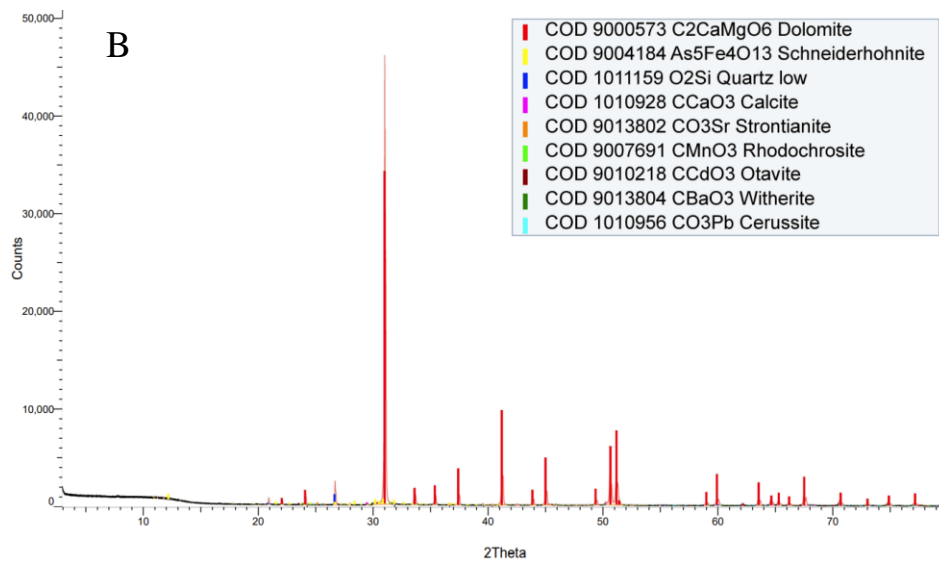


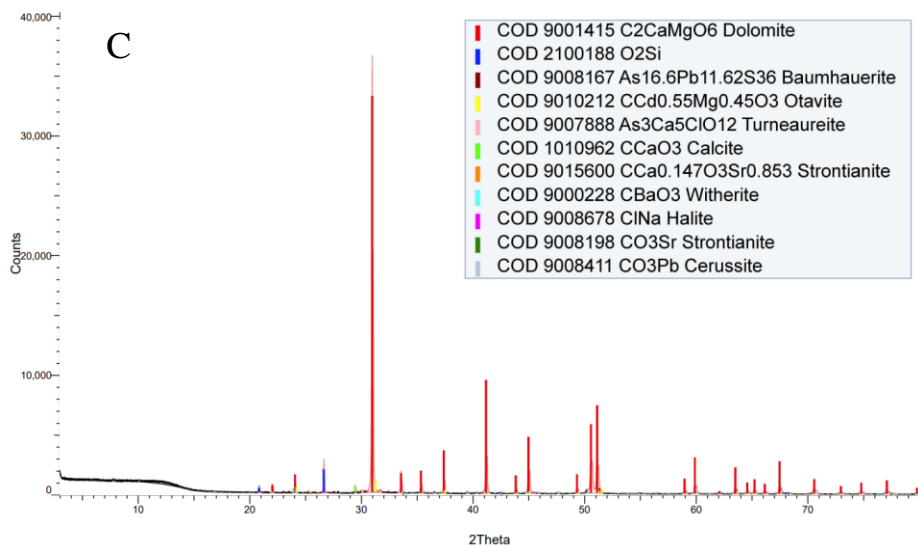
Fig. 4.20. Semiquantitative analyses from high-resolution XRD (Fig. 4.21) conducted on the powdered dolomite samples collected from dolomite core flooded with PW type I: A) Control sample, B) Inlet, C) Center, and D) Outlet.



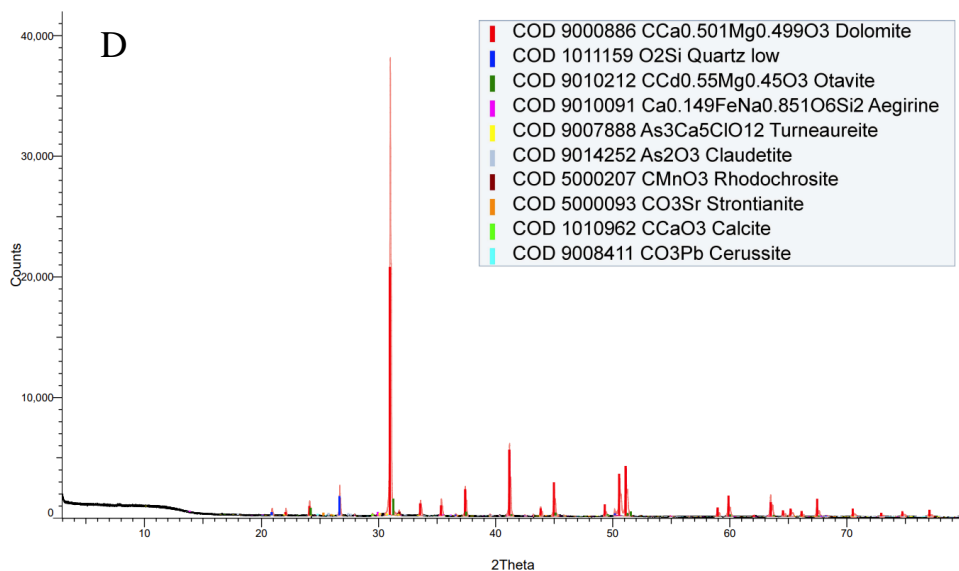
Index	Show	Name	Compound Name	Formula	Y-Scale	S-Q	Icon
1	Yes	COD 9000105	Dolomite	C2CaMgO6	89.52%	94.9%	
2	Yes	COD 9013321	Quartz	O2Si	4.82%	4.5%	
3	Yes	COD 9000097	Rhodochrosite	CMnO3	0.46%	0.4%	
4	Yes	COD 1010962	Calcite	CCaO3	0.29%	0.2%	



Index	Show	Name	Compound Name	Formula	Y-Scale	S-Q	Icon
1	Yes	COD 9000573	Dolomite	C2CaMgO6	74.09%	91.9%	
2	Yes	COD 9004184	Schneiderhohnite	As5Fe4O13	1.20%	4.1%	
3	Yes	COD 1011159	Quartz low	O2Si	2.34%	2.4%	
4	Yes	COD 1010928	Calcite	CCaO3	0.48%	0.5%	
5	Yes	COD 9013802	Strontianite	CO3Sr	0.53%	0.4%	
6	Yes	COD 9007691	Rhodochrosite	CMnO3	0.37%	0.3%	
7	Yes	COD 9010218	Otavite	CCdO3	0.47%	0.2%	
8	Yes	COD 9013804	Witherite	CBaO3	0.36%	0.2%	
9	Yes	COD 1010956	Cerussite	CO3Pb	0.33%	0.1%	

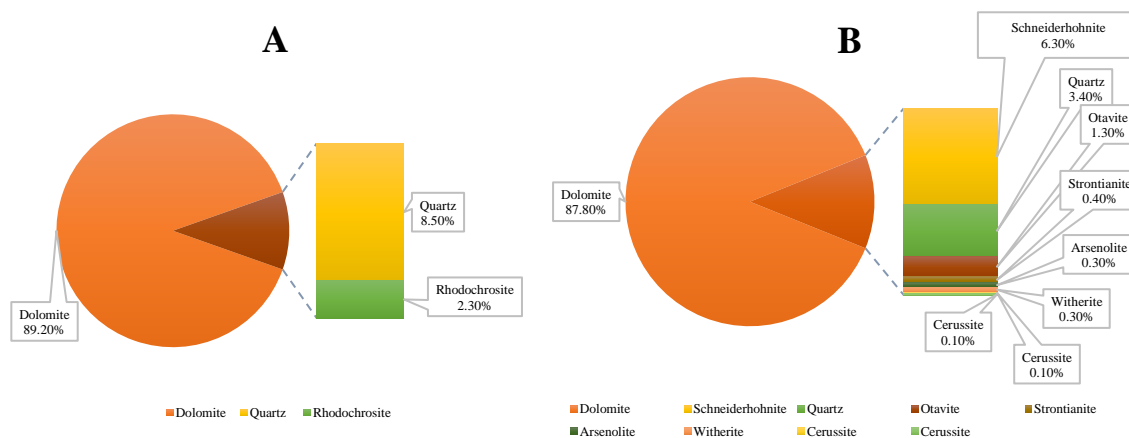


Index	Show	Name	Compound Name	Formula	Y-Scale	S-Q	Icon
1	Yes	COD 9001415	Dolomite	C ₂ CaMgO ₆	90.71%	89.2%	
2	Yes	COD 2100188		O ₂ Si	5.42%	4.5%	
3	Yes	COD 9008167	Baumhauerite	As _{16.6} Pb _{11.62} S ₃₆	0.48%	1.5%	
4	Yes	COD 9010212	Otavite	CCd _{0.55} Mg _{0.45} O ₃	2.78%	1.5%	
5	Yes	COD 9007888	Turneaureite	As ₃ Ca ₅ ClO ₁₂	0.76%	1.1%	
6	Yes	COD 1010962	Calcite	CCaO ₃	1.33%	0.9%	
7	Yes	COD 9015600	Strontianite	CCa _{0.147} O ₃ Sr _{0.853}	0.59%	0.4%	
8	Yes	COD 9000228	Witherite	CBaO ₃	0.95%	0.3%	
9	Yes	COD 9008678	Halite	ClNa	0.53%	0.3%	
10	Yes	COD 9008198	Strontianite	CO ₃ Sr	0.35%	0.2%	
11	Yes	COD 9008411	Cerussite	CO ₃ Pb	0.36%	0.1%	



Index	Show	Name	Compound Name	Formula	Y-Scale	S-Q	Icon
1	Yes	COD 9000886	Dolomite	CCa0.501Mg0.499O3	54.25%	85.1%	
2	Yes	COD 1011159	Quartz low	O2Si	4.28%	5.4%	
3	Yes	COD 9010212	Otavite	CCd0.55Mg0.45O3	3.60%	3.0%	
4	Yes	COD 9010091	Aegirine	Ca0.149FeNa0.851O6Si2	0.80%	1.9%	
5	Yes	COD 9007888	Turneaureite	As3Ca5ClO12	0.64%	1.4%	
6	Yes	COD 9014252	Claudetite	As2O3	0.65%	1.1%	
7	Yes	COD 5000207	Rhodochrosite	CMnO3	0.74%	0.8%	
8	Yes	COD 5000093	Strontianite	CO3Sr	0.70%	0.7%	
9	Yes	COD 1010962	Calcite	CCaO3	0.41%	0.5%	
10	Yes	COD 9008411	Cerussite	CO3Pb	0.42%	0.1%	

Fig. 4.21. Semiquantitative analyses from high-resolution XRD conducted on the powdered dolomite samples collected from filter that filtered PW type I: A) A) Control sample, B) Inlet sample, C) Center sample, and D) Outlet sample.



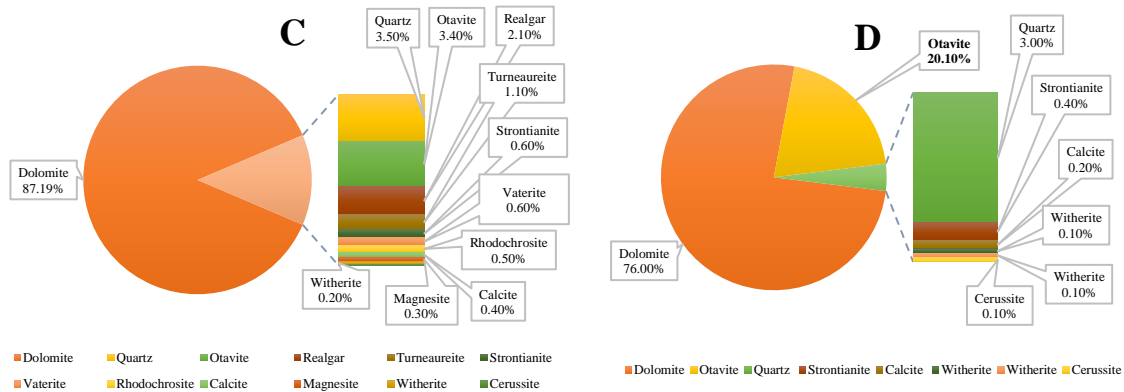
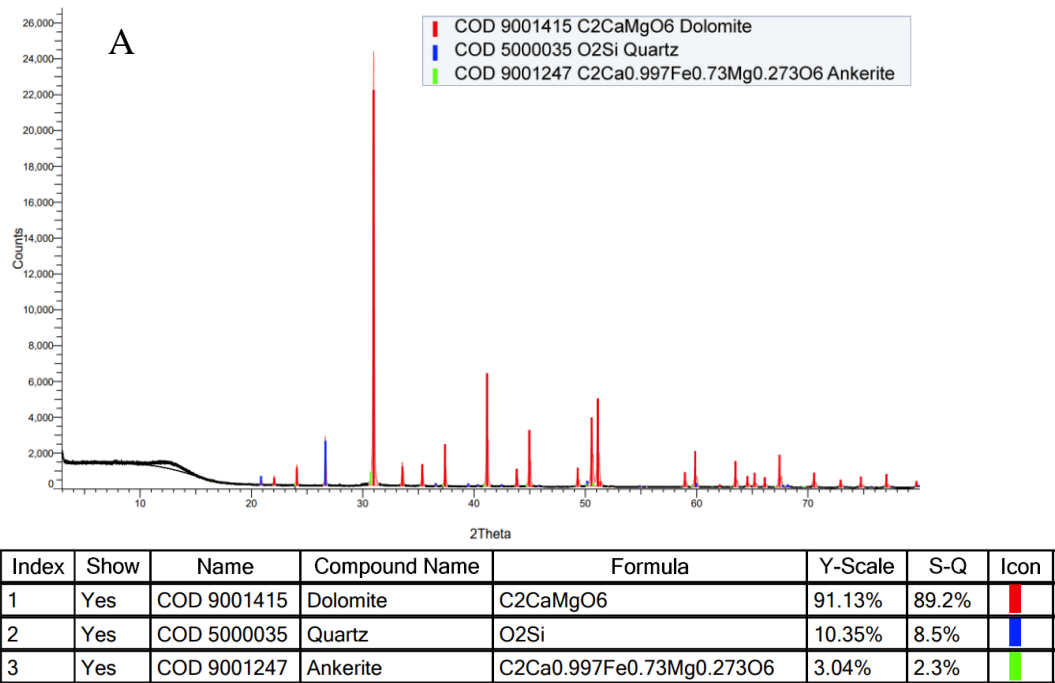
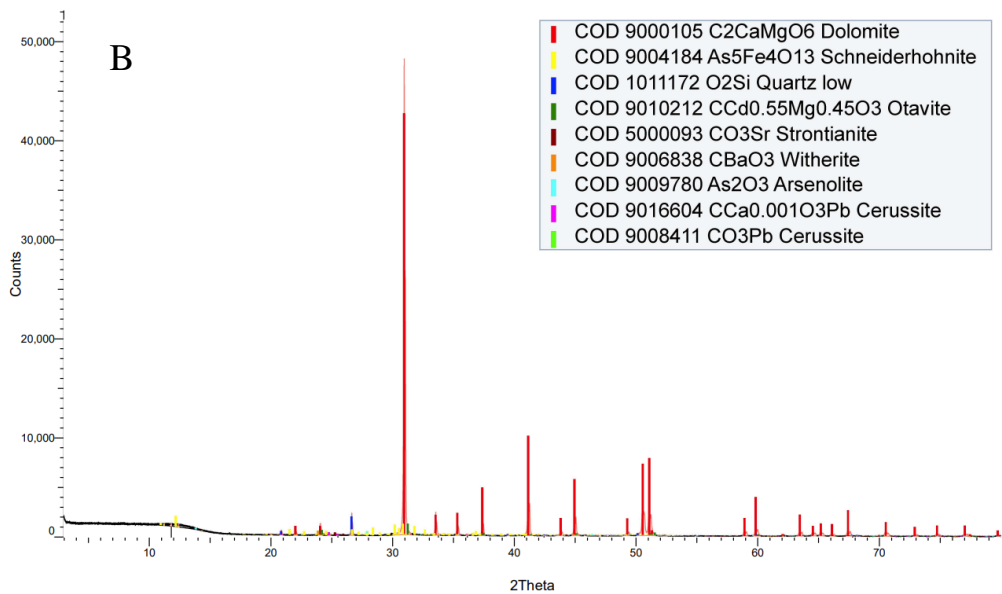
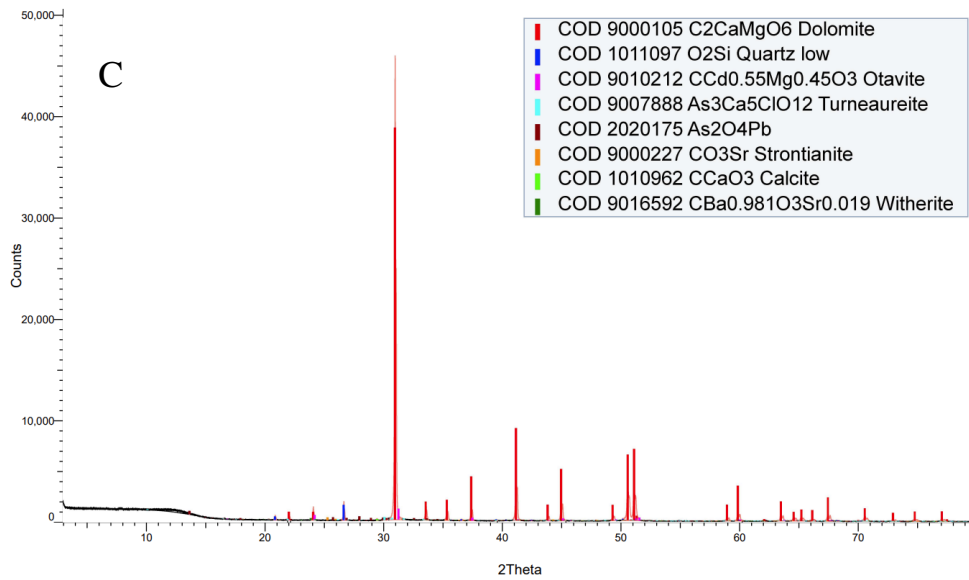










Fig. 4.22. Semiquantitative analyses from high-resolution XRD (Fig. 4.24) conducted on the powdered dolomite samples collected from dolomite core injected with FW type II: A) Control sample, B) Inlet sample, C) Center sample, and D) Outlet sample.

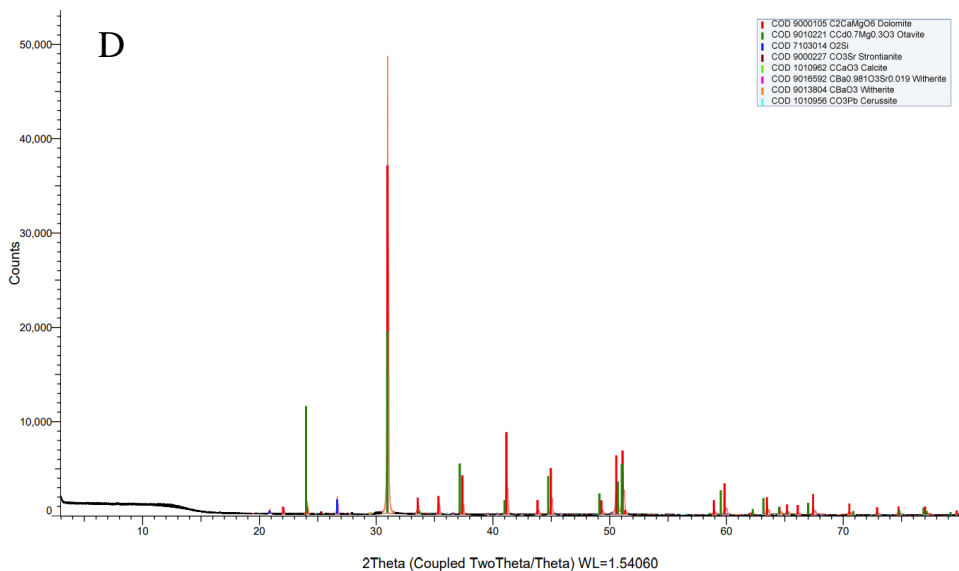




Index	Show	Name	Compound Name	Formula	Y-Scale	S-Q	Icon
1	Yes	COD 9000105	Dolomite	C ₂ CaMgO ₆	88.54%	87.8%	
2	Yes	COD 9004184	Schneiderhohnite	As ₅ Fe ₄ O ₁₃	2.25%	6.3%	
3	Yes	COD 1011172	Quartz low	O ₂ Si	3.81%	3.4%	
4	Yes	COD 9010212	Otavite	CCd _{0.55} Mg _{0.45} O ₃	2.26%	1.3%	
5	Yes	COD 5000093	Strontianite	CO ₃ Sr	0.62%	0.4%	
6	Yes	COD 9006838	Witherite	CBaO ₃	0.92%	0.3%	
7	Yes	COD 9009780	Arsenolite	As ₂ O ₃	0.81%	0.3%	
8	Yes	COD 9016604	Cerussite	CCa _{0.001} O ₃ Pb	0.65%	0.1%	
9	Yes	COD 9008411	Cerussite	CO ₃ Pb	0.59%	0.1%	



Index	Show	Name	Compound Name	Formula	Y-Scale	S-Q	Icon
1	Yes	COD 9000105	Dolomite	C ₂ CaMgO ₆	84.52%	92.4%	
2	Yes	COD 1011097	Quartz low	O ₂ Si	3.32%	3.2%	
3	Yes	COD 9010212	Otavite	CCd _{0.55} Mg _{0.45} O ₃	2.40%	1.5%	
4	Yes	COD 9007888	Turneaureite	As ₃ Ca ₅ ClO ₁₂	0.68%	1.1%	
5	Yes	COD 2020175		As ₂ O ₄ Pb	0.90%	0.8%	
6	Yes	COD 9000227	Strontianite	CO ₃ Sr	0.68%	0.5%	
7	Yes	COD 1010962	Calcite	CCaO ₃	0.29%	0.2%	
8	Yes	COD 9016592	Witherite	CBa _{0.981} O ₃ Sr _{0.019}	0.44%	0.2%	



Index	Show	Name	Compound Name	Formula	Y-Scale	S-Q	Icon
1	Yes	COD 9000105	Dolomite	C2CaMgO6	76.13%	76.0%	
2	Yes	COD 9010221	Otavite	CCd0.7Mg0.3O3	39.82%	20.1%	
3	Yes	COD 7103014		O2Si	3.19%	3.0%	
4	Yes	COD 9000227	Strontianite	CO3Sr	0.59%	0.4%	
5	Yes	COD 1010962	Calcite	CCaO3	0.29%	0.2%	
6	Yes	COD 9016592	Witherite	CBa0.981O3Sr0.019	0.39%	0.1%	
7	Yes	COD 9013804	Witherite	CBaO3	0.32%	0.1%	
8	Yes	COD 1010956	Cerussite	CO3Pb	0.26%	0.1%	

Fig. 4.24 Semiquantitative analyses from high-resolution XRD conducted on the powdered dolomite samples collected from filter that filtered FW type II: A) A) Control sample, B) Inlet sample, C) Center sample, and D) Outlet sample.

The major minerals in the control dolomite sample were dolomite and quartz. However, XRD spectra showed minor content of silica (quartz) and ankerite as well as traces of other carbonate minerals (calcite and rhodochrosite) minerals in some control samples. Various carbonate minerals and oxide phases were detected in the collected dolomite grains, confirming that these minerals precipitated during core-flooding experiments. The type and amount of minerals detected by XRD analysis are considerably distinct from sample to sample.

The composition of the precipitated minerals corresponds to the chemical composition of the employed type of PW and FW. For example, the carbonate minerals phases detected for samples collected from experiments conducted using PW type I-IV are witherite (BaCO_3), strontianite (SrCO_3), otavite (CdCO_3), cerussite (PbCO_3), and arsenic phases (e.g., As_2O_3) (Figs. 4.20 and 4.21), which are known to be more thermodynamically stable at standard conditions (Antao and Hassan, 2009; Anthony et al., 1995). In addition to these minerals, calcite, vaterite, and specific polymetallic oxides were also detected but aragonite was never detected. The detected oxide phases were largely arsenate minerals and coprecipitated arsenate phases such as schneiderhohnite ($\text{As}_5\text{Fe}_4\text{O}_{13}$) and lead arsenate (PbAs_2O_4). These minerals have been found in dolomite of low hydrothermal origin (Anthony et al., 1995). As oxides were detected in samples collected from experiments using both synthetic PW and FW. As is known to form oxide phases in aqueous environments (Neuberger and Helz, 2005), and that it can coprecipitate with carbonate minerals during their transformation from hydrated (e.g., monohydrocalcite) to anhydrous (e.g., calcite and aragonite) carbonate phases in saline water (Fukushi et al., 2011).

The amount of Pb and As carbonate/oxide phases were generally high at the inlet of the core and decreased at the center and outlet of the dolomite core. Conversely, the amounts of Ba and Sr carbonate minerals were low at the inlet of the core and increased at the center and outlet of the dolomite core. On the other hand, the amount of Cd carbonate minerals was low or absent at the inlet and gradually increased at the center, reaching a maximum at the outlet. Sorption/precipitation of Pb and As occurred preferentially closer to the inlet while sorption/precipitation of Ba, Sr, and Cd occurred preferentially away from

the inlet. This is attributed to the different chemical equilibrium and reaction kinetics of these toxic metals.

4.6. Conclusions

The removal of toxic metal is higher under flow than under batch reaction conditions. This is due to the removal of competing cations (Ca and Mg) by advection-dispersion from the pore space which enables higher sorption levels of toxic metals (Ba, Sr, Cd, Pd, and As) and precipitation (mineralization) reactions with alkalinity generated from the dissolution of dolomite. Ba and Sr removal is mainly controlled by nonequilibrium sorption reactions while the removal of Pb and As removal is predominantly controlled by precipitation and/or coprecipitation. Cd removal is controlled by sorption and precipitation reactions depending on the solution composition. Therefore, reducing the surface area of dolomite (e.g., dolomite core size) in contact with PW significantly affects the removal of Ba, Sr, and Cd whereas the removal of Pb and As is only partially affected. The obtained results suggests that the mobility of alkaline earth metals (Ba and Sr) > metalloids (As) > heavy metals (Pb and Cd) through dolomite porous media at both low and high salinity waters conditions. Based on obtained results from SEM, SEM-EDS, and XRD analyses, all tested toxic metals precipitates. Precipitates are characterized by different specific shapes, roundness, and sizes. Mineral precipitation occurs preferentially in locations surrounding the pore thoughts, on grain edges and cavities, and on grain surfaces that are facing the fluid flow directions. Toxic metals precipitate as carbonate minerals such as witherite (BaCO_3), strontianite (SrCO_3), otavite (CdCO_3), cerussite (PbCO_3), and arsenic phases (e.g., As_2O_3) that are associated with

calcite, vaterite, and polymetallic oxides. Sorption and precipitation of Pb and As occurs preferentially at the inlet point of PW into dolomite while sorption and precipitation of Ba, Sr, and Cd occurs preferentially in locations away from inlet point. This result suggests that Pb and As have faster reaction rates than Ba, Sr, and Cd in dolomite. Our results support our finding regarding the key role of alkalinity of PW and dolomite dissolution in promoting the removal of toxic metals from PW via precipitation/coprecipitation as carbonate minerals.

4.7. Funding

This work was supported by the National Science Foundation under Grant CBET-220036.

4.8. Acknowledgments

This is Oklahoma State University Boone Pickens School of Geology contribution number 2023-xx.

4.9. References

- Alexandratos, V. G., Elzinga, E. J., and Reeder, R. J., 2007, Arsenate uptake by calcite: macroscopic and spectroscopic characterization of adsorption and incorporation mechanisms: *Geochimica et Cosmochimica Acta*, v. 71, no. 17, p. 4172-4187.
- Antao, S. M., and Hassan, I., 2009, The orthorhombic structure of CaCO₃, SrCO₃, PbCO₃ and BaCO₃: linear structural trends.: *The Canadian Mineralogist*, v. 47(5), pp.1245-1255.

- Anthony, J. W., Bideaux, R. A., Bladh, K. W., and Nichols, E., Monte C., , 1995, Handbook of Mineralogy: Mineralogical Society of America. Chantilly, VA 20151-1110, USA. <http://www.handbookofmineralogy.org/>.
- Ballinger, D. G., 1979, 1979. Methods for chemical analysis of water and wastes. In United States Environmental Protection Agency.: EPA 600/4-79-020. Environmental Monitoring and Support Laboratory Cincinnati, Ohio., p. 353.352-351 to 353.352-355 (nitrate analysis) and 325.352-351 to 325.352-352 (chloride analysis).
- Çelebi, H., Gök, G., and Gök, O., 2020, Adsorption capability of brewed tea waste in waters containing toxic lead (II), cadmium (II), nickel (II), and zinc (II) heavy metal ions: Scientific reports, v. 10(1), pp.1-12.
- Dixit, S., and Hering, J. G., 2003, Comparison of arsenic (V) and arsenic (III) sorption onto iron oxide minerals: implications for arsenic mobility.: Environmental science & technology,, v. 37(18), pp.4182-4189.
- Drever, J. I., 1997, The geochemistry of natural waters: surface and groundwater environments., v. 436. p87-105.
- Ebrahimi, P., and Vilcáez, J., 2018, Petroleum produced water disposal: Mobility and transport of barium in sandstone and dolomite rocks.: Science of the Total Environment,, v. 634, pp.1054-1063.
- Ebrahimi, P., and Vilcáez, J., 2019a, Transport of barium in fractured dolomite and sandstone saline aquifers: Science of the Total Environment, v. 647, p. 323-333.
- Ebrahimi, P., and Vilcáez, J., 2019b, Transport of barium in fractured dolomite and sandstone saline aquifers.: Science of the Total Environment,, v. 647, pp.323-333.

- Federation, W. E., and Aph Association, 2005, Standard methods for the examination of water and wastewater. : American Public Health Association (APHA): Washington, DC, USA. 21th Edition. , p. pp 4-75 to 74-76 (chloride method 4500-Cl G) and 4504-4127 to 4504-4129 (nitrate method 4500-NO4503 I).
- Feizi, M., and Jalali, M., 2015, Removal of heavy metals from aqueous solutions using sunflower, potato, canola and walnut shell residues.: Journal of the Taiwan Institute of Chemical Engineers., v. 54, pp.125-136.
- Flora, G., Gupta, D., and Tiwari, A., 2012, Toxicity of lead: a review with recent updates: Interdisciplinary Toxicology, v. 5, no. 2, p. 47-58.
- Fukushi, K., Munemoto, T., Sakai, M., and Yagi, S., 2011, Monohydrocalcite: a promising remediation material for hazardous anions: Sci Technol Adv Mater, v. 12, no. 6, p. 064702.
- Guerra, K., Dahm, K., and Dunderf, S., 2011, Oil And Gas Produced Water Management And Beneficial Use in the Western United States,: US Department of the Interior,, p. p. 157.
- Jensen, J., 2020, The Role of Carbonate Minerals in Arsenic Mobility in a Shallow Aquifer Influenced by a Seasonally Fluctuating Groundwater Table (Masters thesis, Utah State University).
- Kharaka, Y. K., Kakouros, E., Thordsen, J. J., Ambats, G., and Abbott, M. M., 2007, Fate and groundwater impacts of produced water releases at OSPER “B” site, Osage County, Oklahoma: Applied geochemistry, v. 22, no. 10, p. 2164-2176.
- Koutros, S., Lenz, P., Hewitt, S. M., Kida, M., Jones, M., Schned, A. R., Baris, D., Pfeiffer, R., Schwenn, M., and Johnson, A., 2018, RE: Elevated bladder cancer in northern

- new England: The role of drinking water and arsenic: JNCI: Journal of the National Cancer Institute, v. 110, no. 11, p. 1273-1274.
- Kowalczyk, E., Givelet, L., Amlund, H., Sloth, J. J., and Hansen, M., 2022, Risk assessment of rare earth elements, antimony, barium, boron, lithium, tellurium, thallium and vanadium in teas: EFSA Journal, v. 20, p. e200410.
- Neuberger, C. S., and Helz, G. R., 2005, Arsenic (III) carbonate complexing: Applied geochemistry, v. 20(6), pp.1218-1225.
- Ng, J. C., Wang, J., and Shraim, A., 2003, A global health problem caused by arsenic from natural sources: Chemosphere, v. 52, no. 9, p. 1353-1359.
- Omar, K., and Vilcaez, J., 2023, Role of alkalinity and dolomite reactivity on toxic metals removal from petroleum produced water by dolomite: Science of the Total Environment
- Omar, K., and Vilcáez, J., 2022, Removal of toxic metals from petroleum produced water by dolomite filtration.: Journal of Water Process Engineering., v. 47, p.102682.
- Pokrovsky, O. S., Schott, J., and Thomas, F., 1999, Processes at the magnesium-bearing carbonates/solution interface. I. a surface speciation model for magnesite: Geochimica et Cosmochimica Acta, v. 63, no. 6, p. 863-880.
- Ribeiro, L. P. S., Puchala, R., Lalman, D. L., and Goetsch, A. L., 2021, Composition of various sources of water in Oklahoma available for consumption by ruminant livestock.: Applied Animal Science., v. 37(5), pp.595-601.
- Saha, S., Basak, B., Hwang, J.-H., Salama, E.-S., Chatterjee, P. K., and Jeon, B.-H., 2020, Microbial Symbiosis: A Network towards Biomethanation: Trends in Microbiology, v. 28, no. 12, p. 968-984.

- Smith, A. H., Lopipero, P. A., Bates, M. N., and Steinmaus, C. M., 2002, Arsenic epidemiology and drinking water standards, Volume 296, American Association for the Advancement of Science, p. 2145-2146.
- Tabatabaeefar, A., Yuan, Q., Salehpour, A., and Rajabi-Hamane, M., 2020, Batch adsorption of lead (II) from aqueous solution onto novel polyoxyethylene sorbitan monooleate/ethyl cellulose microfiber adsorbent: kinetic, isotherm and thermodynamic studies.: *Separation Science and Technology*, , v. 55(6), pp.1051-1061.
- Temple, B. J., Bailey, P. A., and Gregg, J. M., 2020, Carbonate Diagenesis Of The Arbuckle Group North Central Oklahoma To Southeastern Missouri., p. 10-30.
- Tesoriero, A. J., and Pankow, J. F., 1996, Solid solution partitioning of Sr²⁺, Ba²⁺, and Cd²⁺ to calcite: *Geochimica et Cosmochimica Acta*, v. 60, no. 6, p. 1053-1063.
- Watts, P., and Howe, P., 2010, Strontium and strontium compounds, World Health Organization, v. 77.
- Wei, H., Shen, Q., Zhao, Y., Wang, D. J., and Xu, D. F., 2003, Influence of polyvinylpyrrolidone on the precipitation of calcium carbonate and on the transformation of vaterite to calcite. : *Journal of Crystal Growth*, , v. 250(3-4), pp.516-524.
- Yin, X., Jiang, Y., Tan, Y., Meng, X., Sun, H., and Wang, N., 2019, Co-transport of graphene oxide and heavy metal ions in surface-modified porous media: *Chemosphere*, v. 218, p. 1-13.

Zheng, J.-L., Yuan, S.-S., Wu, C.-W., Lv, Z.-M., and Zhu, A.-Y., 2017, Circadian time-dependent antioxidant and inflammatory responses to acute cadmium exposure in the brain of zebrafish: *Aquatic Toxicology*, v. 182, p. 113-119.

CHAPTER V

CONCLUSIONS AND RECOMMENDATIONS

The objectives of my dissertation were in two parts; firstly, to elucidate the controlling factors in the removal of toxic metals from PW by dolomite, and secondly, to assess the feasibility of dolomite filtration as an economically viable method to ease the cost or replace the conventional PW treatment methods. This is significant because it will contribute to solving environmental issues related to the oil and gas industry by making PW more beneficial to be reused by integration for agricultural and industrial purposes. To achieve these objectives, batch sorption and core flooding experiments were conducted at different synthetic PW composition, pH, and salinity conditions to understand the chemophysical factors on toxic metal removal from synthetic PW by dolomite. In addition, XRD and SEM-EDS analysis were performed to illustrate the dolomite efficiency for removing toxic metals from PW. Moreover, the obtained experimental results were used to develop geochemical models for used toxic metals sorption and reactive transport simulations through dolomite as well as for dolomite filter optimization. This will eventually help us in developing dolomite filtration not only for PW treatment but also for PW mining as well.

The dissertation findings were presented in three journal papers. The following are the main conclusions of these journal papers followed by recommendations for future work.

5.1. Conclusions

5.1.1. Removal of toxic metals from petroleum produced water by dolomite filtration

Salinity has a significant impact on the removal of Sr and Ba, but a mild impact on the removal of Cd by dolomite filtration. Dolomite filters are more effective in removing heavy metals (e.g., Pb and Cd) than alkaline earth metals (e.g., Ba and Sr). At salinity levels of PW, the affinity sequence for the sorption of mixture metals on dolomite is $Pb > Cd > As > Ba > Sr$. Opposite to metal-(oxyhydro)oxides the affinity sequence for dolomite at salinity levels of PW is $Ba > Sr$. Removal of Sr, Ba, and Cd from PW by dolomite filtration are kinetically controlled reactions where an increase of pH due to the dissolution of dolomite increases the removal of Sr, Ba, and Cd. This increase is higher for Cd than for Sr and Ba. Sr, Ba, and Cd complexation by guar gum in the aqueous phase hinders their removal by dolomite filters made of large grain size (e.g., 350-600 μm), where trapping of guar gum in small pore throats is not possible. A complete removal of Sr, Ba, and Cd can be obtained by optimizing the relationship between the injection rate and size of the dolomite filter. Overestimated removal levels of Cd and higher removal levels of Sr than Ba, by the formulated reactive transport model highlights the necessity of further experimental research to be able to incorporate molecular scale surface crystal structure and surface morphology parameters into the model.

5.1.2. Role of alkalinity and dolomite reactivity on toxic metals removal from petroleum produced water by dolomite

Batch reaction experiments were conducted to assess the role of alkalinity and dolomite reactivity on the removal of high concentrations (100 mg/L) of toxic metals (Ba, Sr, Cd, Pb, and As) from PW (TDS > 68,000 mg/L) and FW (TDS < 2,000 mg/L) by dolomite.

Ba, Sr, Cd, Pb, and As undergo sorption and precipitation reactions. However, the degree and therefore relevance of both reactions at salinity and alkalinity levels of PW are different depending on the type of metal. Ba, Sr, and Cd mostly undergo sorption reactions, whereas Pb and As undergo both sorption and precipitation reactions. Alkalinity promotes the removal of Ba, Sr, and Cd through sorption reactions by reducing the concentration of H^+ which competes for hydration (sorption) sites of dolomite. Whereas alkalinity (CO_3^{2-} and HCO_3^{2-}) promotes the removal of Pb and As by forming carbonate minerals. Given the role of alkalinity in the removal of Ba, Sr, Cd, Pb and As by sorption and precipitation reactions, dolomite dissolution plays an important role in the removal of toxic metals from PW. This is particularly the case of Pb whose removal rate is proportional to the dissolution rate of dolomite. This conclusion is supported by SEM-EDS mapping results showing different ratios of sorbed and precipitated phases of Ba, Sr, Cd, Pb, and As on dolomite grains, as well as by XRD analysis showing the precipitation of Ba, Sr, Cd, and Pb as carbonate minerals (e.g., witherite, strontianite, otavite, and cerussite), As as oxide (calcium arsenate), and several other minerals phases with complex composition, such as strontium cadmium arsenate ($SrCd(As_2O_7)$) and lead arsenate ($PbAs_2O_4$) when they are all present in PW. Ba precipitates in cavities or between dolomite crystals, Sr on quartz in

dolomite, Cd on ferric dolomite grains, Pb on the dints or inside edges of dolomite grains, and As precipitates directly on the surface of dolomite.

Simulations accounting for complexation reactions in the aqueous and mineral phases, equilibrium precipitation reactions of carbonate minerals, and kinetic dissolution/precipitation reaction of dolomite, confirms the thermodynamic feasibility of small amounts of Sr, and Cd precipitation and much larger precipitation amounts of Pb as carbonate minerals. Comparison between attained removal levels of Ba, Sr, Cd, Pb, and As from PW and FW of the same alkalinity shows that the effect of salinity is very different depending on the type of toxic metal. Salinity inhibits sorption reactions of Ba, Sr, and Cd and it promotes the solubility of Pb, but it does not seem to have any effect on As removal by dolomite.

The findings of this study have large practical implications to predict the fate and transport of toxic metals in saline aquifers injected with PW and to design optimum operational conditions to remove toxic metals from PW by dolomite filtration.

5.1.3. Effect of carbonate minerals precipitation and sorption reactions on the transport of toxic metals in dolomite

The removal of toxic metal is higher under flow than under batch reaction conditions. This is due to the removal of competing cations (Ca and Mg) by advection-dispersion from the pore space which enables higher sorption levels of toxic metals (Ba, Sr, Cd, Pd, and As) and precipitation (mineralization) reactions with alkalinity generated from the dissolution of dolomite. Ba and Sr removal is mainly controlled by nonequilibrium sorption reactions while the removal of Pb and As removal is

predominantly controlled by precipitation and/or coprecipitation. Cd removal is controlled by sorption and precipitation reactions depending on the solution composition. Therefore, reducing the surface area of dolomite (e.g., dolomite core size) in contact with PW significantly affects the removal of Ba, Sr, and Cd whereas the removal of Pb and As is only partially affected. The obtained results suggests that the mobility of alkaline earth metals (Ba and Sr) > metalloids (As) > heavy metals (Pb and Cd) through dolomite porous media at both low and high salinity waters conditions. Based on obtained results from SEM, SEM-EDS, and XRD analyses, all tested toxic metals precipitates. Precipitates are characterized by different specific shapes, roundness, and sizes. Mineral precipitation occurs preferentially in locations surrounding the pore thoughts, on grain edges and cavities, and on grain surfaces that are facing the fluid flow directions. Toxic metals precipitate as carbonate minerals such as witherite (BaCO_3), strontianite (SrCO_3), otavite (CdCO_3), cerussite (PbCO_3), and arsenic phases (e.g., As_2O_3) that are associated with calcite, vaterite, and polymetallic oxides. Sorption and precipitation of Pb and As occurs preferentially at the inlet point of PW into dolomite while sorption and precipitation of Ba, Sr, and Cd occurs preferentially in locations away from inlet point. This result suggests that Pb and As have faster reaction rates than Ba, Sr, and Cd in dolomite. Our results support our finding regarding the key role of alkalinity of PW and dolomite dissolution in promoting the removal of toxic metals from PW via precipitation/coprecipitation as carbonate minerals.

5.2. Recommendations for Future Studies

In this dissertation, I managed to obtain our objectives for elucidating the chemo-physical controlling factors influencing toxic metals removal from synthetic produced

water (PW) by dolomite. I also managed through this project to confirm that this new dolomite filtration method is economically feasible due to its low cost and highly efficient for removal of toxic metals from PW at low pH and high salinity conditions. In addition, the obtained results were represented in geochemical models and simulations. However, there are many additional other questions that have yet to be answered due to the scope and time limit of this PhD project. In this section, I would like to propose some recommendations for future investigations:

- My studies focused on a suite of heavy metals, metalloids, and alkaline earth metals (Pb, Cd, As, Ba, Sr) which are commonly found in PW. However, there are other toxic metals and radionuclides in PW that can be removed using a similar approach presented in my dissertation.
- My experimental and computational studies used ambient temperature without considering bio-intervention. I recommend conducting investigations using similar methodologies under high temperatures and/or bio-mediation.
- I used only synthetic PW in experimental studies, and I suggest conducting similar studies on natural PW from different petroleum plays in the United States.
- I utilized only natural dolomite from the Arbuckle Group for all my experimental studies and suggest using dolomite from different origins, metamorphic dolomite, and activated dolomite.
- More computational work is needed for developing new geochemical models for 3D reactive transport for rare and critical elements present in PW and this will be helpful in PW mining.

- I recommend conducting more investigations on our new dolomite filtration method on the field and regional scales.

REFERENCES

- Alexandratos, V. G., Elzinga, E. J., and Reeder, R. J., 2007, Arsenate uptake by calcite: macroscopic and spectroscopic characterization of adsorption and incorporation mechanisms: *Geochimica et Cosmochimica Acta*, v. 71, no. 17, p. 4172-4187.
- Alley, B., Beebe, A., Rodgers Jr, J., and Castle, J. W., 2011, Chemical and physical characterization of produced waters from conventional and unconventional fossil fuel resources.: *Chemosphere*, v. 85(1), pp.74-82.
- Antao, S. M., and Hassan, I., 2009, The orthorhombic structure of CaCO₃, SrCO₃, PbCO₃ and BaCO₃: linear structural trends.: *The Canadian Mineralogist*, v. 47(5), pp.1245-1255.
- Anthony, J. W., Bideaux, R. A., Bladh, K. W., and Nichols, E., Monte C., 1995, *Handbook of Mineralogy: Mineralogical Society of America*. Chantilly, VA 20151-1110, USA. <http://www.handbookofmineralogy.org/>.
- Anthony, J. W., Bideaux, R. A., Bladh, K. W., and Nichols, M. C., 2007, Borates, Carbonates, Sulfates. In *Handbook of Mineralogy: Mineralogical Society of America*, v. V.
- Ávila, I., Crnkovic, P. M., Milioli, F. E., and Luo, K. H., 2012, Investigation of the pore blockage of a Brazilian dolomite during the sulfation reaction: *Applied Surface Science*, v. 258, no. 8, p. 3532-3539.
- Balci, N., Demirel, C., Ön, S. A., Gültekin, A. H., and Kurt, M. A., 2018, Evaluating abiotic and microbial factors on carbonate precipitation in Lake Acigöl, a hypersaline lake in Southwestern Turkey: *Quaternary International*, v. 486, pp.116-128.
- Ballinger, D. G., 1979, 1979. Methods for chemical analysis of water and wastes. In *United States Environmental Protection Agency*.: EPA 600/4-79-020. Environmental Monitoring and Support Laboratory Cincinnati, Ohio., p. 353.352-351 to 353.352-355 (nitrate analysis) and 325.352-351 to 325.352-352 (chloride analysis).
- Bettermann, P., and Liebau, F., 1975, The transformation of amorphous silica to crystalline silica under hydrothermal conditions.: *Contributions to Mineralogy and Petrology*, v. 53(1), pp.25-36.
- Brady, P. V., Papenguth, H. W., and Kelly, J. W., 1999, Metal sorption to dolomite surfaces. This work supported by the United States Department of Energy under contract DE-AC04-94AL85000.1: *Applied Geochemistry*, v. 14, no. 5, p. 569-579.

- Brown, G. E., and Parks, G. A., 2001a, Sorption of Trace Elements on Mineral Surfaces: Modern Perspectives from Spectroscopic Studies, and Comments on Sorption in the Marine Environment: *International Geology Review*, v. 43, no. 11, p. 963-1073.
- Brown, J. G. E., and Parks, G. A., 2001, Sorption of trace elements on mineral surfaces: Modern perspectives from spectroscopic studies, and comments on sorption in the marine environment.: *International Geology Review*, v. 43(11), pp.963-1073.
- Brown, J. G. E., and Parks, G. A., 2001b, Sorption of trace elements on mineral surfaces: Modern perspectives from spectroscopic studies, and comments on sorption in the marine environment.: *International Geology Review*, , v. 43(11), pp.963-1073.
- Çelebi, H., Gök, G., and Gök, O., 2020, Adsorption capability of brewed tea waste in waters containing toxic lead (II), cadmium (II), nickel (II), and zinc (II) heavy metal ions: *Scientific reports*, v. 10(1), pp.1-12.
- Chen, X., Zhang, D., Larson, S. L., Ballard, J. H., Knotek-Smith, H. M., Nie, J., Hu, N., Ding, D., and Han, F. X., 2021, Microbially Induced Carbonate Precipitation Techniques for the Remediation of Heavy Metal and Trace Element–Polluted Soils and Water.: *Water, Air, & Soil Pollution*, v. 232(7), pp.1-15.
- Clark, C. E., and Veil, J. A., 2009, Produced water volumes and management practices in the United States: Argonne National Laboratory.
- Collins, A. G., 1969, Chemistry of some Anadarko basin brines containing high concentrations of iodide: *Chemical Geology*, v. 4, no. 1-2, p. 169-187.
- Da'ana, D. A., Zouari, N., Ashfaq, M. Y., Abu-Dieyeh, M., Khraisheh, M., Hijji, Y. M., and Al-Ghouti, M. A., 2021, Removal of toxic elements and microbial contaminants from groundwater using low-cost treatment options: *Current Pollution Reports*, v. 7, no. 3, p. 300-324.
- Dixit, S., and Hering, J. G., 2003, Comparison of arsenic (V) and arsenic (III) sorption onto iron oxide minerals: implications for arsenic mobility.: *Environmental science & technology*, v. 37(18), pp.4182-4189.
- Drever, J. I., 1997, *The geochemistry of natural waters: surface and groundwater environments.*, v. 436. p87-105.
- Ebrahimi P, Vilcáez J. Effect of brine salinity and guar gum on the transport of barium through dolomite rocks: Implications for unconventional oil and gas wastewater disposal. *Journal of Environmental Management* 2018a; 214: 370-378.
- Ebrahimi P, Vilcáez J. Petroleum produced water disposal: Mobility and transport of barium in sandstone and dolomite rocks. *Science of The Total Environment* 2018b; 634: 1054-1063.
- Ebrahimi P, Vilcáez J. Transport of barium in fractured dolomite and sandstone saline aquifers. *Science of The Total Environment* 2019; 647: 323-333.
- Ebrahimi, P., and Borrok, D. M., 2020, Mobility of Ba, Sr, Se and As under simulated conditions of produced water injection in dolomite: *Applied Geochemistry*, v. 118, p. 104640.

- Ebrahimi, P., and Vilcáez, J., 2018, Petroleum produced water disposal: Mobility and transport of barium in sandstone and dolomite rocks.: *Science of the Total Environment*, v. 634, pp.1054-1063.
- Ebrahimi, P., and Vilcáez, J., 2018a, Effect of brine salinity and guar gum on the transport of barium through dolomite rocks: Implications for unconventional oil and gas wastewater disposal: *Journal of Environmental Management*, v. 214, p. 370-378.
- Ebrahimi, P., and Vilcáez, J., 2019b, Transport of barium in fractured dolomite and sandstone saline aquifers.: *Science of the Total Environment*, v. 647, pp.323-333.
- Emmons, R. V., Shyam Sunder, G. S., Liden, T., Schug, K. A., Asfaha, T. Y., Lawrence, J. G., Kirchhoff, J. R., and Gionfriddo, E., 2022, Unraveling the Complex Composition of Produced Water by Specialized Extraction Methodologies.: *Environmental Science & Technology*, v. 56(4), pp.2334-2344.
- Engle, M. A., Cozzarelli, I. M., and Smith, B. D., 2014, USGS investigations of water produced during hydrocarbon reservoir development, US Department of the Interior, US Geological Survey.
- Fard, A. K., McKay, G., Chamoun, R., Rhadfi, T., Preud'Homme, H., and Atieh, M. A., 2017, Barium removal from synthetic natural and produced water using MXene as two dimensional (2-D) nanosheet adsorbent: *Chemical Engineering Journal*, v. 317, p. 331-342.
- Federation, W. E., and Aph Association, 2005, Standard methods for the examination of water and wastewater. : American Public Health Association (APHA): Washington, DC, USA. 21th Edition. , p. pp 4-75 to 74-76 (chloride method 4500-Cl G) and 4504-4127 to 4504-4129 (nitrate method 4500-NO4503 I).
- Feizi, M., and Jalali, M., 2015, Removal of heavy metals from aqueous solutions using sunflower, potato, canola and walnut shell residues.: *Journal of the Taiwan Institute of Chemical Engineers*, v. 54, pp.125-136.
- Flora, G., Gupta, D., and Tiwari, A., 2012, Toxicity of lead: a review with recent updates: *Interdisciplinary Toxicology*, v. 5, no. 2, p. 47-58.
- Fu, F., and Wang, Q., 2011, Removal of heavy metal ions from wastewaters: a review: *Journal of environmental management*, v. 92, no. 3, p. 407-418.
- Fukushi, K., Munemoto, T., Sakai, M., and Yagi, S., 2011, Monohydrocalcite: a promising remediation material for hazardous anions: *Sci Technol Adv Mater*, v. 12, no. 6, p. 064702.
- Gadhamshetty, V., Shrestha, N., Chilkoor, G., and Bathi, J. R., 2015, Emerging Environmental Impacts of Unconventional Oil Development in the Bakken Formation in the Williston Basin of Western North Dakota, Hydraulic Fracturing: *Environmental Issues*, Volume 1216, American Chemical Society, p. 151-180.
- Ghaemi, A., Torab-Mostaedi, M., and Ghannadi-Maragheh, M., 2011, Characterizations of strontium(II) and barium(II) adsorption from aqueous solutions using dolomite powder: *Journal of Hazardous Materials*, v. 190, no. 1, p. 916-921.

- Groundwater Protection Council, 2015. Produced Water Reuse in Oklahoma: Regulatory Considerations and References.
- Gruszecka-Kosowska, A., Baran, P., Wdowin, M., and Franus, W., 2017, Waste dolomite powder as an adsorbent of Cd, Pb(II), and Zn from aqueous solutions: *Environmental Earth Sciences*, v. 76, no. 15, p. 521.
- Guerra, K., Dahm, K., and Dundorf, S., 2011, *Oil And Gas Produced Water Management And Beneficial Use in the Western United States*,: US Department of the Interior,, p. p. 157.
- Guerra, K., Dahm, K., and Dundorf, S., 2011a, *Oil and gas produced water management and beneficial use in the Western United States*: US Department of the Interior.
- Guerra, K., Dahm, K., and Dundorf, S., 2011b, *Oil and gas produced water management and beneficial use in the Western United States*: U.S. Department of the Interior Bureau of Reclamation.
- Guerra, K., Dahm, K., and Dundorf, S., 2011c, *Oil And Gas Produced Water Management And Beneficial Use in the Western United States*,: US Department of the Interior,, p. p. 157.
- Gutiérrez-Ravelo, A., Gutiérrez, Á. J., Paz, S., Carrascosa-Iruzubieta, C., González-Weller, D., Caballero, J. M., Revert, C., Rubio, C., and Hardisson, A., 2020, Toxic metals (Al, cd, pb) and trace element (b, ba, co, cu, cr, fe, li, mn, mo, ni, sr, v, zn) levels in sarpa salpa from the north-eastern atlantic ocean region: *International Journal of Environmental Research and Public Health*, v. 17, no. 19, p. 7212.
- Hakami, M., Tizaoui, C., Kochkodan, V., and Hilal, N., 2013, Effect of hydrodynamic operations, salinity, and heavy metals on ha removal by microfiltration ceramic tubular membrane: *Separation Science and Technology*, v. 48, no. 4, p. 564-570.
- Hanes, R., Parker, M., Slabaugh, B., Weaver, J., and Walters, H. G., Analytical Methods for Maintaining Quality Assurance of Recycled Fracturing Fluids, in *Proceedings International Symposium on Oilfield Chemistry2003b*, Volume All Days: SPE-80221-MS.
- Hanes, R., Parker, M., Slabaugh, B., Weaver, J., and Walters, H., Analytical methods for maintaining quality assurance of recycled fracturing fluids, in *Proceedings International Symposium on Oilfield Chemistry2003*, OnePetro.
- Hanes, R., Parker, M., Slabaugh, B., Weaver, J., and Walters, H., Analytical methods for maintaining quality assurance of recycled fracturing fluids, in *Proceedings International Symposium on Oilfield Chemistry2003a*, OnePetro.
- Hayes, K. F., and Katz, L. E., 1996, Application of X-Ray Absorption Spectroscopy for Surface Complexation Modeling of Metal Ion Sorption in Brady, P. V., ed., *Physics and Chemistry of Mineral Surfaces*, CRC Press, p. 77.
- Holail, H., and Al-Hajari, S., 1997, Evidence of an authigenic origin for the palygorskite in a Middle Eocene carbonate sequence from North Qatar.: *Qatar Univ. Sci. J.*, v. 17, 405– 418.
- Igunnu, E. T., and Chen, G. Z., 2014, Produced water treatment technologies: *International journal of low-carbon technologies*, v. 9, no. 3, p. 157-177.

- Ingles, M., and Anadon, P., 1991, Relationship of clay minerals to depositional environment in the non-marine Eocene Pontils Group, SE Ebro Basin (Spain). *J. Sed. Petrol.*, v. 61, 926–939.
- Ivanets, A. I., Kitikova, N. V., Shashkova, I. L., Oleksienko, O. V., Levchuk, I., and Sillanpää, M., 2016, Using of phosphatized dolomite for treatment of real mine water from metal ions: *Journal of Water Process Engineering*, v. 9, p. 246-253.
- Ivanets, A. I., Shashkova, I. L., Kitikova, N. V., and Drozdova, N. V., 2014, Extraction of Co(II) ions from aqueous solutions with thermally activated dolomite: *Russian Journal of Applied Chemistry*, v. 87, no. 3, p. 270-275.
- Jensen, J., 2020, *The Role of Carbonate Minerals in Arsenic Mobility in a Shallow Aquifer Influenced by a Seasonally Fluctuating Groundwater Table* (Masters thesis, Utah State University).
- Jensen, J., 2020, *The Role of Carbonate Minerals in Arsenic Mobility in a Shallow Aquifer Influenced by a Seasonally Fluctuating Groundwater Table* (Masters thesis, Utah State University).
- Jiménez, S., Micó, M., Arnaldos, M., Medina, F., and Contreras, S., 2018, State of the art of produced water treatment: *Chemosphere*, v. 192, p. 186-208.
- Kaasa, B., and Østvold, T., 1996, Alkalinity in oil field waters-what alkalinity is and how it is measured.
- Kaczmarek, S. E., Gregg, J. M., Bish, D. L., Machel, H. G., Fouke, B. W., Macneil, A. J., Lonnee, J., and Wood, R., 2017, Dolomite, very high-magnesium calcite, and microbes—Implications for the microbial model of dolomitization, *Characterization and Modeling of Carbonates—Mountjoy Symposium 1, Volume 109, SEPM (Society for Sedimentary Geology)*, p. 0.
- Kaveeshwar, A. R., Kumar, P. S., Revellame, E. D., Gang, D. D., Zappi, M. E., and Subramaniam, R., 2018, Adsorption properties and mechanism of barium (II) and strontium (II) removal from fracking wastewater using pecan shell based activated carbon: *Journal of Cleaner Production*, v. 193, p. 1-13.
- Kharaka, Y. K., Kakouros, E., Thordsen, J. J., Ambats, G., and Abbott, M. M., 2007a, Fate and groundwater impacts of produced water releases at OSPER "B" site, Osage County, Oklahoma: *Applied Geochemistry*, v. 22, no. 10, p. 2164-2176.
- Kharaka, Y. K., Kakouros, E., Thordsen, J. J., Ambats, G., and Abbott, M. M., 2007b, Fate and groundwater impacts of produced water releases at OSPER "B" site, Osage County, Oklahoma: *Applied geochemistry*, v. 22, no. 10, p. 2164-2176.
- Kharaka, Y. K., Kakouros, E., Thordsen, J. J., Ambats, G., and Abbott, M. M., 2007, Fate and groundwater impacts of produced water releases at OSPER "B" site, Osage County, Oklahoma: *Applied geochemistry*, v. 22, no. 10, p. 2164-2176.
- Kim, Y., Kwon, S., and Roh, Y., 2021, Effect of divalent cations (Cu, Zn, Pb, Cd, and Sr) on microbially induced calcium carbonate precipitation and mineralogical properties.: *Frontiers in Microbiology*, v. 12, p.646748.

- Koutros, S., Lenz, P., Hewitt, S. M., Kida, M., Jones, M., Schned, A. R., Baris, D., Pfeiffer, R., Schwenn, M., and Johnson, A., 2018, RE: Elevated bladder cancer in northern new England: The role of drinking water and arsenic: JNCI: Journal of the National Cancer Institute, v. 110, no. 11, p. 1273-1274.
- Kowalczyk, E., Givelet, L., Amlund, H., Sloth, J. J., and Hansen, M., 2022, Risk assessment of rare earth elements, antimony, barium, boron, lithium, tellurium, thallium and vanadium in teas: EFSA Journal, v. 20, p. e200410.
- Kumari, D., Qian, X. Y., Pan, X., Achal, V., Li, Q., and Gadd, G. M., 2016, Microbially-induced carbonate precipitation for immobilization of toxic metals.: Advances in applied microbiology,, v. 94, pp.79-108.
- Lasaga, A. C., 1984, Chemical kinetics of water-rock interactions: Journal of Geophysical Research: Solid Earth, v. 89, no. B6, p. 4009-4025.
- Lin, C. Y., Musta, B., and Abdullah, M. H., 2013, Geochemical processes, evidence and thermodynamic behavior of dissolved and precipitated carbonate minerals in a modern seawater/freshwater mixing zone of a small tropical island: Applied geochemistry, v. 29, p. 13-31.
- Lutz, B. D., Lewis, A. N., and Doyle, M. W., 2013, Generation, transport, and disposal of wastewater associated with Marcellus Shale gas development: Water Resources Research, v. 49, no. 2, p. 647-656.
- Mohammadi, M., Ghaemi, A., Torab-Mostaedi, M., Asadollahzadeh, M., and Hemmati, A., 2015, Adsorption of cadmium (II) and nickel (II) on dolomite powder: Desalination and Water Treatment, v. 53, no. 1, p. 149-157.
- Morton, R. B., 1986, Effects of brine on the chemical quality of water in parts of Creek, Lincoln, Okfuskee, Payne, Pottawatomie, and Seminole Counties, Oklahoma, University of Oklahoma.
- Morton, R. B., 1986a, Effects of brine on the chemical quality of water in parts of Creek, Lincoln, Okfuskee, Payne, Pottawatomie, and Seminole Counties, Oklahoma, 89.
- Morton, R. B., 1986b, Effects of brine on the chemical quality of water in parts of Creek, Lincoln, Okfuskee, Payne, Pottawatomie, and Seminole Counties, Oklahoma, University of Oklahoma.
- Mukherjee, S., Mukhopadhyay, S., Zafri, M. Z. B., Zhan, X., Hashim, M. A., and Sen Gupta, B., 2018, Application of guar gum for the removal of dissolved lead from wastewater: Industrial Crops and Products, v. 111, p. 261-269.
- Murray, K. E., 2014, Class II underground injection control well data for 2010–2013 by geologic zones of completion, Oklahoma: Oklahoma Geological Survey Open File Report OF1.
- Neuberger, C. S., and Helz, G. R., 2005, Arsenic (III) carbonate complexing: Applied geochemistry, v. 20(6), pp.1218-1225.

- Ng, J. C., Wang, J., and Shraim, A., 2003, A global health problem caused by arsenic from natural sources: *Chemosphere*, v. 52, no. 9, p. 1353-1359.
- Ogolo, N. A., Akinboro, O. G., Inam, J. E., Akpokere, F. E., and Onyekonwu, M. O., Effect of Grain Size on Porosity Revisited, in *Proceedings SPE Nigeria Annual International Conference and Exhibition 2015*, Volume All Days: SPE-178296-MS.
- Omar, K., and Vilcáez, J., 2022, Removal of toxic metals from petroleum produced water by dolomite filtration.: *Journal of Water Process Engineering*, v. 47, p.102682.
- Omar, K., and Vilcaez, J., 2023, Role of alkalinity and dolomite reactivity on toxic metals removal from petroleum produced water by dolomite: *Science of the Total Environment*
- Peter, A., Sharma, S. K., and Obot, I. B., 2016, Anticorrosive efficacy and adsorptive study of guar gum with mild steel in acidic medium: *Journal of Analytical Science and Technology*, v. 7, no. 1, p. 26.
- Pokrovsky, O. S., Mielczarski, J. A., Barres, O., and Schott, J., 2000b, Surface Speciation Models of Calcite and Dolomite/Aqueous Solution Interfaces and Their Spectroscopic Evaluation: *Langmuir*, v. 16, no. 6, p. 2677-2688.
- Pokrovsky, O. S., Schott, J., and Thomas, F., 1999, Dolomite surface speciation and reactivity in aquatic systems: *Geochimica et Cosmochimica Acta*, v. 63, no. 19-20, p. 3133-3143.
- Pokrovsky, O. S., Schott, J., and Thomas, F., 1999, Processes at the magnesium-bearing carbonates/solution interface. I. a surface speciation model for magnesite: *Geochimica et Cosmochimica Acta*, v. 63, no. 6, p. 863-880.
- Pokrovsky, O. S., Schott, J., and Thomas, F., 1999a, Dolomite surface speciation and reactivity in aquatic systems: *Geochimica et Cosmochimica Acta*, v. 63, no. 19, p. 3133-3143.
- Pokrovsky, O. S., Schott, J., and Thomas, F., 1999b, Dolomite surface speciation and reactivity in aquatic systems: *Geochimica et Cosmochimica Acta*, v. 63, no. 19-20, p. 3133-3143.
- Pokrovsky, O., and Schott, J., 2002, Surface chemistry and dissolution kinetics of divalent metal carbonates: *Environmental science & technology*, v. 36, no. 3, p. 426-432.
- Pokrovsky, O., Mielczarski, J., Barres, O., and Schott, J., 2000, Surface speciation models of calcite and dolomite/aqueous solution interfaces and their spectroscopic evaluation: *Langmuir*, v. 16, no. 6, p. 2677-2688.
- Ribeiro, L. P. S., Puchala, R., Lalman, D. L., and Goetsch, A. L., 2021, Composition of various sources of water in Oklahoma available for consumption by ruminant livestock.: *Applied Animal Science*, v. 37(5), pp.595-601.
- Rozell, D. J., and Reaven, S. J., 2012, Water pollution risk associated with natural gas extraction from the Marcellus Shale: *Risk Analysis: An International Journal*, v. 32, no. 8, p. 1382-1393.

- Ryan, B. H., Kaczmarek, S. E., and Rivers, J. M., 2019, Dolomite dissolution: An alternative diagenetic pathway for the formation of palygorskite clay.: *Sedimentology*, v. 66(5), pp.1803-1824.
- Saha, S., Basak, B., Hwang, J.-H., Salama, E.-S., Chatterjee, P. K., and Jeon, B.-H., 2020, Microbial Symbiosis: A Network towards Biomethanation: *Trends in Microbiology*, v. 28, no. 12, p. 968-984.
- Scanlon, B. R., Reedy, R. C., Xu, P., Engle, M., Nicot, J. P., Yoxtheimer, D., Yang, Q., and Ikonnikova, S., 2020, Can we beneficially reuse produced water from oil and gas extraction in the U.S.: *Science of The Total Environment*, v. 717, p. 137085.
- Scientific Committee on Health and Environmental Risk, 2012. Assessment of the tolerable daily intake of barium.
- Shabani, B., and Vilcáez, J., 2017, Prediction of CO₂-CH₄-H₂S-N₂ gas mixtures solubility in brine using a non-iterative fugacity-activity model relevant to CO₂-MEOR: *Journal of Petroleum Science and Engineering*, v. 150, p. 162-179.
- Shabani, B., Pashin, J., and Vilcáez, J., 2020, TOUGHREACT-CO₂Bio – A new module to simulate geological carbon storage under biotic conditions (Part 2): The bio-geochemical reactive transport of CO₂-CH₄-H₂-H₂S gas mixtures: *Journal of Natural Gas Science and Engineering*, v. 76, p. 103190.
- Shaffer, D. L., Arias Chavez, L. H., Ben-Sasson, M., Romero-Vargas Castrillón, S., Yip, N. Y., and Elimelech, M., 2013, Desalination and Reuse of High-Salinity Shale Gas Produced Water: Drivers, Technologies, and Future Directions: *Environmental Science & Technology*, v. 47, no. 17, p. 9569-9583.
- Silva, C., Smith, B. J., Ray, J. T., Derby, J. R., and Gregg, J. M., 2020, Diagenesis of Hunton Group Carbonates (Silurian) West Carney Field, Logan and Lincoln Counties, Oklahoma, U.S.A: *Midcontinent Geoscience*, v. 1, p. 30-51.
- Smith, A. H., Lopipero, P. A., Bates, M. N., and Steinmaus, C. M., 2002, Arsenic epidemiology and drinking water standards, Volume 296, American Association for the Advancement of Science, p. 2145-2146.
- Srivastava, N. K., and Majumder, C. B., 2008, Novel biofiltration methods for the treatment of heavy metals from industrial wastewater: *Journal of Hazardous Materials*, v. 151, no. 1, p. 1-8.
- Steeffel, C. I., and Lasaga, A. C., 1994, A coupled model for transport of multiple chemical species and kinetic precipitation/dissolution reactions with application to reactive flow in single phase hydrothermal systems: *American Journal of Science*, v. 294, no. 5, p. 529.
- Stumm, W., 1992, *Chemistry of the Solid-Water Interface: Processes at the Mineral-Water and Particle-Water Interface in Natural Systems*, Wiley.
- Stumm, W., and Morgan, J. J., 1996, *Aquatic Chemistry* (3rd ed.). New York, Wiley-Interscience. Chaps 3 and 4. Detailed systematics of acid-base reactions, the carbonate system, and alkalinity titrations.

- Tabatabaeefar, A., Yuan, Q., Salehpour, A., and Rajabi-Hamane, M., 2020, Batch adsorption of lead (II) from aqueous solution onto novel polyoxyethylene sorbitan monooleate/ethyl cellulose microfiber adsorbent: kinetic, isotherm and thermodynamic studies.: *Separation Science and Technology*, , v. 55(6), pp.1051-1061.
- Temple, B. J., Bailey, P. A., and Gregg, J. M., 2020, Carbonate Diagenesis Of The Arbuckle Group North Central Oklahoma To Southeastern Missouri., p. 10-30.
- Tesoriero, A. J., and Pankow, J. F., 1996, Solid solution partitioning of Sr²⁺, Ba²⁺, and Cd²⁺ to calcite: *Geochimica et Cosmochimica Acta*, v. 60, no. 6, p. 1053-1063.
- Thompson, J. B., and Ferris, F. G., 1990, Cyanobacterial precipitation of gypsum, calcite, and magnesite from natural alkaline lake water.: *Geology* v. 18, 995e998.
- Thompson, J. B., Schultze-Lam, S., Beveridge, T. J., and Des Marais, D. J., 1997, Whiting events: Biogenic origin due to the photosynthetic activity of cyanobacterial picoplankton.: *Limnol. Oceanogr.*, v. 42, 133e141.
- Tucker, M. E., and Wright, V. P., 2009, *Carbonate Sedimentology*, Wiley.
- Van Cappellen, P., Charlet, L., Stumm, W., and Wersin, P., 1993, A surface complexation model of the carbonate mineral-aqueous solution interface: *Geochimica et Cosmochimica Acta*, v. 57, no. 15, p. 3505-3518.
- Verrecchia, E. P., and Le Coustumer, M. N., 1996, Occurrence and genesis of palygorskite and associated clay minerals in a Pleistocene calcrete complex, Sde Boqer, Negev Desert, Israel.: *Clay Miner.*, , v. 31, 183–202.
- Vilcáez, J., 2020, Reactive transport modeling of produced water disposal into dolomite saline aquifers: Controls of barium transport: *Journal of Contaminant Hydrology*, v. 233, p. 103600.
- Vilcáez, J., York, J., Youssef, N., and Elshahed, M., 2018, Stimulation of methanogenic crude oil biodegradation in depleted oil reservoirs: *Fuel*, v. 232, p. 581-590.
- Watts, P., and Howe, P., 2010, Strontium and strontium compounds, World Health Organization, v. 77.
- Watts, P., England, S., and Howe, P., 2010, Strontium and strontium compounds: World Health Organization, 1020-6167.
- Wei, H., Shen, Q., Zhao, Y., Wang, D. J., and Xu, D. F., 2003, Influence of polyvinylpyrrolidone on the precipitation of calcium carbonate and on the transformation of vaterite to calcite. : *Journal of Crystal Growth*, , v. 250(3-4), pp.516-524.
- Wolery, T. J., Jackson, K. J., Bourcier, W. L., Bruton, C. J., Viani, B. E., Knauss, K. G., and Delany, J. M., 1990, Current Status of the EQ3/6 Software Package for Geochemical Modeling, *Chemical Modeling of Aqueous Systems II*, Volume 416, American Chemical Society, p. 104-116.

- Xu, T., Sonnenthal, E., Spycher, N., and Pruess, K., 2006, TOUGHREACT—A simulation program for non-isothermal multiphase reactive geochemical transport in variably saturated geologic media: Applications to geothermal injectivity and CO₂ geological sequestration: *Computers & Geosciences*, v. 32, no. 2, p. 145-165.
- Yamkate, N., Chotpantararat, S., and Sutthirat, C., 2017, Removal of Cd²⁺, Pb²⁺, and Zn²⁺ from contaminated water using dolomite powder: Human and Ecological Risk Assessment: *An International Journal*, v. 23, no. 5, p. 1178-1192.
- Yin, X., Jiang, Y., Tan, Y., Meng, X., Sun, H., and Wang, N., 2019, Co-transport of graphene oxide and heavy metal ions in surface-modified porous media: *Chemosphere*, v. 218, p. 1-13.
- Yost, E. E., Stanek, J., DeWoskin, R. S., and Burgoon, L. D., 2016, Overview of Chronic Oral Toxicity Values for Chemicals Present in Hydraulic Fracturing Fluids, Flowback, and Produced Waters: *Environmental Science & Technology*, v. 50, no. 9, p. 4788-4797.
- Zheng, J.-L., Yuan, S.-S., Wu, C.-W., Lv, Z.-M., and Zhu, A.-Y., 2017, Circadian time-dependent antioxidant and inflammatory responses to acute cadmium exposure in the brain of zebrafish: *Aquatic Toxicology*, v. 182, p. 113-119.
- Zielinski, R. A., and Budahn, J. R., 2007, Mode of occurrence and environmental mobility of oil-field radioactive material at US Geological Survey research site B, Osage-Skiatook Project, northeastern Oklahoma: *Applied Geochemistry*, v. 22, no. 10, p. 2125-2137.

VITA

Khalid Majeed Haji Omar

Candidate for the Degree of

Doctor of Philosophy

Dissertation: CHEMICAL AND PHYSICAL CONTROLS OF TOXIC METALS
REMOVAL FROM PETROLEUM PRODUCED WATER BY
DOLOMITE FILTRATION

Major Field: Geology

Biographical:

Education:

Completed the requirements for the Doctor of Philosophy in Geology at Oklahoma State University, Stillwater, Oklahoma in May, 2023.

Completed the requirements for the Master of Art in Earth Sciences at Western Michigan University, Kalamazoo, Michigan in 2017.

Completed the requirements for the Bachelor of Science in Geology at Salahaddin University, Erbil, Kurdistan, Iraq in 2008.

Experience:

Graduate Research and Teaching Associate at Oklahoma State University. Hydrogeologist/ Geophysicist at Groundwater Directorate of Duhok City, Duhok, Kurdistan, Iraq, Geologist at Michigan Geological Survey, Kalamazoo, MI, Consulting Geologist at Cielo Engineering, Duhok, Kurdistan, Iraq, and a Mining Geologist at Kurdistan Geological Survey, Duhok, Kurdistan, Iraq.

Professional Memberships:

Association of Environmental and Engineering geologists, Society for Sedimentary Geology, Society of Exploration Geophysicists, Geological Society of America, American Institute of Professional Geologists, American Geophysical Union, American Association of Petroleum Geologists, Oklahoma City Geological Society, Tulsa Geological Society.